# 10Investigation of the uptake, co-localisation, biological effects, and toxicity mechanism(s) of carboxyl-modified polystyrene nanoparticles (COO-PS-NPs) onto human bronchial epithelial (BEAS-2B) cells

by

**Mohammed Salem Shuwaikan**

A thesis submitted to the School of Biosciences
of The University of Birmingham
for the degree of
**DOCTOR OF PHILOSOPHY IN TOXICOLOGY**

School of Biosciences
The University of Birmingham
March 2014

- *‘‘The cell never acts; it reacts’’* - **Ernst Haeckel** (1986)

## ABSTRACT

Carboxyl-modified polystyrene nanoparticles (COO-PS-NPs) have many potential applications, for example drug-delivery systems, but their toxicity remains poorly assessed. In the current study, characterisation, uptake and toxicity of two sized COO-PS-NPs in cultured BEAS-2B lung epithelial cells were investigated.

The 20nm sized COO-PS-NPs tended to aggregate heavily in the cell culture media yielding larger aggregates, in contrast the 100nm COO-PS-NPs were stable. Electron and confocal microscopy demonstrated that COO-PS-NPs rapidly accumulate in vesicle-like structures within cells and fluorescent organelle co-staining showed the presence of 20nm COO-PS-NPs in mitochondria and the 100nm COO-PS-NPs in Golgi apparatus. Cellular studies revealed that COO-PS-NPs cause GSH depletion and induce ROS generation resulting in oxidative stress. Studies in a cell-free system showed that COO-PS-NPs directly deplete levels of GSH in solution. Size- and concentration-dependent DNA strand breaks (by comet assay) were also observed and both 20nm and 100nm COO-PS-NPs induced caspases-3/7 activation in a $Ca^{2+}$ independent manner, however a significant decrease in cell viability was observed only at high concentrations of 20nm COO-PS-NPs.

In summary, this *in vitro* study demonstrated that toxicity of the 20nm COO-PS-NPs is mediated by oxidative stress after co-localisation to the mitochondria and that further studies are needed to assess the safety of COO-PS-NPs.

## ACKNOWLEDGEMENTS

I would like to express my thanks foremost to ALLAH (The God) for everything and then to the government of Saudi Arabia for offering this opportunity to do a PhD and for financial support of all the studying fees and life expenses during this research project.

Academically, I would like to express my sincere gratitude towards my supervisor, Dr. Nik Hodges. I appreciate his vast knowledge, skills, understanding, patience, brilliant advices for practical experiments, time he has given to me and assistance in writing letters required to Saudi Arabia Cultural Bureau (SACB) and reports (e.g. GRS2 monthly reports and annual reports). His guidance at all levels of my PhD including through writing this thesis was priceless and his selfless time and care were sometimes all that kept me going on. I would like also to thank Prof. Kevin Chipman for taking time out from his busy schedule to give advices particularly at the beginning of my project and Dr. Michaella Kendall for support she provided throughout my research project and for reading chapter three of my thesis.

I would like to express special thanks to Dr. Mohammed Baalousha for technical assistance with DLS and TEM instruments for COO-PS-NPs characterisation and for invaluable suggestions and insightful comments he provided regarding this issue. Appreciation also goes out to Dr.Stephen Baker for assistance in evaluating the metal content of the samples and to Dr. Sayeed Haque who helped me with statistical analysis of results and advices at times of critical need. I must also acknowledge the members and

staff of the 4th floor for exchanging knowledge and skills as well as the technicians in the centre for electron microscopy, Mr. Paul Stanley and Mrs. Theresa Morris, who provided assistance with sample preparations for TEM imaging.

I would further like to thank all of my friends, my lab mates and my fellow PhD students for creating a wonderful environment to work which make my time here interesting, very enjoyable and more fun during the 4-years PhD with special thanks to Lorna Thorne for venting out the frustration during my research program.

A very special gratitude goes to my parents, the special ones, words cannot express how grateful I am to them for encouraging me and for instilling confidence in me to take this opportunity to achieve my dream in continuing higher education and pursuing my PhD. I would also like to thank my brothers and sisters for the spiritual support and great help they provided to me through my entire life particularly through this period of my carrier. Their dua'a (prayer) for me was what sustained me thus far. At the end, I would like to express sincere appreciation to my beloved wife for sleepless nights she spent and for being always there in the moments where no one was there to stand by me. I would say that without your love, continuous support and encouragement I would not have achieved my PhD.

# TABLE OF CONTENT

## LIST OF FIGURES

## LIST OF TABLES

# LIST OF ABBREVIATIONS

| Abbreviation | Name |
|---|---|
| A549 | Human lung carcinoma cells |
| AFM | Atomic force microscopy |
| Ag-NPs | Silver nanoparticles |
| AIF | Apoptosis-inducing factor |
| ANOVA | Analysis of variance |
| AP-1 | Activator protein 1 |
| AP-2 | Adaptor protein 2 (complex) |
| ATP | Adenosine triphosphate |
| ATPase | Adenosine triphosphatase |
| AU-NPs | Gold nanoparticles |
| BAPTA-AM | 1,2-bis-(O-Aminophenoxy)-ethane-N,N,N',N'-tetraacetic acid tetraacetoxymethyl ester |
| BEAS-2B | Bronchial epithelial cells |
| BSA | Bovine serum albumin |
| BSO | Buthionine sulfoximine |
| C3A | Rat carcinoma hepatocyte cells |
| $Ca^{2+}$ | Calcium |
| CB-NPs | Carbon nanoparticles |
| CIM | Cell imaging media |
| CLSM | Confocal laser scanning microscope |
| COO-PS-NPs | Carboxyl-modified polystyrene nanoparticles |
| Cu | Copper |
| DAPI | 4',6-diamidino-2-phenylindole |
| DCF | 2',7'-dichlorofluorescein |

| | |
|---|---|
| $dH_2O$ | Distilled water |
| DLS | Dynamic light scattering |
| DMSO | Dimhethyl sulfoxide |
| DNA | Deoxyribonucleic acid |
| ENPs | Engineered nanoparticles |
| EGFR | Epidermal growth factor receptor |
| ER | Endoplasmic reticulum |
| FACS | Fluorescence-activated cell sorting (flow cytometry) |
| Fe | Ferrous (iron) |
| FITC | Fluorescein isothiocyanate |
| FPG | Formamidopyrimidine glycosylase |
| GA | Glutaric acid dialdehyde (or glutaraldehyde) |
| GFP | Green fluorescent protein |
| GPx | Glutathione peroxidase |
| GSH | Glutathione (reduced) |
| GSSG | Glutathione disulfide (oxidized) |
| GST | Glutathione-S-transferase |
| 16HBE14o | Polarized human bronchial epithelial cells |
| $H_2DCF$ | 2',7'-dichlorodihydrofluorescein |
| $H_2DCF$-DA | 2',7'-dichlorodihydrofluorescein diacetate |
| HeLa | cervical epithelial adenocarcinoma cells |
| HEPA-1 | hepatoma cells |
| HepG2 | human carcinoma hepatocyte cells |
| HMEC | human microvascular endothelial cells |
| $HNO_3$ | Nitric acid |
| HO• | Hydroxyl radical |

| | |
|---|---|
| $H_2O_2$ | Hydrogen peroxide |
| ICP-MS | Inductively coupled plasma-mass spectrometry |
| IL | Interleukins |
| $IP_3$ | Inositol 1,4,5-triphosphate |
| IRHCs | Isolated rat hepatocyte couplets |
| LAMP-1 | Lysosomal membrane glycoprotein-1 compartment |
| LB | Lysogeny broth |
| LDH | Lactate dehydragenase |
| LHC-9 | Lechner and LaVeck serum-free cell-culture medium |
| LMPA | Low melting point agar |
| MAPK | Mitogen activated protein kinase |
| MDCK | Madin-Darby canine kidney cells |
| MRI | Magnetic resonance imaging |
| MSC | Mesenchymal stem cells |
| MSTO-211H | Mesothelioma cells |
| MTT | 3-(4,5-dimethylthiazol-2-yl)-2,5-diphenyltetrazolium bromide |
| MWCNT | Multi-wall carbon nanotubes |
| 1321N1 | Human astrocytoma cells |
| NADPH | Nicotinamide adenine dinucleotide phosphate |
| NFAT | Nuclear factor of activated T-cells |
| NBF | Neutral buffered formalin solution |
| NFκB | Nuclear factor-kappa B |
| NH-PS-NPs | Amine-modified polystyrene nanoparticles |
| NH-Si-NP | Amino-modified silica nanoparticles |
| nm | Nanometre(s) |
| NMPA | Normal melting point agar |
| NPs | Nanoparticles |

| | |
|---|---|
| NTA | Nanoparticle tracking analysis |
| $O_2•^-$ | Superoxide anions |
| $OH^•$ | Hydroxyl radical |
| OPT | O-Phthalaldehyde |
| $OsO_4$ | Osmium tetraoxide |
| 8-oxodG | 8-oxo-7,8-dihydro-2′-deoxyguanosine |
| PC-12 | Pheochromocytoma cells |
| PI | Propidium iodide |
| PBS | Phosphate-buffered saline |
| $PO_4$-EDTA | Phosphate ethylenediaminetetraacetic acid |
| PS | Phosphatidylserine |
| PS-NPs | Polystyrene nanoparticles |
| PTP | Permeability transition pore |
| RAECM | Rat alveolar epithelial cell monolayers |
| RAW 264.7 | Mouse leukaemic monocyte macrophage cells |
| ROO• | Peroxy radical |
| ROS | Reactive oxygen species |
| SEM | Scanning electron microscopy |
| SFM | Serum-free medium |
| SiNP | Silica nanoparticles |
| SOD | Superoxide dismutase |
| SR | Sarcoplasmic reticulum |
| SYBR | Synergy brands, Inc |
| TCA | Trichloroacetic acid |
| $TiO_2$-NPs | Titanium dioxide nanoparticles |
| TEM | Transmission electron microscopy |
| TNF-α | Tumor necrosis factor alpha |

| | |
|---|---|
| U251 | Human neuronal glioblastoma (astrocytoma) cells |
| UFPs | Ultrafine particles |
| Zn | Zinc |
| ZnO-NPs | Zinc oxide nanoparticles |
| ζ-potential | Zeta potential |

# CHAPTER ONE:

# GENERAL INTRODUCTION

## 1.1 Engineered nanoparticles

Nanoparticles (NPs) including engineered nanoparticles (ENPs) are defined in a size-based way, although the precise definition varies. Revell, for instance, has described ENPs as extremely small laboratory man-made materials with one or more dimensions of a diameter of 100 nanometres (nm) or less [Revell (2006)] while Varela and colleagues have defined them as ultrafine particles that have at least two dimensions with less than 100nm in length [varela et al (2012)]. On the other hand, Stone and colleagues identified ENPs as having three dimensions with length less than 100nm [Stone et al (2010)]. The European Commission has reported that "nanomaterial means a natural, incidental or manufactured material containing particles, in an unbound state or as an aggregate or as an agglomerate and where, for 50% or more of the particles in the number size distribution, one or more external dimensions is in the size range 1-100nm". [Commission Recommendation on the Definition of Nanomaterial (Brussels, 2011, published online)]. Whatever the precise definition, ENPs are extremely small and they therefore can easily penetrate through to all cells and reach almost all the areas of the body.

ENPs are known to demonstrate large surface area to volume ratio due to their small size. This means that a large number of total atoms are exposed on the outer surface of ENPs (compared to atoms engulfed inside) and this would enhance their energy and consequently increase their chemical functional reactivity compared to their counterparts

of the large scale particles towards biological systems [Oberdörster et al (2005b), Vippola et al (2009)]. In other words, ENPs have significant adsorption capacities (because of their large surface area) that would improve their biological activity as dynamic carrier systems for other probes (e.g. drugs) and bio-molecules (e.g. proteins) in biological systems [Fröhlich[b] (2012)]. Subsequently, this would enhance the drug efficacy when physically adsorbed (or covalently bound) onto the surface of the ENPs because they would provide effective drug transportation to the target of interest with good protection against digestion and/or extracellular degradation upon metabolism [Mailänder and Landfester (2009)].

The surface of ENPs can be modified (with functional group) or coated (with other material) to change their physicochemical properties [De Jong et al (2008)]. These consist of the ENPs attributes (such as size, shape, surface charge, functional group, chemical composition and porosity) in addition to the surrounding media-dependent characteristics (including bio-degradation, solubility (hydrophobicity/hydrophilicity) and aggregation/dispersion status) [Nel et al (2009)]. The ENPs physicochemical characteristics play a major role in determining the uptake, bioactivity, translocation and biodegradability of ENPs in biological systems [Alvarez-Román et al (2004)] as well as determining the ENPs-drug binding, adsorption, trafficking and fate [Olivier et al (2004), Rejman et al (2004)].

Over the past couple of decades, ENPs have attracted the attention of scientists and people from different fields including industries because of the unique physicochemical properties (including electronic, magnetic and optical characteristics) of

ENPs compared with traditional materials of large-scale size. These properties make them scientifically and economically important with uses in electrical and medical products as well as in wider range of applications [Yang et al (2010)] showing a very promising future for ENPs. They have also been used in medical sciences and technologies [Murthy (2007), Yang et al (2007)] such as diagnostics (e.g. contrast agents in magnetic resonance imaging (MRI)) [Mailänder and Landfester (2009)], therapeutics (i.e. drug/gene delivery and cancer detection) [Panyam and Labhasetwar (2010)] and in materials used for bone and hip replacements [Yang et al (2010)]. In addition, they are used in several applications including cosmetics and daily personal care products (e.g. sun lotions, deodorants and toothpaste), dyes for the textile industry [Wong et al (2006)] and in criminal detection (such as latent fingerprints identification) [Sametband et al (2007), Amey et al (2009)]. Thus, ENPs can be exploited broadly in several applications depending on their increased surface area compared to their unit mass [Allaker et al (2008)]. As many as 1500 ENPs-based containing consumer products have been estimated to be recently in market [Marquis et al (2009), Zhu et al (2010), The Nanotechnology Consumer Products Inventory (published online)].

## 1.2 Carboxyl-modified polystyrene nanoparticles and their applications

Polystyrene nanoparticles (PS-NPs) are polymers without transition metals or minerals [Brown et al (2001)]. They are monodisperse of variable size [Holzapel et al (2005)] with a minimal negative charge but are often considered neutral as they do not

have a specific functional group [Lundqvist et al (2008)]. The carboxyl-modified polystyrene nanoparticles (COO-PS-NPs) are polar negatively charged polymeric nanoparticles with several carboxyl groups attached covalently to their surfaces [Alvarez-Román et al (2004), Mailänder and Landfester (2009)].

These polymeric nanoparticles have been widely used in a variety of fields such as biomedical applications (as carriers for several bio-molecules such as antibodies, peptides or proteins and drugs to different tissues and organs), electrical applications and catalysts [Liu and Liu (2009)]. In addition, PS-NPs can be used as a research model for long-term exposure studies since they are not significantly biodegradable and can be detected easily in cells [Mailänder and Landfester (2009)]. Fluorescent PS-NPs have been used for sensing trace amounts of infectious diseases such as malaria and a PS-NPs-based diagnosis test has been used to identify malaria in Thailand [Tallury et al (2010)]. PS-NPs are the most widely used polymeric nanoparticles as drug-carriers because they are commercially available at inexpensive cost with high stability in biological systems [Liu and Liu (2009)]. However, they have hydrophobic surfaces which would result in a non-specific adsorption of bio-molecules and they hence need to be modified by adding certain functional (carboxylic or amino) groups to allow covalent binding of bio-molecules onto their surfaces [Liu and Liu (2009), Hai et al (2009)].

## 1.3 Routes of human exposure to ENPs

The human body can come in contact with ENPs released into the environment from different sources including industrial plants, chemical storage, waste handling, transportation means and ENPs-based products as well as to ENPs that escape to the soil and groundwater through agricultural applications such as ENPS-containing pesticides. ENPs have been used in a wide range of application and consequently human exposure to ENPs are potential through various routes including inhalation (from air), digestion (or ingestion from food and water), dermal penetration (from clothes and skin products) and injection (Fig. 1.1). However, inhalation seems to be the foremost exposure route of ENPs targeting the nose, nasal cavity and alveolar cells in the lungs (passing through the respiratory tract) and travels to other organs via the circulation system. The large surface area of the lungs is a major reason that makes them the target for the inhaled NPs [Mühlfeld et al (2007)].

## 1.4 Possible adverse effects of exposure to ENPs and translocation to different organs

The use of ENPs containing products and nanotechnology applications is growing fast. The profit of medical ENPs-based application industry for example, such as ENPs containing artificial hip replacements [De Jong and Borm (2008)], is expected to reach $1 trillion by 2015 [Nel et al (2006)]. As a result, it is inevitable to avoid the

exposure to ENPs that may result in harmful consequences to human and thus, the awareness about the possible toxic consequences of the ENPs in biological systems has recently increased [Agarwal et al (2013)]. Accordingly, the nanotoxicological studies have been focusing on understanding the cells-ENPs interactions, developing risk assessment of ENPs on human health and environment, determining the concentrations (doses) for ENPs cytotoxicity and assessing the potential associated adverse health consequences of exposure to ENPs at the molecular level [Agarwal et al (2013)]. This is essential to ensure that they are safe to be used for example in medical applications and products used on a daily basis. Although not all ENPs used in applications might be harmful, the internalisation of the ENPs into cells can possibly cause adverse health impacts (Fig. 1.2). The exposure rate of the human body to ENPs, concentration, metabolism, accumulation in organs and secretion of ENPs out of the body are vital factors in evaluating possible risks of ENPs.

As previously mentioned, lungs (by inhalation), gastro-intestinal tract (by ingestion) and skin (by dermal contact) are the most likely portals of NPs entry into human body. Other possible routes (such as injections) are limited to deliberate exposure to ENPs. The internalised ENPs (through the entry points due to their small size) can gain access to the circulatory system where they can be translocated within the body to other organs and tissues.

This ENPs translocation through systemic circulation (i.e. blood stream) and distribution to different organs might have adverse effects on the human health. Thrombus formation, for example, measured after 2 and 6h in blood of human subjects

was increased following short exposure (1-2h) to dilute diesel exhaust (350µg/$m^3$) [Lucking et al (2008)]. Moreover, the effect of 60nm sized PS-NPs of three different surface modifications; neutral (unmodified) PS-NPs, negatively charged (carboxyl-modified) COO-PS-NPs and positively charged (amine-modified) NH-PS-NPs on thrombosis (and hemostasis) has also been studied in vivo and the results showed that although neutral and negatively charged COO-PS-NPs had no or weak effect, the positively charged NH-PS-NPs (60nm size) enhanced thrombus formation significantly in hamster after intravenous injection (at 50 and 500µg/kg body weight) and intratracheal administration (at 5000µg/kg body weight) [Nemmar et al (2002)]. Similarly, other study has revealed that continuous intravenous administration of the positively charged NH-PS-NPs (60nm size) in ear veins of rat model has increased the thrombus formation in a dose-dependent manner while the negatively charged COO-PS-NPs did not affect thrombosis [Silva et al (2005)].

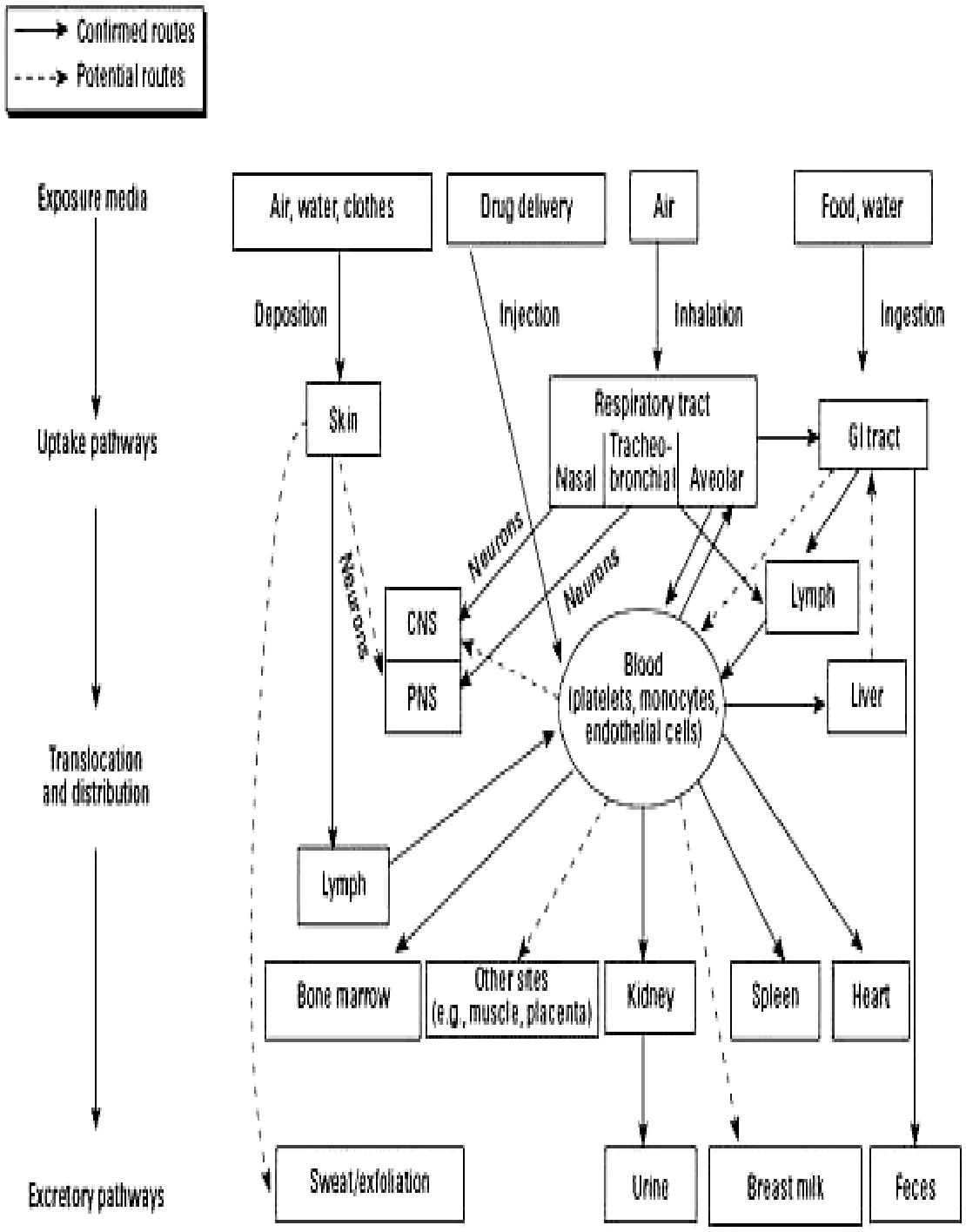


Fig 1.1 Routes of ENPs uptake and translocation into human body including inhalation, digestion, injection and skin (adopted from: "Oberdörster et al[b] (2005)").

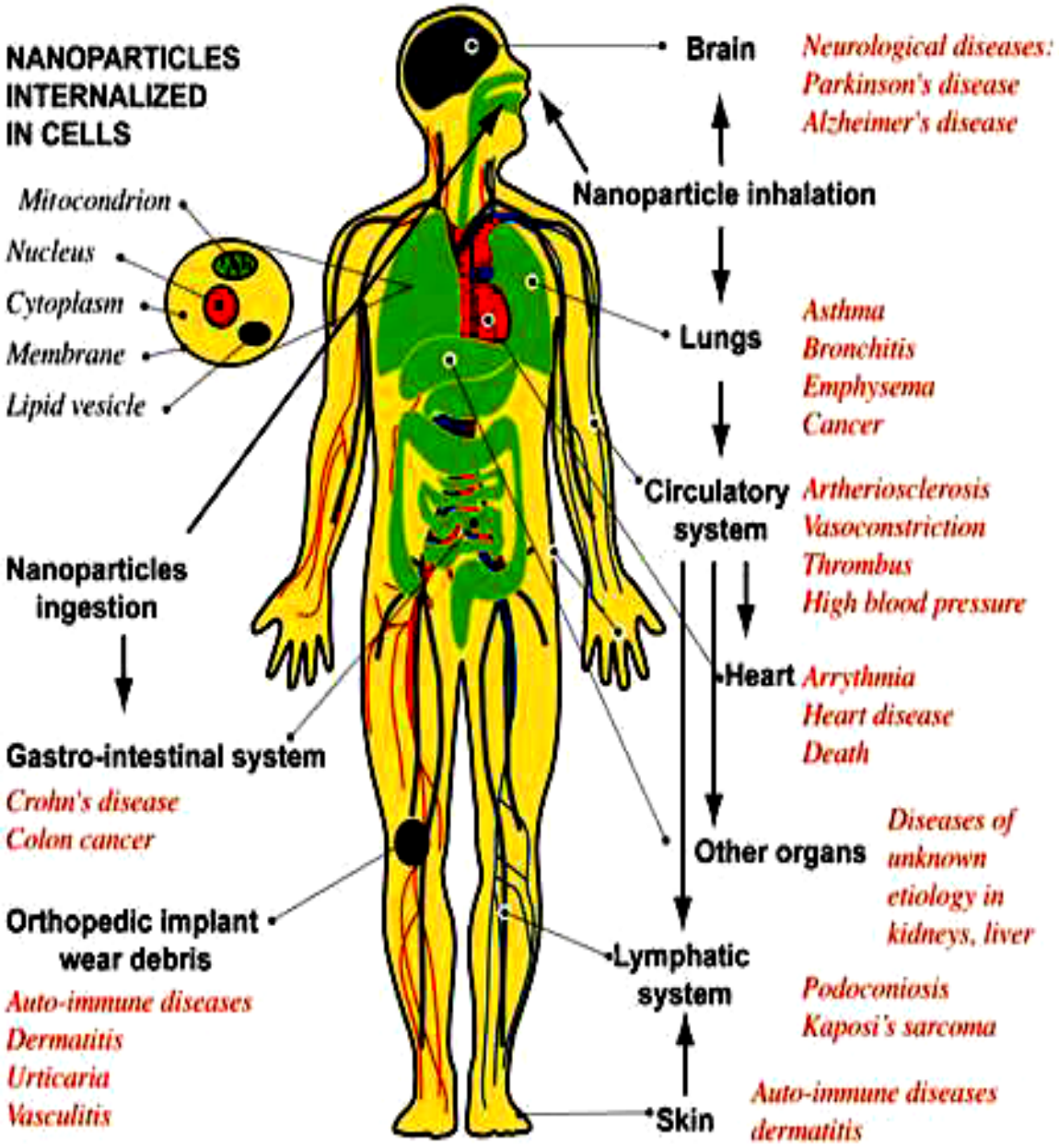


Fig 1.2 diagram of diseases and possible effects of ENPs internalisation into different organs of the human health (adopted from a report by Institute of Science In Society (ISIS) released in March 2010). The potential effects include asthma, bronchitis, lung cancer, neurodegenerative diseases (such as Parkinson), colon cancer, arteriosclerosis, heart diseases and autoimmune diseases leading potentially at the end to death, however these effects will depend on the physicochemical properties of particular ENPs.

## 1.5 Cellular uptake of ENPs and co-localisation into different compartments

Due to their large surface area-to-volume ratio, ENPs are suggested to behave in a different way to large-scaled particles of the same materials. However, relatively little is known about the cellular uptake and possible biological effects of ENPs on health and the environment are poorly understood.

Proteins are known to compete to be adsorbed onto the surfaces of ENPs in biological environments forming a transient "corona" complex which is likely to enhance the physical adhesion (interaction) of ENPs on the cell surface (this may be through plasma membrane receptors) by biologically identifying the ENP before being ingested into the cell or organelle where they can dissociate again [Ehrenberg and McGrath (2005), Cedervall et al[b] (2007), Lynch et al (2007)]. This ENPs-protein corona, in addition to the ENPs shape and size, has been therefore proposed to determine the ENPs interactions with cells and with other molecules in biological fluids as well as determining their cellular fate and sub-cellular co-localisation [Lundqvist et al (2008), Rocker et al (2009), Hellstrand et al (2009), Jiang et al[b] (2010)]. Therefore, understanding the corona formation and ENPs binding properties to bio-molecules will be helpful to gain knowledge about the biological effects of ENPs mainly at the cellular level.

Adsorption of protein on ENPs (i.e. ENP-protein corona association/dissociation) was reported to depend on the ENP size and chemical surface as well as on the protein identity and concentration in the surrounding environment [Cedervall et al (2007)]. Lundqvist and colleagues have studied the effect of the 60nm

sized PS-NPs of the three different surface modifications; neutral (unmodified) PS-NPs, negatively charged (carboxyl-modified) COO-PS-NPs and positively charged (amine-modified) NH-PS-NPs on formation of human plasma protein-nanoparticles corona using two sizes of each (50 and 100nm). They have found that both size and surface properties play a key role in determining the compositions of the protein coronas formed from human plasma on the different particles of identical materials [Lundqvist et al (2008)]. However, it has been reported recently that proteins exist in biological systems that might decrease the targeted cellular uptake of ENPs, potentially by wrapping and shielding the ligands (e.g. proteins used for modification on ENPs) and hence preventing specific binding to receptors on the cell surface leading to decrease in the pool of ENPs available to interact with cells [Salvati et al (2013)].

It has been speculated that several physicochemical properties of the ENPs including their surface charge (that might be modified by functional group or protein), size and morphology as well as the cell line would play major role in the cellular uptake of the ENPs [Mailänder and Landfester (2009)]. It has been stated: "Since cell membranes are negatively charged, positively charged ENPs were expected to be taken up even more efficiently than negatively charged ENPs " [Mailänder and Landfester (2009)]. In agreement with this statement, Lorenz and colleagues reported that ENPs with positively charged surfaces (e.g. functionalized with cationic group) were efficiently internalised into mesenchymal stem (MSC) cells and cervical epithelial adenocarcinoma (HeLa) cells compared to uncharged (non-functionalized) ones [Lorenz et al (2006)].

However, the negatively charged ENPs might gain access into the cell after attaching to a positively charged bio-molecule on the cell membrane.

The uptake of different sizes (20 - 1010nm) of fluorescently labeled PS-NPs by several cell lines including ECV 304, Hepa 1–6, HepG2, HNX 14C, KLN 205 and HUVEC was studied and the results demonstrated that the uptake of the 20nm was detected in all cells, however the detection of large PS-NPs (≥ 93nm) was cell type-dependent [(Zauner et al (2001)]. Moreover, the uptake of 200nm sized red fluorescent COO-PS-NPs was minimal in rat carcinoma hepatocytes (C3A), human carcinoma hepatocytes (HepG2) and isolated rat hepatocyte couplets (IRHCs) and happened after long period of exposure time (> 30 minutes) compared with their 20nm counterparts which were absorbed much earlier (~10 minutes) in all cell lines investigated particularly in the C3A cells [Johnston et al (2010)]. This would indicate the impact of size on the cellular uptake of ENPs. The results also showed that in contrast to the gradual increase in the uptake of the 20nm COO-PS-NPs over time in the serum containing medium, COO-PS-NPs aggregated in the serum free medium (SFM) which reduced their uptake into cells [Johnston et al (2010)]. It has been observed that only albumin in the serum-containing media can significantly increase the size of the COO-PS-NPs due to aggregation, whereas most other serum proteins have a stabilizing effect on them [Fatisson et al (2012)].

The surface charge of the particles has been suggested to affect the attachment of particles to and interaction with the cell membrane and hence influence their cellular uptake [Mailänder and Landfester (2009)]. The previous study by Lorenz and colleagues has also reported that positively charged ENPs were co-localised in MSCs and HeLa cells

mainly in endosomes whereas they were found attached to the cell surface in Jurkat and KG1a cells [Lorenz et al (2006)]. In earlier study by Johnston and colleagues, the 20nm sized PS-NPs were co-localised in the tubulin cytoskeleton, in compartments between neighbouring cells and then in the mitochondria after 10, 30 and 60 minutes respectively but not in early endosomes, lysosomes, or nucleus. In contrast, the 200nm sized PS-NPs were found to be only bound the cell surface after 30 minutes of exposure and upwards [Johnston et al (2010)].

Taken together, these findings would suggest that the cellular uptake of ENPs, clearance, efficiency and subsequent toxicity are influenced by several factors including size, shape, functional group and surface charge of ENPs in addition to exposure time, cell line and serum content of the biological fluid (e.g. cell culture media) which all can affect the ENPs adherence and interaction with cells [He et al (2010), Tsuji et al (2006)]. It seems that cells might utilize different uptake mechanism for ENPs internalisation and/or that the charge located on the surface of ENPs could be influenced perhaps by the surroundings environment (such as the media) to undergo modification that may facilitate their uptake and translocation to various sites within the cell.

## 1.6 Mechanism of cellular uptake of ENPs

At the cellular level, it is important to understand the uptake pathway(s) of ENPs since this would possibly affect their co-localisation within cell compartments and

this would hence help in controlling the intracellular fate and target of drug by nano-carriers [Palakurthi et al (2011)].

The permeable plasma membrane is composed of phospholipid bilayers with embedded proteins to function as a selective barrier that surrounds the cell to isolate its cytoplasm (protecting the intracellular components in the interior from the outside environment) and to regulate the biological communication as well as the selective exchange of substances and materials in and out of the cell [Zhao et al (2011)]. The interaction of ENPs with the plasma membrane of the cell is the first step towards the cellular internalisation of ENPs and the co-localisation in or near the intracellular organelles. However, the uptake mechanism(s), the cellular fate and the consequent toxicological effects of ENPs in biological systems are not fully understood because a variety of ENPs, various cell lines, several practical methods and different experimental conditions (e.g. time, concentration, size of ENPs) employed in different studies. This has resulted in different (and possibly controversial) results.

Uptake of ENPs (or other materials and viruses) into cells is known as endocytosis [Palakurthi et al (2011)]. Endocytotic mechanism is an active (i.e. energy-dependent) transport system in which ENPs gain entry to a cell without passing directly through the cell membrane in multiple stages as the cell encloses them when in contact with its exterior membrane in intracellular vesicles (pockets originate from its membrane) to bring them from outside into the cell [Sahay et al (2010), Zhao et al (2011)]. Endocytosis consists mainly of two categories, depending on the size and nature of the engulfed molecules, which are phagocytosis (i.e. cell eating or engulfment of large sized

insoluble objects > 750nm) and pinocytosis (i.e. cell drinking or engulfment of fluids, solutions and soft objects) [Conner and Schmid (2003)]. Pinocytosis itself can be categorized in four groups (with distinctive morphologies depending on the mechanism of the vesicle formation) including macro-pinocytosis, clathrin-mediated (or receptor-mediated) endocytosis, caveolin-mediated endocytosis and clathrin- and caveolin-independent [Conner and Schmid (2003), Geiser (2010), Dos Santos et al (2011)]. These different endocytotic mechanisms are illustrated diagrammatically (Fig. 1.3 A). It has been reported that phagocytosis is restricted to particular cell types including macrophages, monocytes, neutrophils and dendritic cells [Prokop and Dvidson (2008)] which form the mononuclear phagocyte immune system [Hume (2006)] whereas pinocytosis occurs in all types of cell [Palakurthi et al (2011)]. Some features of these different endocytotic mechanisms are summarized in brief in the next section.

Phagocytosis is an endocytotic mechanism in which the attachment of a large size object to the cell membrane would trigger specific surface receptors to signal and initiate membrane-origin phagosome (large endosome vesicle) that encapsulates the foreign material and deliver the ingested cargo to lysosome where it can be destroyed by the lysosomal degradative enzymes [Samaj et al (2004)]. Macro-pinocytosis is a nonspecific mechanism in which large vesicle is generated by bending the cell membrane with the particles containing extracellular fluid inside the cell before the two ends get closer to each other and fuse together forming large vesicle (named macro-pinosome) [Conner and Schmid (2003)]. The clathrin- and caveolin-independent endocytosis is also a non-specific mechanism to engulf substances. It involve formation of lipid rafts that are

small size cholesterol-rich domains with diameter of 40-50nm which can be captured by endocytotic vesicle, followed by internalisation [Dos Santos et al (2011].

In the clathrin- (or receptor-) mediated endocytosis (Fig. 1.3 B), clathrin (large specific protein molecule) is concentrated along specific regions of the inner surface of the cell plasma membrane forming clathrin-coated pits. On the opposite outer side of these pits, receptors would specifically bind to ENPs (or other ligands) and clathrin is then linked to receptors by AP-2 adaptors (complex) stimulating this clathrin-coated pit to grow inside the cell to form a coated endocytotic vesicle in the cell cytoplasm bringing the enclosed substances into the cell. The vesicle is detached and fuses in the cytoplasm with lysosomes releasing the ligands from the receptors to digest the contents or discharge them while the receptors are sent back to the plasma membrane for recycling [Bauer et al (2008)]. Since the endocytotic clathrin-coated pit has about 120nm in diameter [Lunov et al[a] (2011)], this clathrin-mediated endocytosis would internalise only small area of the cell surface with engulfed molecules and small volume of extracellular fluid.

Regarding caveolin-mediated endocytosis (Fig. 1.3 C), it has been speculated that caveolin protein is produced in the endoplasmic reticulum (ER) and is transferred to the Golgi apparatus to be organized with phospholipid rafts into higher-order oligomers. Cholesterol is then added upon exiting the Golgi apparatus forming a caveolae-lipids associated structures that fuse into the plasma membrane forming caveolae pits (of 60-80nm diameter) that have hairpin-like shapes [Parton et al (2007)]. Caveolae pit stays stable at the plasma membrane until it is induced by ENP (probably due to increase in

their sizes) for internalisation into the cell and this pit with the content is released to fuse either with the early endosomes or cavesomes [Parton et al (2007)].

It has also been suggested that ENPs are able to enter cells through non-endocytotic mechanisms including passive transport (e.g. diffusion and permeation (trans-cellular pathway) through holes in the plasma membrane) or even through promoting cell membrane rupture and other unclear mechanism(s) before accumulating near plasma membrane and/or gaining access to different organelles (such as mitochondria, nucleus, etc) [Li et al (2003), Geiser et al (2005), Tsoli et al (2005), Porter et al (2006), Rothen-Rutishauser et al (2006), Johnston et al (2010), Yacobi et al (2010)]. In contrast, other studies have demonstrated that ENPs uptake may be achieved via endocytotic mediated mechanisms [Stearns et al (2001), Chithrani et al (2006)].

Receptor- (clathrin-) mediated endocytosis was speculated to be the most effective uptake mechanism for ENPs [Decuzzi et al (2008)]. Nonetheless, it seems that determining the mechanism(s) responsible for the internalisation of ENPS into cells is complicated and several factors might be involved in the ENPs interactions with and uptake into cells and intracellular organelles such as size of ENPs [Rejman et al (2004)], shape [Geng et al (2007)] and surface charge [Dausend et al (2008), Mailänder and Landfester (2009)]. One study has suggested that ENPs with a size $\leq$ 200nm diameter are internalised via clathrin-mediated endocytosis while these ENPs that have a size > 200nm diameter are ingested via caveolin-dependent endocytosis [Rejman et al (2004)]. In addition, a stronger driving force and additional energy have been hypothesized to be essential for the uptake of large sized ENPs [Gao et al (2005)]. Another study has

proposed macro-pinocytosis to be the uptake mechanism of positively charged PS-NPs into the cytoplasm of the human epithelial cervical cancer (HeLa) cells whereas negatively charged PS-NPs were hypothesized to be cellularly internalised by unknown dynamin- and clathrin-independent pathway [Dausend et al (2008)]. Moreover, it has been reported that ENPs with positive charge are generally internalised into cells in much high rate when compared with these that carry negative charge [Höcherl et al (2012)].

In addition to the size and surface charge of ENPs, it has been anticipated that other physicochemical characteristics (including the chemical composition, shape and structure of NPs) and the formation of ENP-protein corona [Höcherl et al (2012)] as well as the cell line (due to distinct cell properties) [Zauner et al (2001), Cortez et al (2007)] are overall most likely to contribute to the uptake phenomenon. Consequently, different ENPs might possibly have more than one intracellular fate and uptake mechanism into different cell lines. Moreover, the increase in size of ENPs after agglomeration has to be taken into account when analyzing the internalisation mechanism. Moreover, electrostatic attractive forces between charged ENPs and oppositely charged molecules embedded or attached to the cell membrane have been suggested to cause the cell membrane to wrap around the ENP and promote endocytosis [Li et al (2010)].

Confocal microscopy was used to investigate and compare routes of uptake and fate of fluorescent cationic amino-modified polystyrene nanoparticles (NH-PS-NPs) of 60nm diameter in five different cell lines including macrophages (RAW 264.7), human bronchial epithelial cells (BEAS-2B), human microvascular endothelial cells (HMEC), hepatoma cells (HEPA-1) and pheochromocytoma cells (PC-12) as ports of entry or

systemic targets for ENPs [Xia et al (2008)]. The experimental data proposed that the uptake pathway and toxicity mechanism of NH-PS-NPs are cell line-specific with different toxic impact on these cells showing that the HMEC, HEPA-1 and PC-12 cells were relatively resistant to these NH-PS-NPs compared to highly toxic effect observed in the other two cell lines after 16h. NH-PS-NPs were found in lysosomes (lysosomal membrane glycoprotein-1 compartment; LAMP-1) in RAW 264.7 cells leading to mitochondrial damage and caspases-activated apoptosis initiated by intracellular $Ca^{2+}$ release after lysosomal permeabilization into the cytosol. In BEAS-2B cells, NH-PS-NPs have been suggested to be taken up by caveolae causing necrotic cell death associated with induction of mitochondrial clustering and ATP depletion [Xia et al (2008)]. In both cell lines, however no mitochondrial co-localisation with NH-PS-NPs has been observed which would suggest that this damage of mitochondria is not a result of a direct interaction between NH-PS-NPs and mitochondria.

In summary, several endocytotic mechanisms may contribute to the cellular internalisation (uptake) of ENPs depending on their size, chemical composition and surface charge. However, the uptake mechanism of ENPs is still not well in-depth known and seems to be more complicated than the simple vesicle formation. It may include different stages where a portion of the plasma membrane is invaginated in the first stage of this pathway and pinched off to create membrane-bound vesicles (known as endosomes) which encompass the particles and import them into the cell. Secondly, these endosomes carry the engulfed particles to specialized vesicular structures. Finally, the content is transported across the cell to different intracellular compartments.

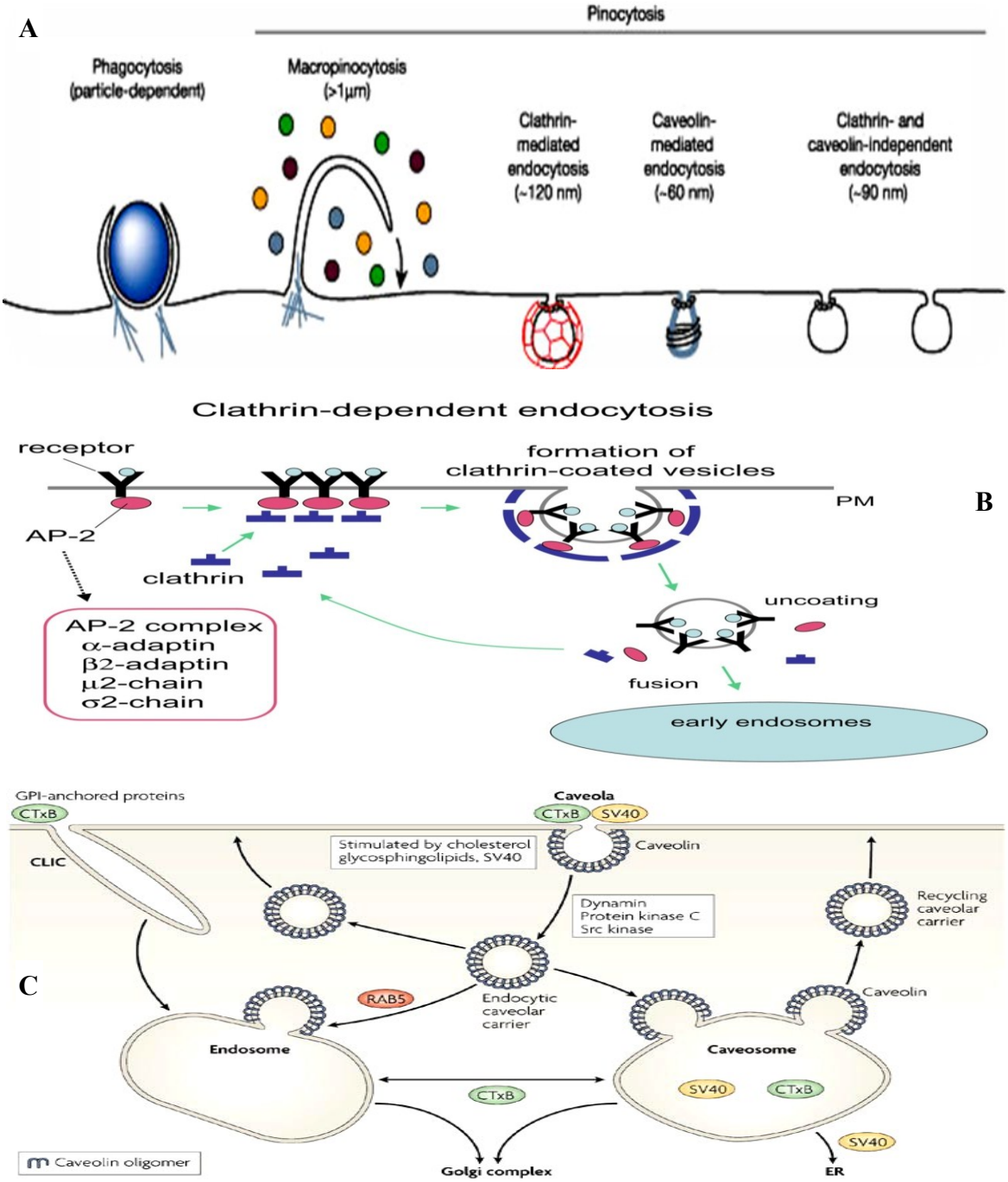


Fig. 1.3 (A) Different types of endocytosis that involves creating endosomes to engulf and deliver ENPs to different cell compartments (adopted from: "Conner and Schmid (2011)"). (B) Mechanism of clathrin-mediated endocytosis in which the clathrin are linked to receptors by AP-2 complexes forming clathrin-coated vesicles that are detached from plasma membrane and delivered to early endosomes (adopted from: "Grant et al (2006)") while in caveolae-mediated endocytosis (C), caveolae pits with hairpin-like shapes are induced by ligands on membrane before internalised into cell (adopted from: "Parton et al (2007)").

## 1.7 Toxicity of ENPs and possible mechanism of cellular death

Following body exposure to ENPs, they can be distributed to various organs where they can interact with cells and might cause cyto- and geno-toxicity, if they are not cleared out (excreted or digested). These ENPs toxicity can be shown as inflammation, generation of reactive oxygen species (ROS), GSH depletion, DNA damage and injury of cells and tissues [Nel et al (2006)]. Moreover, retention of ENPs in the body for a long time after uptake (mainly via inhalation) and translocation (within the blood stream) to different organs has been reported to cause their potential toxicological effects to increase [Seaton et al (2010)].

The cellular defensive antioxidant system is composed of enzymatic molecules (such as catalase, superoxide dismutase, glutathione peroxidase and glutathione reductase) in addition to non-enzymatic antioxidants (such as copper and iron chelators, flavonoids as well as vitamins A, E and C) [Mohora et al (2009)]. Glutathione (γ-L-Glutamyl-L-CysteinylGlycine), in its reduced form (GSH), is one of the critical cellular defensive non-enzymatic antioxidant (reducing) agents that can modulate the ROS level [Green et al (2006)]. It is a very small molecule (having low molecular weight) composed of three amino acids that are γ-glutamic acid, cysteine, and glycine with a sulfhydryl (thiol) unit [Jefferies et al (2003)]. This tripeptide is produced in high concentration (~ 15 mM) due to its significant importance [Deponte (2012)] in the cytosol of almost all mammalian cells through the γ-glutamyl cycle [Pastore et al (2003)]. GSH synthesis is an ATP-dependent process in which γ-glutamic acid is conjugated through its γ-carboxyl

group with cysteine by the action of γ-glutamylcysteine ligase forming γ-GlutamylCysteinyl to which glycine is then added by a GSH synthetase enzyme to produce GSH (Fig. 1.7 A) [Meister (1988), Bains et al (1997), Green et al (2006)]. It is the fundamental non-protein thiol source and the total cellular GSH is found mainly in the cytosol (80-85%) and mitochondria (10-15%) while small amounts were found in the nucleus and endoplasmic reticulum [Lu (2013), Green et al (2006)]. Although this ubiquitous tri-peptide plays a major role in many cellular biological processes and mechanisms (such as regulating gene expression, apoptosis, DNA synthesis and repair, protein synthesis, proliferation, apoptosis and serving as a form of cysteine moiety storage), it functions foremost as an antioxidant system to protect cells by detoxifying chemical xenobiotics and neutralizing toxins including pollutants and ROS which can build up in cells and cause damage by oxidative stress [Meister (1988), Stephen et al (1996), Grant et al (1996), Baudouin-Cornu et al (2012), Lu (2013)]. Table 1.1 summarizes the defensive role of GSH against some of the toxic molecules in the cell [Jefferies et al (2003)].

The sulfur (thiol, -SH) group of cysteine is responsible for the biological reactivity of GSH by allowing it to donate an electron to other unstable ROS molecules that are highly reactive due to a lack of balanced electron pairs [Bains et al (1997)]. By donating an electron, the GSH molecule itself becomes unstable and so it seeks stability via binding other GSH molecules through the glutathione peroxidase enzyme which forms a di-sulphur bond between the two GSH molecules (Fig. 1.7 B) creating one molecule of glutathione disulfide (GSSG); the oxidized form of glutathione (M.W. of 612

g/mol) [Kulinskii et al (2009), Marquis et al (2009)]. GSSG can be reduced afterward most efficiently by glutathione reductase using nicotinamide adenine dinucleotide phosphate (NADPH) to yield the GSH molecule (M.W. of 307 g/mol). GSH represents > 90% of the total non-protein sulfur in cells while GSSG (named glutathione disulfide) represents < 10% of the total glutathione concentration [Meister (1988), Bains et al (1997), Bass et al (2004)]. The cellular redox homeostasis (i.e. the oxidation/reduction balance) of GSH is important in the regulation of many cellular metabolic processes since it maintains cell viability. It has been speculated that a minor level of GSH depletion and GSSG accumulation (by ROS) has protective effects. This low level depletion can act as a sensor to trigger the activation of a group of antioxidant and detoxification enzymes, known as phase II enzymes (including NADPH quinone oxidoreductase (NQO1), catalase, superoxide dismutase, glutathione-S-transferase (GST) isoenzymes, glutathione peroxidase (GPx) and glutathione reductase) to produce more GSH and other protective antioxidant molecules [Nel et al (2006)]. On the other hand, higher levels of cytotoxic oxidative stress due to failure to provide sufficient protection and ROS overproduction may cause adverse damaging effects [Xia et al (2006)]. Therefore, the measurement and monitoring of changes in intracellular GSH level and ROS production can give an indication about the cellular ENPs-induced oxidative stress state and the toxicological effects of ENPs.

| Biological molecule | Toxic effect | GSH protective role |
|---|---|---|
| Oxidizing agents | ROS generation that can cause oxidative damage to lipids, DNA and proteins | ROS and RNS are reduced and inactivated by interacting with GSH to generate the oxidized form of glutathione molecule (GSSG) that has a disulphide bond. |
| RNS | Inactivation of respiratory chain complexes that would lead to inhibition of protein and DNA synthesis | |
| Chemical carcinogens | Cancer induction | GSH participates in phase II detoxification by conjugating xenobiotics to produce inactive hydrophobic less toxic compounds (mercapturic acids) that can be effectively transported and excreted. |

Table 1.1 A summary of GSH protective role against some biological molecules that can have harmful effects on the cell. Modified from Jefferies et al (2003).

Few studies hypothesize that ENPs may be useful as they can act as oxygen radical scavengers [Kajita et al (2007), Tsai et al (2007)]. However, ENPs-derived oxidative stress caused by inducing the generation of ROS has been postulated to play a major role in the toxicological cellular response. ROS may either directly affect the integrity and functionality of proteins, membrane lipids and DNA by oxidation [Unfried et al (2008)] or may indirectly induce cellular responses by affecting the calcium ($Ca^{2+}$) sensitive signaling pathways [Ermak and Davis (2002)]. ENPs-stimulated oxidative stress can cause the release of $Ca^{2+}$ from their major stores, in endoplasmic reticulum (ER) or sarcoplasmic reticulum (SR), through calcium channel leading to $Ca^{2+}$ level elevation in the cell cytoplasm [Donaldson et al (2003)].

ROS are very transient free radicals that are chemically highly reactive molecules containing oxygen. They include superoxide anions ($O_2^{\bullet -}$), hydroxyl radical (HO•), peroxy radical (ROO•), and hydrogen peroxide ($H_2O_2$) [Waris et al (2006), Genestra et al (2007), Rigas et al (2008)]. They are produced at low concentrations as natural byproducts of many aerobic cellular metabolism processes (e.g. oxygen metabolism and inflammation) to play a role in gene regulation and intracellular signal transduction process in the cell by acting as secondary messengers and inducing cellular apoptosis [Valko et al (2006)]. Under normal circumstances, ROS can be detoxified within cells to regulate their concentrations and preserve the ROS formation/detoxification balance through the cellular defense anti-oxidant system. $H_2O_2$, for example, is detoxified to $H_2O$ and $O_2$ either by glutathione peroxidase in mitochondria or by catalases in peroxisomes (in cytosol) [Mohora et al (2009)]. However, failure to maintain and stabilize the balanced level of ROS by defensive anti-oxidant mechanisms would disrupt the redox status resulting in abnormal ROS accumulation caused by uncontrolled formation (overproduction) of these oxidants within the cell or tissue in a way that exceeds the cellular defense anti-oxidant capacity [Stone and Donaldson (2006)]. As a result, the cellular redox homeostasis would be shifted toward more oxidized conditions that represent an oxidative stress status [Ermak and Davis (2001)]. ROS accumulation may cause toxic effects leading to cell death owing to damage and oxidation of wide range of cellular bio-molecules such as DNA, protein and lipids [Stone and Donaldson (2006), Magder (2006), Marquis et al (2009)]. Thus, ROS need to be continuously detoxified by antioxidants including enzymes (e.g. catalase,

superoxide dismutase, glutathione peroxidase and glutathione reductase) and other non-enzymatic molecules (e.g. glutathione (GSH), copper and iron chelators, flavonoids as well as vitamins A, E and C) [Mohora et al (2009)].

2',7'-dichlorodihydrofluorescein diacetate ($H_2$DCF-DA); a non-fluorescent dye that is able to cross the cell membrane, is one of the most widely used probes to evaluate intracellular oxidative stress. Within cells, $H_2$DCF-DA is hydrolyzed by esterases yielding a fluorescent 2′,7′-dichlorofluorescein product ($\lambda_{ex}$ 512nm / $\lambda_{em}$ 530nm) that can be measured as an indicator for NP-induced ROS formation as it reacts with ROS in the presence of cellular peroxidises [Bass et al (1983), Hanley et al (2008)]. However, cytochrome *c* that is released from the mitochondria during apoptosis has been reported to be a strong oxidative catalyst for $H_2$DCF-DA and may result in the overestimation of oxidative stress, therefore $H_2$DCF-DA should be used carefully for oxidative stress measurements when apoptosis occurs as a result of nanoparticle exposure [Lawrence et al (2003)]. MitoSOX Red ($\lambda_{ex}$ 510nm/$\lambda_{em}$ 580nm), a selective non-fluorescent probe, can also be used to identify superoxides within the mitochondria and locate ROS produced as a result of NP-mediated toxicity [Robinson et al (2006)].

Under normal conditions, the intracellular $Ca^{2+}$ plays a vital role in several biological processes of cell life and death via a signaling mechanism that can regulate several cellular events. These events include cytokine gene expression, redox-sensitive mitogen activated protein kinase (MAPK) family activation as well as the activation of a number of redox-sensitive transcription factors such as activator protein 1 (AP-1), nuclear factor-kappa B (NFκB) and nuclear factor of activated T-cells (NFAT) [Dolmetsch et al

(1997), Donaldson et al (2003)]. This would consequently induce the expression and release of pro-inflammatory cytokines such as tumor necrosis factor alpha (TNF-α) and interleukins (ILs).

In abnormal conditions including ROS overproduction and/or ROS elimination deficiency, $Ca^{2+}$ level would be increased in the cytoplasm (in cellular response to oxidative stress) by activating inositol 1,4,5-triphosphate ($IP_3$), a signaling molecule for $IP_3$-sensitive calcium channels to release $Ca^{2+}$ from ER and/or by inhibiting the $Ca^{2+}$ adenosine triphosphatase (ATPase), a calcium pump that eleminates $Ca^{2+}$ from cytoplasm into ER/SR stores [Donaldson et al (2003)]. It has been proposed that ROS overload can also alter calcium pumps on the cell plasma membrane allowing the $Ca^{2+}$ to enter the cell from the outside space [Roveri et al (1992), Fusi et al (2001)]. This at the end would result in excessive accumulation of massive amounts of $Ca^{2+}$ in the cytosol which may cause cytotoxicity and lead to cell death [Zhivotovsky and Orrenius (2011)]. Alternatively, elevated $Ca^{2+}$ in cytosol can induce $Ca^{2+}$ uptake into the mitochondria through the $Ca^{2+}$ uniporter-mediated pathway to reach high levels (of hundred μM) [Roy and Hajnoczky (2008)]. This would disrupt the function of mitochondria (due to swelling of mitochondria and alteration of its outer membrane permeability) and provoke the release of cytochrome *c* and other mitochondrial apoptosis-stimulating factors into the cytoplasm which would end up hence with apoptosis induction [Roy and Hajnoczky (2008)]. Therefore, the $Ca^{2+}$ level in cells following exposure to chemicals can be studied to explore the mechanism through which they can exert their deleterious effect on cells.

DNA is an important target for ROS generated either naturally during various endogenous metabolical processes or by exogenous chemical oxidants (such as toxic substances) and is vulnerable daily to thousands of oxidative damages [Ames et al (1993)]. Overwhelming the cellular antioxidant defense system capacity by ROS generation would disrupt the cellular redox homeostasis leading to toxic oxidative stress due to ROS accumulation and hence to adverse biological consequences. Unneutralized ROS induced by ultrafine particles (UFPs, which are NPs with size < 100nm and referred to as NPs hereafter) have been revealed to be able to react with several bio-molecules in the cell (mostly DNA) causing DNA damage (by guanine oxidation that generates 8-oxo-7,8-dihydro-2′-deoxyguanosine (8-oxodG) product) and lipid peroxidation and resulting therefore in cell destruction [(Brown et al (2004), Risom et al (2005)]. Several NPs (such as carbon black and welding fume) have showed genotoxic effects [Donaldson et al (2005)].

Apoptosis is an energy-dependent programmed (carefully regulated) cell death mechanism that involves several cellular morphological changes including membrane blebbing, chromatin condensation, fragmentation of nucleus and DNA, loss of mitochondrial membrane potential and cell shrinkage [Porter (1999)]. It is a complicated, crucial and essential cell self-destruction process for the development and homeostasis of multicellular organisms [Hengartner (2000), Elmore (2007)]. Two major apoptotic pathways were identified, that are the intrinsic mitochondrial-mediated apoptosis (fig. 1.4) and the extrinsic plasma membrane death receptor-mediated apoptosis (fig. 1.5), however, the endpoints of both apoptotic pathways involve the release of several death-

inducing molecules and caspases activation [Hengartner (2000)] and evidences shows that there is significant cross-link between the two apoptotic mechanisms [Elmore (2007)].

In the intrinsic pathway (fig. 1.4), death signal induction (due to oxidative stress, unrepaired DNA damage or others) would trigger the activation of some pro-apoptotic proteins (such as Bax) and the translocation of them to the mitochondria leading to the deactivation of the anti-apoptotic proteins (such as bcl-2 and Bcl-xL) and causing mitochondrial swelling and disruption of the outer membrane [Hengartner (2000)]]. The intermembrane proteins including the pro-apoptotic cytochrome c (*cyt C*) would be released upon this disruption through the transition pore to the cytosol where it combinds the apoptosome protein complex to activate the apoptotic protease activating factor-1 (Apaf-1) and pro-caspase-9 in the presence of dATP leading to further caspase cascade activation and cell death initiation [Beurel and Jope (2006)].

In contrast, the extrinsic pathway (fig.1.5) activation involves the binding of the ligands to cell-membrane death receptors (such as the tumor necrosis factor (TNF) family) and the recruitment of cytoplasmic adaptor proteins (such as Fas-Associated protein with Death Domain (FADD)) which would trigger the formation of death-inducing signaling complex (DISC), stimulate the caspase cascade and initiate apoptosis [Beurel and Jope (2006)].

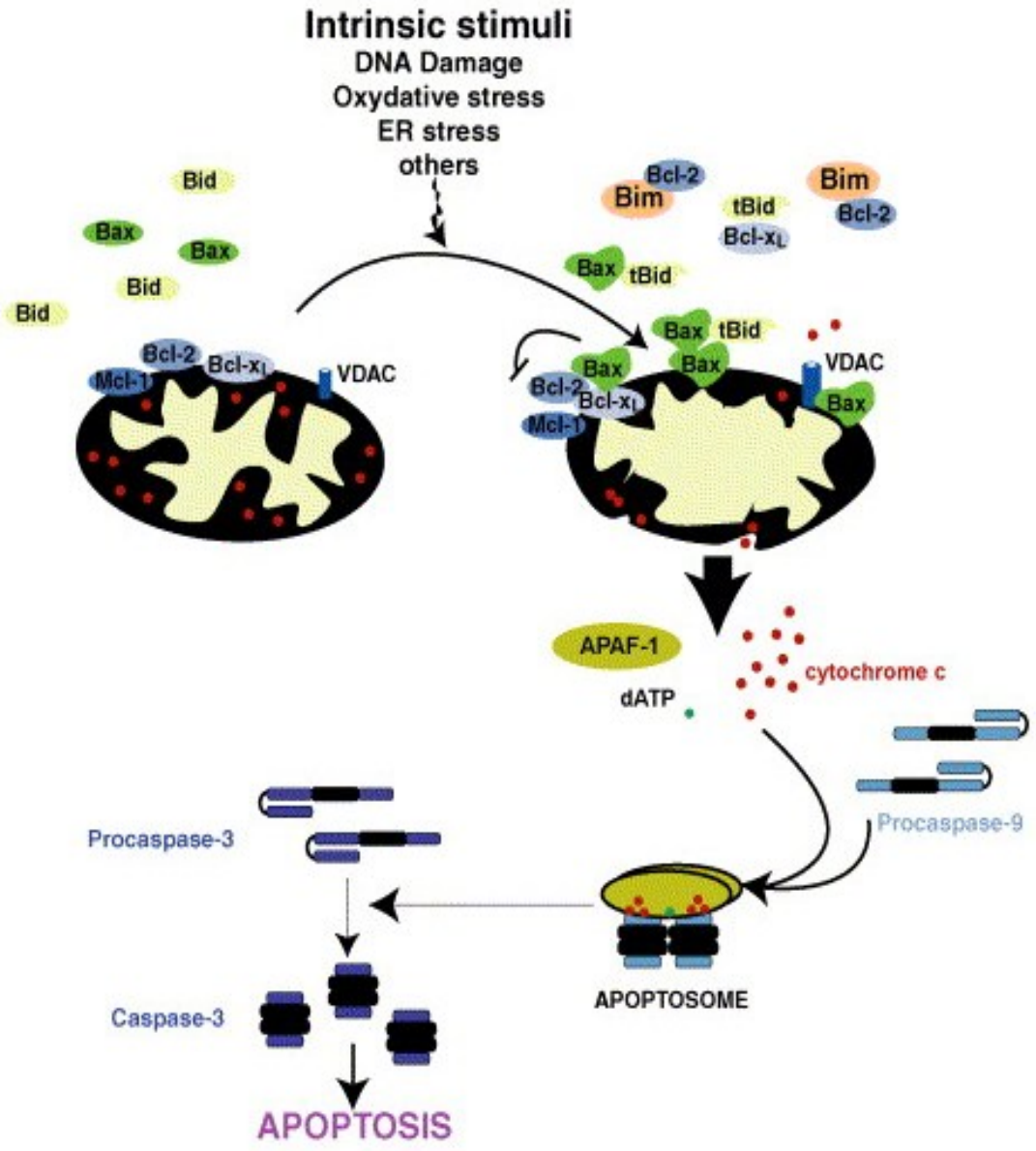


Fig. 1.4 This diagram shows the intrinsic pathway of apoptosis that is triggered by internal cell signalling (such as DNA damage and oxidative stress) which would lead to mitochondria disruption, release of cytochrome c and caspase cascade activation resulting in the cell-self destruction. (Adopted from: "Beurel and Jope (2006)")

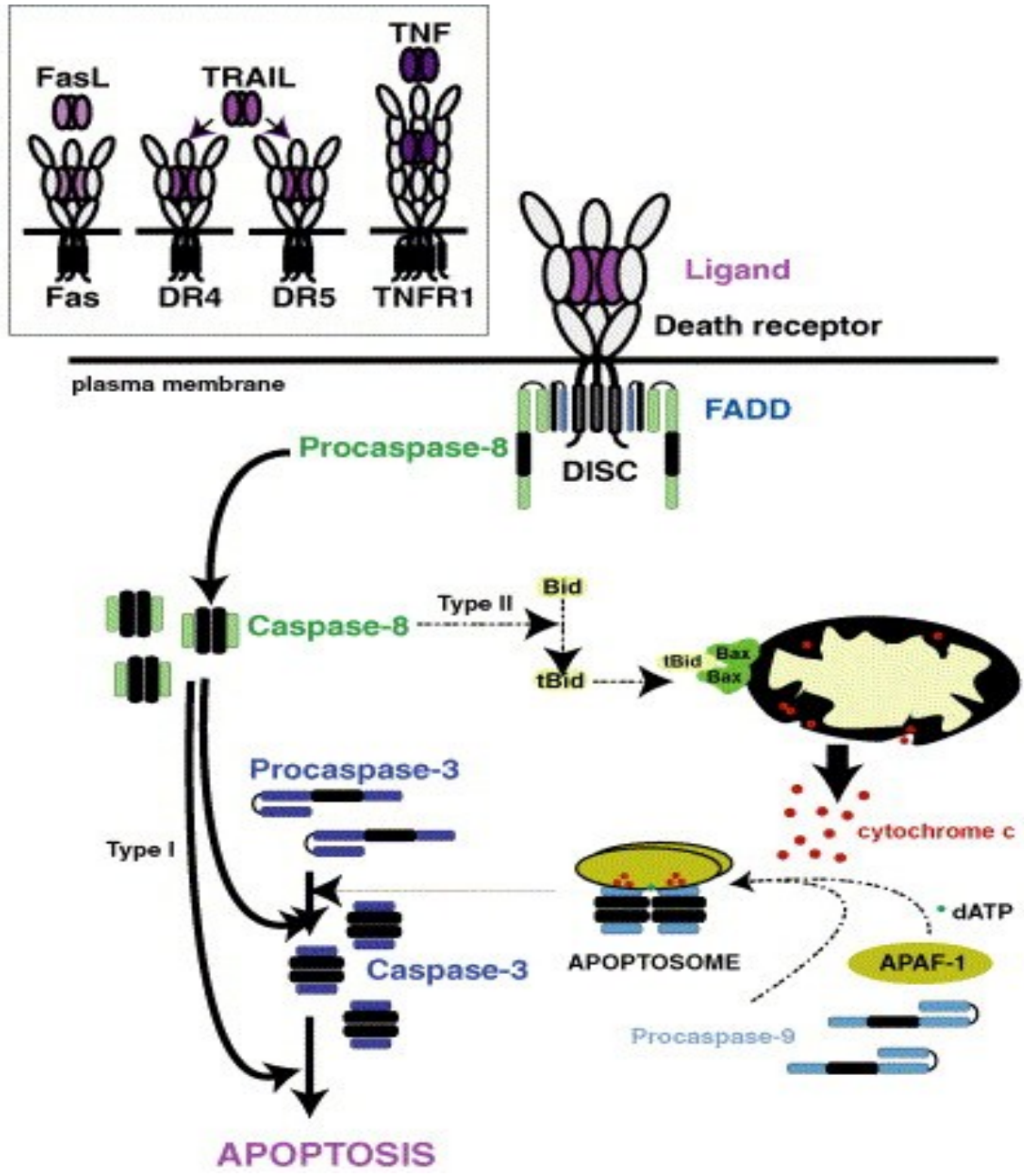


Fig. 1.5 This diagram shows the extrinsic signalling pathway of apoptosis that is stimulated when the ligands (such as Fas) bind to the apoptosis-inducing receptors on the cell plasma membrane. This would activate a caspase cascade resulting in apoptosis. (Adopted from: "Beurel and Jope (2006)")

Apoptosis has been reported in several studies using various material- and inorganic-based ENPs in different cell lines such as $TiO_2$ in BEAS-2B cells [Park et al (2008), Shi et al (2010)], Cu-NPs in PC12 cells [Xu et al (2012)] as well as COO-PS-NPs and NH-PS-NPs in Caco-2 cells [Thubagere and Reinhard (2010)]. The ENPs-induced apoptotic pathway was proposed to depend on the composition, concentration, size and charge of ENPs in addition to the type of the exposed cells [De Stefano et al (2012)]. Apoptosis is a well-controlled and regulated cellular process of programmed cell death that is involved in various normal physiological and abnormal pathological events [Riedl and Shi (2004)].

Caspases play a fundamental role in apoptosis and in inflammation as well [Boatright and Salvesen (2003)]. They are conserved intracellular cysteine protease enzymes that are classified, depending on their role in the apoptotic cascade, into the initiator caspases with long pro-domain (including caspase-2, -8, -9, and -10) and the effector caspases with short pro-domain (that consist of caspase-3, -6, and -7) [Zhivotovsky and Orrenius (2011), Riedl and Shi (2004), Shi (2002)]. Caspases are synthesized and stored within cells in inactive forms (known as pro-enzymes or zymogens) that need to undergo activation to stimulate apoptosis that is triggered either by extrinsic (receptor-mediated) pathway at the plasma cell membrane that includes cell surface death ligand-receptors binding (such as tumor necrosis factor (TNF) family; e.g. FAS) or by intrinsic pathway which is mediated by the mitochondria-stress response that is mediated by numerous intracellular death stimulus [Parrish et al (2013), Cullen and Martin (2009), Riedl and Shi (2004)]. These caspases can cleave after the aspartate

residues with Asp-Glu-Val-Asp (DEVD) sequence of amino acids in key intracellular substrates [Elmore (2007)]. Caspase-3 and -7 are central components in executing the apoptotic pathway and need to be activated by other activators (of catalysis or another initiator caspases) in a downstream cascade that result at the end into apoptosis (a commitment of cell death) [Cullen and Martin (2009)]. Therefore, the assessment of caspase-3/7 activation can give a clear indication about the mechanism through which the ENPs-stimulated cell death takes place.

A reliable assay to investigate the caspase-3 and -7 activities was consequently used in this study to monitor the apoptosis in BEAS-2B cells treated with different concentrations of the 20nm or 100nm sized COO-PS-NPs. In the enzymatic caspase-3/7 assay, a specific pro-luminescent DEVD-containing lysis buffer reagent is typically used as a substrate that is cleaved by the activated caspase-3/7 in the apoptotic cell lysate to release the aminoluciferin which becomes luminescent only in the presence of luciferase enzyme [Wesierska-Gadek et al (2005)]. The luminescence can be measured (at $\lambda_{ex}$ 360nm and $\lambda_{em}$ 460nm) using a plate-reading luminometer and the signal is directly proportional to the amount of caspase-3/7 activity [Carrasco et al (2003)].

Autophagy (i.e. self-eating) is a regulated intracellular pro-survival mechanism that is activated in response to different intra- and extracellular stress including oxygen and nutrition deficiency (starvation), endoplasmic reticulum stress, oxidative stress and infection [Zhong et al (2013), De Stefano et al (2012), Glick et al (2010), He and klionsky (2009)]. It is a cell survival machinery that serves to maintain the homeostasis (the balance required between synthesis and catabolism) in cells and hence play

important roles in several cellular processes such as metabolism and cell growth by controlling the intracellular degradation and removal of damaged cellular components (of aged organelles, dysfunctional aggregated bio-molecules and/or unwanted pathogens) [Zhong et al (2013), De Stefano et al (2012), Glick et al (2010), He and klionsky (2009)]. In this catabolic multi-steps mechanism, a phagophore (which is a cell membrane-originated sac) segregates and surrounds damaged proteins, aged organelles and contagious pathogens in the cytosol forming autophagosome that is double-membrane structure vesicle (Fig. 1.6). The cargo containing autophagosome is transferred and fused with lysosome forming autolysosomes where the content of materials is digested and degraded by hydrolytic enzymes (hydrolases) to its basic main components which are then released into the cytoplasm for reuse in cell growth and other synthesis processes [Xie and Klionsky (2007), Stern et al (2012), Zhong et al (2013)].

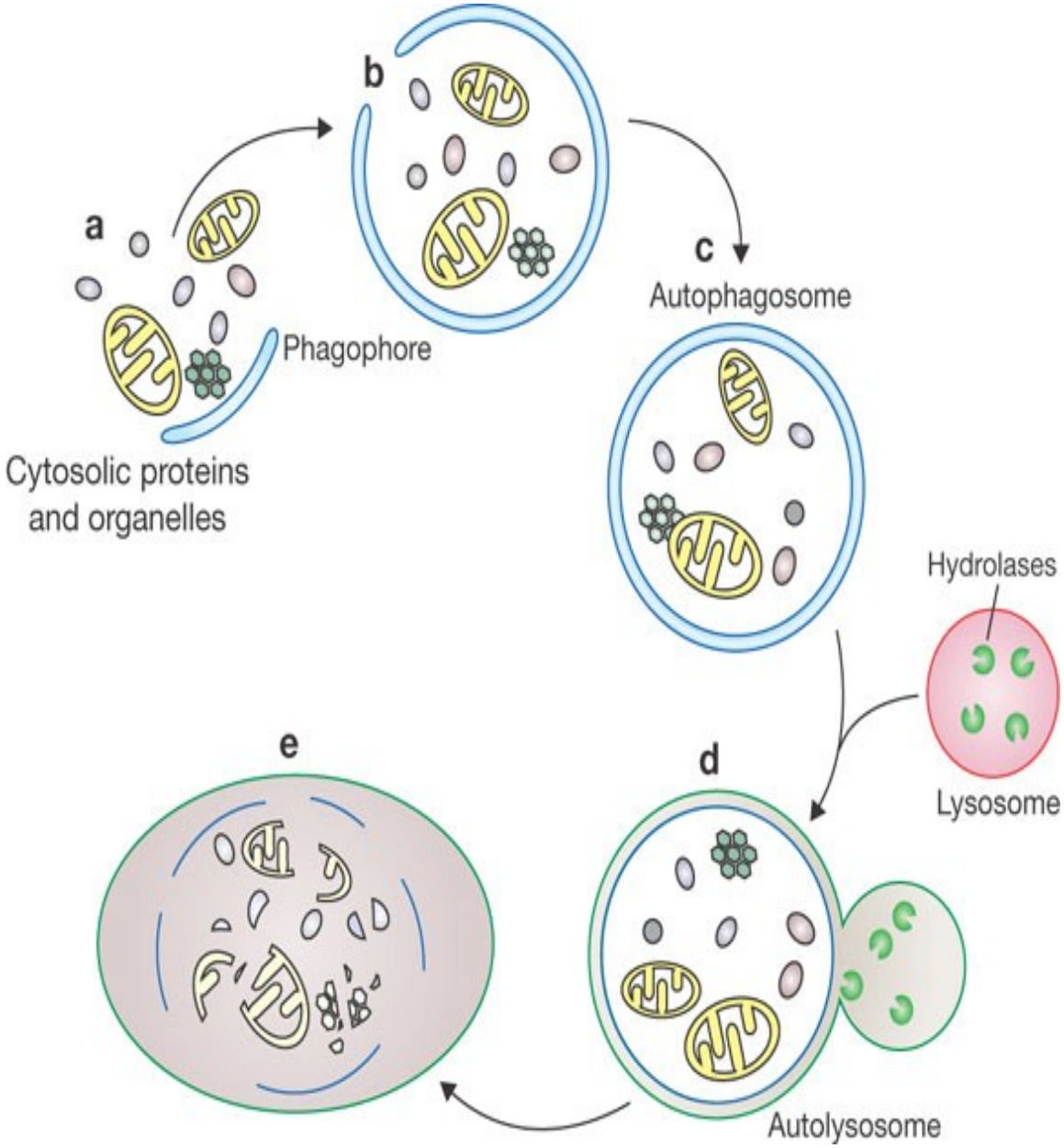


Fig. 1.6 In this diagram, a membrane sac (phagophore) is expanded to separate the cytosolic material (**a**, **b**); forming an autophagosome (that is a double-membrane vesicle) containing damaged proteins, aged organelles and/or contagious pathogens (**c**); which fuses in turn with a lysosome in the cytoplasm to form an autolysosome (**d**); where the content is lysed and degraded by the lysosomal hydrolases (**e**). (Adopted from: "Xie and Klionsky (2007)").

Some literatures indicated that nanoparticles engulfed in lysosomes can have cellular toxicological effects by causing lysosomal dysfunctions and inducing autophagy [Stern et al (2012)]. Autophagy, in turn, has been also suggested to potentially cause cell damage and to involve in some diseases (such as cancer and muscular disorder) [Shintani and Klionsky (2004)].

The toxicological effects of ENPs on cells have been recently suggested to be mediated via autophagy which might be induced (due to oxidative stress) or interrupted (due to mitochondrial damage or lysosomal enzymes inhibition) leading to accumulation of autophagosomes in both cases [Zhong et al (2013), De Stefano et al (2012), Stern et al (2012)]. $TiO_2$-NPs, Si-NPs and AU-NPs, for example, have been reported to activate autophagy [De Stefano et al (2012), Stern et al (2012)] whereas drug delivery-polymeric NPs were reported to co-localise in the mitochondria of rat macrophages causing mitochondrial decay and leading to toxicity by disrupting autophagy [Eidi et al (2012)]. Lysosomal rupture induced by positively charged NH-PS-NPs (~100nm size), but not by negatively charged COO-PS-NPs, was also reported in human macrophages associated with ROS generation and mitochondrial membrane damage [Lunov et al[b] (2011)] and such damage can block the autophagosome-lysosome fusion (i. e. prevention of autolysosome formation that is an essential step in autophagy) causing autophagy dysfunction [Stern et al (2012)]. Nevertheless, the autophagic pathway (that involves regulated lysosomal degradation) has been speculated to be the most effective process for self-destruction in cells that cannot undergo apoptosis [Levine and Yuan (2005)] and in cells exposed to non bio-degraded ENPs [Zabirnyk et al (2007)].

LC3-II (microtubule-associated protein 1 light chain 3) is an ubiquitin-like protein that is converted from cytoplasmic LC3-I upon autophagic pathway activation and hence can be investigated on the autophagosome membrane (by western blot or TEM) as an autophagy biomarker for autophagosome formation to identify the autophagy-mediated cytoxicity in ENPs-treated cells [Wu et al (2014), Zhong et al (2013), Barth et al (2010)]. However, since accumulation of autophagosomes can indicate either autophagy induction or a disruption, other assays should be conducted to clarify the two options [Zhong et al (2013)].

It has been shown that NPs can generate more ROS than its larger-sized counterpart after incubation with $H_2$DCF-DA (ROS-sensitive probe) either in cells (such as Mono Mac 6 macrophages) or cell-free system [Wilson et al (2002)] and this is most likely due to their larger surface area that allow active interactions with cellular components. In addition to ROS generation, NPs have been suggested to cause intracellular $Ca^{2+}$ alteration, activation of transcription factors (such as NF-κB) and induction of production of cytokines (such as TNF-α) [Brown et al (2004)]. The co-localisation of NPs [Li et al (2003), Xia et al (2006)] and cationic PS-NPs [Xia et al (2006)] in the mitochondria has been reported to cause mitochondrial injury and dysfunction due to membrane damage leading hence to toxic oxidative stress. Another study has investigated the intracellular co-localisation and the potential cellular effects of the negatively charged COO-PS-NPs and the results showed size-dependent internalisation into cells with no considerable difference in ROS generation between the 20nm COO-PS-NPs and their 200nm counterparts although the 20nm COO-PS-NPs were

toxic while 200nm ones were not [Fröhlich et al (2009)]. The 20nm COO-PS-NPs were co-localised into endosomes and lysosomes (and rarely in the nucleus) but not into the mitochondria or endoplasmic reticulum resulting in cellular damage and death that can be linked to induction of apoptosis or necrosis [Fröhlich et al (2009)]. Furthermore, Bhattachajee et al have also illustrated that the production of intracellular ROS in mitochondria is an important mechanism for cytotoxicity [Bhattacharjee et al (2010)].

A

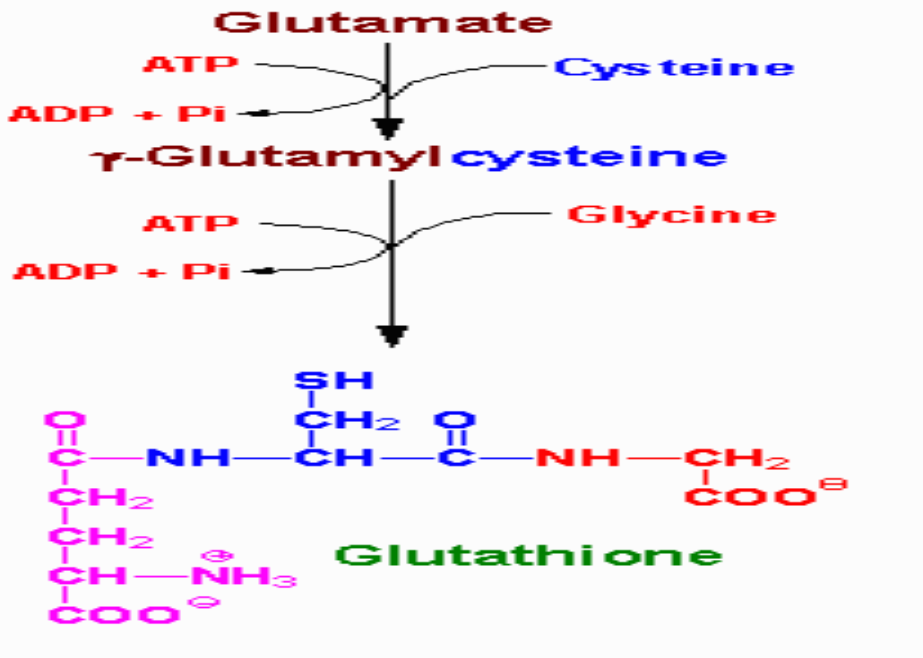


B

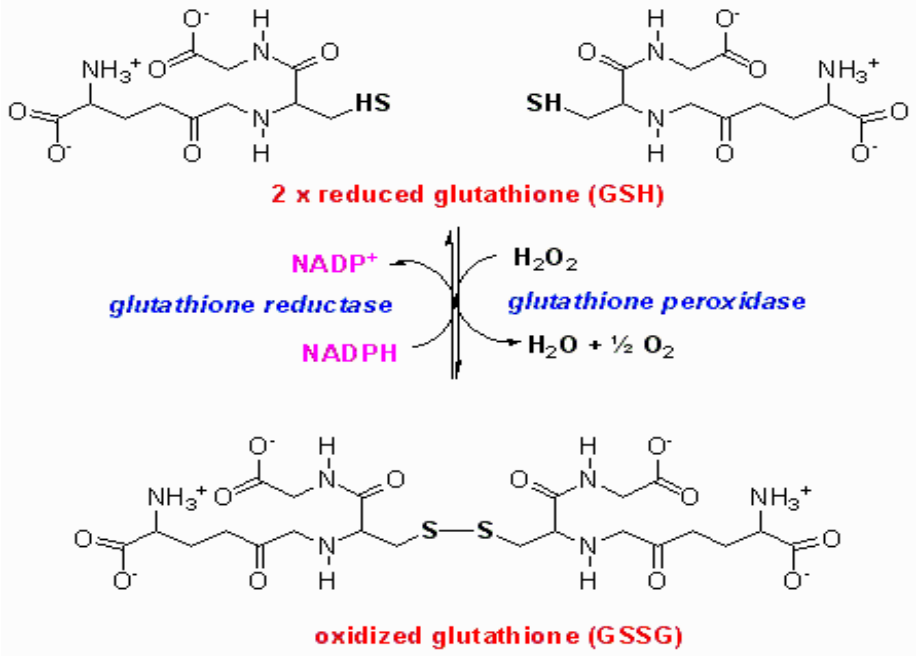


Fig. 1.7 (A) GSH synthesis in cells by condensing glutamate with cysteine via γ - glutamylcysteine synthetase enzyme to produce γ-GlutamylCysteinyl and glycine is then added by GSH synthetase enzyme (published online, adopted from: "http://www.gsh.com.tw/images/glutathione_synthesis.gif"). (B) ROS (e.g. $H_2O_2$) scavenging by intracellular GSH that is oxidized to produce GSSG while the harmful $H_2O_2$ is converted to water releasing oxygen molecule (published online, adopted from: "http://david-bender.co.uk/metonline/CHO/favism/images/GSH.png").

## 1.8 Influence of the ENPs physicochemical properties on uptake, co-localisation and toxicity

Several physicochemical properties of ENPs are important from toxicological perspective as they are associated with the ENPs-mediated adverse health effects and thus alterations in these characteristics were thought to affect the biological and environmental toxicity of ENPs. It has been reported that even slight changes or adjustment in the essential physicochemical properties of ENPs can have significant impacts on their functions, cellular uptake, bio-distribution, fate, clearance, efficiency and toxicity in any biological application [He et al (2010), Yang et al (2010)]. Thus, investigating the physicochemical properties that might control the cell-ENPs interactions would help in understanding the behavior of ENPs, the cellular responses towards them and the adverse health risk which would return back with benefit on the design of ENPs to be safely used (or at least with less harmful side-effects) in numerous applications.

Size (that is inversely correlated with the surface area) and surface charge of the ENPs seem to be the most significant parameters that play important role in controlling their cytotoxicity, metabolism, distribution and uptake [Panyam and Labhasetwar (2010), Bhattacharjee et al (2010)]. The small-sized NPs would have larger surface area with higher number of particles per unit mass and increased reactivity (due to larger absorption capacity and higher binding energy per atom) [Roduner (2006)] increasing hence their biological effect compared to their larger-sized counterparts. It has been reported that the small size of ENPs may cause them to be more toxic [Lam et al

(2004)] and have relatively higher intracellular uptake (2.5 ~ 6 fold) in general [Desai et al (1997)] due to their easier penetration into cells compared to macroparticles of the same substance. Confocal microscopy results for the uptake of different sizes (20 and 200nm) of fluorescently labeled COO-PS-NPs by rat hepatocytes (C3A) and human hepatocytes (HepG2) revealed that the internalisation occurred in a size-dependent manner [Johnston et al (2004)]. Moreover, the uptake of different sizes (20, 40 and 100nm) of fluorescently labeled COO-PS-NPs into human astrocytoma (1321N1) and human lung carcinoma (A549) was investigated and results showed faster uptake of the 40nm (compared to the 20nm or 100nm particles) in both cell lines which suggest different mechanisms of internalisation for the different sized COO-PS-NP [Varela et al (2012)].

Several studies have revealed that the charge of the ENPs significantly affects their ability to be internalised (by determining the cellular endocytosis mechanism) and cytotoxicity. Harush-Frenkel and colleagues have showed that positively charged (i.e. cationic) ENPs have accumulated at the plasma membrane in cells when clathrin- and caveolin-dependent endocytosis is strictly inhibited however the amount of negatively charged (i.e. anionic) ENPs being taken up into human cervical epithelial carcinoma (HeLa) cells is not affected [Harush-Frenkel et al (2007)]. These outcomes indicate that cationic ENPs have more potential to be internalised via clathrin-mediated pathways when compared to anionic ENPs that use other pathways. In agreement with that, it has pointed out that charging ENPs positively may improve their capability as drug delivery system due to the strong attraction of cationic ENPs by the negatively charged plasma

membrane of cells and weak ENPs-cell membrane electrostatic repulsion forces [He et al (2010)]. Moreover, Harush-Frenkel and colleagues have showed in another study that some anionic but not cationic ENPs were accumulated in the lysosomes where they undergo a degradative pathway (Fig. 1.8) after being taken up into polarized epithelial Madin-Darby canine kidney (MDCK) cells by different endocytotic pathways [Harush-Frenkel et al (2008)].

A relationship between surface charge and cellular uptake was clearly observed when polymeric carboxyl- (COO-) or amino- (NH-) modified ENPs have been used [Lorenz et al (2006), Mailänder et al (2009)]. Using confocal fluorescence microscopy and fluorescence-activated cell sorting (FACS) technique, a study has revealed that NH-PS-NPs have utilized the clathrin-mediated pathway to gain entry into mesenchymal stem cells (MSC) due to the positive charge of amino groups whereas their unmodified counterparts (with no functional groups) were internalised via a clathrin-independent endocytosis [Jiang et al[a] (2010)]. In further study by Jiang and colleagues as well, the negatively charged COO-PS-NPs were quickly and effectively taken up into the MSCs cell line by clathrin-mediated endocytosis compared to the negatively charged non-functionalized PS-NPs that were internalised via macro-pinocytosis [Jiang et al (2011)]. In both cases, the accumulation rate of plain non-functionalized PS-NPs in MSCs is much lower than their modified counterparts (that have functional group of either NH- or COO- on their surfaces) showing the role of the functional groups in the cell-ENPs interactions. Likewise, positively charged gold nanoparticles (AU-NPs) were found to be more rapidly uptaken than the neutral or negatively charged ones [Zhu et al (2010)]. The uptake of PS-

NPs into rat alveolar epithelial cell monolayers (RAECM) assessed by confocal microscopy was increased (20–40 times) as the charge became less negative/more positive at equivalent size [Yacobi et al (2008)]. In contrast, another study by Bhattacharjee and colleagues revealed that positively charged amino-modified silica nanoparticles (NH-Si-NP) were more cytotoxic than their negatively charged carboxyl-modified (COO-SiNP) and neutral unmodified (SiNP) counterparts. They have shown that treatment with NH-Si-NP led to more reduction in the mitochondrial metabolic activity of macrophage (NR8383) cells and generation of intracellular ROS at the highest level with protective effect of vitamins (E and C) against the cytotoxicity of the $NH_2$-SiNP suggesting a role of oxidative stress in the mechanism of cytotoxicity [Bhattacharjee et al (2010)].

It is important to bear in mind that ENPs might tend to aggregate in biological systems and this would reflect the size of the aggregates more than the size of the nanoparticles themselves. Therefore, investigating the ENPs physicochemical characteristics in biological environments or systems is essential for in vitro studies. The dynamic light scattering (DLS) system, also named photon correlation spectroscopy, is the most-used method for ENPs size characterisation in solution however, it is preferable to use other different techniques such as electron microscopy methods (e.g. Transmission Electron Microscopy (TEM)) for size characterisation. The same DLS technique can be used for zeta-potential measurement as an estimation of surface charge.

Moreover, the experimental conditions (including the agglomeration tendency of ENPs) and the characteristics of the target cells in addition to the ENPs

physicochemical properties, are important parameters that have been suggested to influence the toxicity, translocation along with intracellular trafficking and uptake of the ENPs into cells [Oberdörster et al (2005a), Patil et al (2007), Qiao et al (2007), Rothen-Rutishauser et al (2007), Unfried et al (2008), Yacobi et al (2007)].

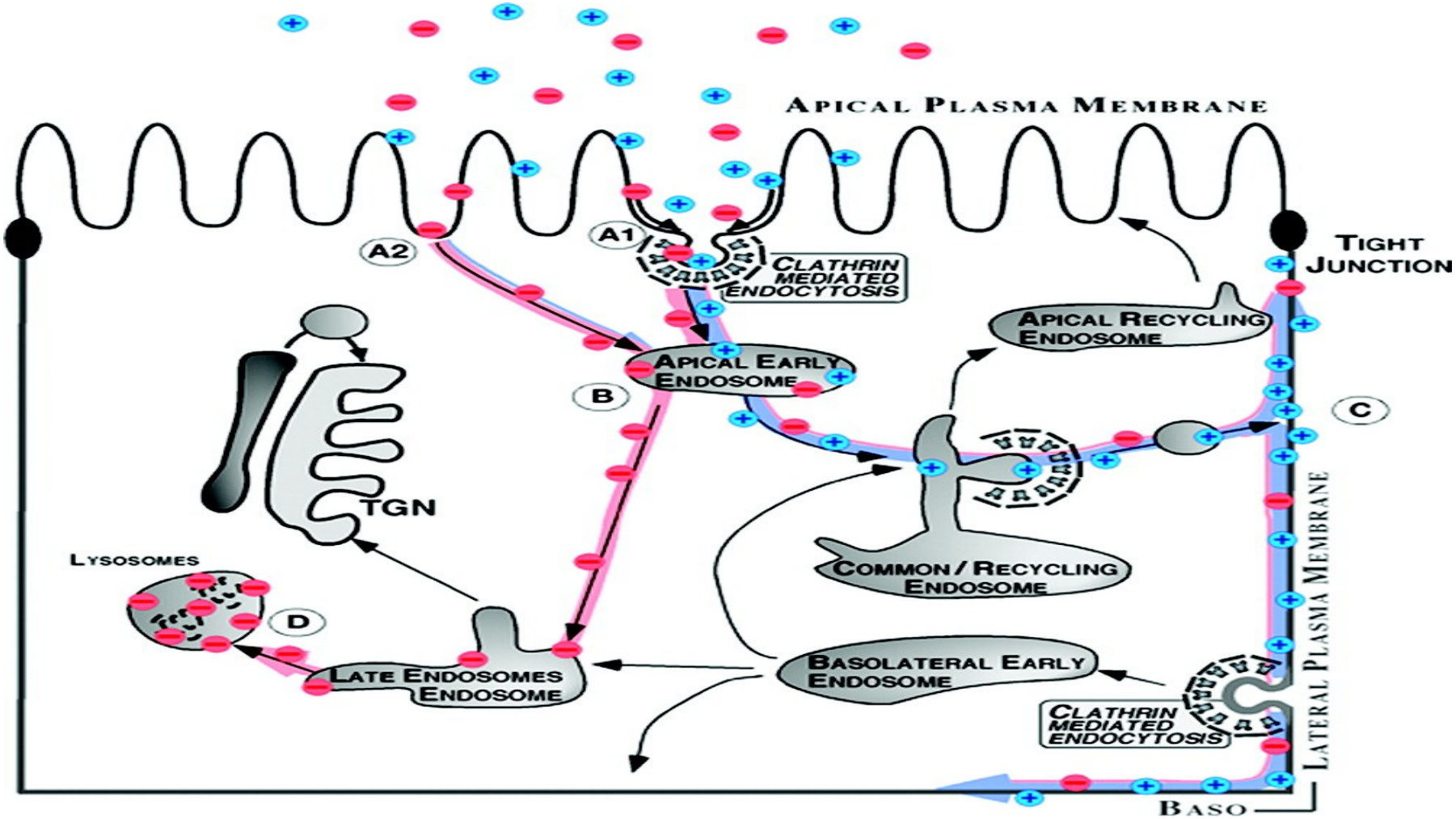


Fig. 1.8 Surface charge of ENPs determines their intracellular pathways in polarized epithelial MDCK cells. Cationic and anionic ENPs are internalised differently. (adopted from "Harush-Frenkel et al (2008)").

## 1.9 Aims of the current study

Nanoparticles (NPs) including COO-PS-NPs have many potential applications, as drug delivery system for example, however their toxicity remains poorly assessed. The current thesis undertook an *in vitro* study to evaluate the potential toxicological effects of COO-PS-NPs on the cellular activities of cultured BEAS-2B lung epithelial cells. Since the toxicity of other ENPs has been shown to be concentration- and size-dependent [Fröhlich et al[b] (2012)], several concentrations of two different sizes (20nm and 100nm diameter) of the same red fluorescent negatively charged COO-PS-NPs were used for investigation of toxicity at different time points to evaluate the possible impacts of these important parameters. The cellular uptake and co-localisation of COO-PS-NPs within specific organelles was also studied as NPs need to gain access to inside the cell to exert their effect [Lovric et al (2005)].

Furthermore, the aggregation of COO-PS-NPs was characterised in the culture media as well as in the stock solution for comparison to relate their physical behavior to effects in biological systems. Although the surface charge of the COO-PS-NPs was also characterised, its role in toxicity was not investigated herein, but may be need to be taken in consideration in further projects.

# CHAPTER TWO:

# GENERAL MATERIALS AND METHODS

## 2.1 Chemical reagents and cell culture labware products

All chemicals were used without additional purification and were obtained mainly from Sigma Aldrich (Dorset, UK) or Fisher Scientific (Loughborough, UK) unless otherwise stated. The LHC-9 serum-free medium (SFM) and commercial red fluorescent ($\lambda_{ex}$ @ 580nm/ $\lambda_{em}$ @ 605nm) carboxyl-modified polystyrene nanoparticles (COO-PS-NPs), with 20nm (F-8786) and 100nm (F-8801) average nominal diameter sizes, were purchased from Invitrogen (Paisley, UK). Phosphate buffer saline (PBS) tablets were from Oxoid Ltd (Basingstoke, UK) and trypsin-ethylenediaminetetraacetic acid (trypsin-EDTA, 1X, 0.05% – 0.02% in D-PBS) was from PAA Laboratories GmbH (Cölbe, Germany), Bradford reagent was from Bio-Rad Laboratories GmbH (München, Germany) and hydrogen peroxide ($H_2O_2$, 30%) was from BDH Laboratory Supplies (Poole, UK). Cell culture plastic and glass labware products (including multi-well plates, flasks, micro-tips, disposable polystyrene serological pipettes, conical and micro-centrifuge tubes, cryo-vials, cell scrapers, reservoirs, cuvettes and microscope slides) were purchased primarily from Corning Incorporated Life Sciences (NY, USA) however some labwares were also obtained from SPL Life Sciences (Pocheon-city, South Korea), VWR International (Lutterworth, UK), Greiner Bio-One (Stonehouse, UK) or Fisher Scientific.

## 2.2 BEAS-2B Cell culture

*In vitro* models seem to be more attractive for preliminary assessment of the potential toxicological effects of ENPs due to several reasons including the high expense of *in vivo* experiments, ethical concerns raised as a result of the increased number of animals required for laboratory testing as well as governmental and public urging to develop alternatives to animal testing. Furthermore, i*n vitro* studies are faster with vast control of the experimental conditions compared with *in vivo* ones and the quantity of ENPs used for *in vitro* experiments will be minimal which would make these models of low cost. Nevertheless, selecting the most appropriate representative cell line as a realistic *in vitro* model that resembles (and specifically relevant to) the target organ of interest *in vivo* is crucial in investigating the potential toxicological effects of ENPs. Lungs are the main target for ENPs following exposure by inhalation and human epithelial cells (BEAS-2B) were therefore used in this study as they were found to be relevant representatives to the lung.

The BEAS-2B cells used in this *in vitro* study are immortalized normal human bronchial epithelial cell line derived from non-cancerous person [ATCC (published online)]. The growth properties of these cells were transformed to expand their capabilities to divide and replicate continuously without altering their phenotype and genotype. This would avoid the replicative senescence status that primary cells are normally arrested in after a fixed number of replications and hence enable researchers to maintain consistency during *in vitro* experiments.

The use of serum-free medium (SFM) to culture cells in vitro has many advantages since it increases the cell culture productivity by eliminating the cytotoxicity due to serum cytotoxins and cutting down the risk of possible contamination that may come from serum microbiological contaminants [Newman (2003), Van der Valk et al (2004), Brunner et al (2010)]. SFM has an improved consistency as a result of reducing substantial quantitative and qualitative batch-to-batch variation, hence enhance the control of cell culture conditions of sterilization and safety [Newman (2003), Van der Valk et al (2004), Brunner et al (2010)]. Thus SFM used in cell culture tends to improve the consistency of experimental results. SFM is also preferred since serum production is complicated and costly in addition to avoiding the controversial ethical issue of using animal-derived components in media [Newman (2003), Van der Valk et al (2004)]. Furthermore, SFM is used for in vitro studies of nanoparticles since serum containing media may affect the ENPs internalisation into cells due to serum proteins adsorption onto the ENPs surface which might increase or decrease their uptake in vitro [Chithrani et al (2006)]. It has been stated that cells react in response to substances that are in contact with their membranes or already taken inside, but not to the floating ones in the media [Teeguarden et al (2007)]. Thus, cells need to be washed several times (with PBS) at the end of the treatment to eliminate the unbound and non-internalised COO-PS-NPs and cells will be re-incubated with fresh SFM.

All cell culture work was conducted aseptically using a class II tissue culture cabinet and all solutions, supplies, reagents and materials were autoclaved and sterilized by wiping with 70% ethanol as necessary before being used to avoid contamination that

may interfere with conducted assays as well as alter cell morphology, growth, viability and production. Materials in contact with the cells were tested on a regular basis to prevent contamination and recognize any of its potential sources in early stages. All labwares used for cell cultures were coated with type-I rat tail collagen (6.66 µg collagen/$cm^2$ for 2h) before being used and all solutions used in cell culture were pre-warmed to 37ºC in a water bath (SUB14, Grant Instruments (Cambridge) Ltd, Shepreth, UK).

### 2.2.1 Maintenance

BEAS-2B cell line was obtained from the Health Protection Agency (Cat no. 95102433). These adherent cells were routinely cultured in a suitable Lechner and LaVeck serum-free cell-culture medium (LHC-9 SFM), maintained at 37ºC and 5% $CO_2$ in a humidified incubator (MCO-15AC, Sanyo Electric Co. Ltd, Osaka, Japan) and fresh media was supplied every 2-3 days after cell washing with PBS. Flasks were checked microscopically for confluence. When cells were about 90% confluent (every 3–4 days), they were washed with PBS to remove dead cells and trypsinised with trypsin-EDTA (37ºC for 5-7 min) to detach them from surfaces. The flasks were tapped firmly to certain detachment of cells and fresh media (5 ml) were then added to neutralize the enzymatic activity of trypsin. Cells were mono-dispersed by pipetting before centrifuging the cell suspension at 1200 rpm (MSE Falcon 6/300, MSE Ltd., London, UK) for 5 min and the resulted cell pellet was re-suspended in 1 ml media.

### 2.2.2 Passage

For cell sub-cultures, cells were passaged into new T75 and T25 flasks (at 1:3 and 1:6 split ratio respectively). Each batch of BEAS-2B cells were used for 10 passages or fewer. For experiments, cell number was counted using a Neubauer haemocytometer (Weber International Ltd, Teddington Middlx, UK) and cells were reseeded into appropriate multi-well plates using fresh LHC-9 SFM. Cells were seeded at $2\times10^4$ cells/100µl LHC-9 SFM/well in 96-well plates, at $2\times10^5$ cells/2ml LHC-9 SFM/well in 12-well plates and at $5\times10^5$ cells/5ml LHC-9 SFM/well in 6-well plates. The multi-well plates were maintained at 37ºC in 5% $CO_2$ humidified incubator for 24h to allow cells to adhere and grow to be approximately 85% confluent. For the cell treatment with nanoparticles, cells were washed next day with PBS to remove suspended dead cells and incubated in fresh LHC-9 SFM for 10min at 37°C in a 5% $CO_2$ humidified incubator before being treated individually with single definite dose of various concentrations of nanoparticles. However, information about the chemical composition and ingredients of LHC-9 SFM were considered proprietary for the manufacturer and undivulgable.

## 2.3 Treatment with COO-PS-NPs

In this study, red fluorescently-labelled, negatively charged, carboxyl-modified polystyrene nanoparticles (COO-PS-NPs) were used because they are pure (with high quality and no contamination as manufacturer claimed) and are abundantly available at

quite low cost. The 20nm and 100nm COO-PS-NPs were selected for the current study since these sizes are relevant to the NPs-based applications.

According to the manufacturer, the red fluorescent carboxyl-modified polystyrene nanoparticles (commercially named latex beads or FluoSpheres) are spherical beads with red dyes integrated in the core ($\lambda_{ex}$ @ 580nm/ $\lambda_{em}$ @ 605nm) which means that the fluorescent nanoparticles have the same surface properties and composition of non-fluorescent particles. This would allow evaluation of toxicity, assessment of uptake and easy detection of localisation of the COO-PS-NPs of similar composition under identical conditions in the living cells without help of other substances that might change their size or composition. Moreover, these nanoparticles have attached carboxylic acids on their surface which make them negatively charged and were supplied as suspensions (2% solids) in 2mM sodium azide containing water. These COO-PS-NPs are stable for at least one year (as stated by the supplier) when recommended storage conditions are strictly fulfilled (2-6º C, protected from light). More information about the chemical composition of COO-PS-NPs, their structure and configuration were considered proprietary for the manufacturer and undivulgable.

### 2.3.1 Dosage of COO-PS-NPs

Although freshly prepared solution of ENPs using the powder form was argued to be the most suitable [Stone et al (2010)], the suspension form of COO-PS-NPs (i.e. dispersed in a solution) was chosen in this study to avoid problems of reproducibility of dispersion. A freshly-prepared diluted solution of fluorescent 20nm COO-PS-NPs (1:10)

in LHC-9 SFM was used as well as a stock solution of 100nm COO-PS-NPs (without dilution) for the treatment of cells in multi-well plates.

It has been shown that the response of cells is proportional to surface area of ENPs ($cm^2$) in media volume (ml) [Oberdörster et al[a] (2005)]. In agreement with that, Sager and Castranova concluded that using surface area as a dose unit in the toxicity assessment studies is more reliable than the mass-based dose [Sager and Castranova (2009)]. Moreover, there will be a huge variation in the number of the particles of the different size nanoparticles exposed to the living system if weight (i.e. mass) per volume was the approach used to express concentration (mg/ml or µg/ml) and this might affect the results [Varela et al (2012)]. Therefore, the surface area ($cm^2$) of ENPs per volume unit (ml) of media is used in this study as a concentration of COO-PS-NPs for cell treatment. Using the surface area of ENPs per volume ($cm^2$/ml) will allow discriminate between the size effect and concentration effect when studying the internalisation, toxicity, characterisation and mechanism of action. The surface area for the COO-PS-NPs was calculated according to this equation:

$$\frac{6 \bullet 10^7 \bullet x}{y \bullet z}$$

$x$ = particle weight (g) per ml $y$ = density (g/ml) $z$ = diameter (nm)

The concentrations used for treatments were in range to 25–300 $cm^2$/ml. Triplicate (or at least duplicate) wells were conducted in every experiment for each treatment and each experiment was repeated independently at least three separate times unless mentioned.

### 2.3.2 Dispersion of COO-PS-NPs

In aqueous systems, ENPs form aggregates (i.e. tightly associated particles) and/or agglomerates (i.e. loosely associated particles) and in both cases the nanoparticles are held together by relatively weak attractive forces including Van der Waals forces, electrostatic forces as well as surface tension in the absence of the repulsion interactions [Revell (2006)]. This presence of aggregation (due to high surface energy) can alter the physicochemical characteristics of the ENPs including their size from the initial state [Donaldson et al (2001)] and they hence need to be dispersed by external forces (e.g. extensive sonication or strong agitating) to deagglomerate them before being added to the biological system. This is essential in order to simulate real exposure conditions and to avoid the inaccurate evaluation of the ENPs toxicity and co-localisation [Magdolenova et al (2012)]. Nevertheless, avoiding sonication was recommended as sonication might cause alteration in the ENPs characteristics [Teeguarden et al (2007)].

The samples of COO-PS-NPs were hence dispersed to minimise aggregation by vortexing at maximum speed for 2minutes in order to reduce particle interactions (avoiding heating of the nanoparticles that may alter their characteristics in suspension) [Oberdörster et al[a] (2005)]. The prepared COO-PS-NPs solutions were immediately used for cell treatment and added to cell cultures (80–90% confluence) at various concentrations and cells were incubated for different time points at 37ºC in a 5% $CO_2$ humidified incubator. Samples were also retained for nanoparticle characterisation (See section 2.4).

In some experiments, chemicals of buthionine sulfoximine (BSO), hydrogen peroxide ($H_2O_2$, 30%) or etoposide were used as positive controls whereas cells in the absence of nanoparticles (non- treated cells in medium only) were used as negative controls.

## 2.4 Characterisation of COO-PS-NPs

Characterisation of COO-PS-NPs (including size, surface charge, elements contamination and shape) is performed in the stock solutions and in the cell culture media using different techniques. This is required for monitoring and understanding the changes of the physicochemical properties in the biological solutions.

### 2.4.1 Determination of the COO-PS-NPs size and surface charge

Dynamic Light Scattering (DLS) technique was applied for COO-PS-NPs characterisation to evaluate the hydrodynamic diameter and surface charge using Nano-ZS Zetasizer Instrument (Malvern Instruments Ltd., Worcestershire, UK). At incubation temperature (37°C), samples of stock solution and various dilutions of COO-PS-NPs in LHC-9 SFM (2.5–300 $cm^2$/ml) were vortexed for 2 min and transferred to 1ml clear cuvettes. At a scattering angle of 90°, the average size of nanoparticles was measured in triplicate (with 20 single measurements per sample) and calculated to assess the aggregation state of the nanoparticles. The zeta potential (ζ-potential) is the electric potential difference between the surface of the particle and the suspension medium in the colloidal system where one state of matter (gas, liquid or gas) is dispersed very well in

another [McFadyen and Fairhurst (1993)]. ζ-potential is not the surface charge itself but it is proportional to the surface charge of ENPs [Fubini et al (2010)]. The ζ-potential was determined in the stock and diluted samples of COO-PS-NPs in triplicate with 10 single measurements per sample. The average size and ζ-potential were assessed using COO-PS-NPs diluted in ultrapure de-ionized water (Milli-Q $dH_2O$) (300 $cm^2$/ml) in order to find out how size and surface charge may change in relation to the media compositions and to determine whether particles aggregate or not under experimental conditions. Furthermore, characterisation was also carried out at room temperature (25°C) to observe the effect of temperature on the physicochemical characteristics of COO-PS-NPs.

### 2.4.2 Composition quantification of COO-PS-NPs by ICP-MS

Inductively coupled plasma mass spectrometry (ICP-MS) is a sensitive analytical technique used for detecting many of the elements (metals and non-metals) in the periodic table at concentrations as low as parts per million [Scheffer et al (2008)]. This analysis is based on ionizing the samples yielding a plasma from which the ions are then separated and quantified. Each element is identified as a signal pulse depending on its unique mass spectrum and quantities of elements are proportional to their signal intensities (received on a detector) [Laborda et al (2011)].

For sample preparation, 100µl of COO-PS-NPs (20nm or 100nm) were separately aliquoted and centrifuged for 5min at 5000rpm using a benchtop microcentrifuge (5415D, Eppendorf AG, Hamburg, Germany) and the supernatants were carefully aspirated. Nitric acid ($HNO_3$, 70% analytical grade) (Fisher Scientific Ltd,

Loughborough, UK) was used for nanoparticle digestion due to its oxidizing ability, chemical compatibility, purity, low cost and availability. Each delicate pellet of nanoparticles was acidified in tightly capped glass vial in 57µl of $HNO_3$ and the samples were then incubated for 24h at 37°C. Next day, the samples were diluted to 2ml with MQ $dH_2O$ (approximately 2% final concentration of $HNO_3$) and filtered through a 32mm acrodisc syringe filters with a sterile 0.2µm supor membrane (Pall Life Sciences, Portsmouth, UK). A blank sample (57µl $HNO_3$) was prepared and diluted in the same way as the other samples and all samples were then subjected to analysis by ICP-MS.

### 2.4.3 Determination of COO-PS-NPs size and morphology (shape) by TEM

Transmission electron microscopy (TEM) is an ideal analytical tool for NPs characterisation to study their structural appearance (shape and size) [Mühlfeld et al (2007)] using high magnification at very short wavelengths to get high resolution imaging capacity. Fig. 2.1 illustrates the main steps for cell sample preparation for examination by TEM including fixation, post-fixation, dehydration, embedding, sectioning and staining [Bozzola (2007), Schrand et al (2010)] following the treatment with the ENPs of interest.

Samples of the 20nm and 100nm sized COO-PS-NPs in stock solution were analyzed individually by TEM to investigate their actual size and the probable aggregation. Sample preparation was carried out by directly placing 10µl (tiny drop) of the sample of interest upon the grid allowing the sample to settle. The residuals were then removed with filter paper, the drop was left to dry on grids for about 2 minutes and was

negatively stained by adding 10µl (tiny drop) of 1% Uranyl acetate for about 1 minute before washing it off. The TEM grids were then mounted individually on sample receiver, inserted into the vacuum chamber and imaged by TEM (JEOL, model 1200EX) instrument (JEOL, Tokyo, Japan) operating at accelerating voltage of 80 kV.

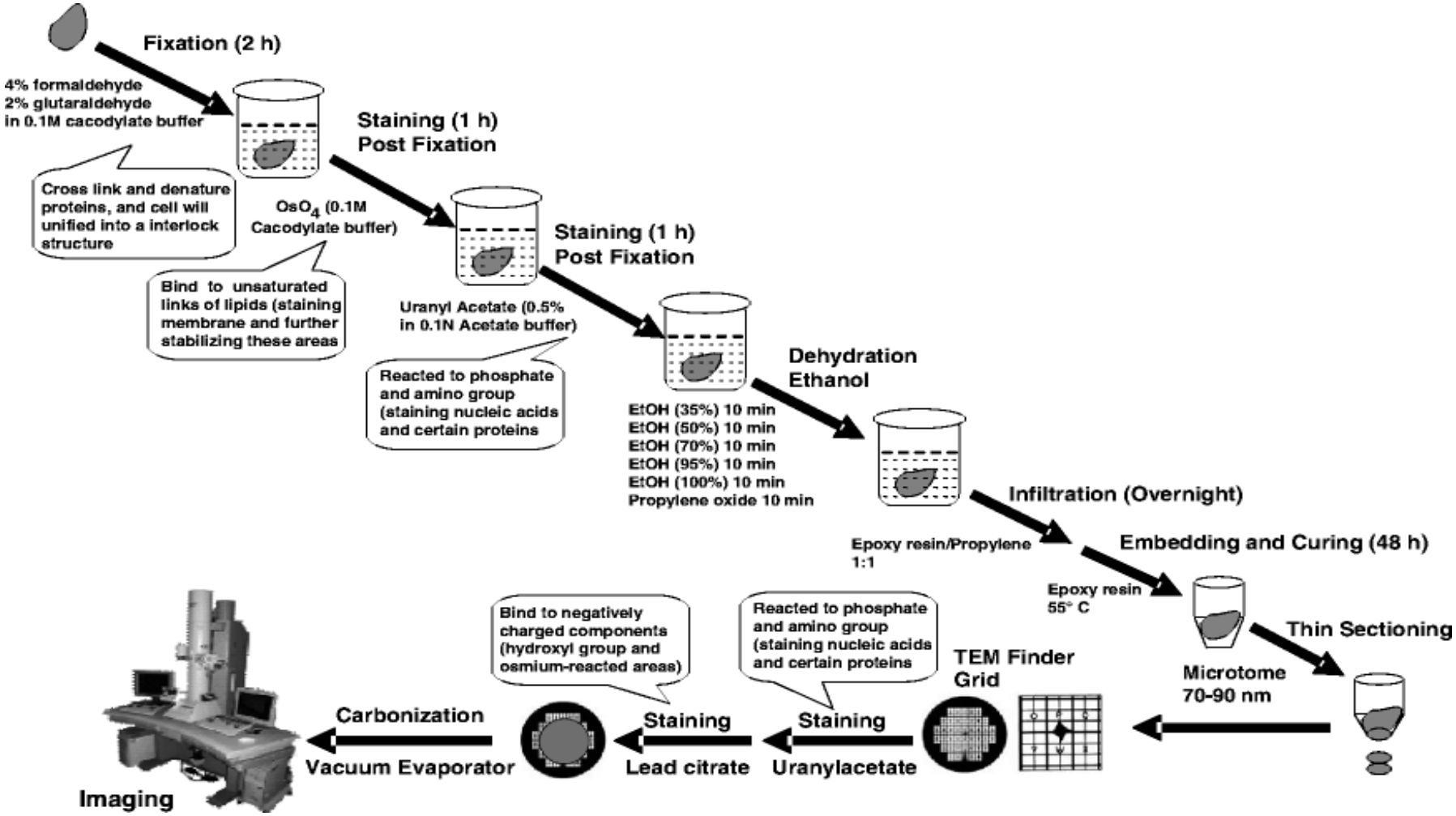


Fig. 2.1 The major steps in cell sample preparation for TEM imaging following the treatment. (adopted from "Nagashima (2011)").

## 2.5 Measurement of the mitochondrial activity by MTT assay

Only in viable cells, the active mitochondrial reductase (dehydrogenase) enzyme can reduce the yellow MTT (3-(4,5-dimethylthiazol-2-yl)-2,5-diphenyltetrazolium bromide) salt into water-insoluble purple formazan crystals [slater et al 1963)] (Fig. 2.2). The purple formazan salts can be dissolved by DMSO and the optical density of the formazan concentration can be quantified spectrophotometerically to indicate the metabolic activity of cells which is directly proportional to the growth and number of viable cells [Mosmann (1983), Lanone et al (2009)].

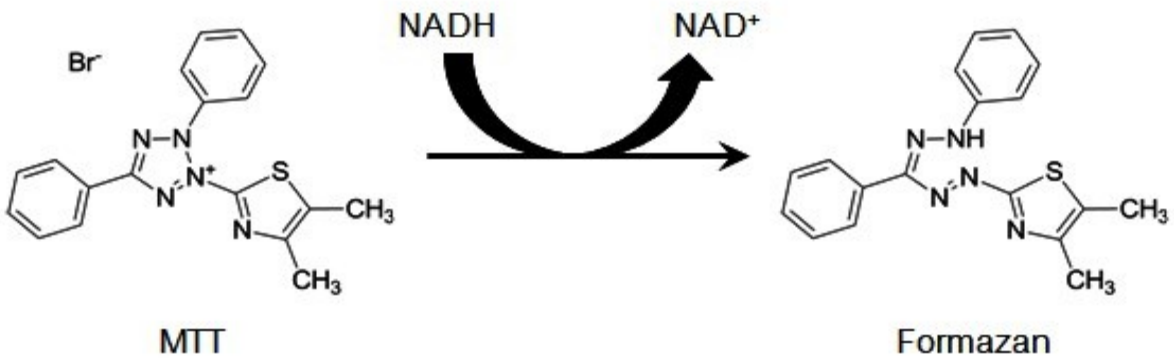


Fig. 2.2 Reduction of yellow tetrazolium salt (MTT) to water-insoluble purple formazan crystals by the active mitochondrial reductase enzyme of the viable cells as an indication of viability. [adapted from "Assay Guidance Manual by Sittampalam et al (2004)"]

The rapid colorimetric MTT assay is broadly used nowadays to quantitatively assess the potential toxicological effect of materials on the cell mitochondria activity and that directly proportional to the number of living cells in treated samples [Van Meerloo et

al (2011)]. This convenient cytotoxicity assay was applied in this study to evaluate the BEAS-2B cell viability (since cytotoxicity results in loss of mitochondrial activity) after 24h incubation with different single concentrations of 20nm and 100nm of COO-PS-NPs.

BEAS-2B cells seeded in 96-well plastic tissue culture plates were incubated with various concentrations of COO-EPSNP at 37ºC in a 5% $CO_2$ humidified incubator for 1, 4, 6, 12, 18 and 24h. Following treatment, old media was discarded, cells were washed with 100µl PBS and 100µl fresh LHC-9 SFM was added. 25µl of MTT solution (of 5mg/ml PBS) was then added to each well and cells incubated for 3h at 37ºC. Media containing MTT solution were then aspirated and 200µl of dimethylsulfoxide (DMSO)/well were added before covering the plates with foil and agitating gently on rocker for 1h at RT to dissolve the purple formazan crystals. Absorbance was read at a wavelength of 590nm using a micro-well plate reader (FL 600, Bio-Tek Instruments Inc., Winooski, USA) against DMSO as a blank. The mean of mitochondrial metabolic activity that represent the cellular viability at different concentrations was expressed as a percentage of non-treated cells (negative control).

$$100 - \left[\frac{(x \bullet 100)}{y}\right]$$

$x$ = treated sample absorbance $y$ = control (non-treated) sample absorbance

The above formula was applied in this cytotoxicity experiment for calculating the living cells which have active mitochondrial function that enable them to reduce MTT salts into water-insoluble purple formazan crystals via mitochondrial dehydrogenases.

## 2.6 Measurement of ROS generation by $H_2$DCF-DA assay

In this study, the formation of ROS (mainly $H_2O_2$) was examined by a fluorometric assay using 2',7'-dichlorodihydrofluorescein diacetate ($H_2$DCF-DA) to detect cellular oxidative stress induction caused by reactive oxygen species in BEAS-2B cells after treatment with different concentrations of COO-PS-NPs.

$H_2$DCF-DA is a hydrophobic membrane-permeable non-polar non-fluorescent dye that is able to freely enter across the cell membrane [LeBel et al (1992)]. It is one of the most widely used probes to detect oxidative stress by measuring the intracellular ROS production (mainly $H_2O_2$) using flow cytometry [LeBel et al (1992)]. Within cells, $H_2$DCF-DA is hydrolyzed by intracellular esterases so the diacetate groups are cleaved and removed yielding a polar non-fluorescent 2',7'-dichlorodihydrofluorescein ($H_2$DCF) derivative that is trapped in the cell. This $H_2$DCF derivative is then oxidized in the presence of intracellular ROS (chiefly peroxides such as $H_2O_2$) and transformed by peroxidases into green fluorescent 2′,7′-dichlorofluorescein (DCF) product which can be quantified by flow cytometer ($\lambda_{ex}$ 512nm / $\lambda_{em}$ 530nm) [Bass et al (1983), LeBel et al (1992), Wang and Joseph (1999), Müller et al (2008), Hanley et al (2008)]. The produced fluorescence would be directly proportional to the overall intracellular ROS concentration and can used as an indicator for ENPs-induced ROS formation.

BEAS-2B cells cultured in 12-well plastic tissue culture plates were treated with various concentrations of COO-PS-NPs and cells were incubated at 37ºC for 24h. This assay was also conducted on BEAS-2B cells after incubation with a range of COO-PS-NPs concentrations (25-300 $cm^2$/ml) for different time points (1, 4, 6, 12 and 18h). At

the end of treatments, cells were washed with 1ml PBS and incubated in media containing 200µl $H_2$DCF-DA (10µM final concentration) at 37ºC for 45min. In the main lab, cells were washed with PBS, trypsinised (500µl/well, 5-7 min at 37ºC), neutralized with media (500µl/well), centrifuged at 4000 rpm for 4 min and each pellet was then re-suspended in 400µl PBS before being transferred to a FACS tube. The analysis was run to measure the COO-PS-NPs induced ROS generation by a Becton Dickinson FACS Calibur flow cytometer instrument (BD Science, San Jose, USA) using 488nm laser for excitation to count ten thousand cells (events) from each sample and detect them in channel FL-1.

CellQuest software program (Pro-V 5.2.1, BD Science) was used for data acquisition while the Weasel software program (V 3.1, Walter and Eliza Hall Institute (WEHI), Melbourne, Australia) was used for data display, gating and analysis. The cellular debris was gated out from the analysis and the median of fluorescence was calculated. $H_2$DCF-DA was also incubated with the COO-PS-NPs in the absence of cells to check the possibility of nanoparticles interference with the assay. The results were expressed after being calibrated with the blank (i.e. the blank was subtracted from each sample).

## 2.7 Determination of the total reduced glutathione (GSH) level

### 2.7.1 GSH assay

Briefly, BEAS-2B cells cultured in 6-well plastic tissue culture plates were treated with different concentrations of COO-PS-NPs and cells were incubated at 37ºC for 24h. At the end of incubation, a modified protocol based on the fluorometric method described initially by Hissin and Hilf (1976) was used for the measurement of the intracellular GSH content. Media containing the PS-NPs were aspirated and cells in each well were washed twice with 1ml of warm PBS after which cells in each well were scraped into 450µl of ice-cold cell lysis buffer [0.1% Triton X100 in $PO_4$-EDTA buffer (100 mM $NaH_2PO_4$ and 5 mM $Na_2$-EDTA, adjusted to pH 8.0)]. Lysates were transferred to eppendorf tubes on ice and 10–15µl of each sample was retained in a separate tube for protein estimation. Next, 50µl of ice-cold protein precipitation buffer (50% w/v trichloroacetic acid (TCA) in $PO_4$-EDTA buffer) was added to the lysates and samples were centrifuged at 13000rpm for 5min. The resulting supernatants (containing the GSH) were then transferred to new eppendorf tubes. 1.8ml of $PO_4$-EDTA buffer, 100µl of GSH sample solution and 100µl of freshly made O-Phthalaldehyde (OPT, 1mg/ml 100% methanol) (Fisher Scientific Ltd, Loughborough, UK) were mixed in individual 3ml polystyrene fluorescence cuvettes (Sarstedt Ltd, Leicester, UK) and placed in a covered box which was incubated at RT with rocking for 15min. A GSH standard curve was prepared using a freshly made GSH stock solution (0.325 mM, 0.1 mg/ml in PO4-EDTA

buffer) and different concentrations (0-2µg) were treated in the same way as test samples except 5% w/v trichloroacetic acid (TCA) in $PO_4$-EDTA buffer was used. The fluorescence was subsequently read (PerkinElmer LS50B luminescence spectrometer, PerkinElmer, Cambridge, UK) with $\lambda_{excitation}$ @ 340nm (slit width 2.5nm) and $\lambda_{emission}$ @ 420nm (slit width 4.0nm).

### 2.7.2 Bradford assay

This assay was first described by Bradford for protein estimation [Bradford (1976)] and is based on the shift in Coomassie blue G-250 absorbance when binding protein under acidic conditions [Reisner et al (1975)]. The Coomassie dye has a red, green or blue color in the basic (cationic), neutral or acidic (anionic) pH respectively with different absorbance wavelengths and the pH equilibrium is shifted to the anionic status upon the protein binding that occurs mainly through electrostatic (Van der Waals and/or hydrophobic) interactions between the arginine and aromatic (i.e. Try, Tyr and Phe) amino acid residues with the sulfonic group of the dye [Compton and Jones (1985)].

In this assay, the Bradford reagent was diluted (1:5 in $dH_2O$) and filtered into a glass tube. 1ml of this diluted reagent solution was placed separately in 1ml cuvettes (Sarstedt Ltd, Leicester, UK), 2µl of test sample was added and stirred with a plastic rod. A stock solution of BSA (1 mg/ml $dH_2O$) was freshly prepared and different volumes (0, 1, 2, 4, 6, 8 and 10 µg) were treated in the same way as test samples. The cuvettes were placed in a covered box for 10min and the absorbance readings were then taken at 595nm

(UVIKON 922 spectrophotometer, Kontron Instruments, Bletchley, UK) against 1ml diluted Bradford reagent as a blank.

The protein standard curve was plotted using Beer Lambert law, the test sample values were calibrated against the standard curve of GSH and expressed per milligram of cellular protein. The total intracellular GSH concentrations in samples (treated cells and controls) were calculated using the standard curve, normalized to mass of total protein in cells and expressed as nmol/mg of proteins contained in the sample.

## 2.8 Evaluation of the DNA strand breaks by comet assay

The comet assay (known also as single cell gel electrophoresis) is a simple, sensitive and reliable practical method that is widely used for investigating the DNA damage [(Szeto et al (2005)]. The concept behind this assay is to insert the cell in agar (after the treatment is accomplished), unwind the DNA by immersing in highly salted solution (pH>13) before running the electrophoresis to pull the damaged DNA to the anode (the positive pole). The DNA containing strand breaks would migrate more rapidly in agarose gel than intact DNA upon application of an electric field forming a comet tail that can be stained by a DNA fluorescent dye and viewed microscopically. The extent of the stimulus induced DNA damage can be directly related to the amount of DNA strand breaks in the stained comet tail and to the tail length [Singh et al (1988), Collins (2004)]. The assay involves several steps including cell collection and lysis, DNA unwinding,

electrophoresis, staining, cell counting (of at least 100 cells per sample) under the microscope and comet analysis by computer program (Fig. 2.3).

### 2.8.1 Evaluation of the DNA strand breaks in BEAS-2B cells

BEAS-2B cells in 6-well plastic tissue culture plates were treated with different concentrations of PS-NPs and plates were incubated at 37ºC in a 5% $CO_2$ humidified incubator for 24h. At the end of treatment, media containing the PS-NPs were aspirated and cells in each well were washed twice with 2ml PBS before scraping cells into 300µl of PBS. Cell suspensions were centrifuged at 8000rpm for 5min and the supernatants were carefully aspirated and each cell pellet was re-suspended in 150µl of PBS. 30µl of the re-suspended cells was transferred into a clean tube containing 300µl molten 2% low melting point agarose (LMPA, Bioline ltd., London, UK) and mixed well. 150µl of each cell suspension was spread onto a well-labeled glass microscope slide (26x76mm, VWR International BVBA, Leuven, Belgium) pre-coated with normal melting point agarose (NMPA, 0.5% w/v, 48h to dry, Bioline ltd.) and a duplicate slide was prepared the same way. Each of the two slides were covered with a glass cover slip (22x64mm, VWR) avoiding bubbles formation, placed on a metallic tray over ice and left in the cold room (at 4° C) for approximately 20min to allow the agarose to set. When solid, the cover slips were removed and the slides were incubated for 1h at 4° C in foil-wrapped Coplin jars filled with cold lysis buffer (2.5M NaCl, 0.1M $Na_2$-EDTA, 10mM Tris base, 1% sodium N-lauryl sarcosinate, 10% DMSO and 1% Triton X-100). Later, the slides were incubated horizontally in large electrophoresis tank containing cold electrophoresis buffer (300mM NaOH and 1mM $Na_2$-EDTA, pH≥13) for 20min to unwind the DNA and were then

electrophoresed for 20min (32V, 300mA) using a Bio-Rad power pack 200 power supply (Bio-Rad Laboratories, Hercules, USA). Slides were washed (3 x 5 min) with cold neutralization buffer (400mM Tris base, pH 7.5) on paper tissues before staining each slide with 50µl DNA-specific SYBR gold (1:1000 in $dH_2O$, Invitrogen, Paisley, UK), placing new glass cover slips and storing slides in the cold room in a foil-wrapped moist box for analysis (within 24h).

The comets (on slides) were viewed using Axiovert 10 inverted fluorescence microscope (Zeiss Ltd, Göttingen, Germany) using a 20X objective lens. Computerized image analysis was performed using the Comet 4.0 (Comet assay IV) software program (Perceptive Instruments Ltd., Haverhill, UK) and 100 cells per slide were randomly selected and analyzed. The median of tail intensity percentage (i.e. the DNA content percentage in the comet tail) was used to represent the DNA damage level since it is linearly related to the numbers of DNA breaks following treatment [Collins (2004)] and it is not influenced by the time and voltage used for running the electrophoresis showing a robust indicator of DNA damage [Olive and Durand (2005)]. $25cm^2$ and $150cm^2$ were used as dose concentrations of both 20nm and 100nm COO-PS-NPs compared to BSO and untreated cells as positive and negative controls respectively.

### 2.8.2 Estimation of the DNA damage in COO-PS-NPs treated cell lysate and cell suspension

BEAS-2B cells were seeded without treatment in 6-well plastic tissue culture plates at 37ºC in a 5% $CO_2$ humidified incubator for 24h. The media were aspirated

before washing cells twice with 1ml of warm PBS and cells in each well were then scraped into 300µl warm PBS and the cell suspensions were centrifuged at 8000rpm for 5min. The supernatants were then carefully aspirated and each cell pellet was re-suspended in 150µl of PBS. The cell suspensions were categorized in two groups as follows; 1st group samples were treated with different concentrations (25 and 150 $cm^2$/ml) of the 20nm or 100nm COO-PS-NPs for 1h while the 2nd group samples were left untreated. 30µl of the re-suspended cells of each of the two groups was transferred into a clean tube containing 300µl molten 2% low melting point agarose (LMPA, Bioline ltd., London, UK) and mixed well. 150µl of each cell suspension was spread onto a labeled glass microscope slide (26x76mm, VWR International BVBA, Leuven, Belgium) pre-coated with normal melting point agarose (NMPA, 0.5% w/v, 48h to dry, Bioline ltd.). The slides were covered with a glass cover slip (22x64mm, VWR) avoiding bubbles formation, placed on a metallic tray over ice and left in the cold room (at 4° C) for approximately 20min to allow the agarose to set. When solid, the cover slips were removed and the slides were incubated for 1h at 4° C in foil-wrapped Coplin jars filled with cold lysis buffer (2.5M NaCl, 0.1M $Na_2$-EDTA, 10mM Tris base, 1% sodium N-lauryl sarcosinate, 10% DMSO and 1% Triton X-100). Later on, the slides were washed (3 x 5 min) using cold neutralization buffer (400mM Tris base, pH 7.5) on paper tissues. The 2nd group samples were exposed to different concentrations (25 and 150 $cm^2$/ml) of the 20nm or 100nm COO-PS-NPs for 1h before incubating all the slides horizontally in large electrophoresis tank containing cold electrophoresis buffer (300mM NaOH and 1mM $Na_2$-EDTA, pH≥13) for 20min to unwind the DNA. The electrophoresis was run for 20min (32V, 300mA) using a Bio-Rad power pack 200 power supply (Bio-Rad

Laboratories, Hercules, USA) and the other steps were then applied as performed earlier (section 2.9.) to assess the COO-PS-NPs induced DNA damage.

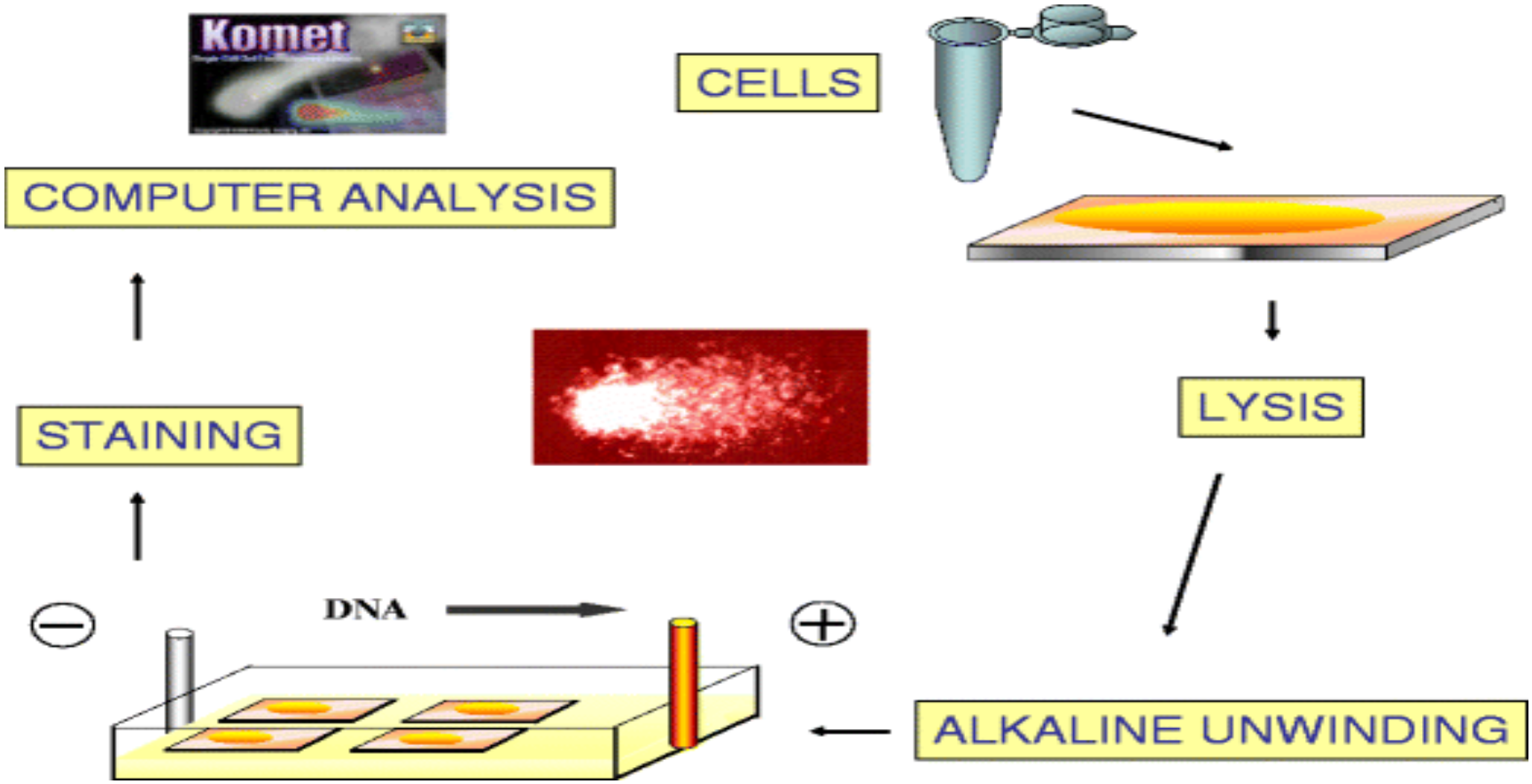


Fig. 2.3 The different steps of the alkaline comet assay including cell collection, lysis, DNA unwinding, electrophoresis and staining before running the comet analysis by computer program under the microscope. (adopted and modified from "Karlsson (2010)").

## 2.9 Observation of COO-PS-NPs cellular uptake and co-localisation

The uptake and co-localisation of ENPs to different organelles were studied in fixed and living BEAS-2B cells using confocal laser scanning microscopy (CLSM) technique.

### 2.9.1 Laser Scanning Confocal Microscopy (LSCM)

LSCM from Nikon (A1R-A1, Nikon Instruments, Surrey, UK) was used to visualize BEAS-2B cells exposed to a range of fluorescence COO-PS-NPs concentrations in order to investigate their internalisation inside these cells.

#### 2.9.1.1 Live cell preparation

BEAS-2B cells were cultured in a T-25 flask at 37ºC in a 5% $CO_2$ humidified incubator and split (when 70% confluent, at 1:25) in a glass bottom MatTek culture dish (35mm, MatTek Corporation, Ashland, USA) allowing cells to adhere and grow overnight at 37ºC in a 5% $CO_2$ humidified incubator. Next day, the media were replaced and cells were incubated with 20nm or 100nm COO-PS-NPs (25 and 150$cm^2$/ml for uptake investigation and 50$cm^2$/ml for Rhodamine staining) at 37ºC in a 5% $CO_2$ humidified incubator for various times (45min, 1h, 5h and 24h for uptake investigation and 24h for Rhodamine staining). After treatment, cells in each dish were washed with 2ml cell imaging media (CIM, Hank's balanced salt solution (HBSS), 10 µM, pH 7.4 and filtered) and another fresh 2ml CIM was added to the cells. Cells were imaged at 37°C by

LSCM using a 60 x oil lens against untreated cells as negative control and images were analyzed using NIS-Elements software.

#### 2.9.1.1.1 Mitochondria staining with rhodamine 123 in live cell

In some experiments, live cells were prepared (section 2.9.1.1) and incubated with 20µl rhodamine 123 (10µM final concentration) for about 30 minutes to stain the mitochondria. Cells were then washed twice in PBS (2 ml/well) and 2ml LHC-9 SFM were placed before imaging by LSCM. The emission signals were collected independently using a serial mode technique to avoid crosstalk between the channels and image was then processed using ImageJ software (1.47V, downloaded from the Research Services Branch, National Institute of Mental Health, Maryland, USA).

### 2.9.1.2 Fixed cells preparation

BEAS-2B cells were cultured overnight on glass cover slips (22x22mm, VWR) in a 6-well plastic tissue culture plate (until 70% confluent). They were then incubated with the 20nm or 100nm COO-PS-NPs (50$cm^2$/ml) for various time points (1, 6 and 24h for WGA-Lectin staining and 24h for DAPI staining) at 37ºC in a 5% $CO_2$ humidified incubator. Following treatment, media containing nanoparticles were discarded and cells were washed with 2ml PBS. Cells were fixed using 2ml neutral buffered formalin (NBF) solution (4% formaldehyde) per well and incubated at 4°C for 10min. NBF was then removed and cells were washed twice with 2ml PBS.

On a glass microscope slide (26x76mm, VWR), a drop of hydramount was put and the cover slip (with the treated cells) was smoothly placed upside down on that drop allowing the hydramount to disperse over the entire section and the cover slip edges were then sealed with nail polish to prevent the sample from drying out. Slides were imaged immediately by confocal microscopy or stored at 4°C in foil (protected from light) for up to two weeks.

#### 2.9.1.2.1 Nucleus staining with DAPI in fixed cells

Following cell fixation with formaldehyde (section 2.10.1.2), a drop of blue-fluorescent DAPI (4',6-diamidino-2-phenylindole) nucleic acid stain (Vector Laboratories Ltd., Peterborough, UK) in Vectashield mounting medium was put on a glass microscope slide (26x76mm, VWR). The cover slip (with the treated cells) was smoothly placed upside down on that drop to stain the nucleus allowing DAPI to disperse over the entire section. The cover slip edges were then sealed with nail polish to prevent the sample from drying out and slides were imaged immediately by confocal microscopy or stored at 4°C in foil (protected from light) for up to two weeks.

#### 2.9.1.2.2 Golgi apparatus staining with WGA-Lectin in fixed cells

Following cell fixation with formaldehyde (section 2.10.1.2), cells were stained for about 45 minutes with WGA-Lectin FITC (2µg/ml in PBS) and washed twice with PBS (2ml/well). A drop of either hydramount or Vectashield with DAPI was put on a glass microscope slide (26x76mm, VWR). The cover slip (with the treated cells) was smoothly mounted upside down on that drop allowing it to disperse over the entire

section. The cover slip edges were then sealed with nail polish to avoid sample drought and samples were imaged immediately by confocal microscopy (Leica) or stored at 4°C in foil (protected from light) up to two weeks.

### 2.9.2 Transmission Electron Microscopy (TEM)

Transmission Electron Microscopy (TEM) can be employed to observe localisation of ENPs within cellular compartments [Mühlfeld et al (2007)] using high magnification at very short wavelengths to get high resolution imaging capacity.

#### 2.9.2.1 Investigation of cellular uptake of suspended COO-PS-NPs by TEM

In details, BEAS-2B cells were cultured at a density of $5\times10^5$ in 5ml of LHC-9 SFM/well on type I rat tail collagen-coated glass cover slip in 6-well plate which was incubated overnight in a 5% $CO_2$ humidified incubator at 37°C. Cells at 85% confluence were then incubated with COO-PS-NPs (1:100 dilutions) for 24h at 37°C. At the end of treatment, media containing nanoparticles were discarded, cells were washed with warm PBS (2ml/well), primarily fixed (to preserve the cell structure) using 3ml of 2.5% glutaraldehyde (GA, glutaric acid dialdehyde) in 0.1M phosphate buffer solution (pH 7.4) for 24h in the fridge at 4°C to reduce autolysis (cell components self-destruction). Cells were then post-fixed for more preservation of the lipids and proteins using 1% osmium tetraoxide ($OsO_4$) in 0.1M phosphate buffer for 1h. Samples were dehydrated (2 x 15 minutes) in a graded ethanol series (50%, 70%, 90% and 100%) and then in propylene oxide (1-2 Epoxypropane, $C_3H_6O$). Samples were then put on a rotator in fume hood in propylene oxide/resin mixture (1:1) for 45 minutes to ensure thorough mixing followed

by full resin for about 1h to aid good infiltration. Resin was polymerized at 60°C overnight (for ~16h) and semi-thin sections (1μm) were cut with an ultra-microtome. Ultra-thin (approximately 80nm) sections, which can endure vacuum (in vacuum chamber) and heat (from electron beam) while imaging with TEM, were obtained afterward using a diamond knife. The sections were mounted independently onto a 200-mesh single slot supporting carbon-coated copper grids, stained with uranyl acetate (2%) and lead citrate before being visualized by TEM (JEOL 1200EX) operating at 80 kV to investigate intracellular localisation of these COO-PS-NPs within BEAS-2B cells.

## 2.10 Investigation of the role of calcium in COO-PS-NPs cytotoxicity

The 1,2-bis-(O-Aminophenoxy)-ethane-N,N,N',N'-tetraacetic acid tetraacetoxymethyl ester, abbreviated BAPTA-AM, is a derivative of the non-fluorescent membrane-permeable $Ca^{2+}$-specific chelator (as a selective sponge of $Ca^{2+}$) where the ester moiety is cleaved in the cell by esterase enzyme (Fig. 2.4) to release the BAPTA that can bind the $Ca^{2+}$ molecules in the cytoplasm [Collatz et al (1997)]. BAPTA-AM was employed in this study to treat the BEAS-2B cells before exposure to COO-PS-NPs in order to investigate the potential role of free cytosolic $Ca^{2+}$ in the mechanism of COO-PS-NPs cytotoxicity using the MTT assay (section 2.5) and in the ROS production using $H_2$DCF-DA assay (section 2.6).

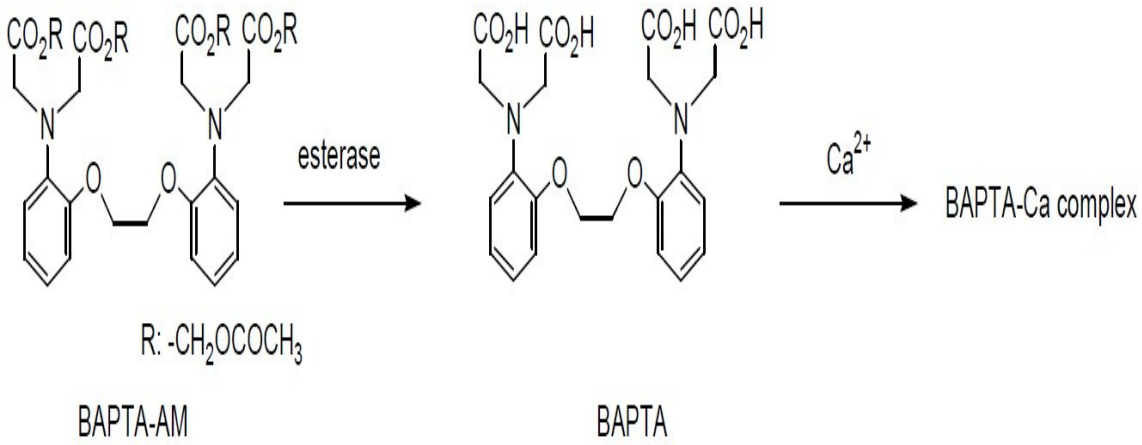


Fig. 2.4 Cleavage of ester moiety of BAPTA-AM by esterase enzyme releasing the BAPTA that selectively bind cytosolic $Ca^{2+}$ molecules forming BAPTA-$Ca^{2+}$ complex. (published online, adopted from: "website of Dojindo Molecular Technologies Inc.")

To evaluate the ability of BAPTA to protect cells against COO-PS-NPs and investigate the cellular death mechanism of these nanoparticles, BEAS-2B cells in 96-well plastic tissue culture were incubated with 5µM BAPTA-AM (Enzo Life sciences Ltd., Exeter, UK) for 1h before washing with 100µl PBS and re-incubation for 24h with concentrations (ranging 25 - 300 $cm^2$/ml) of the 20nm and 100nm COO-PS-NPs at 37ºC. Previously described MTT assay protocol (section 2.5) was applied and the absorbance was read against DMSO as blank and compared to cells exposed to COO-EPSNP but not treated with BAPTA-AM. The same BAPTA-AM treatment was also employed before treating BEAS-2B cell with 20nm and 100nm COO-PS-NPs (at concentrations of 75 and 300 $cm^2$/ml) and the earlier described $H_2$DCF-DA assay protocol (section 2.6) was then used for evaluating ROS generation.

## 2.11 Measurement of caspase-3/7 activity

These caspases can cleave after the aspartate residues with Asp-Glu-Val-Asp (DEVD) sequence of amino acids in intracellular substrates [Elmore (2007)] and many kits that use this pro-luminescent DEVD-based substrate are commercially available to assess the caspases activation following cell treatment with the apoptosis-inducing compound of interest.

BEAS-2B cells seeded in a white-walled 96-well plastic tissue culture plates were incubated individually with various concentrations (25, 50, 75, 150 and 300 $cm^2$/ml) of the 20nm and 100nm COO-EPSNP at 37ºC for 24h. After treatment, old media were aspirated, cells were washed in 100µl PBS, 50µl fresh LHC-9 SFM was added and the plate was left to equilibrate to RT. 50µl of the well-mixed Caspase-Glo 3/7 reagent (G8091, Promega UK Ltd, Southampton, UK) was added and the plate was wrapped in a foil. The foil-wrapped plate was gently agitated for 30sec on a plate shaker to mix the contents, incubated at RT for 1h and the luminescence readings were measured using a Bio-Tek FL 600 micro-well plate reader (Bio-Tek Instruments Inc, Winooski, USA) to monitor the activation of caspase-3/7 in these COO-PS-NPs treated BEAS-2B. Wells containing media alone were used as a blank.

## 2.12 Investigation of the mechanism of the COO-PS-NPs action

### 2.12.1 Measurement of the GSH level in cell-free system

Several eppendorf tubes containing 10µl GSH solution (0.1mg in 1ml $PO_4$-EDTA) were incubated on ice for 1hr with different concentrations (25 and 150 $cm^2$/ml) of the 20nm and 100nm COO-PS-NPs. Next, 50µl of ice-cold protein precipitation buffer (50% w/v trichloroacetic acid (TCA) in $PO_4$-EDTA buffer) was added to each sample before centrifugation at 13000rpm for 5min and the solutions were then transferred individually to new eppendorf tubes. 50µl of that solution were mixed individually in 3ml polystyrene fluorescence cuvettes (Sarstedt Ltd, Leicester, UK) with 0.9ml $PO_4$-EDTA buffer and 50µl freshly made O-Phthalaldehyde (OPT, 1mg/ml 100% methanol) (Fisher Scientific Ltd, Loughborough, UK). The samples were incubated at RT in a covered box with rocking for 15min and the fluorescence was then read (PerkinElmer LS50B luminescence spectrometer, PerkinElmer, Cambridge, UK) with $\lambda_{excitation}$ @ 340nm (slit width 2.5nm) and $\lambda_{emission}$ @ 420nm (slit width 4.0nm).

### 2.12.2 Evaluation of the GSH level in COO-PS-NPs treated cell lysate

To measure the GSH level in BEAS-2B cells, cells were seeded without treatment in 6-well plastic tissue culture plates at 37ºC in a 5% $CO_2$ humidified incubator for 24h. The media were aspirated before washing cells twice with 1ml of warm PBS and cells in each well were then scraped into 450µl ice-cold cell lysis buffer [0.1% Triton X100 in $PO_4$-EDTA buffer (100 mM $NaH_2PO_4$ and 5 mM $Na_2$-EDTA, adjusted to pH

8.0)]. About 10–15µl of each sample were retained in a separate tube for protein estimation and the remainder lysates were incubated independently in new eppendorf tubes with different concentrations (25 and 300 $cm^2$/ml) of the 20nm or 100nm COO-PS-NPs for 1h on ice. Then, 50µl ice-cold protein precipitation buffer (50% w/v trichloroacetic acid (TCA) in $PO_4$-EDTA buffer) was added to the lysates and the other steps of the GSH assay (section 2.7.1) in addition to Bradford assay procedures (section 2.7.2) were then applied as performed earlier.

## 2.13 Statistical Analysis

As mentioned before, all experiments were repeated at least three times unless mentioned. SPSS software (Stat Soft Inc., Tulsa, USA) was applied in performing the entire statistical analysis and $p \leq 0.05$ values were considered statistically significant. The multi-regression and factorial two--way ANOVA was performed for evaluating the significant differences between groups preceded by testing data for the presence of outliers, normal distribution (Kolmogorov–Smirnov's test) and homogeneity of variances (Levene's test). Results were presented graphically by Microsoft Excel and expressed as mean ± SEM that is represented by error bars.

# CHAPTER THREE:

# COO-PS-NPs PHYSICOCHEMICAL CHARACTERISATION

## 3.1 Introduction

The physicochemical properties of engineered nanoparticles (ENPs) determine their behavior in the biological test media and affect their uptake, clearance, sub-cellular internalisation, biological interactions, fate and the toxicity towards living cells [Nel et al (2009)]. Among the physicochemical properties of ENPs of importance are chemical composition, size (hydrodynamic diameter), shape, surface area, surface charge (zeta-potential) and tendency to form agglomerates in biological systems [Stone et al (2010)]. The physicochemical properties of ENPs should be investigated in stock solutions and in biological systems in order to (i) inform on how they would change in cell culture media and other systems and (ii) to understand the role and effects of these characteristics on cellular uptake and toxicity of ENPs [Poda et al (2011)]. Such information about the ENPs characteristics in stock solution and test media will facilitate our understanding of ENP behavior upon contact with cells and their fate in cell culture systems and help in interpreting the results from the cell culture studies.

The Scientific Committee on Emerging and Newly Identified Health Risks (SCENIHR) has declared that characterisation measurements of studied ENPs should be carried out in both the stock solution and after addition to biological system of interest [SCENIHR[a] (2007), SCENIHR[b] (2007)]. The committee also recommended that such measurements should be made in environments similar to and comparable with the real surrounding circumstances of exposure. Shape, size and surface charge of ENPs are among the most important properties that have been suggested to be characterised as they are of high importance in understanding of biological findings. Thus, characteristics of

COO-PS-NPs were studied in the experimental culture media and in cell (in some cases) in addition to the chemical composition of these COO-PS-NPs themselves and different techniques for characterisation were exploited such as DLS, ICP-MS and TEM. Below is a brief description of the basic principles of these techniques before indulging into the key findings.

Dynamic light scattering (DLS) is a fast and accurate scattered laser light intensity detection-based method for measuring the size of NPs in suspensions [Braun et al (2011)]. It has been mentioned that size measurement in biological media by DLS is likely to be inaccurate due to the influence of these media on the NPs sedimentation (agglomeration), however, DLS is widely used solution-based method for NPs characterisations [Baalousha et al[a] (2012)]. DLS measures the fluctuations of the scattered laser intensity over time, which occurs as a result of the Brownian motion (e.g. diffusion) of NPs in suspension. The measured fluctuations are then used to determine the diffusion coefficient of the particles which can be converted to a hydrodynamic diameter of spherical-shape NPs that represents the size of NPs in suspensions [Wang et al (2009), Brar and Verma (2011)].

The surface charge of NPs is another important physicochemical parameter, which determines the behavior of NPs in the test media and their interaction (i.e. uptake, translocation, etc.) with the organism. The surface charge is usually reported as Zeta (ζ-) potential of the NP and is widely used to experimentally characterise NPs [Mohanraj and Chen (2006)]. The ζ-potential is the electrical potential at the shear (slipping) plane of a nanoparticle and is proportional to (but not the same as) the surface potential [McFadyen and Fairhurst (1993)]. One of the commonly available analytical techniques to measure ζ-

potential is DLS using the laser Doppler electrophoresis, which enables measuring the speed of NPs under electric field effect, known as electrophoretic mobility. The ζ-potential can then be calculated from the measured electrophoretic mobility based on the difference (shift) in the frequency between the incident laser beam and the scattered light resulted from hitting the moving NPs in solution [Baalousha et al[b] (2012)]. The ζ-potential depends on the characteristics of both the surrounding media and the surface of the nanoparticle itself. Understanding and controlling the ζ-potential parameter (by changing the environment or altering the surface features) is crucial because it is very strongly correlated with particle aggregations (i.e. stability in dispersion) [Win and Feng (2005)]. Previous studies have shown that ζ-potential is strongly influenced by the properties of the cell culture media or the surrounding environment including pH (activity of hydrogen ions), ionic strength (concentration of free ions) and content of protein such as serum [Sabuncu et al (2012), Pavlin and Bregar (2012)].

The surface charge (represented by ζ-potential) and size (hydrodynamic diameter) of the 20nm and 100nm sized red fluorescently-labeled COO-PS-NPs were measured with a Malvern Nano-ZS Zetasizer instrument as described in the General Materials and Method (section 2.4.1).

Redox cycling metals, such as copper, iron and zinc are important transition metals that contribute in controlling different signaling and metabolic pathways, yet (if they escape the control mechanism) they bind to and interact with particular cell components (such as proteins and DNA molecules) leading to structure deformation, inactivation, dysfunction, DNA damage and cell toxicity [Flora et al (2008)]. These

metals were proposed to cause a ROS-induced oxidative stress in aerobic biological systems resulting in cell death if it exceeds the capacity of cell intrinsic antioxidant defense mechanism [Ercal et al (2001)]. Therefore, the chemical composition and impurities of ENPs needs to be well characterised and quantified to ensure that their toxicity is not related to metals impurities. Thus, the inductively coupled plasma mass spectrometry (ICP-MS) analysis of the inorganic COO-PS-NPs was performed on the stock suspension to characterise their chemical composition and obtain the elemental concentrations of specific metals (e.g. Fe, Zn and Cu). ICP-MS technique is a standard, highly sensitive (with low detection limits), precise and powerful analytical system that can be used for assessment of impurities and metal contaminants in a sample of ENPs [Scheffer et al (2008)]. Furthermore, transmission electron microscopy (TEM) with high spatial resolution is a useful well-established tool for the structural characterisation of ENPs mostly of sizes ≤ 100nm [Schrand et al (2010)]. Jones and Grainger cited several studies that have used this robust technique for characterising the particle size, shape and aggregation/dispersion state in solutions [Jones and Grainger (2009)]. TEM was applied in this study to verify the shape, size and dispersion status of COO-PS-NPs (20nm and 100nm) in stock solution.

## 3.2 Results

### 3.2.1 Hydrodynamic diameter and surface charge

The solutions used for the characterisation by Nano-ZS Zetasizer were prepared using 20nm and 100nm sized COO-EPSNs in a total volume of 1 ml including COO-PS-NPs in undiluted stock solution (SS), COO-PS-NPs (300 $cm^2$/ml) in MQ-$dH_2O$ as well as different concentrations of COO-PS-NPs (25, 50, 75, 150 and 300 $cm^2$/ml) in LHC-9 serum-free media (SFM). Characterisations of COO-PS-NPs solutions were carried out at various temperatures (37°, 20° and 4° C) to investigate the impact of temperature on the ζ-potential and the hydrodynamic diameter of these COO-PS-NPs. COO-PS-NPs characterisation was performed since size in addition to the surface charge and the surface chemistry are important parameters for predicting the aggregation, the interaction with cells and the potential adverse toxicological impact that they can cause.

The ζ-potential measurements demonstrated that all COO-PS-NPs were negatively charged in the prepared solutions and at different temperatures, with various concentrations and in distinct media. In addition, apart from solutions prepared by the 20nm and 100nm sized COO-PS-NPs in $dH_2O$, results (table 3.1) showed that the negative charges at 20° C measured in SS and in serum-free media (SFM) were lower in general than that at 37° C and at 4° C. In other words, the ζ-potential measured at 20° C declined compared with that at 37° C before it increase when recorded at 4° C reaching a higher level - to some extent - than that at 37° C (Fig. 3.1 and Fig. 3.3). For instance, the ζ-potential of 20nm and 100nm sized COO-PS-NPs in SS were -57.68 mV and -53.19

mV successively at 37° C (incubation temperature in cell culture) compared with -54.75 and -46.70 successively at 20°C (room temperature) and -63.90 and -55.89 successively at 4°C (storage condition temperature).

Moreover, with regard to the 20nm and 100nm sized COO-PS-NPs re-suspended in MQ-d$H_2O$ the negative charge increased as the temperature decreased, yet this increase was larger and more obvious in the 100nm sized COO-PS-NPs (mainly between 37° and 20° C). Furthermore, with increasing the concentration of 20nm and 100nm sized COO-PS-NPs in SFM - despite the 50 and 75 $cm^2$/ml - we can clearly notice an increase in the negative surface charge at constant temperature. Additionally, the negative charges of different concentrations of the 20nm sized COO-PS-NPs were decreased by 3-4 folds in SFM and the 20nm sized COO-PS-NPs were likewise decreased by 2-4 folds in SFM at various temperatures compared to the same sized COO-PS-NPs in SS or in MQ-d$H_2O$.

Concerning the hydrodynamic diameter (size) of both sized COOH-PS-NPs in SS, the outputs of the DLS instrument (Table 3.2) showed that their sizes are larger than the primary nominal sizes quoted by the supplier at all the three temperatures (i.e. 37°, 20° and at 4° C) investigated. The size of the 100nm COO-PS-NPs was increased by more than 12% whereas the size of the 20nm COO-PS-NPs was amplified by more than 300% at all the three temperatures. Moreover, the hydrodynamic diameters of both sized COO-PS-NPs measured in MQ-d$H_2O$ and LHC-9 SFM were also altered from that measured in SS which clearly indicates the effective role of the suspension media on the size of the ENPs. This alteration was detected at all various temperatures investigated. This increase in hydrodynamic diameter is in line with the decrease in the ζ-potential.

In addition, temperature can affect the size of ENPs as there were significant differences in the hydrodynamic diameters of both sized COO-PS-NPs measured at various temperatures. The results (Fig. 3.5 and Fig. 3.7) showed significant differences in the hydrodynamic diameters of the 100nm sized COO-PS-NPs measured at 37°, 20° and 4° C in MQ-d$H_2O$ and LHC-9 SFM, however, a significant difference in the 20nm sized COO-PS-NPs in LHC-9 SFM was only found between sizes measured at 37° and at 4° C. The highest hydrodynamic diameters of the 20nm sized COO-PS-NPs in LHC-9 SFM measured at 20° and at 4° C were recorded at the concentration of 300 $cm^2$/ml while the highest measured at 37° C was at the concentration of 75 $cm^2$/ml. On the other hand, the highest hydrodynamic diameters of the 100nm sized COO-PS-NPs in LHC-9 SFM measured at 20° C and at 4° C were recorded at the concentration of 25 $cm^2$/ml while the highest measured at 37° C was at the concentration of 75 $cm^2$/ml.

| | The measured surface charge of the 20nm COO-PS-NPs (mV) | | | | | | |
|---|---|---|---|---|---|---|---|
| °C | in SS | 300 $cm^2$/ml in $dH_2O$ | 25 $cm^2$/ml in LHC-9 SFM | 50 $cm^2$/ml in LHC-9 SFM | 75 $cm^2$/ml in LHC-9 SFM | 150 $cm^2$/ml in LHC-9 SFM | 300 $cm^2$/ml in LHC-9 SFM |
| 37 | -57.68 ± 3.05 | -51.91 ± 4.30 | -13.57 ± 1.16 | -13.67 ± 1.24 | -16.05 ± 1.70 | -15.09 ± 1.20 | -17.31 ± 1.88 |
| 20 | -54.75 ± 2.24 | -58.73 ± 1.58 | -12.53 ± 0.79 | -12.43 ± 0.57 | -13.19 ± 0.87 | -14.05 ± 1.16 | -14.97 ± 1.07 |
| 4 | -63.90 ± 2.62 | -66.36 ± 2.20 | -15.74 ± 0.82 | -15.28 ± 0.64 | -15.82 ± 0.72 | -16.58 ± 1.12 | -18.63 ± 1.04 |

| | The measured surface charge of the 100nm COO-PS-NPs (mV) | | | | | | |
|---|---|---|---|---|---|---|---|
| °C | in SS | 300 $cm^2$/ml in $dH_2O$ | 25 $cm^2$/ml in LHC-9 SFM | 50 $cm^2$/ml in LHC-9 SFM | 75 $cm^2$/ml in LHC-9 SFM | 150 $cm^2$/ml in LHC-9 SFM | 300 $cm^2$/ml in LHC-9 SFM |
| 37 | -53.19 ± 1.21 | -35.33 ± 4.37 | -15.24 ± 1.17 | -14.51 ± 1.38 | -17.08 ± 2.07 | -18.27 ± 2.02 | -21.44 ± 2.55 |
| 20 | -46.70 ± 1.50 | -62.88 ± 1.18 | -14.09 ± 0.50 | -14.16 ± 0.86 | -16.24 ± 0.95 | -16.29 ± 0.86 | -19.21 ± 1.30 |
| 4 | -55.89 ± 1.14 | -69.75 ± 1.06 | -17.04 ± 1.00 | -18.11 ± 1.00 | -18.47 ± 1.62 | -19.96 ± 0.88 | -23.02 ± 1.34 |

Table 3.1 The measurements of COO-PS-NPs surface charge at 37°C (incubation temperature), 20°C (room temperature) and 4°C (storage temperature). ζ-potential was measured in duplicate with total of ten samples ($n$=10) and was carried out in stock solution (SS), MQ-$dH_2O$ and serum free cell culture media (LHC-9 SFM). Different concentrations of the 20nm and 100nm nominal sized COO-PS-NPs were investigated in LHC-9 SFM because these concentrations were used for the cell treatment. Data of the surface charge values in this table represent the mean ± SD.

| | The measured size of the 20nm COO-PS-NPs (nm) | | | | | | |
|---|---|---|---|---|---|---|---|
| °C | in SS | 300 $cm^2$/ml in $dH_2O$ | 25 $cm^2$/ml in LHC-9 SFM | 50 $cm^2$/ml in LHC-9 SFM | 75 $cm^2$/ml in LHC-9 SFM | 150 $cm^2$/ml in LHC-9 SFM | 300 $cm^2$/ml in LHC-9 SFM |
| 37 | 61.760 ± 0.74 (PDI=0.383) | 58.914 ± 1.00 | 2083.60 ± 130.57 | 1979.20 ± 500.44 | 2635.20 ± 289.60 | 1715.20 ± 178.77 | 1912.20 ± 268.04 |
| 20 | 60.740 ± 0.44 | 55.000 ± 0.70 | 1312.60 ± 204.82 | 1547.16 ± 424.38 | 1154.42 ± 148.13 | 1657.40 ± 189.54 | 2016.60 ± 577.63 |
| 4 | 61.414 ± 1.10 | 52.426 ± 2.67 | 1069.22 ± 235.62 | 1711.40 ± 345.74 | 1280.80 ± 214.47 | 1117.36 ± 378.94 | 1839.80 ± 106.62 |

| | The measured size of the 100nm COO-PS-NPs (nm) | | | | | | |
|---|---|---|---|---|---|---|---|
| °C | in SS | 300 $cm^2$/ml in $dH_2O$ | 25 $cm^2$/ml in LHC-9 SFM | 50 $cm^2$/ml in LHC-9 SFM | 75 $cm^2$/ml in LHC-9 SFM | 150 $cm^2$/ml in LHC-9 SFM | 300 $cm^2$/ml in LHC-9 SFM |
| 37 | 115.960 ± 2.08 (PDI=0.06) | 135.920 ± 2.58 | 154.94 ± 5.20 | 164.64 ± 5.32 | 176.64 ± 9.21 | 172.08 ± 4.30 | 167.94 ± 2.52 |
| 20 | 113.880 ± 1.21 | 129.120 ± 1.10 | 264.52 ± 4.67 | 230.70 ± 2.90 | 245.34 ± 5.37 | 228.26 ± 2.37 | 203.94 ± 2.36 |
| 4 | 112.880 ± 3.71 | 107.218 ± 5.50 | 251.24 ± 8.94 | 220.88 ± 7.82 | 224.22 ± 7.84 | 235.92 ± 11 | 198.36 ± 8.06 |

Table 3.2 Summary of the measurements of COO-PS-NPs size at 37°C (incubation temperature), 20°C (room temperature) and 4°C (storage temperature). This hydrodynamic diameter was measured in duplicate with total of five samples ($n$=5) and was carried out in stock solution (SS), MQ-$dH_2O$ and LHC-9 SFM. Different concentrations of the 20nm and 100nm nominal sized COO-PS-NPs were investigated in LHC-9 SFM because these concentrations were used for the cell treatment. Data of the hydrodynamic diameter values in this table represent the mean ± SD. PDI refers to the polydispersity index.

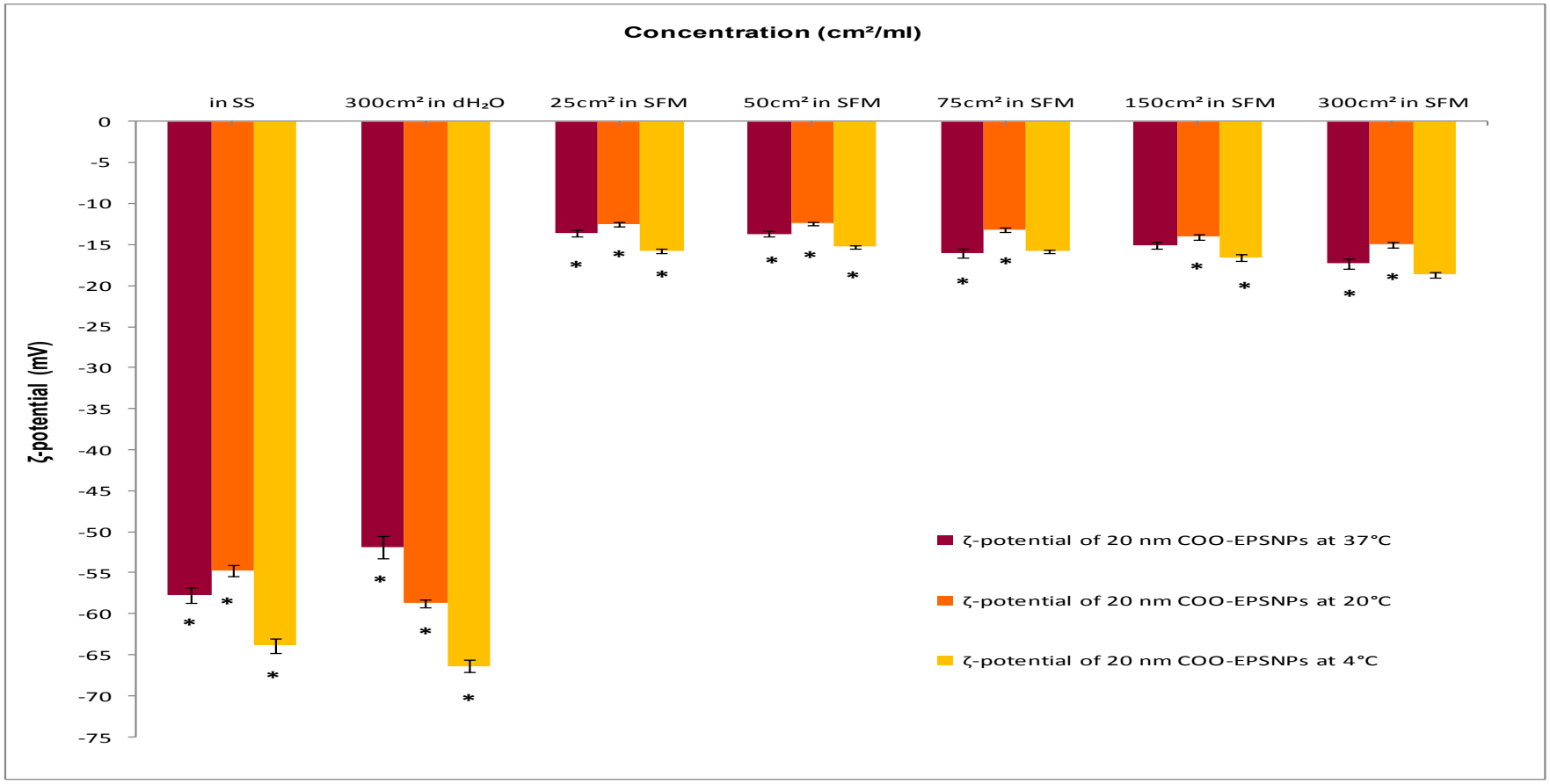


Fig. 3.1 The ζ-potential (surface charge) of 20nm COO-EPSNs in SS, in MQ-$dH_2O$ as well as in LHC-9 SFM revealed significant difference (*) between measurements recorded at 37° (dark red), 20° (orange) and 4° C (yellow). The ζ-potential was measured in duplicate with total of about ten samples ($n$=10). The error bars illustrated on the graph represent the standard error of the mean (± SEM).

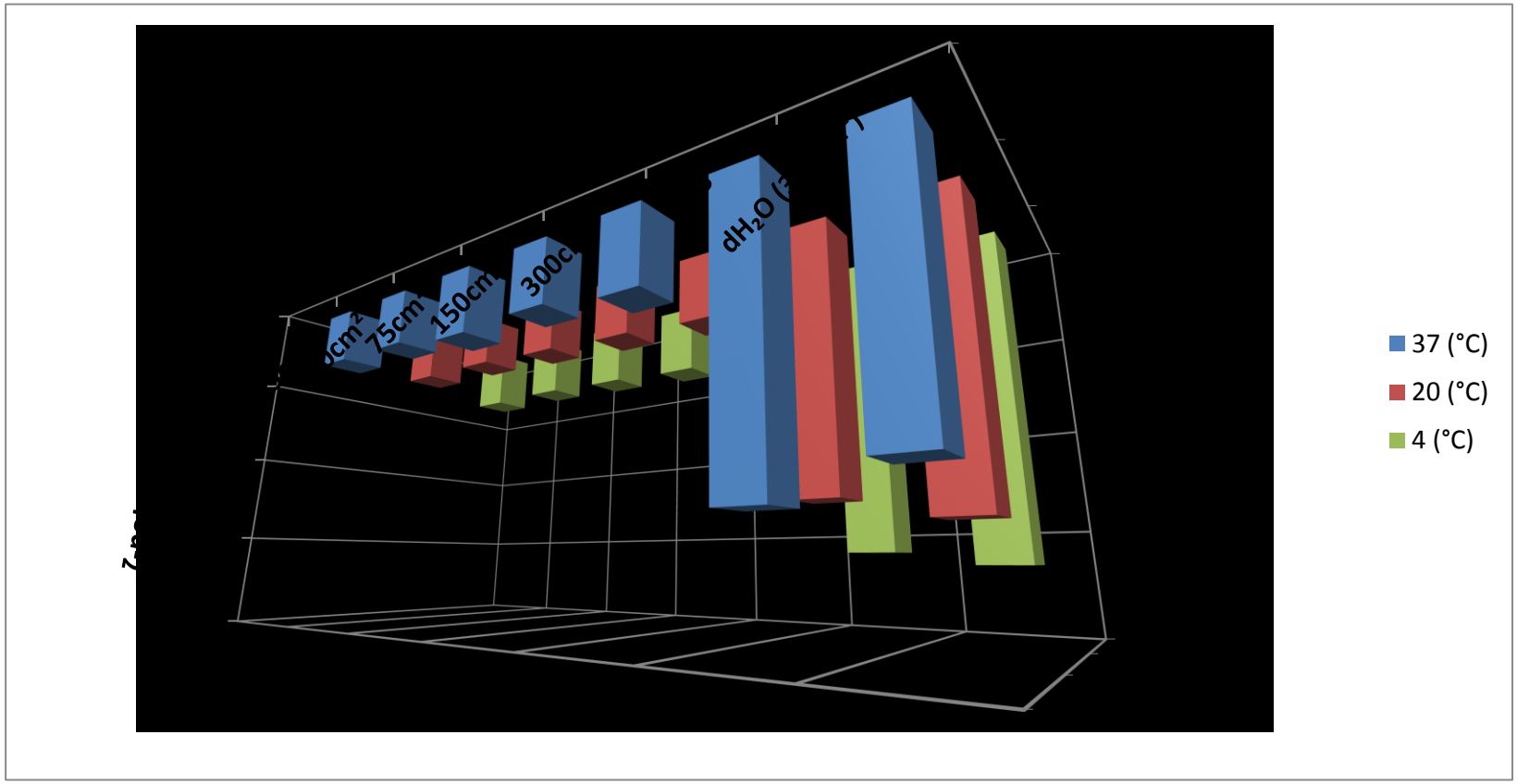


Fig. 3.2 This graph shows a 3-D plot of the ζ-potential (surface charge) against the different concentrations of 20nm COO-EPSNs in LHC-9 SFM, in SS as well as in MQ-$dH_2O$ and the temperature (at 37°, 20° and 4° C). This is to reveal the different parameters on one graph.

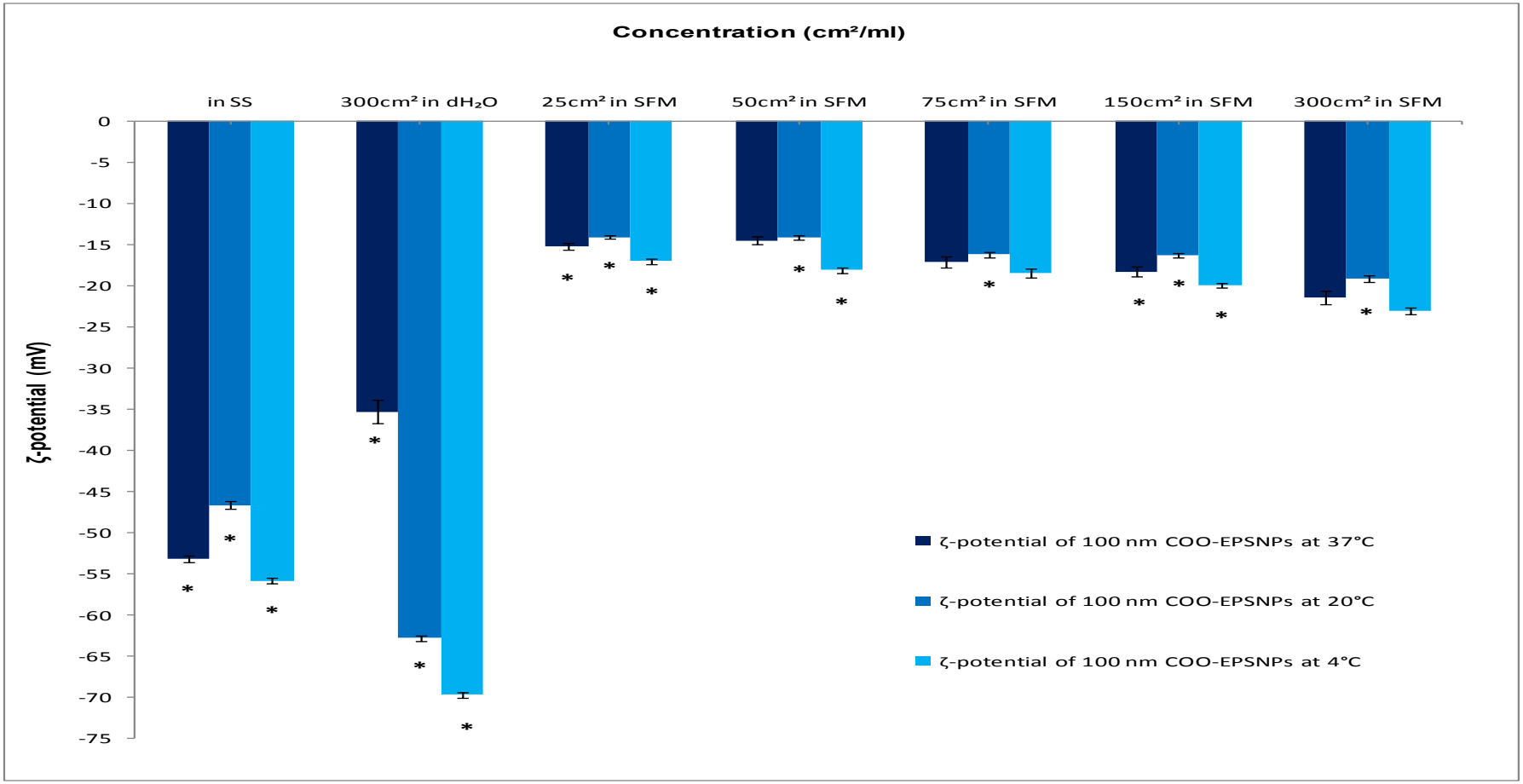


Fig. 3.3 The ζ-potential (surface charge) of 100nm COO-EPSNs in SS, in MQ-d$H_2O$ as well as in LHC-9 SFM revealed significant difference (*) between measurements recorded at 37° (navy blue), 20° (blue) and 4° C (turquoise). The ζ-potential was measured in duplicate with total of ten samples ($n$=10).The error bars illustrated on the graph represent the standard error of the mean (± SEM).

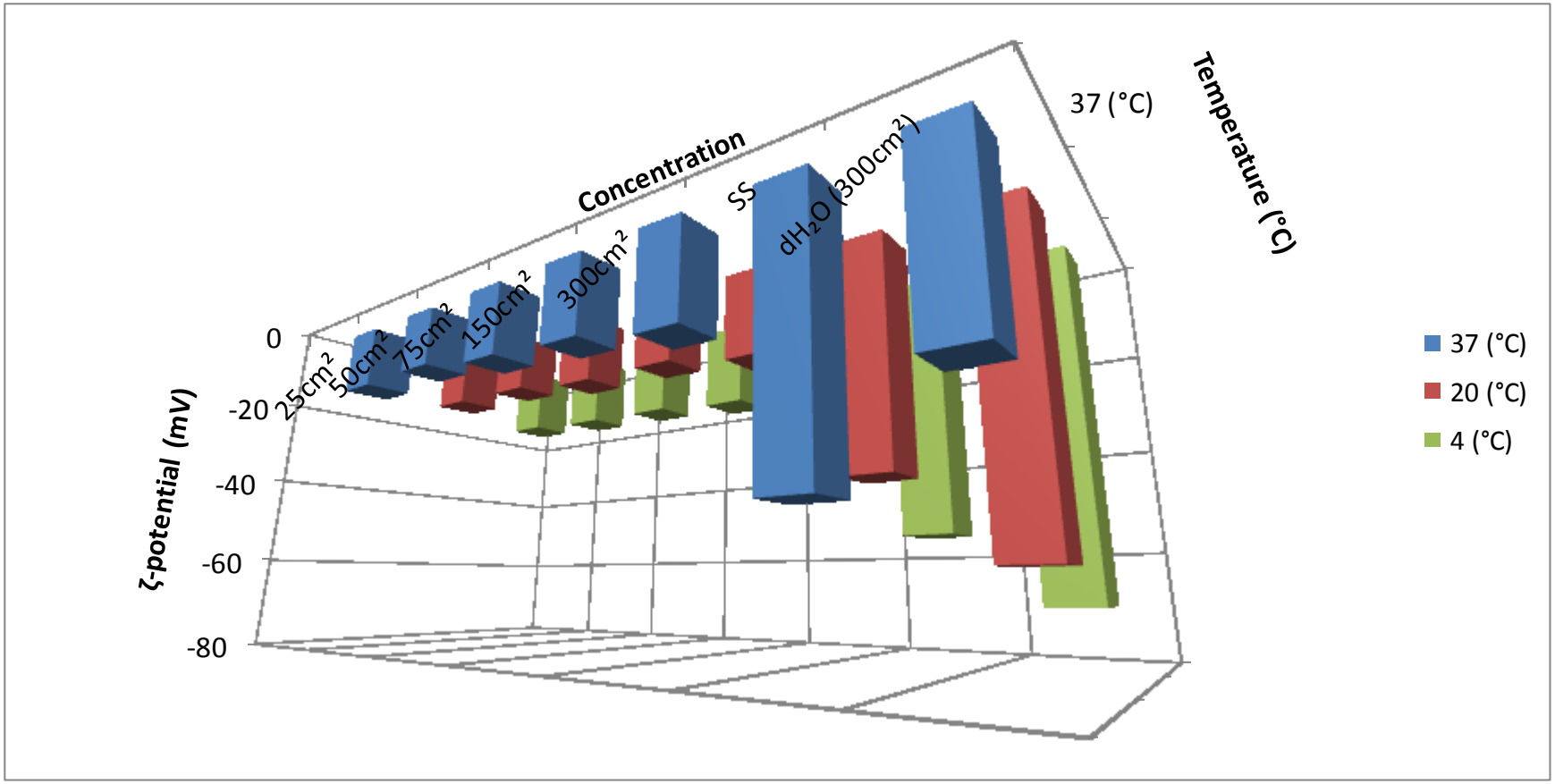


Fig. 3.4 This graph shows a 3-D plot of the ζ-potential (surface charge) against the different concentrations of 100nm COO-EPSNs in LHC-9 SFM, in SS as well as in MQ-$dH_2O$ and the temperature (at 37°, 20° and 4° C). This is to display the different parameters on one graph.

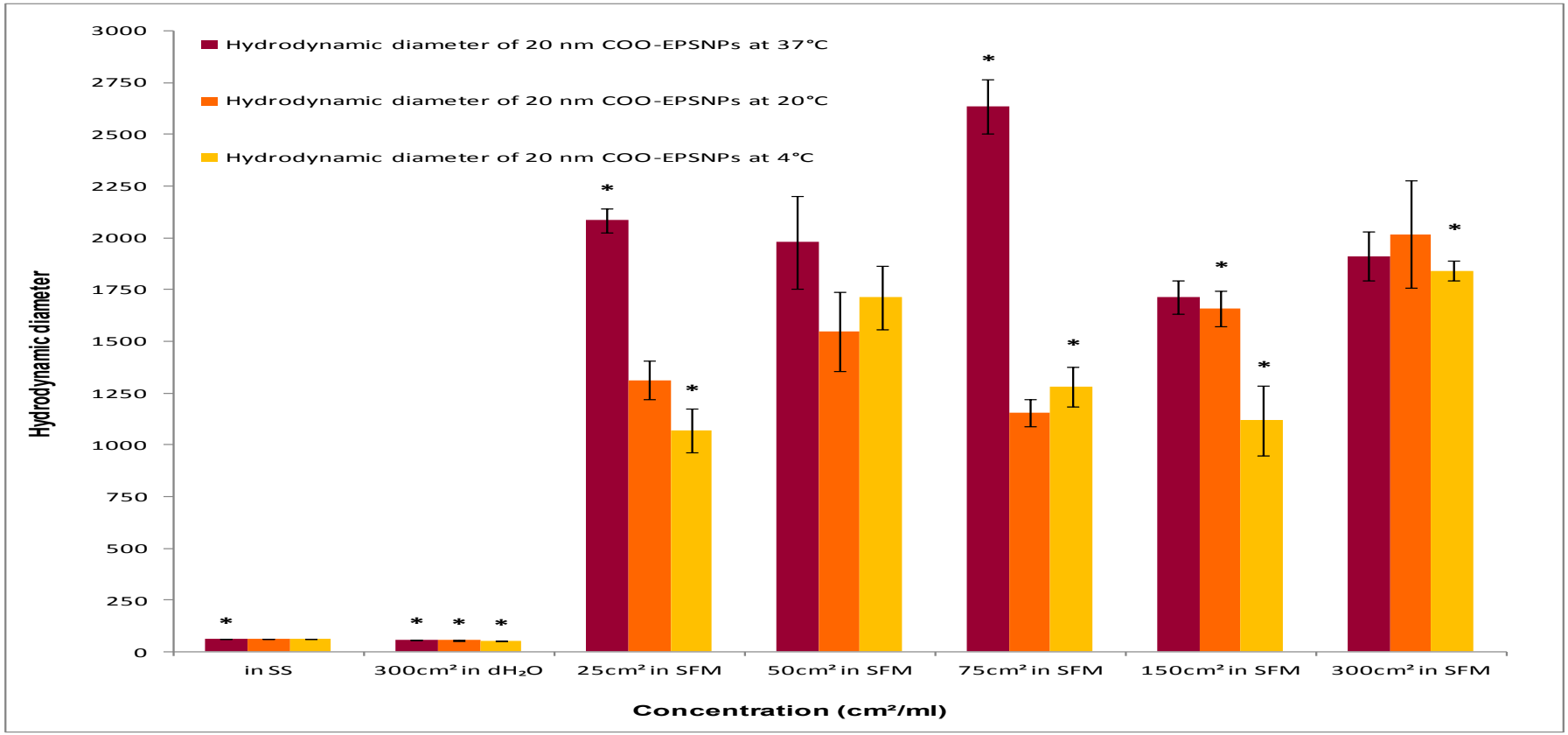


Fig. 3.5 The hydrodynamic diameter values of 20nm COO-EPSNs in SS, in MQ-d$H_2O$ and in LHC-9 SFM were measured at 37° (dark red) as well as at 20° (orange) and 4° C (yellow). The size of 20nm COO-EPSNs measured in LHC-9 SFM revealed significant difference (*) between 4° and 37° C. Significant difference in sizes of the COO-EPSNs were also observed in MQ-d$H_2O$ between all temperatures. Generally, the 20nm COOH-PS-NPs tend to aggregate heavily in the LHC-9 SFM. The hydrodynamic diameter was measured in duplicate with total of five samples ($n$=5). The error bars illustrated on the graph represent the standard error of the mean (± SEM).

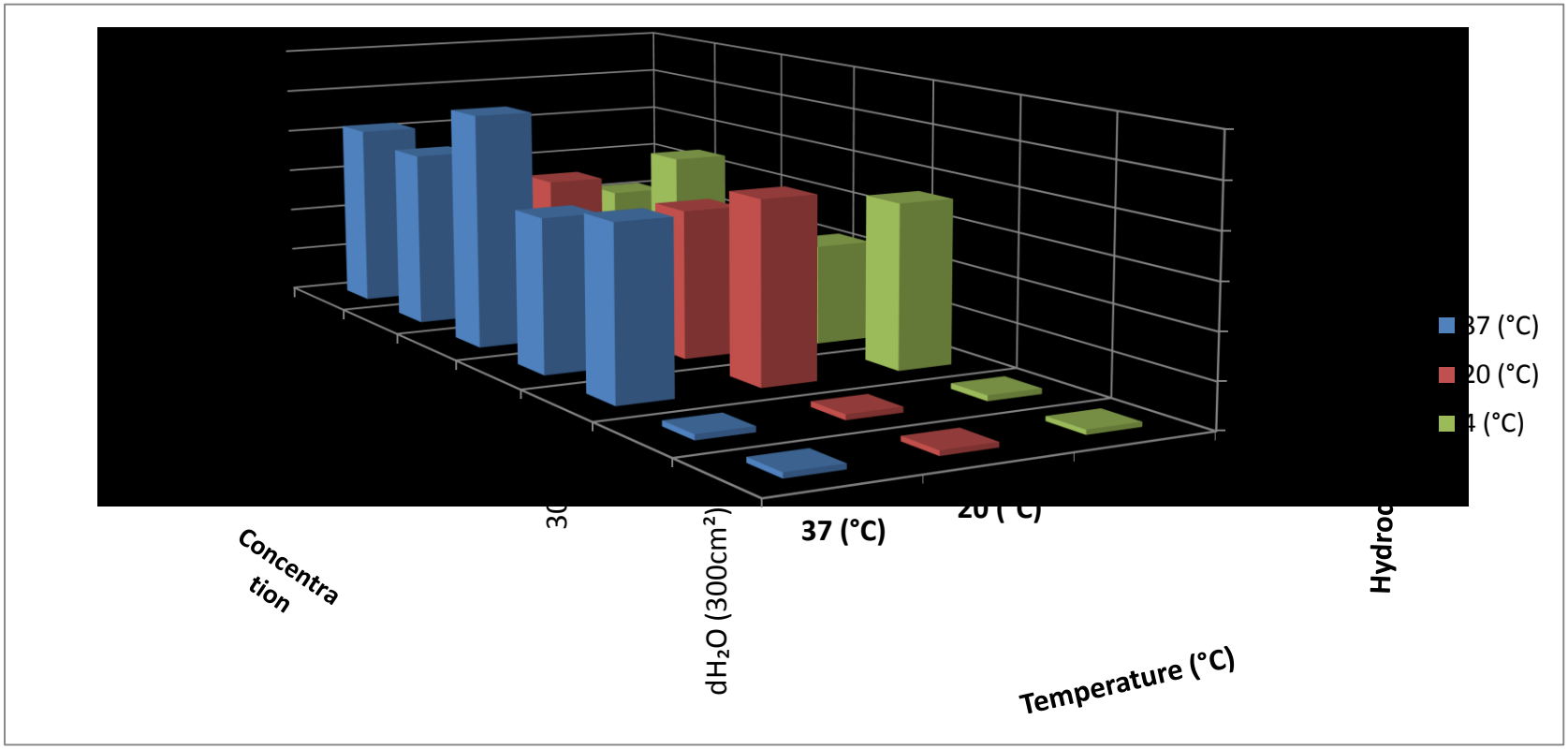


Fig. 3.6 This graph shows a 3-D plot of the hydrodynamic diameter against the different concentrations of 20nm COO-EPSNs in LHC-9 SFM, in SS as well as in MQ-$dH_2O$ and the temperature (at 37°, 20° and 4° C). This is to display the different parameters on one graph.

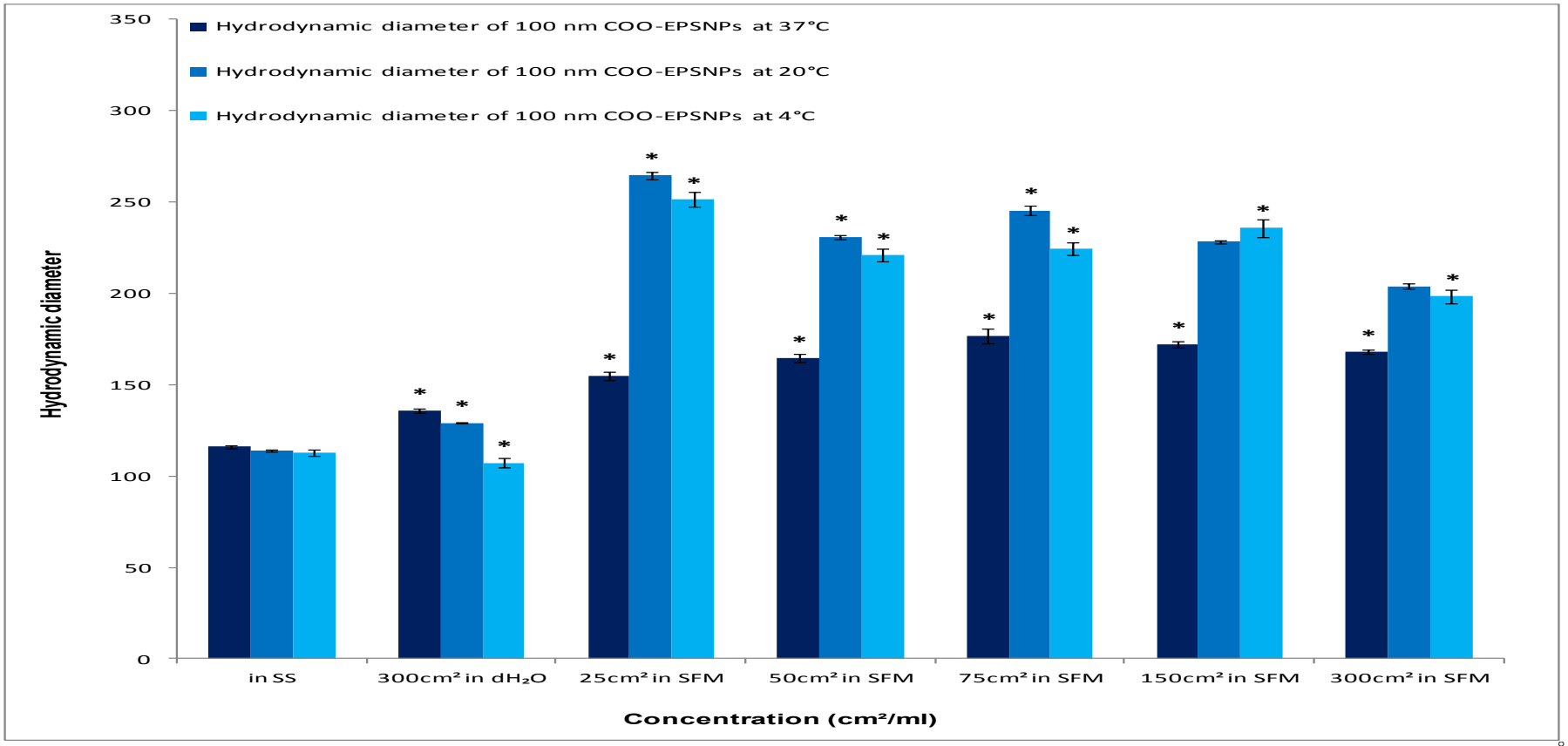


Fig. 3.7 The hydrodynamic diameter values of 100nm COO-EPSNs in SS, in MQ-d$H_2O$ as well as in LHC-9 SFM were reported at 37° (navy blue), 20° (blue) and 4° C (turquoise). No significant differences in size were monitored in high concentrations of the 100nm COO-EPSNs in LHC-9 SFM between 20° and 4° C. Significant difference in sizes of the 100nm COO-EPSNs in MQ-d$H_2O$ were observed between all temperatures but not in the 100nm COO-PS-NPs in SS. It seems that the 100nm COOH-PS-NPs tend to be more stable than their 20nm counterparts in all media. The hydrodynamic diameter was measured in duplicate with total of five samples ($n$=5). The error bars illustrated on the graph represent the standard error of the mean (± SEM).

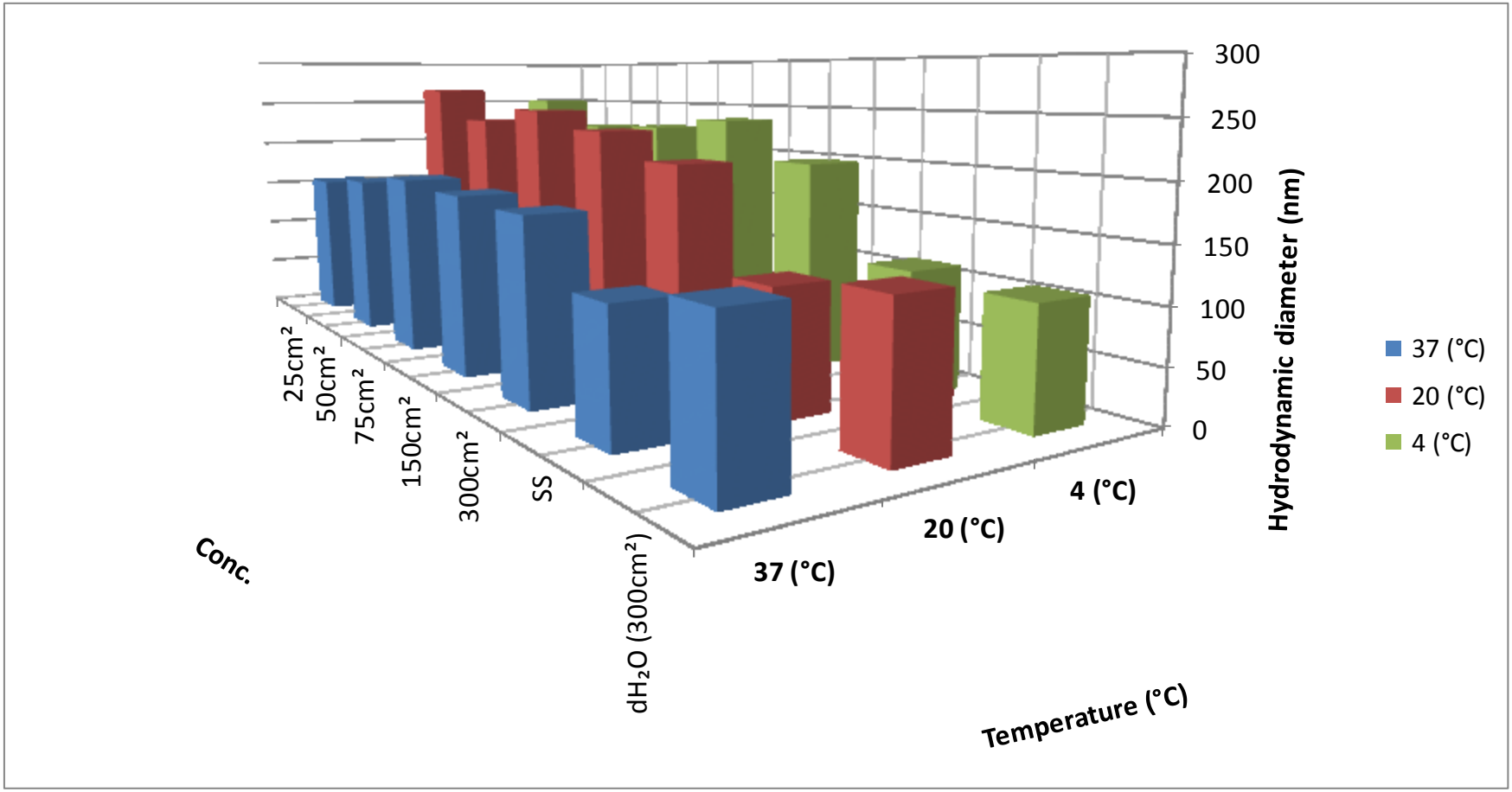


Fig. 3.8 This graph shows a 3-D plot of the hydrodynamic diameter against the different concentrations of 20nm COO-EPSNs in MQ-$dH_2O$, in SS as well as in LHC-9 SFM and the temperature (at 37°, 20° and 4° C). This is to display the different parameters on one graph.

### 3.2.2 Core size and morphology

The specifications of the 20nm and 100nm sized COO-PS-NPs regarding their shape and size were studied by TEM with a voltage of 80 kV (as described earlier in section 2.4.2). The images were taken in SS before running the other experimental studies to monitor their shape, compare their sizes with measurements taken by DLS method and correlate the results with the possible toxicological effects in BEAS-2B cells.

TEM images of these COO-PS-NPs (Fig. 3.9 and Fig. 3.10) revealed that both of the 20nm and 100nm sized COO-PS-NPs have spherical shapes. The ImageJ (which is an image processing) software was used to investigate the size distribution (i.e. frequency of number) of the 20nm and 100nm sized COO-PS-NPs and the results of analysis of TEM images of these nanospheres (Fig. 3.11) demonstrated that the average of size number of the 20nm COO-PS-NPs was around 27.4 ± 4.8nm while the number average of the 100nm COO-PS-NPs was about 86.0 ± 6.2nm. This indicates that their primary individual sizes did not appear to differ much from what was declared in the manufacturer bulletin. Both the 20nm and the 100nm sized COO-PS-NPs show aggregations that may be occurred during sample preparations, however the agglomeration level of the 20nm COO-PS-NPs was much higher than their 100nm counterparts.

A

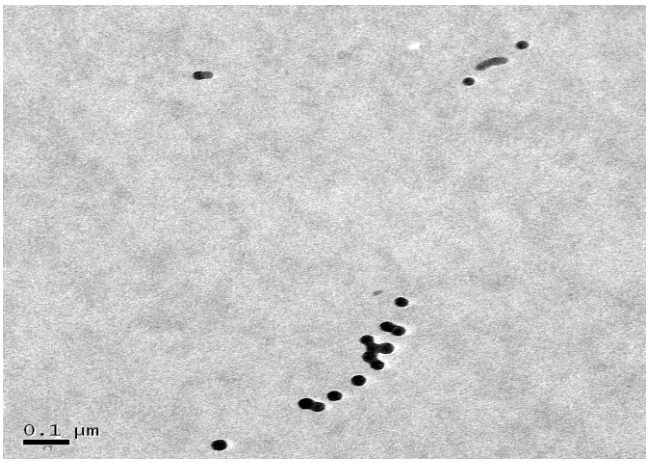


B

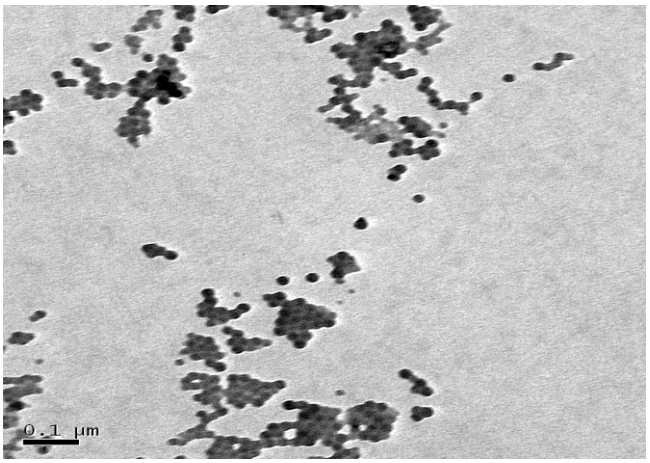


C

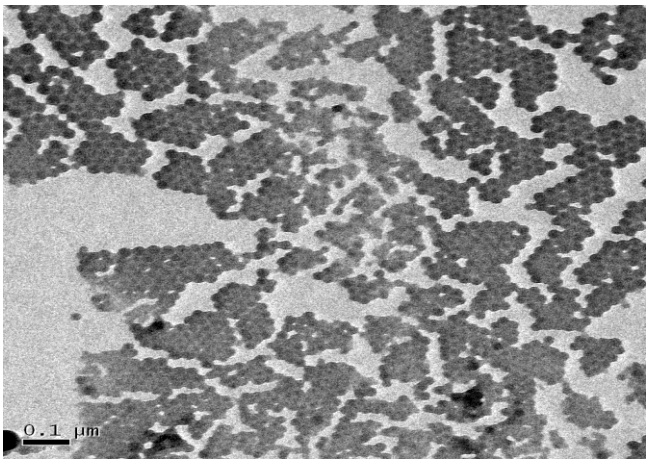


Fig. 3.9 TEM images of the 20nm COO-PS-NPs showing dispersed (A), slightly aggregated (B) and more aggregated (C) nanoparticles. However, agglomeration in image (c) might be due to the drying effect of the sample preparation The scale bar is 0.1 µm.

A

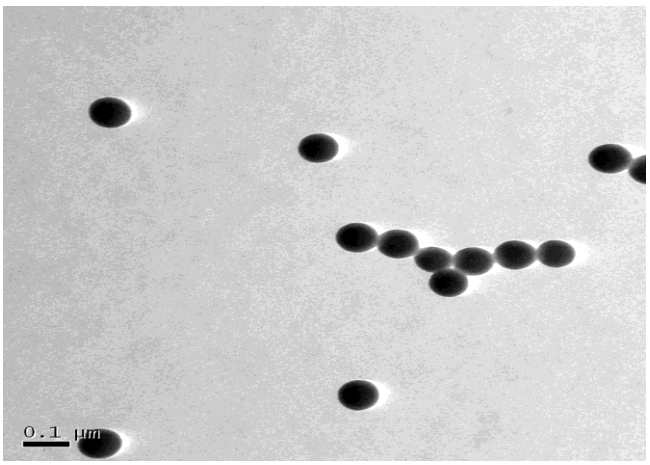


B

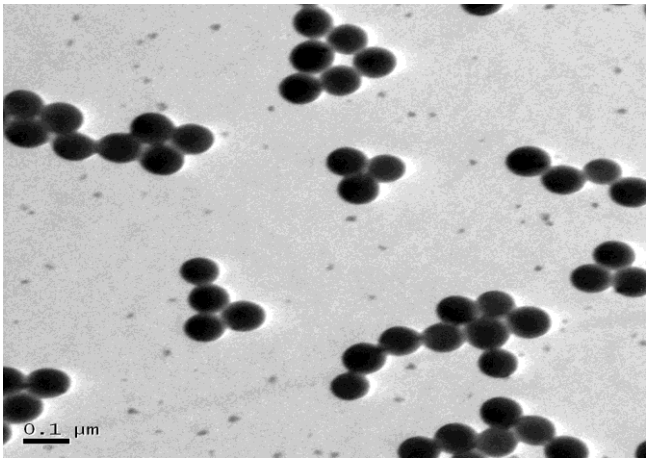


C

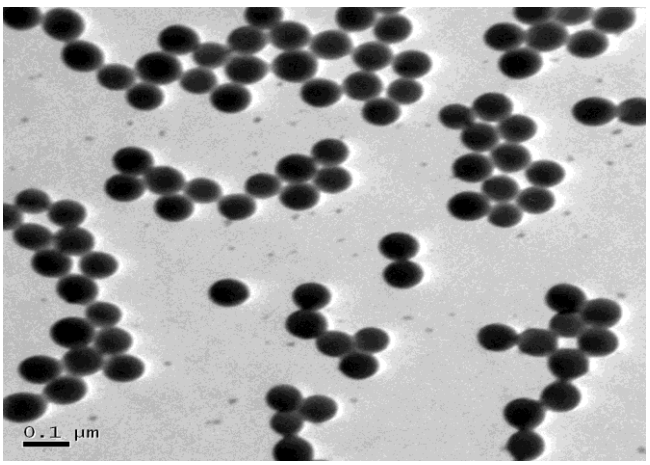


Fig. 3.10 TEM images of the 100nm COO-PS-NPs showing dispersed (A), slightly aggregated (B) and a bit more aggregated (C) nanoparticles. The scale bar is 0.1 µm.

A

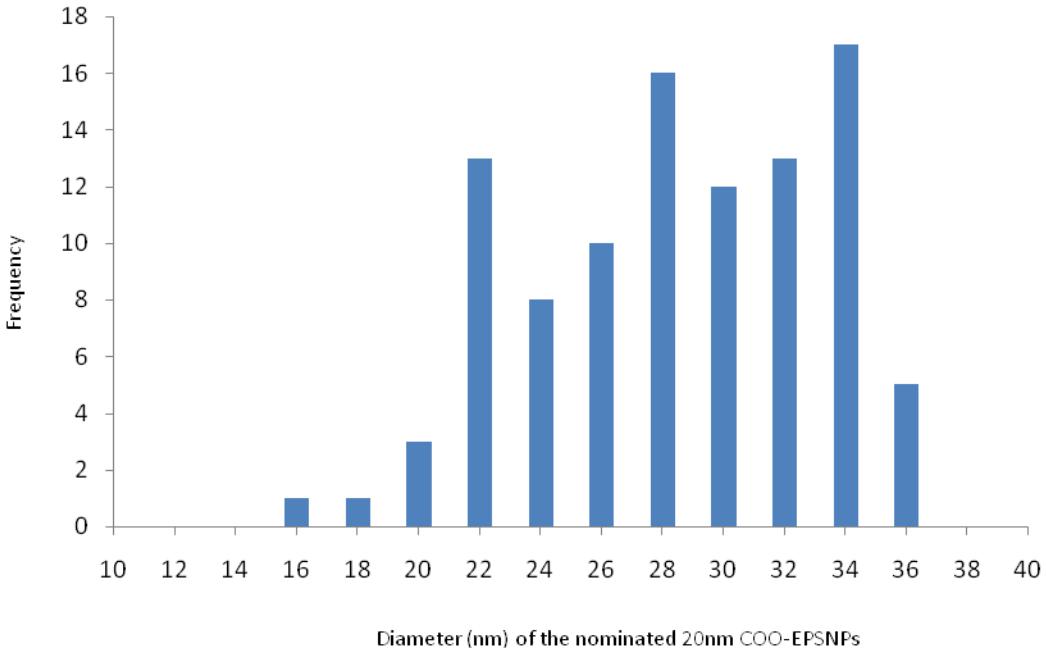


B

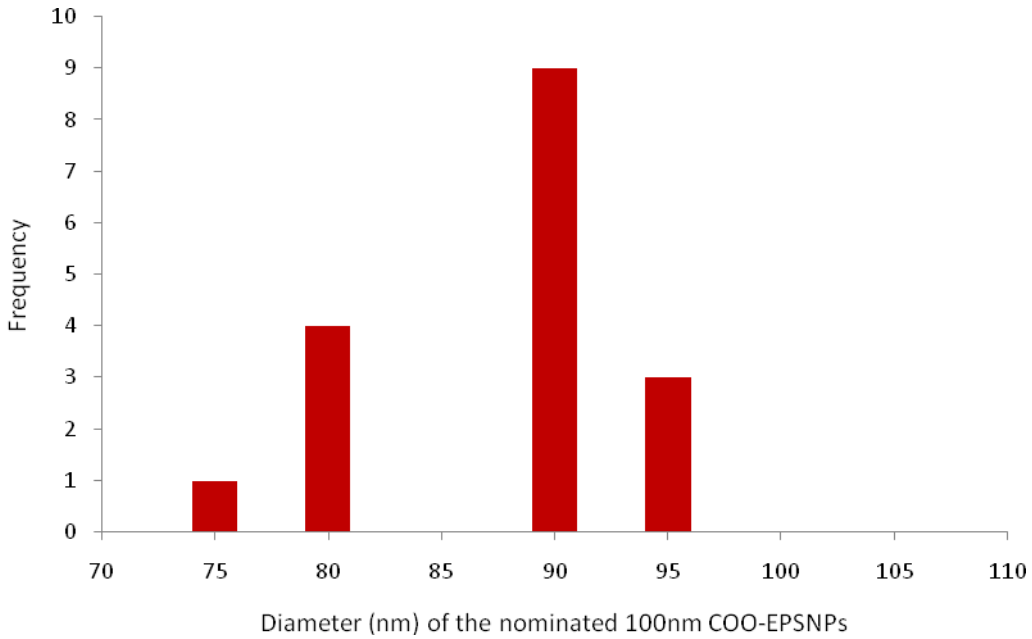


Fig. 3.11 Analyses of TEM images of the 20nm (A) and 100nm (B) sized COO-PS-NPs were conducted using ImageJ software to investigate the number of size distribution of these nanospheres. The results showed that the number average of the 20nm COO-PS-NPs was around 27.4 ± 4.8nm while the number average of the 100nm COO-PS-NPs was 86.0 ± 6.2nm

### 3.2.3 Chemical composition and impurities

The chemical composition of COO-PS-NPs stock solution was investigated for metal contamination using ICP-MS. Copper (Cu), iron (Fe) and zinc (Zn) were the three main chemical elements quantitatively determined in stock solution samples. In this ICP-MS method, the solution sample is vaporized and transported to inductively coupled plasma where it is ionized and the resulted cloud of ions is then analyzed by mass spectrometer to determine the elemental composition as the signal intensity is specifically and directly correlated to the observed content of chemical elements [Scheffer et al (2008)]. The results of the COO-PS-NPs samples analyzed by ICP-MS method illustrated that Cu was the lowest element and Zn was the highest element present in both samples. Nevertheless, these metals were significantly very low since there were only trace amounts of Cu (3.64, 3.17 ppb), Fe (61.95, 40.12 ppb) and Zn (93.2, 91.25 ppb) in the stock solution samples of the 20nm and 100nm COO-PS-NPs respectively (Fig. 3.12).

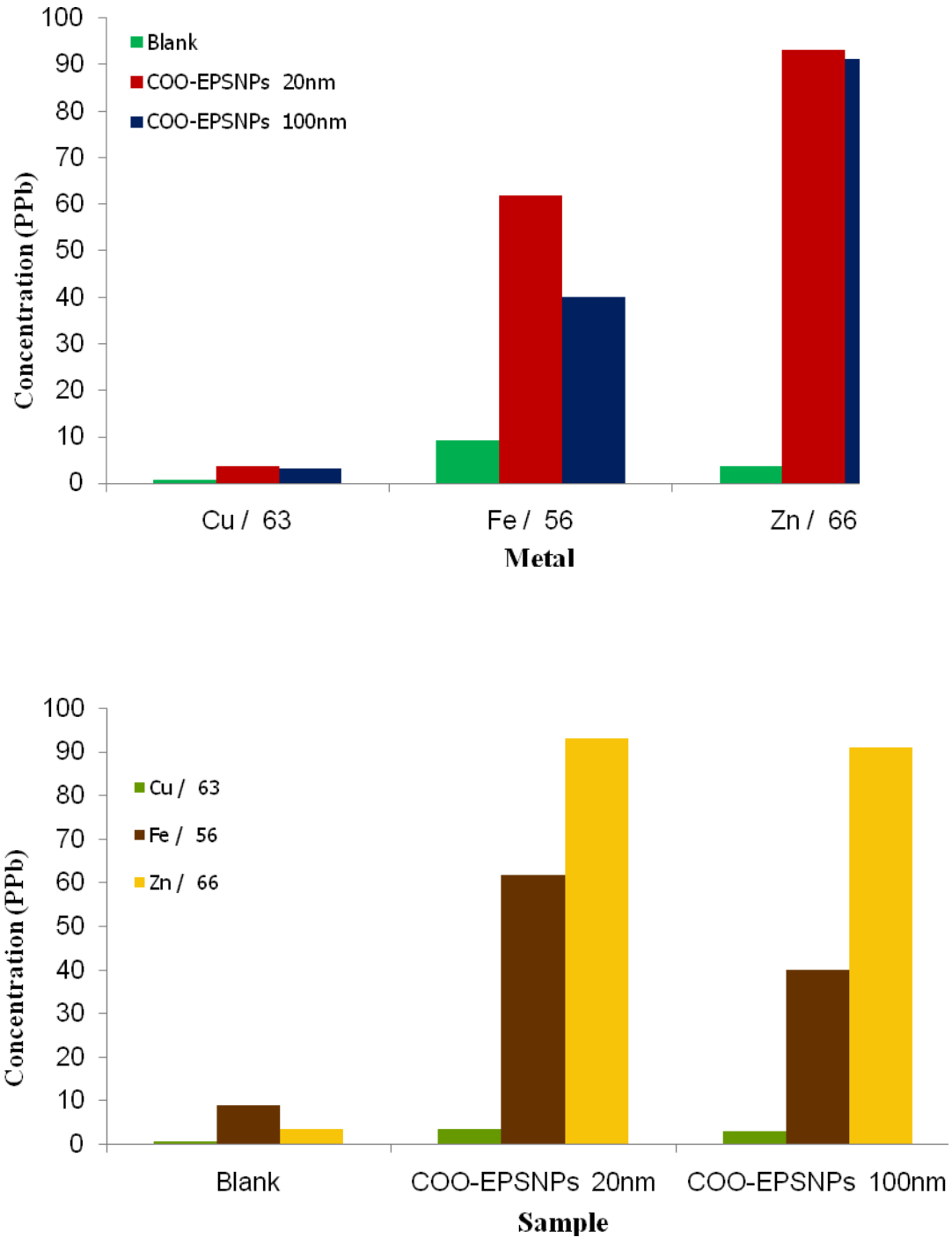


Fig. 3.12 Aanalysis of the chemical composition carried out two times ($n$=2) on stock solutions of COO-EPSNs shows only trace amounts (ppb) of Cu (3.64, 3.17), Fe (61.95, 40.12) and Zn (93.2, 91.25) in the 20nm and 100nm sized respectively. The results were plotted in this figure as concentration versus metal content (above) and as concentration versus sample (below).

## 3.3 Discussion

In the current study, COO-EPSNPs were physicochemically characterized using various techniques. Hydrodynamic diameter of COO-EPSNP was evaluated by DLS technique in solutions of different concentrations of the 20nm and 100nm sized COO-EPSNPs in LHC-9 serum free media to investigate NP aggregation status (i.e. dispersed particles unite together forming clusters) in cell culture media. Size measurements were also performed in the stock solution and in distilled water. The DLS method was applied as well for the surface charge measurements in the same aqueous solutions. The readings at low temperatures (4°C and 20°C) were recorded as well to explore the impact of the temperature change on the nanoparticle size and surface charge. The chemical purity of these nanoparticles was investigated to identify and quantify trace elemental composition while their shape and size were also assessed with the TEM.

The shape, size and dispersion of the 20 and 100nm sized COO-PS-NPs in stock solution were studied by TEM (see section 2.4.2) before running the other experimental studies. The TEM images (Fig 3.5 and 3.6) revealed that these COO-PS-NPs have spherical shapes and that their size is slightly changed. The diameter of these nanospheres measured with TEM was smaller than the hydrodynamic diameter obtained by DLS technique. This can be clearly seen when TEM images were analyzed using ImageJ software that measured the size distribution since the number average of the 20nm COO-PS-NPs was about 27.4 ± 4.8 nm while the number average of the 100nm COO-PS-NPs was 86.0 ± 6.2 nm. DLS technique is based on measuring the scattered light intensity of NPs and thus it calculates the z-average of the size of NPs (i.e. the diameter of core and surrounding shell) whereas the TEM is a number counting-based

system that measures the number average of diameter of only the core of NPs [Hassellov et al (2008)]. This would explain the difference in the measurement of the size of NPs resulted from the two techniques as the measurement of the nominated COO-PS-NPs (in particular the 20nm) by the DLS was higher than the size values of the same COO-PS-NPs measured by TEM. This difference could also be as a result of the bias caused by DLS instrument in consequence of the presence of small aggregates (even if they are small) formed in the solution that would affect the high sensitivity of DLS instrument [Farkas et al (2011)]. In general, characterization of NPs using several techniques might lead to inconsistent results that may vary significantly due to several reasons including (i) the difficulties and limitations of individual analytical method, (ii) the sample preparation difficulties that can end up with imprecise characterizations [Poda et al (2011)] or (iii) simply the fact that different techniques measure different aspects of the NPs [Shang et al (2014), Hassellov et al (2008)].

The size characterization results of the COO-PS-NPs at 37°C by DLS demonstrated aggregations of the 20nm COO-PS-NPs in the LHC-9 SFM (appeared as increase of hydrodynamic diameter of NPs) compared to these in the SS and in the MQ-$dH_2O$ (Fig. 3.5). In contrast, the 100nm COO-PS-NPs appeared to stay mono-dispersed (i.e. single particles or as loose agglomerates) in the stock solution at the room temperature (20°C) and limited accumulation was observed in SFM (Fig. 3.7). NPs adsorb surrounding proteins on their surfaces which would change the NPs size by forming a protein-NPs corona and this adsorption can mediate the toxicity of NPs and influence the human health [Kendall et al (2004), Cedervall et al[b] (2007]. The state of

NPs aggregation was reported to decrease inversely with increasing the particle size [Gharagozloo and Goodson (2011)]

The classical DLVO theory, (identified after independent work by the Russian scientists Derjaguin B. and Landau L., and Dutch scientists Verwey E. and Overbeek J. [Froberg et al (1999)]), suggests that the balance between the electrostatic repulsive forces (between the NPs that carry the same surface electric charge) and the Van der Waals attractive forces (between the electrons of one NP and the nuclei of another) would create an effective steady energy barrier that can preserve the dispersion condition of the NPs (i.e. prevent aggregation) in a colloidal system [Fubini et al (2010)]. The electrostatic repulsive forces are dominant and strong while the Van der Waals attractive forces are weak and are affected by distance between NPs [Fubini et al (2010)]. It is known that NPs dispersed in aqueous solution are subjected to Brownian motion (that is a randomly and continuously movement of particles in a suspension) [Shang et al (2014)] and would result in collision (hitting) of the suspended NPs with each other and with the surrounding fluid molecules.

The NPs dispersed in aqueous solution are in stable condition and would need the kinetic energy (generated by NPs collisions) to be high enough to overcome the total energy barrier and to disrupt the electrostatic boundary (between the nanoparticle outer surface and the medium layer surface) causing a drop in the ζ-potential [Freitas and Müller (1998)]. When the balanced energy barrier is disturbed, NPs get closer to each other and thus, the Van der Waals attractive forces would strive to pull them together into contact and cause them to agglomerate. High temperature has been proposed to increase kinetic energy since it can affect the Brownian motion of NPs in solutions [Freitas and

Müller (1998), Zhang et al (2012); Attachment Efficiency of Nanoparticle Aggregation in Aqueous Dispersions: Modeling and Experimental Validation]. This would reduce the energy barrier [Chen et al (2012)] stimulating consequently the NPs aggregation. In addition, Both the NP's size and concentration can also affect the aggregation kinetics [Metin et al (2014); Aggregation kinetics and shear rheology of aqueous silica suspensions]. This means that high temperature, high NP's concentration and small NP's size would all increase the aggregation kinetics, reduce the NPs dispersion stability and cause NPs aggregation.

In the current study, the ζ-potential of the 20nm sized COO-PS-NPs (Fig. 3.1) measured at high temperatures (20° and 37°C) was found generally less than that measured at low temperature (4°) which might indicate that increasing the temperature caused a decrease in the total negative charge of the COO-PS-NPs (most clear in the MQ-$dH_2O$). Furthermore, the ζ-potential of both sized COO-PS-NPs diluted in LHC-9 SFM were significantly smaller than the equivalent sized COO-PS-NPs in the SS or in the MQ-$dH_2O$ at all concentrations investigated (Table 2). This decrease in ζ-potential is perhaps due to (i) adsorption of protein molecules present in the LHC-9 SFM onto the surfaces of COO-PS-NPs [Dos Santos et al (2011)] and/or (ii) effective neutralization of COO-PS-NPs charge occurred by interactions with divalent cations of salts in the surrounding media [Wei and Khun (2014)]. This drop in ζ-potential would consequently decrease the electrostatic repulsion between NPs reducing at the end the stability of the COO-PS-NPs and increasing their tendency to aggregate [Wei and Khun (2014)]. The data showed that the decrease of the value of the negative charge seems to be directly proportional to decreasing concentrations of COO-PS-NPs (of the 20nm or 100nm) in the culture media.

This would suggest that more anions (COO-) with negative charge are present in the high concentrations of COO-PS-NPs solutions compared to fewer NPs in low concentrations of COO-PS-NPs where cations in the media can neutralize the negative charge and so decrease the total negative charge.

NPs that have a high ζ-potential (above +/- 30 mV) are stable in suspension because charges on the particle surface act to enhance the repulsive forces between particles minimizing the particles attractions and preventing their aggregation [Mohanraj and Chen (2006), Bihari et al (2008), Gowda et al (2009)]. In other words, the higher the ζ-potential (in number not in value) is, the higher the repulsion between the NPs, the higher the energy barrier and the more stability status (dispersion of these nanoparticles) in the solution. According to that, the decrease in the ζ-potential of the COO-PS-NPs observed at high temperature (37°C) would directly have an impact on dispersion state of the NPs as they tend to aggregate due to the loss (or decline) of the inter-particles repulsion leading to size augmentation.

In summary, the electrostatic repulsive forces are dominant and strong enough to resist agglomeration by maintaining the equilibrium energy state and preventing the COO-PS-NPs from attracting each other through keeping appropriate distance between these NPs, according to the classical DLVO theory. Thus, the COO-PS-NPs would be in a state of dispersion in a solution. Increasing the temperature increases (e.g. 37C) would accelerate the Brownian motion of these COO-PS-NPs (mainly at high concentrations of the 20nm COO-PS-NPs) and increase the kinetic energy to overcome the total energy barrier allowing the NPs to get close to each other to the extent that Van der Waals forces would attract them to each other and get them in contact causing agglomeration.

However, the stability of NPs solution is yet a complicated issue and other forces such as the acid-base (AB) forces (including the hydrogen-bonding force, hydrophobic interaction force and hydration forces) might play a role in administrating the stability of NPs and have been suggested therefore to be taken in consideration (by involving them into what is known as the extended DLVO theory) to give a more accurate explanation for the NPs agglomeration [Petosa et al 2010, Chen et al (2012)].

Furthermore, the charge of NPs is important for their stability and salts have been proposed to electrostatically obscure this charge causing NPs aggregation [Soenen et al (2011)]. Charge neutralizations of the COO-PS-NPs might therefore have taken place due to COO-PS-NPs interactions with salts present in culture media leading to a drop in the stability of the NPs and cause NPs agglomeration. In addition, it is also possible that proteins in the culture media may have higher affinity to bind and coat the 20nm sized COO-PS-NPs which have larger surface area for interaction compared to the 100nm COO-PS-NPs although LHC-9 SFM contain low protein compared to normal serum-supplemented medium. Low aggregation occurred in the 100nm COO-PS-NPs can be attributed to the difficulties for the protein molecules to completely enclose the large size (of 100nm) COO-PS-NPs and consequently their size have partially increased to some extent but they overall stay more stable (Fig. 3.7). Proteins are known to instantly be adsorbed on the surface of NPs forming a coating surface, known as protein corona [Cedervall et al[a] (2007), Lynch and Dawson (2008)]. This protein corona can mediate the NPs reactions in biological systems through several mechanisms including modification of the characteristics of NPs surfaces, amendment of the active function of protein,

protein content reduction in the biological system and increase of tendency of NPs for aggregation [Fubini et al (2010), Lynch et al (2013)].

The analysis of the Cu, Fe and Zn in the COO-PS-NPs sample in stock solution demonstrates that there were only trace amounts of these elements present in the COO-PS-NPs (Fig. 3.12). These results showing very low concentrations of elements are significant as they would show that the possible toxicological impact of these COO-PS-NPs (if there are any, see chapter 5) are unlikely be related to metal elements content. Moreover, it is worthy to mention that these concentrations were in the stock solution and the dilution of the COO-PS-NPs by the media would make the amount of the elements even smaller.

# CHAPTER FOUR:

# UPTAKE, INTERNALISATION AND CO-LOCALISATIOIN

## 4.1 Introduction

The assessment of the cellular uptake of ENPs is of fundamental importance as particles must penetrate across the cell membrane and get into the cells before they can cause any cell-specific damage and hence understanding internalisation of particles into cells is crucial for the risk assessment of the ENPs-containing products in order to predict their consequences in the human body [Lovrić et al (2005)]. In addition, it has been suggested that ENPs-induced biological effects may be due to ENPs internalisation and co-localisation to specific organelles such as mitochondria [Li et al (2003), Oberdörster et al[b] (2005)] or near the nucleus [Bhattacharya et al (2009)] causing oxidative stress, DNA damage and cell death following cellular accumulation of ENPs [Oh et al (2010)]. Moreover, ENPs intracellular co-localisation and distribution to specific organelles can be investigated using various fluorescent markers for staining and distinguishing definite cellular compartments. In the current study, co-localisation experiments were conducted to image the intracellular fate of COO-PS-NPs and to investigate whether there was any specific uptake by specific organelles. Such information may aid in understanding the mechanism behind their possible toxicological effect on cells and in monitoring the ENPs delivery as drug-carrier systems.

Several experimental techniques are available for the study of uptake and co-localisation on ENPs including advanced microscopic techniques such as confocal laser scanning microscopy (CLSM) and transmission electron microscopy (TEM) as well as spectroscopic techniques such as fluorescent flow cytometry. Each of these approaches has advantages and disadvantages for the study of NPs uptake. The advantages of

implementation of each of these techniques to study NPs uptake have been discussed briefly below.

TEM is a commonly used method for ENPs detection in biological systems and assessment of uptake into sub-cellular components (e.g. mitochondria, Golgi apparatus, endoplasmic reticulum) at high spectral resolution [Lee et al (2010)]. Nevertheless, it is sometimes difficult to distinguish between the ENPs and the other cell components in the 2-dimensional black and white images because some organelles are dense and have the potential to cause scattering of high-velocity electrons [Nagashima et al (2011)]. This is particularly a problem for PS-NPs which are not electron dense like metal NPs and also prone to artifacts during sample preparation. In addition, the cell imaging is not easily possible since cultured cells need to undergo various stages of toxic, is cost- and time-consuming and complicated sample preparation procedure required for imaging following the desired time and dose treatment including fixation, dehydration, thin sectioning and staining with heavy-metal dyes [Lee et al (2010), Schrand et al (2010), Mühlfeld et al (2007)]. This would also make live imaging not possible. In contrast, CLSM allows live cell imaging and can be used to perform time-course studies but is complicated and the use of a high-energy laser beam over long time can result in bleaching of fluorescent ENPs making it difficult to distinguish the fluorescent ENPs within the cell [Frigault et al (2009)]. In addition, the repeated exposure of living cell to highly-intensive illumination may cause excitation of fluorescence ENPs and hence initiate phototoxicity on account of the oxygen-dependent reaction of free radicals that can damage sub-cellular compartments and lyse the cell [Frigault et al (2009)]. Table 4.1 summarises the advantages and disadvantages of TEM and CLSM.

| | TEM | CLSM |
|---|---|---|
| Adv. | 1. Ideal tool used commonly for monitoring and detection of non-fluorescent ENPs in cells.<br>2. High resolution so it provides information about size and morphological structure.<br>3. Evaluation of cellular distribution and uptake into sub-cellular components (e.g. mitochondria, Golgi apparatus, endoplasmic reticulum) at high spectral resolution. | 1. Allows imaging of ENPs in live cell.<br>2. Allow performing time-course studies. |
| Disadv. | 1. Complicated, time-consuming and costly procedures required for optimal sample preparation including fixation, dehydration, thin sectioning and staining with heavy-metal dyes.<br>2. Possibility of toxicity of cultured cells through various stages of sample preparation.<br>3. Artifacts due to sample preparation.<br>4. Difficulty in distinguishing the ENPs (particularly PS-NPs which are not electron dense-like metal NPs) from other cell components in 2-D black and white images as some organelles are dense and have the potential to cause scattering of high-velocity electrons resulting in unwanted interfere.<br>5. Live imaging is not possible. | 1. Can result in bleaching of fluorescent ENPs due to the use of a high-energy laser beam over long time which might make it difficult to distinguish the fluorescent ENPs within the cell.<br>2. Repeated exposure of living cell to intensive illumination may cause phototoxicity leading to damage of sub-cellular organelles and cell lysis due to the reaction with free radicals. |

Table 4.1 The advantages and disadvantages of TEM and CLSM techniques used for imaging of ENPs in cells.

Quantification of fluorescently labelled ENPs uptake is generally performed by flow cytometry, however, real NP uptake evaluation by flow cytometry method presents a challenge because of the difficulties in distinction between the internalised ENPs and the plasma-adsorbed ENPs upon their interaction with the cell surface following exposure [Dausend et al (2008), Vranic et al (2013), Gottstein et al (2013)]. Thus, these different approaches (flow cytometry, CLSM and TEM) were applied in this study to overcome

their own limitations and validate the results regarding the COO-PS-NPs basic cellular uptake and co-localisation.

## 4.2 Results

### 4.2.1 Uptake of COO-PS-NPs into BEAS-2B cells

#### 4.2.1.1 Quantification by flow cytometry

In summary, after 24h incubation of BEAS-2B cells independently with different concentration of COO-PS-NPs, cells were washed three times with PBS (to remove the membrane-bound COO-PS-NPs), trypsinised, centrifuged and re-suspended in PBS before analysis by flow cytometry (Becton Dickinson FACS Calibur from BD Science, San Jose, USA) equipped with a 488nm laser [Zucker et al (2010)] (section. 2.6). Data acquisition was performed by CellQuest software (Pro-V 5.2.1, BD Science) and the results were analysed by Weasel program (V 3.1, WEHI, Melbourne, Australia) and reported (Fig. 4.1) as the mean of the cell fluorescence intensity (as uptake indication) obtained after analyzing 10,000 events (cells) in the gate. Error bars are the standard error of the mean (± SEM) between 4 independent samples ($n$=4).

Results of statistical analysis of two-way ANOVA conducted using SPSS revealed that there were significant main effects of the size ($F(1, 30) = 524.356$, $p < .001$) and the concentration ($F(4, 30) = 108.255$, $p < .001$) of COO-PS-NPs as well as a significant interaction effect of size and concentration ($F(4, 30) = 83.875$, $p < .001$) on the intensity of the COO-PS-NPs in BEAS-2B cells. This means that both factors (size and concentration) affect the uptake output and that the outcome resulted from changes in one factor (size for example) depended on the level of the other factor (the concentration) indicating a relationship between the size and concentration of the COO-PS-NPs in affecting their uptake in BEAS-2B cells.

The results (Fig. 4.1) showed that when the 100nm sized COO-PS-NPs were used for exposure, the intensity of red fluorescence was concentration dependent and has been the highest for cells treated with 300 $cm^2$/ml while the lowest was when cells were incubated with 25$cm^2$/ml. Interestingly, the relative levels of fluorescence in cells treated with 20nm COO-PS-NPs was approximately an order of magnitude lower than for cells treated with 100nm COO-PS-NPs of the equivalent concentration suggesting that the 100nm particles were more readily taken up into the cells. Furthermore, in both cases the uptake appeared to plateau at concentration of 150$cm^2$/ml and above.

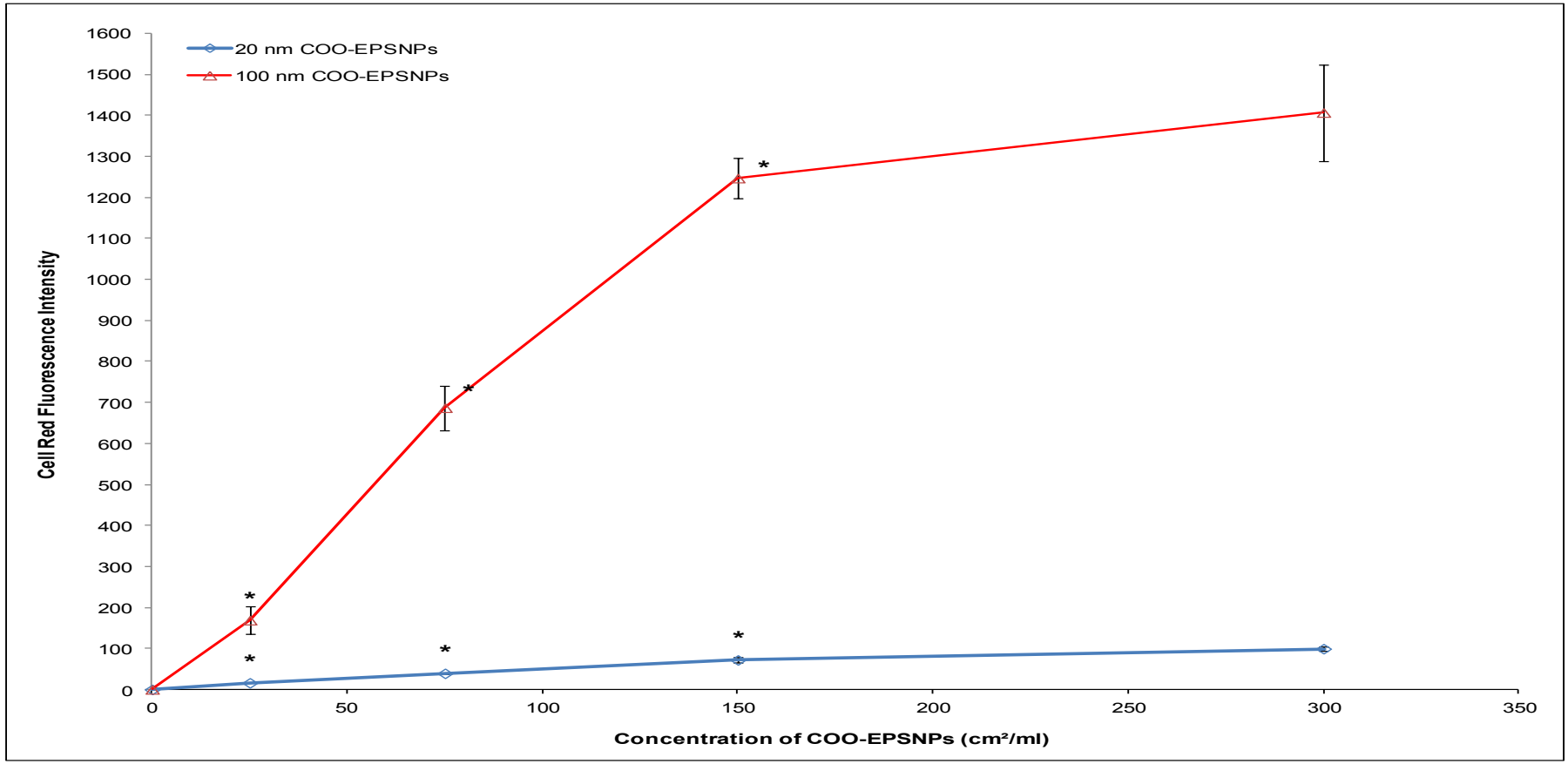


Fig. 4.1 Intracellular uptake of various concentrations of 20nm COO-EPSNs (blue) and 100nm (red) in BEAS-2B cells. The intensity of fluorescence is correlated with the uptake of the COO-PS-NPs into cells. Significant difference in uptake of the 20nm COO-EPSNs and 100nm COO-EPSNs was observed. Measurements of at least 4 samples ($n$=4) were recorded using flow cytometry and the error bars on the graph represent the standard error of the mean (± SEM).

#### 4.2.1.2 Uptake of COO-PS-NPs into BEAS-2B cells by CLSM

CLSM (A1R-A1, Nikon Instruments, Surrey, UK) was used to monitor the internalisation of the red fluorescently labeled 20nm and 100nm sized COO-PS-NPs into live BEAS-2B cells. Cells were independently exposed to 25 and 150 $cm^2$/ml for several time points (45 min, 1h, 5h and 24h) at 37˚C, washed three times with PBS and investigated for uptake of these nanoparticles.

As can be visually seen (Fig. 4.2), the 20nm and 100nm sized red fluorescent-labelled COO-PS-NPs were internalised into BEAS-2B cells within less than an hour (45 minutes) of exposure. Moreover, Fig. 4.2 demonstrated that the amount of internalisation increased over time and that the uptake of the larger 100nm COO-PS-NPs was greater than the 20nm COO-PS-NPs at the same time point in agreement with the flow cytometry data. Furthermore, the uptake increased with increasing the concentration used for cell treatments for both sizes of the nanoparticles. In addition, no distinct evidence of damage to BEAS-2B cell membrane was observed and cells seem able to preserve their morphological structure without serious injuries or major modifications even after incubation for 24h in agreement with the cytotoxicity data in chapter five.

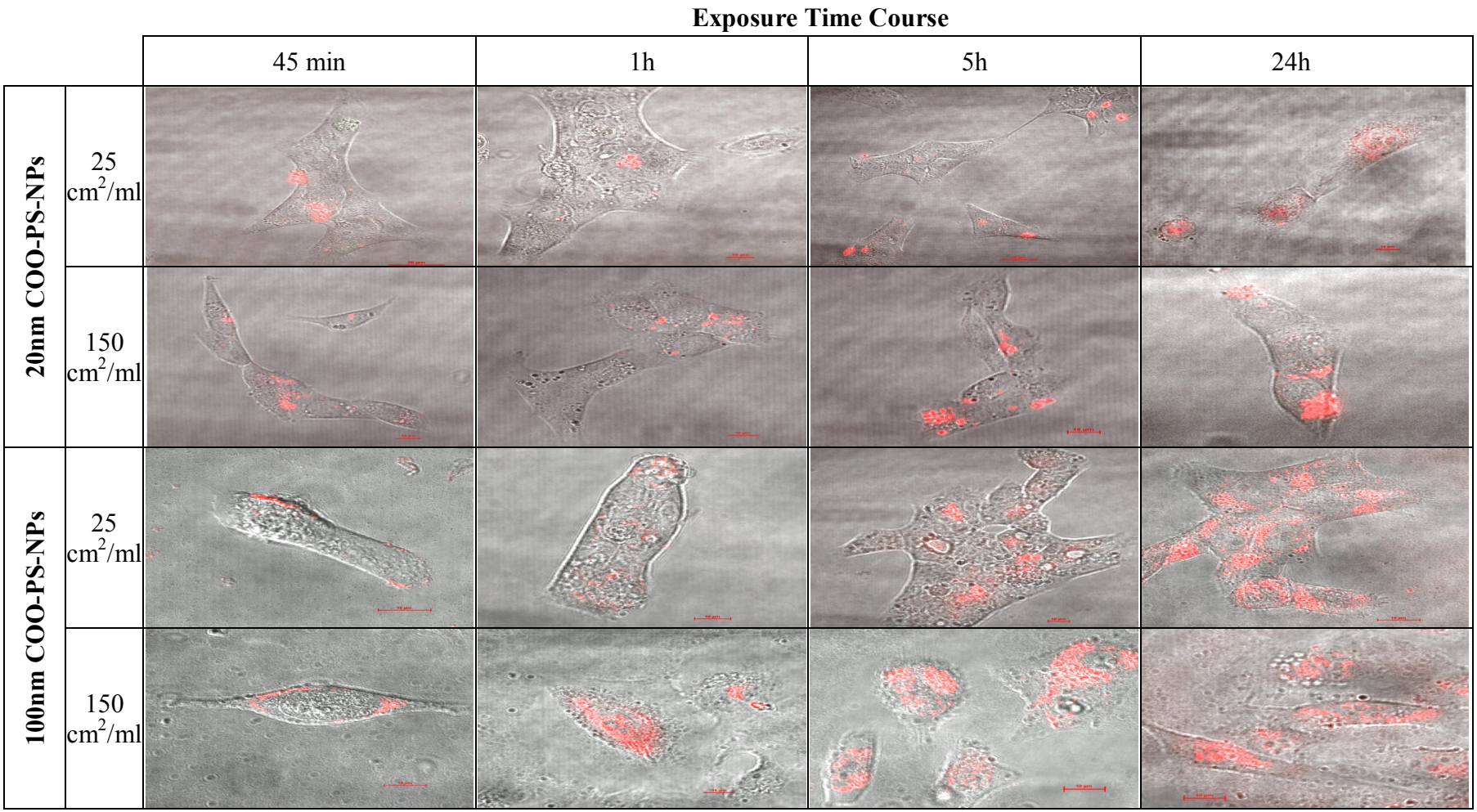


Fig. 4.2 Confocal microscopy images of uptake of 20nm and 100nm red COO-PS-NPs (of 25 or 150 $cm^2$/ml) after various time points (45min, 1, 5 and 24h) in live BEAS-2B cells. Visually, it can be seen that uptake was a concentration-, size- and time-dependent process.

#### 4.2.1.3 Uptake of COO-PS-NPs into BEAS-2B cells by TEM

TEM is a powerful technique that was used not only in investigating the physicochemical characteristics of the COO-PS-NPs regarding their size and shape as well as the agglomeration status (section 3.2.2) but also for fluorescent COO-PS-NPs detection inside cells and co-localisation within sub-cellular compartments at high spatial resolution [Lee et al (2010)]. Since that is pivotal for studying the use of ENPs in several applications such as drug carrier system. It was utilized with high pressure in this study to examine the uptake of 20nm and 100nm COO-PS-NPs in fixed BEAS-2B cell samples. The digital microphotograph images (Fig. 4.3) showed a cellular uptake of the 100nm COO-PS-NPs that were found mostly in the cytoplasm and around the nucleus. The images also showed the 100nm COO-PS NPs between cells and in attached to the outer cell membrane as well as in vesicle-like structures. The TEM images (Fig 4.4) demonstrated that it is confusing and difficult to detect the 20nm COO-PS-NPs in BEAS-2B cells potentially due to their small size and low electron density [Ng et al (2010)].

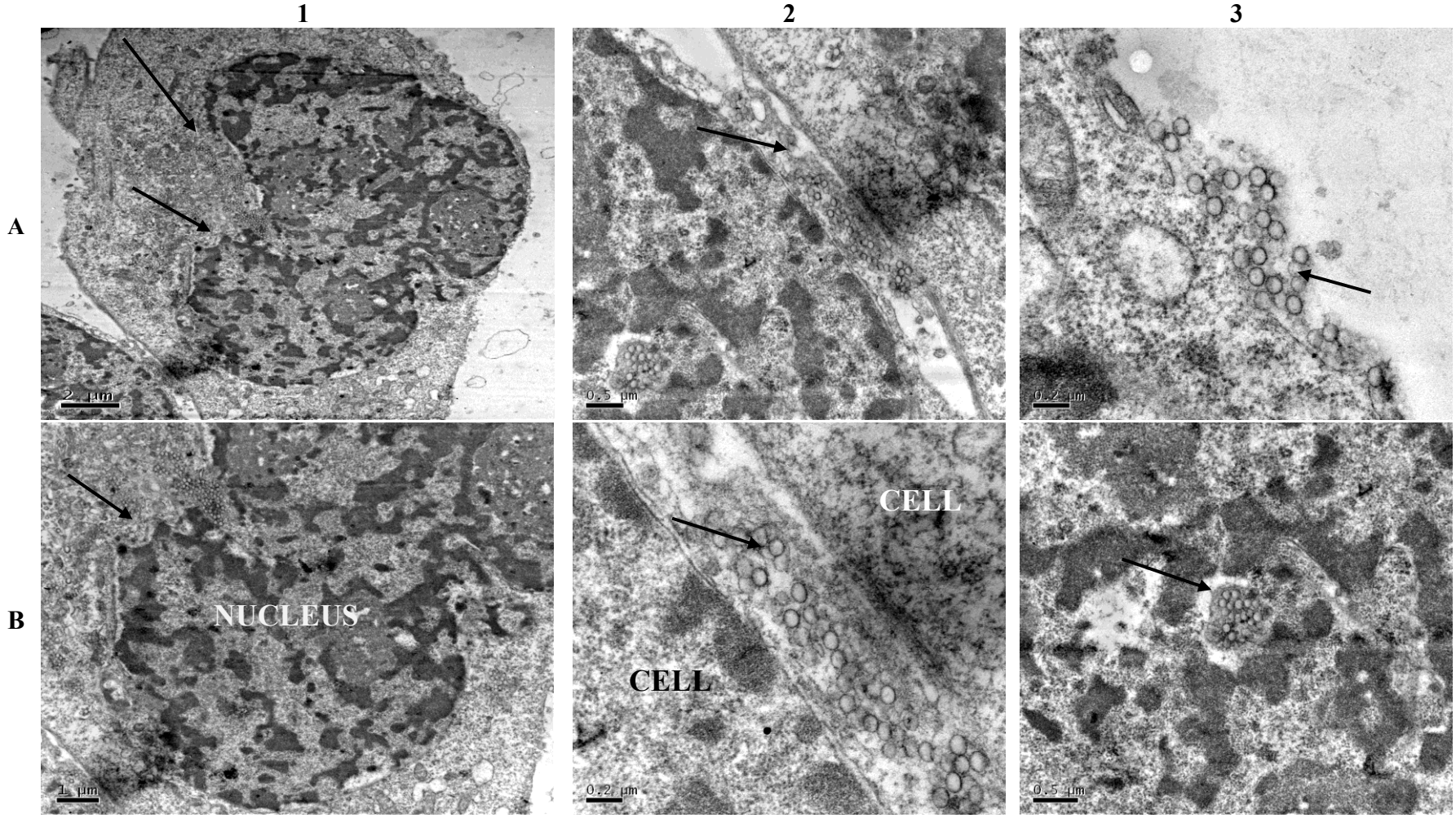


Fig. 4.3 TEM images of cellular uptake of the 100nm COO-PS-NPs (50cm$^2$/ml). Arrows point out to these COO-PS-NPs that can be seen in the cytoplasm around the nucleus (1A and 1B), between cells (2A and 2B), attached to the cell membrane (3A) and in a vesicle-like structure (3B).

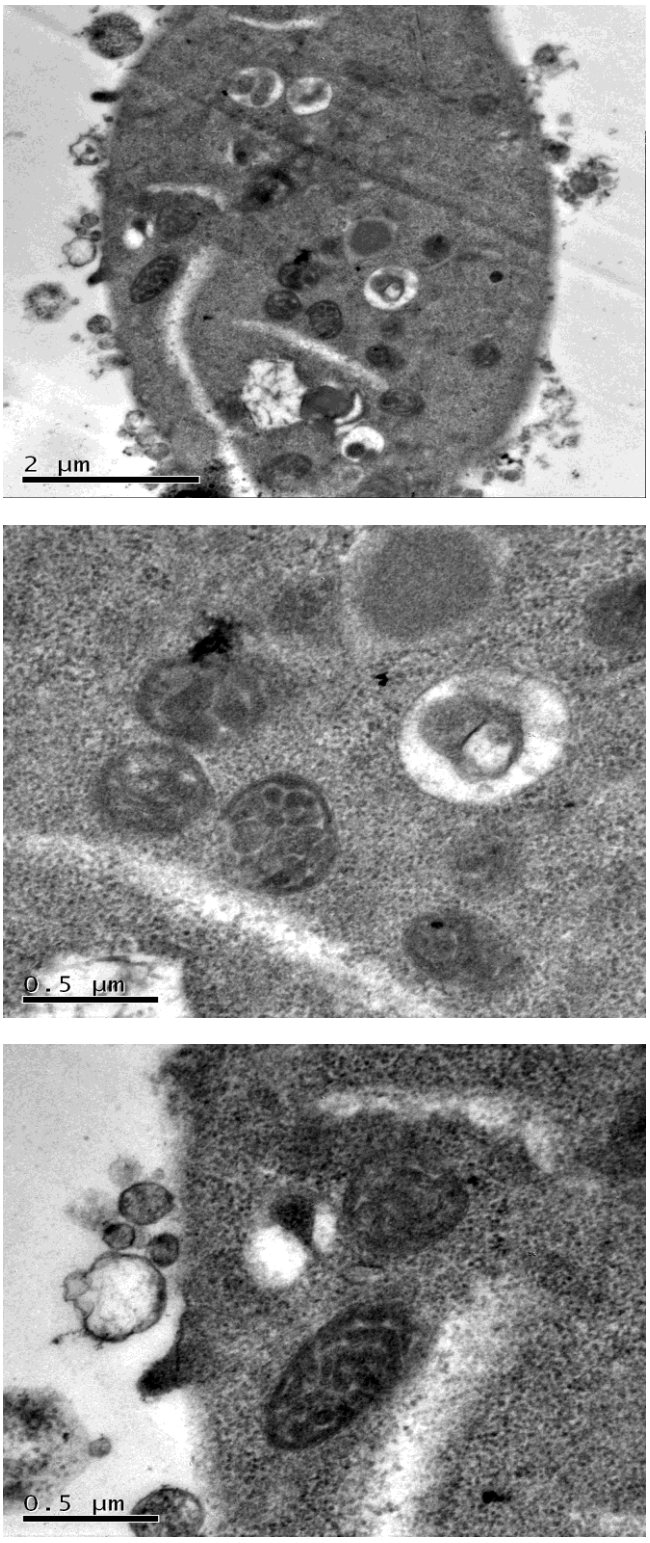


Fig. 4.4 TEM images of BEAS-2B cells incubated with 20nm COO-PS-NPs (50cm$^2$/ml) showing (A) the whole cell, (B) section inside the cell and (C) the outer cell membrane. It was confusing and difficult to detect and visualize the 20nm COO-PS-NPs in the cytoplasm or cell compartments because of their small size and low electron density.

### 4.2.2 Co-localisation of COO-PS-NPs in the nucleus, mitochondria and Golgi apparatus of BEAS-2B cells by CLSM

To study the possible co-localisation of red fluorescent COO-PS-NPs in various sub-cellular organelles of BEAS-2B cells, different stains were used to co-stain BEAS-2B cells following 24h exposure to 50cm$^2$/ml COO-PS-NPs. The mitochondria was marked with the green Rhodamine 123 dye in living cells whereas the blue DAPI was used for staining the nucleus and green WGA-lectin was used for staining the Golgi apparatus in fixed cells. The treated BEAS-2B cells were imaged by LSCM (Nikon A1R-A1 or Leica) using a 60X oil lens against untreated cells as negative control and images were analyzed using ImageJ software.

The red fluorescent COO-PS-NPs were distributed widely throughout the cytoplasm and could be seen as foci of accumulated fluorescence that appears as bright red clusters. The 20nm sized COO-PS-NPs were found around the blue DAPI-stained nuclei (Fig. 4.5 A). Some of these 20nm COO-PS-NPs seemed to be located inside the mitochondria as yellow fluorescence dots were seen as a result of the red particles and the green mitochondria overlay (Fig. 4.8 A). Moreover, very few COO-PS-NPs sized 20nm were situated in the green lectin-stained Golgi and only after 24h incubation (Fig. 4.9 and Fig. 4.10). On the other hand, it seems that the 100nm red COO-PS-NPs colocolise more inside the Golgi apparatus mainly after 24h incubation and partially after 6h incubation (Fig. 4.11 and Fig. 4.12). Furthermore, it was difficult to clearly observe co-localisation of the 100nm COO-PS-NPs inside the mitochondria (B and D).

A

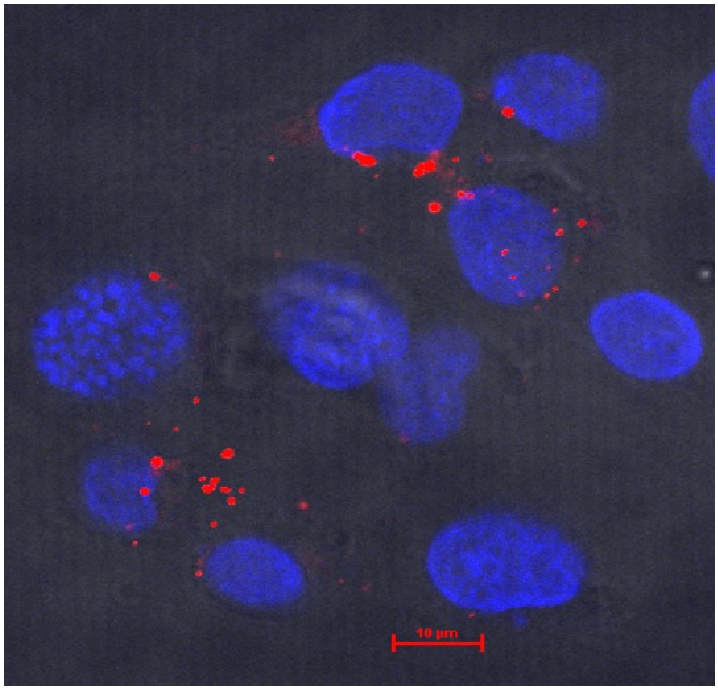


B

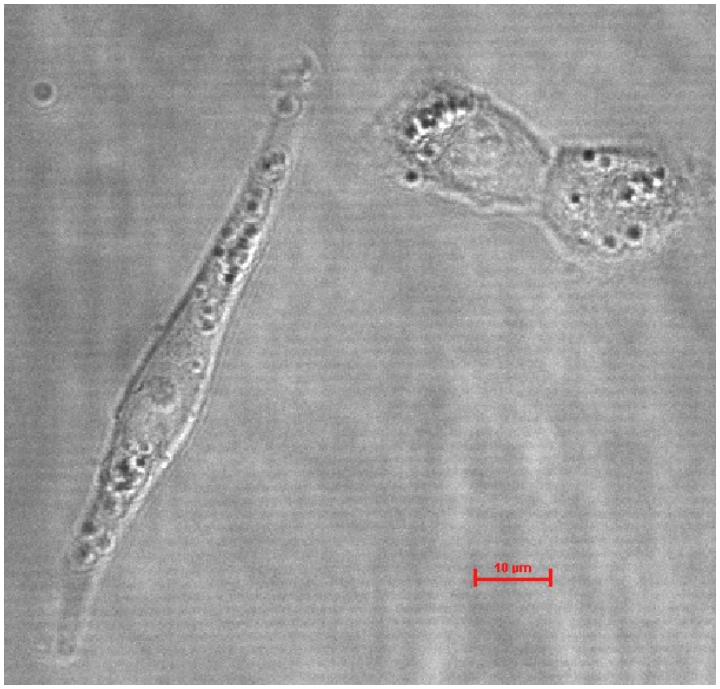


Fig. 4.5 Red fluorescent COO-PS-NPs (20nm, 50cm$^2$/ml) were observed as clusters in the cytoplasm around the blue DAPI-stained nucleus in fixed BEAS-2B cells imaged by CLSM indicating the intracellular uptake (A) in comparison to the non-treated cells (B). The scale bar is 10 µm.

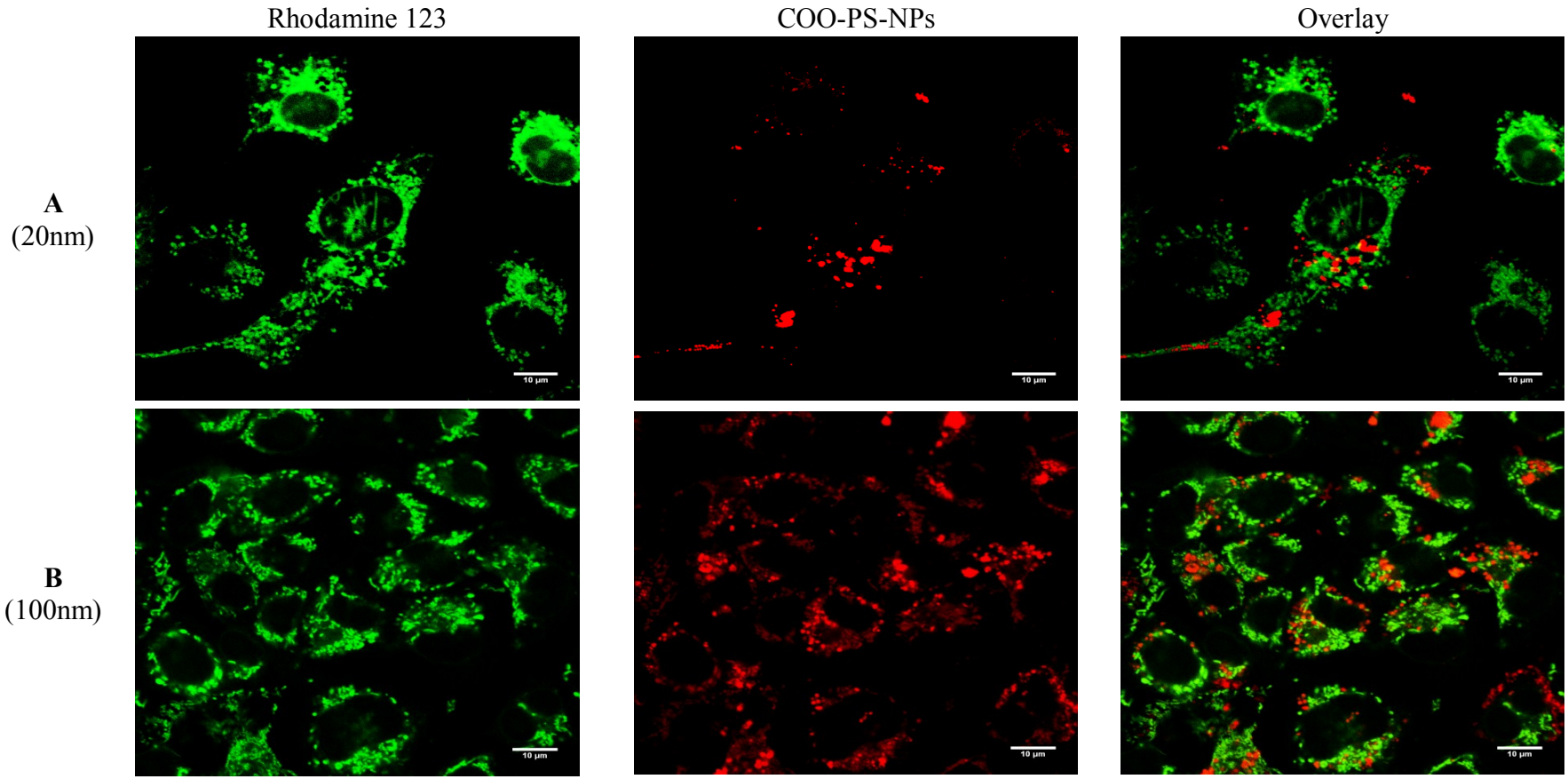


Fig. 4.6 CLSM images of green rhodamine-stained mitochondria in BEAS-2B cells after 24h incubation with 50 $cm^2$/ml COO-PS-NPs sized 20nm (A) or 100nm (B) to monitor their co-localisation. Images were presented to show the mitochondria stained with rhodamine 123 (left column), the red COO-PS-NPs (middle column) and the overlay of red COO-PS-NPs and green-stained mitochondria (right column). The scale bar is 10 µm

**A**
(20nm)

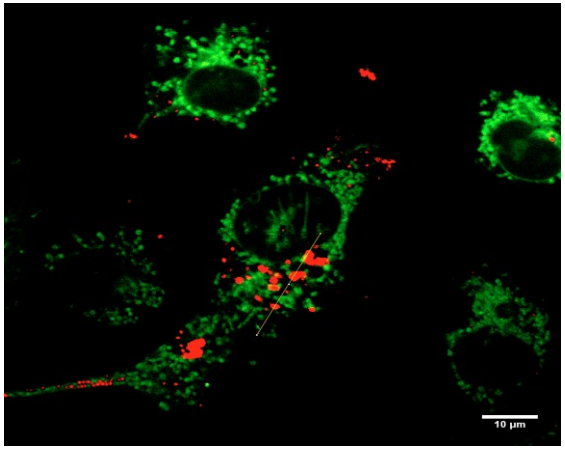


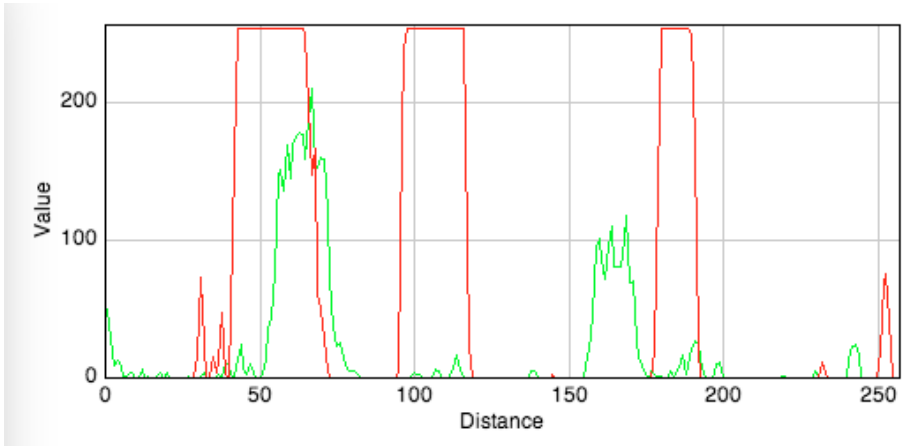


**B**
(100nm)

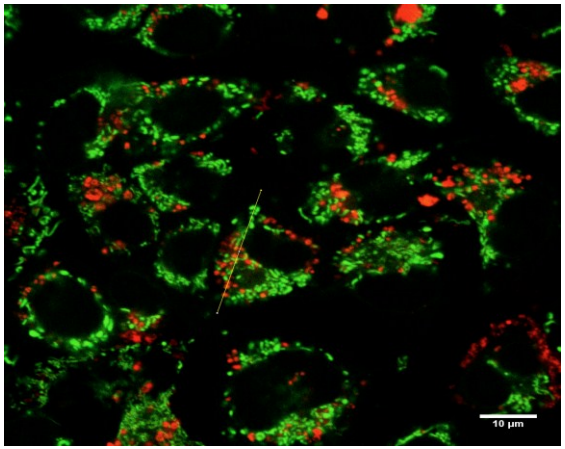


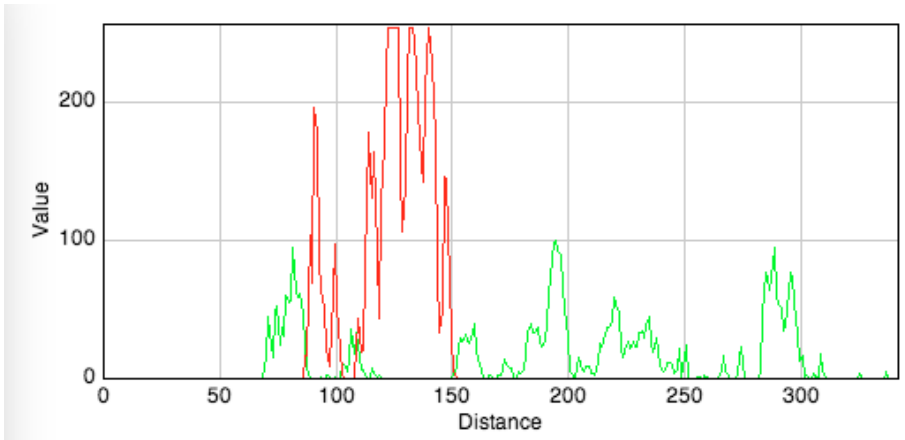


Fig. 4.7 The graph of quantification of the red COO-PS-NPs showed some colocalisation of the 20nm red COO-PS-NPs in the Rhodamine 123 green-stained mitochondria (A) as the red and green channels were overlapped. Meanwhile, no clear co-localisation of the 100nm red COO-PS-NPs could be seen inside the mitochondria (B) since no clear red and green overlapping was displayed. The scale bar is 10 µm

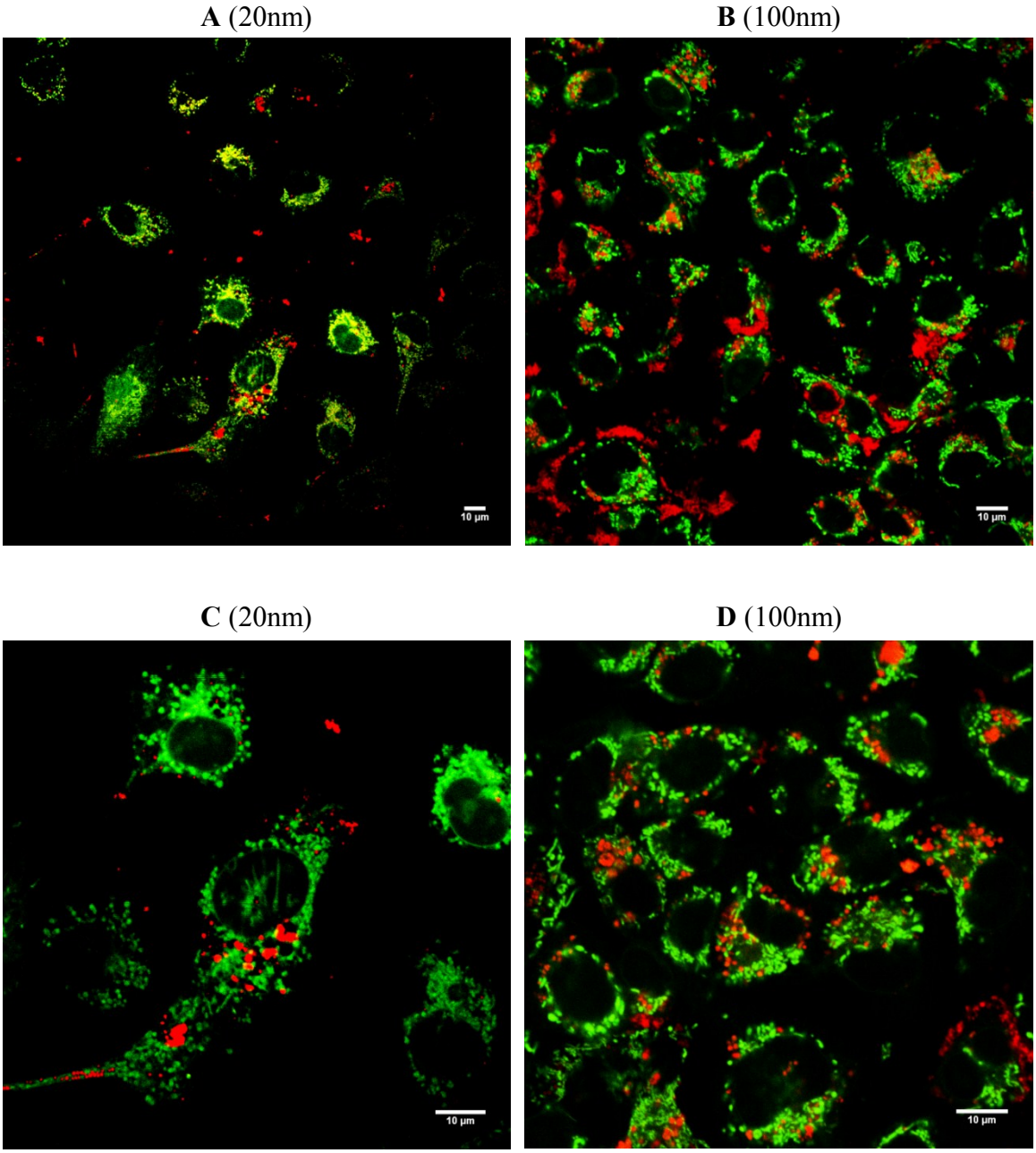


Fig. 4.8 BEAS-2B cells were incubated with 50 $cm^2$/ml of the 20nm or 100nm red fluorescent COO-PS-NPs for 24h followed by mitochondria staining with green Rhodamine 123 for 30 minutes. Confocal images of the 20nm red COO-PS-NPs (A and C) revealed some co-localisation inside the mitochondria as yellow dots resulted from the overlay of the red and green fluorescence. Meanwhile, it was hard to clearly see co-localisation of the 100nm sized red COO-PS-NPs inside the green rhodamine-stained mitochondria (B and D). The scale bar is 10 µm

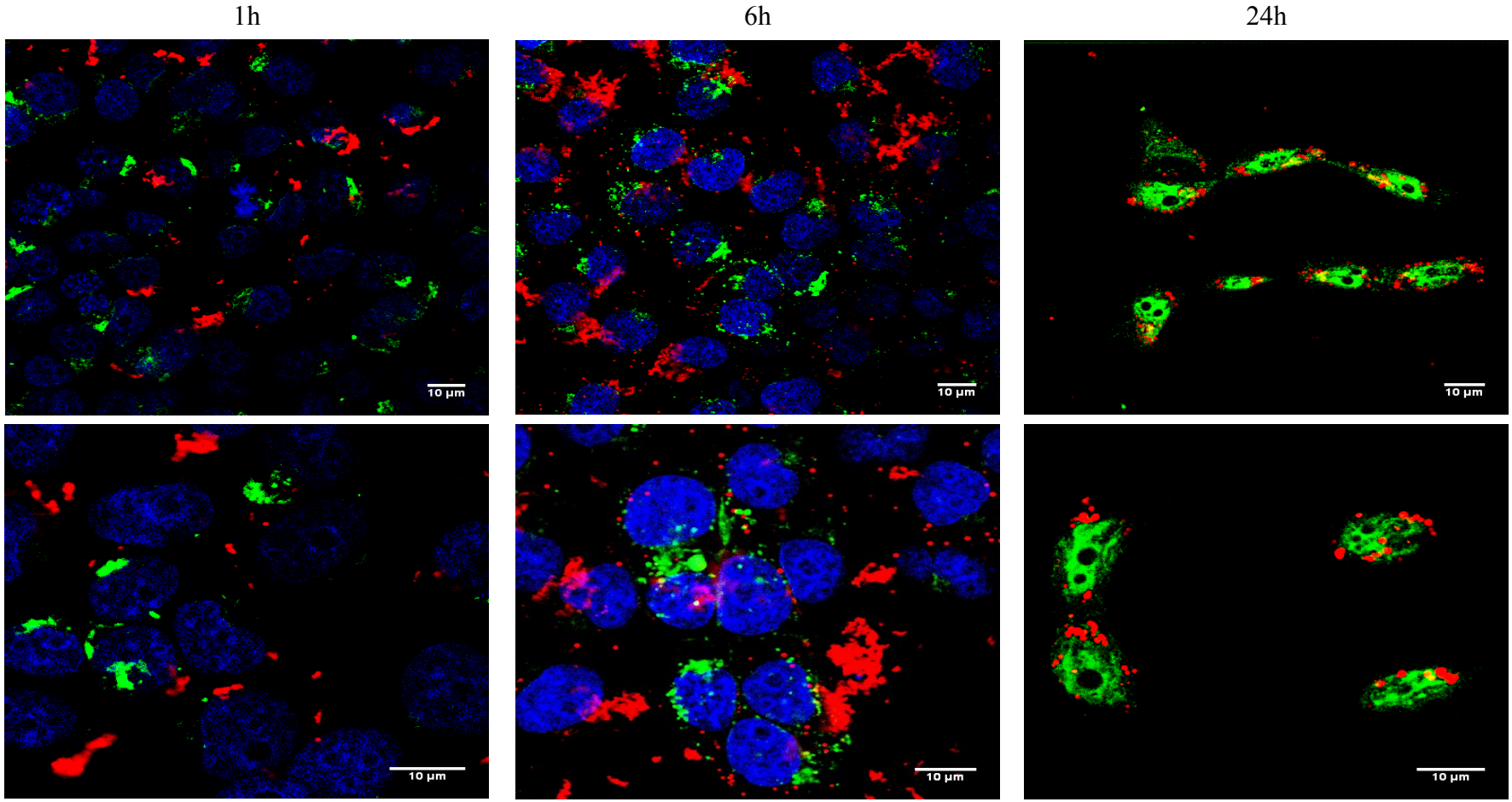


Fig. 4.9 CLSM images of red 20nm COO-PS-NPs (50 $cm^2$/ml) in green lectin-stained Golgi in BEAS-2B cells after 1h (left columns), 6h (middle columns) and 24h (right columns) incubations. Partial co-localisation of 20nm COO-PS-NPs in the Golgi apparatus can be seen only after 24h. The blue DAPI was utilized for 1 and 6h studies to stain the nucleus. Scale bar is 10µm.

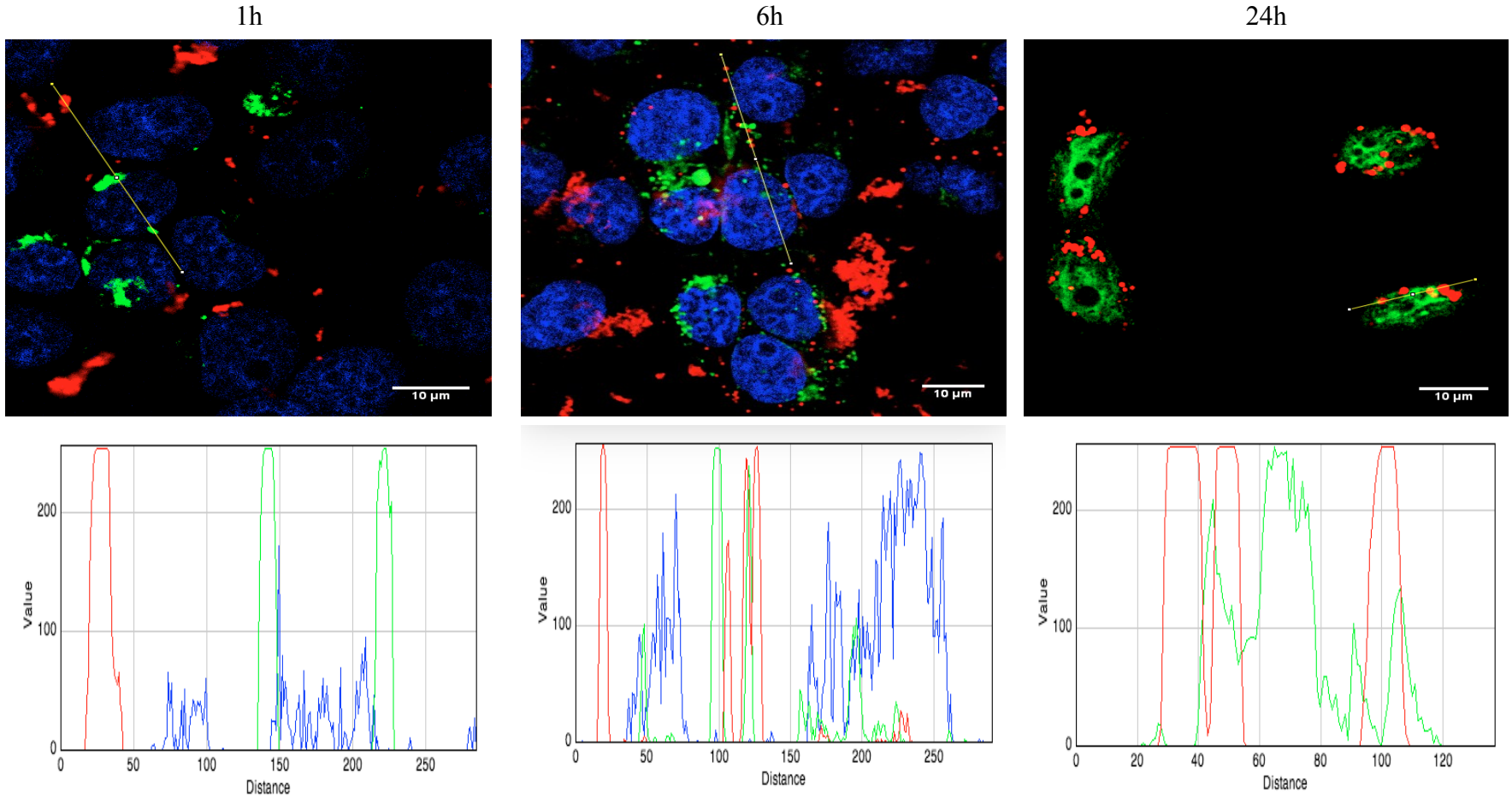


Fig. 4.10 The graph of quantification of the 20nm red COO-PS-NPs showed obvious red and green channels overlapping after 24h incubation (right column), partial overlapping after 6h incubation (middle column) but no overlapping after 1h incubation (left column). This overlapping indicates colocalisation of the 20nm red COO-PS-NPs in the lectin green-stained Golgi apparatus of BEAS-2B cells. The blue DAPI was utilized for staining the nucleus. The scale bar is 10µm.

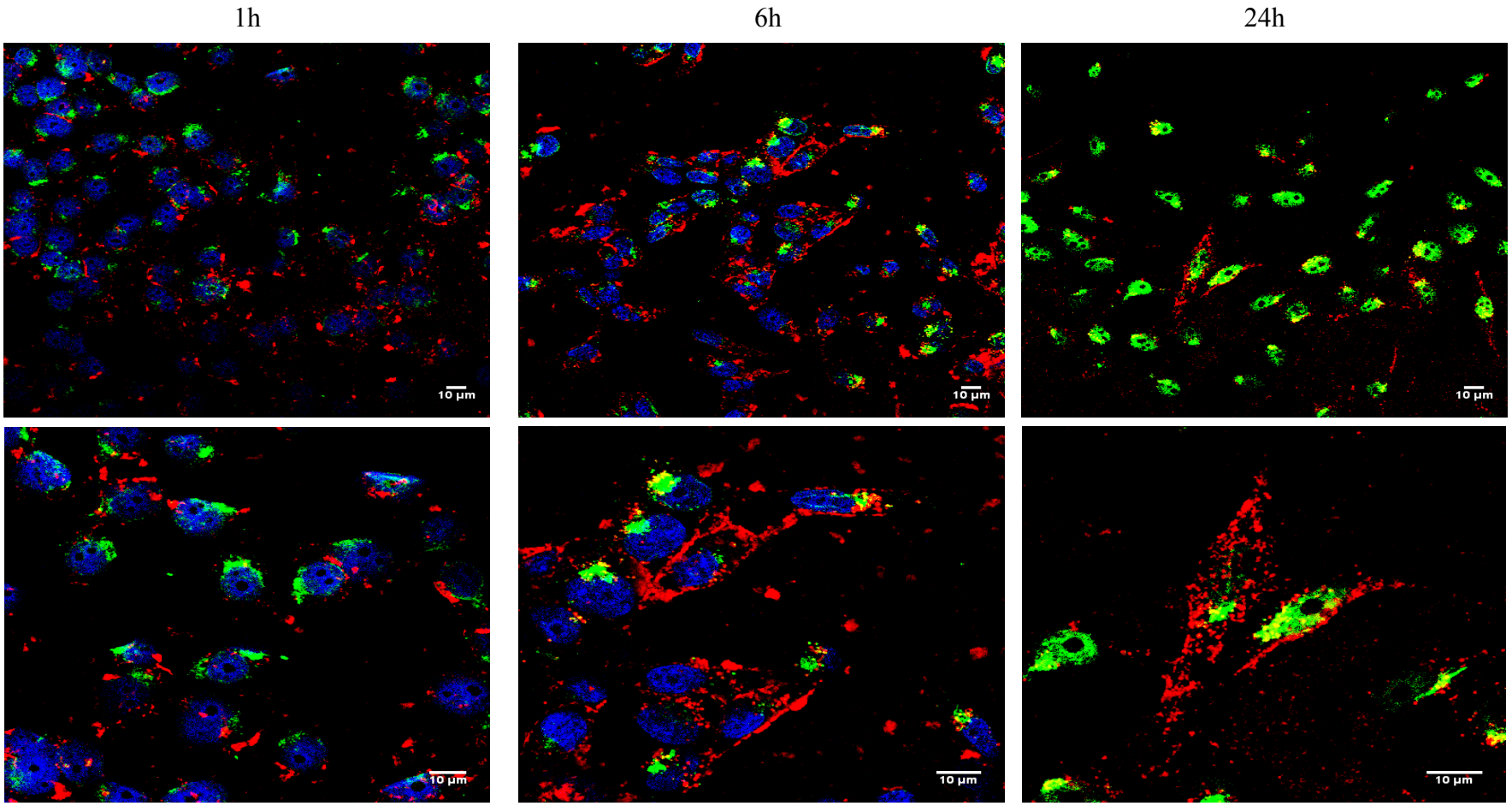


Fig. 4.11 CLSM images of red 100nm COO-PS-NPs (50 $cm^2$/ml) in green lectin-stained Golgi in BEAS-2B cells after 1h (left columns), 6h (middle columns) and 24h (right columns) incubations. Some co-localisation of the 100nm COO-PS-NPs in the Golgi apparatus can be seen mainly after 24h and partly after 6h. Scale bar is 10µm.

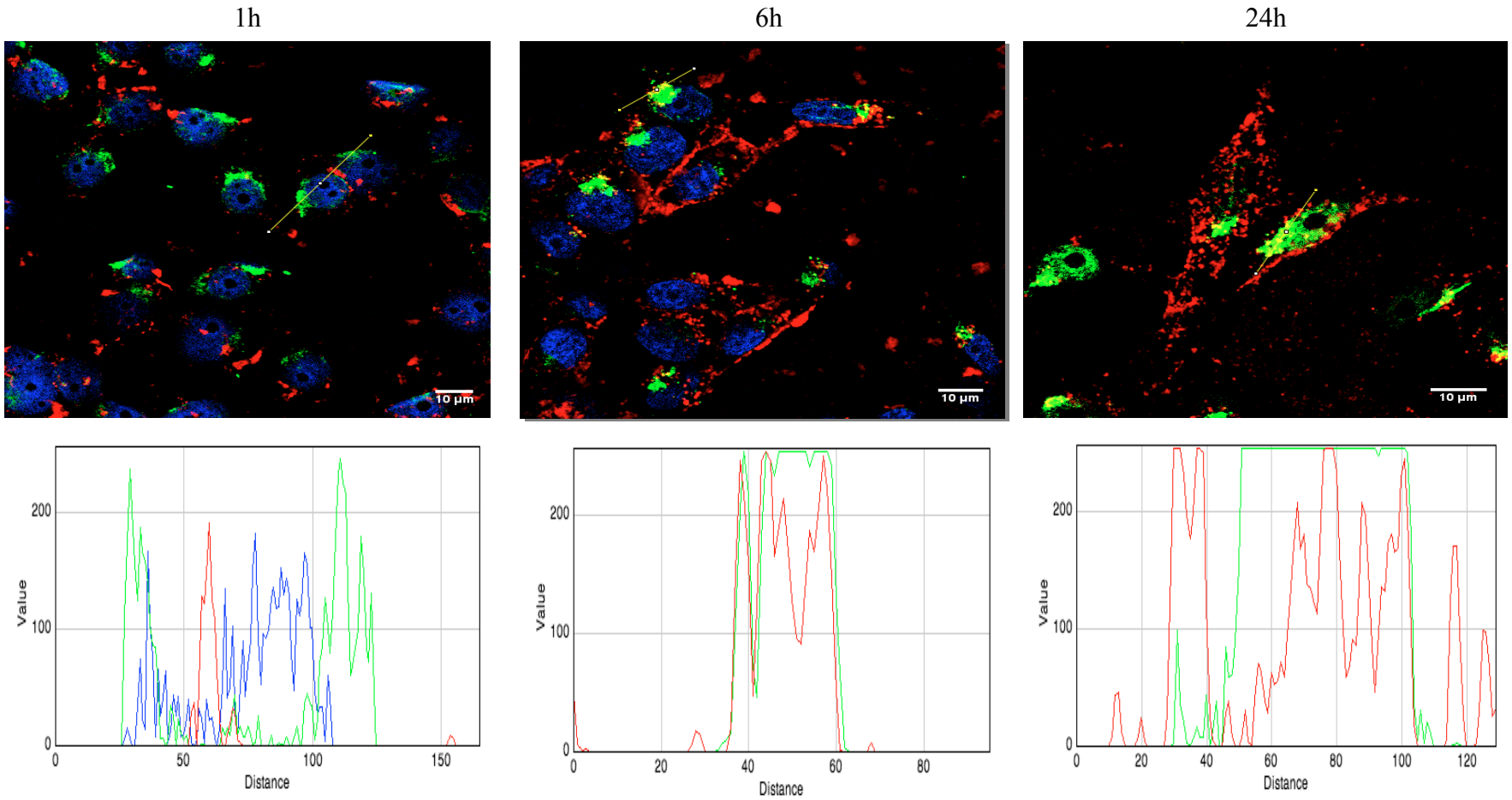


Fig. 4.12 The graph of quantification of the 100nm red COO-PS-NPs showed obvious red and green channels overlapping after 24h incubation (right column) and 6h incubation (middle column) but partial overlapping after 1h incubation (left column). This overlapping indicates colocalisation of the 100nm red COO-PS-NPs in the lectin green-stained Golgi apparatus of BEAS-2B cells. The blue DAPI was utilized for staining the nucleus. The scale bar is 10µm.

## 4.3 Discussion

The evaluation of ENPs cellular uptake has been known to be important since the biological influences that these ENPs can cause depend on their ability to get across the plasma membrane to the interior of cells. Therefore, COO-PS-NPs uptake into BEAS-2B cells was assessed in this study using flow cytometry, CLSM and TEM techniques. CLSM was utilized to observe the internalisation of two concentrations of the fluorescent COO-PS-NPs at several time points while studying the uptake by TEM and FACS was performed after 24h. The intracellular co-localisation of these COO-PS-NPs was accomplished using various fluorescent markers for staining and labeling specific organelle within live or fixed cells following the incubation with the COO-PS-NPs.

For the internalisation assessment by flow cytometry, BEAS-2B cell samples were treated independently with various concentrations (25-300 $cm^2$/ml) of 20nm and 100nm COO-PS-NPs and the relative fluorescence intensity was then measured. The measurements were then plotted against the concentration (dose) used for the treatment for 24h exposure to find out the COO-PS-NPs uptake status in these cells. The flow cytometry results (Fig. 4.1) displayed that the lowest fluorescence intensity was in cells exposed to 25$cm^2$/ml COO-PS-NPs and then increased with increasing the concentration to reach the highest level at 300$cm^2$/ml. This was the pattern of both the 20 and the 100nm COO-PS-NPs and confirms that the internalisation of these particles was proportional to the external concentration used in the experiment indicating a concentration-dependent process. There was no significant increase further than the 150$cm^2$/ml (as verified statistically) since the curve attained a stable level (plateau)

probably as a result of saturation status. This might indicate some kind of active internalisation of COO-PS-NPs (before saturation at 150cm$^2$/ml) and this is in agreement with what has been hypothesized that the cellular uptake of ENPs is active process which involves enclosing them by the cell membrane prior to internalisation [Gao et al (2005)]. Moreover, it has been proposed the cellular uptake of ENPs is controlled by a thermodynamic equilibrium where the internalisation increases with the time and concentrations until it reaches a plateau [Chithrani et al (2006), Zhang et al (2009)]. In addition, it can be clearly seen that the fluorescence intensity of the 100nm COO-PS-NPs (even as low as the 25cm$^2$/ml) are much more than the 20nm COO-PS-NPs intensity at all concentrations in BEAS-2B cells. This means that more of the larger sized COO-PS-NPs (of 100nm) were internalised into BEAS-2B cells compared to the small size COO-PS-NPs (of 20nm) showing an indirect correlation between the size of ENPs and their uptake. This is concordant with other studies which reported greater uptake of the larger ENPs compared with the smaller ones and argued the 100-200nm to be the optimum size for ENPs internalisation [Win et al (2005)]. This can be attributed to the heavy aggregation of the 20nm sized COO-PS-NPs observed in the LHC-9 SFM.

As mentioned above, the cellular uptake of ENPs has been hypothesized to be active process in which the cell membrane surrounds the ENPs to engulf them [Gao et al (2005)]. The size characterisation of COO-PS-NPs by DLS has revealed significant size changes in the 20nm COO-PS-NPs (Fig. 3.9) due to significant aggregation (i.e. size/diameter augmentation) at 37˚C in the LHC-9 cell culture media compared with the 100nm ones that showed less agglomeration. Consequently, the aggregated 20nm COO-PS-NPs in LHC-9 would yield larger sized COO-PS-NPs (Fig. 3.9 C taken by TEM) that

require more time and energy to be enclosed by the membrane and engulfed into the cells resulting therefore in lower uptake into BEAS-2B cells compared to 100nm ones. This would explain the low amount of the 20nm COO-PS-NPs in comparison to the 100nm COO-PS-NPs at equivalent concentration and exposure time.

For investigating the COO-PS-NPs uptake into BEAS-2B cells using CLSM, cells were incubated individually with either 25 or 150 $cm^2$/ml of the 20nm and 100nm COO-PS-NPs in a time course study. The high concentration of COO-PS-NPs (300 $cm^2$/ml) was not used in cell treatment for imaging in order to avoid the potential of saturation during uptake process. The first thing observed was that COO-PS-NPs did not cause obvious alterations in the morphology of BEAS-2B cells even after incubation for 24h (Fig. 4.2) for example: condensed chromatin or membrane blebbing –both features of apoptosis. These data are in agreement with the cell viability studies (chapter 5). Furthermore, confocal images (incorporated in Fig. 4.2) showed COO-PS-NPs accumulation that seems to be mainly inside the BEAS-2B living cells that were washed with PBS to remove the membrane-attached (non-internalised) particles before imaging. Although, quantification of the nanoparticles by cell section scan was not performed, the intracellular uptake of both sizes of COO-PS-NPs could be observed as they appear to accumulate inside cells in a proportional way to the concentrations used and to the incubation time. It is unlikely that these are plasma membrane-bound COO-PS-NPs considering the negative potential of cell membrane and the electrostatic repulsion that would occur between the cell and the anionic COO-PS-NPs unless they were neutralized after being coated with protein. Moreover, both size of the 20nm and 100nm red fluorescent COO-PS-NPs were internalised into BEAS-2B cells at low concentration

(25cm$^2$/ml) and could be easily identified inside cells as early as 45 minutes after incubation (Fig. 4.2). In addition, it is also apparent that the uptake of the 100nm COO-PS-NPs was more rapid than that observed for the 20nm sized COO-PS-NPs which tend to be limitedly internalised possibly due to their heavy aggregation tendency in cell culture media (LHC-9) that has been observed and characterised by DLS. This is also agrees with the flow cytometry results. It seems that the 100nm COO-PS-NPs nevertheless have found a pathway to escape the plasma membrane and get access to the interior of the cells probably using a non-endocytotic mechanism since endocytosis is limited to the uptake of objects that have dimensions of less than 80nm [Joris et al (2013)]. The microscopic images obtained by CLSM technique for live BEAS-2B cells (Fig. 4.2) are consistent with the flow cytometry results (Fig. 4.1) even if flow cytometry is considered a semi-quantitative analysis that does not discriminate between extracellular membrane-bound ENPs and those internalised inside the cell [Oh et al (2010)]. These results confirm that the internalisation of COO-PS-NPs was proportional to the experimental concentration and incubation time.

The results obtained by flow cytometry and CLSM were also validated by TEM after 24h incubation with 20nm and 100nm COO-PS-NPs (50 cm$^2$/ml) at 37$^{\circ}$C. Albeit it is fairly difficult to distinguish between some spherical cellular structures (such as vesicles) and the polymer-based ENPs of the same size range since they are electron lucent spherical-like nanoparticles [Mühlfeld et al (2007)], the results verified the uptake of the COO-PS-NPs of 20nm and 100nm size into the BEAS-2B cells as they were found (to appear as bright objects) into the cytoplasm, possibly in vesicles, but not in the

nucleus of BEAS-2B cells (Fig. 4.3). These COO-PS-NPs would appear as white dots (or small vesicles-like shape) since they are not heavy dense metals [Ng et al (2010)].

Furthermore, the COO-PS-NPs co-localisation with some sub-cellular components, including the nucleus, the mitochondria and the Golgi apparatus, were monitored by CLSM using organelle specific colored-dyes. The CLSM images showed that the 20nm sized red fluorescent COO-PS-NPs (of the 20 and COO-PS-NPs) were not found inside the nucleus (Fig. 4.5 A) and this would point at the difficulty for COO-PS-NPs to go through the nuclear membrane. There was some evidence that 20nm red COO-PS-NPs were located within the mitochondria (A of Fig. 4.6 and Fig. 4.7) and inside the Golgi just when incubated for 24h (Fig. 4.9 and Fig. 4.10). In contrast, no clear co-localisation of the 100nm COO-PS-NPs inside the mitochondria (Fig. 4.8 B and D) but these 100nm COO-PS-NPs could be seen contained by the Golgi apparatus mostly after 24h and somewhat after 6h (Fig. 4.11 and Fig. 4.12).

It is worthy to mention that it has been hypothesized that the cell (line) type [Zauner et al (2001), He et al (2010)], incubation time [Win et al (2005)], ENPs concentration [Jiang et al (2011)] as well as several ENPs physicochemical characteristics including size [Rejman et al (2004)], shape [Chithrani et al (2006)] and functional group [Yamamoto et al (2002), Makino et al (2003), Dausend et al (2008), Harush-Frenkel et al (2008), Jiang et al (2011)] are all important parameters that influence ENPs-cell binding and interaction and therefore the ENPs cellular uptake. In this study, the flow cytometry, CLSM and TEM techniques have been used to investigate the uptake behavior and co-localisation of different sizes and concentrations of red

fluorescent COO-PS-NPs in BEAS-2B cells upon several exposure time points. The results have showed that the uptake of the COO-PS-NPs has increased in general with increasing the concentration and time of incubation, however, the internalisation of larger size (100nm) COO-PS-NPs is higher than the small sized (20nm) ones at equivalent concentration used (in $cm^2$/ml) and incubation time point. This indicates that the COO-PS-NPs were internalised into BEAS-2B cells in a size-, concentration- and time-dependent mode. In all cases, COO-PS-NPs were found to be distributed in the cytoplasm and around the nucleus but not inside it. No clear co-localisation of the 100nm red COO-PS-NPs was observed in the mitochondria (Fig. 4.8 B and D) while some of the 20nm red COO-PS-NPs were colocolised in the mitochondria (A of Fig. 4.6 and Fig. 4.7). Regarding the co-localisation inside the Golgi apparatus, the 20nm red COO-PS-NPs were found in the Golgi only when after 24h (Fig. 4.9 and Fig. 4.10) whereas the 100nm COO-PS-NPs could be seen in the Golgi apparatus mostly after 24h and to some extent after 6h (Fig. 4.11 and Fig. 4.12).

# CHAPTER FIVE:

# CELL TOXICITY AND MECHANISM OF ACTION

## 5.1 Introduction

The emerging use of ENPs in various applications due to their distinctive properties has focused attention on, and raised the concern of, possible harmful interactions with biological systems and their possible toxicological consequences. As part of this, it is essential to investigate the mechanisms of toxicity of ENPs using in vitro system to enable better risk assessment to be undertaken. This includes an assessment of both their long and short term cytotoxicity as well as their potential genotoxicity. In fact, several in vivo and in vitro studies have confirmed the toxicity of different ENPs in various cell lines including amino-modified polystyrene nanoparticles (NH-PS-NPs) in mouse leukaemia monocyte macrophages (RAW 264.7) and normal human bronchial epithelial cells (BEAS-2B) cells [Xia et al (2008)], zinc oxide nanoparticles (ZnO-NPs) and titanium dioxide ($TiO_2$-NPs) in human skin fibroblast cells [Dechsakulthorn et al (2007)], multi-wall carbon nanotubes (MWCNT) in $A_3$ and human lung mesothelioma (MSTO-211H) cells [Hu et al (2010)] as well as starch-coated Ag-NPs in U251 cells [AshaRani et al (2009)]. Several techniques can be utilized to investigate cell morphology and viability at the cellular and molecular levels following exposure to ENPs including MTT assay, ROS analysis, cytokine release test in addition to exploring their cellular uptake and sub-cellular co-localisation through cell-stain microscopy imaging [Lai et al (2013)]. In this study, the cyto-toxicological effects of COO-PS-NPs in human bronchial epithelial cells (BEAS-2B) were evaluated by investigating the cell viability by MTT test and examining the oxidative stress status of cells (production of ROS and GSH depletion), while the genotoxicity was studied using the comet assay to detect the DNA

strand breaks. In addition, the possible mechanism(s) of action was investigated to begin to understand the cellular pathways of toxicity caused by COO-PS-NPs.

Reactive oxygen species (ROS) are transient free radicals that are chemically highly reactive and contain oxygen [Jefferies et al (2003)]. Examples of ROS include superoxide anions ($O_2^{\bullet -}$), hydroxyl radical ($OH^{\bullet}$) and peroxy radical ($ROO^{\bullet}$) in addition to the non-radical species hydrogen peroxide ($H_2O_2$) that is considered a ROS [Halliwell (1999), Waris et al (2006), Genestra et al (2007), Rigas et al (2008)]. Endogenous ROS are produced at low concentrations [Zhang and Gutterman (2007)] as natural byproducts of several aerobic cellular metabolism processes (e.g. the electron transport chain) [Boveris and Chance (1973)]. They can play a role in gene regulation and intracellular signal transduction process in the cell by acting as second messengers including regulation of apoptosis [Valko et al (2006)]. It has been reported that elevated levels of ROS, in response to various chemical stimuli and physical stresses, can activate several mitogen-activated protein kinase (MAPK) family that are involved in the regulation of cellular survival and adaptation processes including gene expression, proliferation, differentiation, protein synthesis and programmed cell death (apoptosis) [Chang and Karin (2001), Kyriakis and Avruch (2001)].

Under normal circumstances, cells are in equilibrium state where ROS are maintained at low levels by cellular defensive antioxidant systems [Mohora et al (2009)]. For example, $H_2O_2$ is detoxified to $H_2O$ and $O_2$ either by the action of glutathione peroxidase in mitochondria or catalase in peroxisomes (in cytosol) [Mohora et al (2009)]. Excessive uncontrolled ROS overproduction and/or failure to maintain and stabilize the balanced level of ROS by defensive anti-oxidant mechanisms can disrupt the reduction-

oxidation (redox) equilibrium status resulting in abnormal ROS accumulation within the cell in a way that exceeds the cellular defensive antioxidant capacity. Abnormal ROS accumulation may cause toxic effects that result in cell death owing to damage of wide range of biological molecules (such as DNA, protein and lipids) and cellular organelles (such as mitochondria, that might suffer mitochondria membrane permeability transition) [Magder (2006), Marquis et al (2009)].

It has been observed that direct ENPs-mitochondria interaction can damage the inner membrane of mitochondria disrupting the electron transport chain (of the oxidative phosphorylation) due to deregulation of the redox potential of this mitochondria membrane [Soenen et al (2011)]. Mitochondrial membrane damage might induce production of ROS and this has been related to cationic PS-NPs concentration-dependent cytotoxicity [Xia et al (2006)]. ENPs-induced ROS production has been suggested to cause cellular cytotoxicity since these ROS, if excessively produced but not effectively buffered, can react with and damage cellular bio-molecules including lipid, DNA and protein causing lipid peroxidation, DNA damage and protein oxidation respectively [Lewinski et al (2008)]. This study has demonstrated (chapter 4) that COO-PS-NPs were at least partially colocalised in the mitochondria and it was essential therefore to investigate whether this can cause cellular ROS generation and depletion of intracellular GSH in BEAS-2B cells resulting in oxidative stress induction. In addition, ENPs cellular internalisation is an important requirement for their biomedical use as drug delivery molecules however, they should not cause severe or complicated effects on targeted cells [Soenen et al (2011)]. Therefore, the biological impacts related to time of exposure to COO-PS-NPs in BEAS-2B cells were investigated in this study in addition to the

cytotoxicity effects of their size and concentration as well. Further investigations of other cellular parameters to explore possible toxicological effects of COO-PS-NPs were conducted and endpoints measured included cell viability assessment by MTT assay, ROS generation analysis, depletion of intracellular GSH, DNA damage detection by comet assay, caspase-3/7 activation and probable role of calcium in COO-PS-NPs induced cell death. Moreover, mechanistic studies in cell free systems were also undertaken and we present evidence that COO-PS-NPs are able to directly bind to free GSH in solution and that this is the mechanism of cellular depletion of GSH.

## 5.2 Results

### 5.2.1 Cytotoxicity assessment

#### 5.2.1.1 Evaluation of cell viability by MTT assay

BEAS-2B cell were cultured and incubated with different concentrations of COO-PS-NPs for various time points (1, 4, 6, 18 and 24h) before cell viability was assessed by the MTT assay [Mosmann (1983)] to investigate possible cytotoxicity of COO-PS-NPs. Cell viability was expressed as a percent as compared to the control (untreated cells).

Statistical analysis (multiple regression) was undertaken using SPSS to predict cell viability from size, concentration and time. The results revealed that the viability of cells is dependent on concentration ($p < 0.05$) and time ($p < 0.05$) but independent from size ($p > 0.05$). This means that time of incubation and concentration of COO-PS-NPs (but not size of COO-PS-NPs) can affect the cell viability indicating a relationship between exposure time and COO-PS-NPs concentration in changing the viability of BEAS-2B cells treated with COO-PS-NPs. The multiple regression model with all three predictors, i.e. independent variables, predicted the viability of BEAS-2B cells $F(3, 428) = 4.414$, $p < 0.05$, $R^2 = 0.023$. The model to predict the viability of treated cells is:

$$\text{Viability} = 0.965 + 0.01\ \text{size} + 0.013\ \text{time} - 0.024\ \text{concentration}.$$

The results (Fig. 5.1) showed a significant decline in viability of BEAS-2B cells (related to mitochondrial activity) when treated with 20nm COO-PS-NPs only at the concentration of 300cm$^2$/ml in a time-dependent manner. Apart from that, the results

clearly show that all other concentrations (25 and 150 $cm^2$/ml) of the 20nm sized COO-PS-NPs and all concentrations (25, 150 and 300 $cm^2$/ml) of the 100nm sized COO-PS-NPs investigated had no effect on cellular viability of BEAS-2B cells over time as assessed by the MTT assay. Interestingly, they resulted in a slight increase in mitochondrial activities of BEAS-2B cells which might indicate enhanced cell growth.

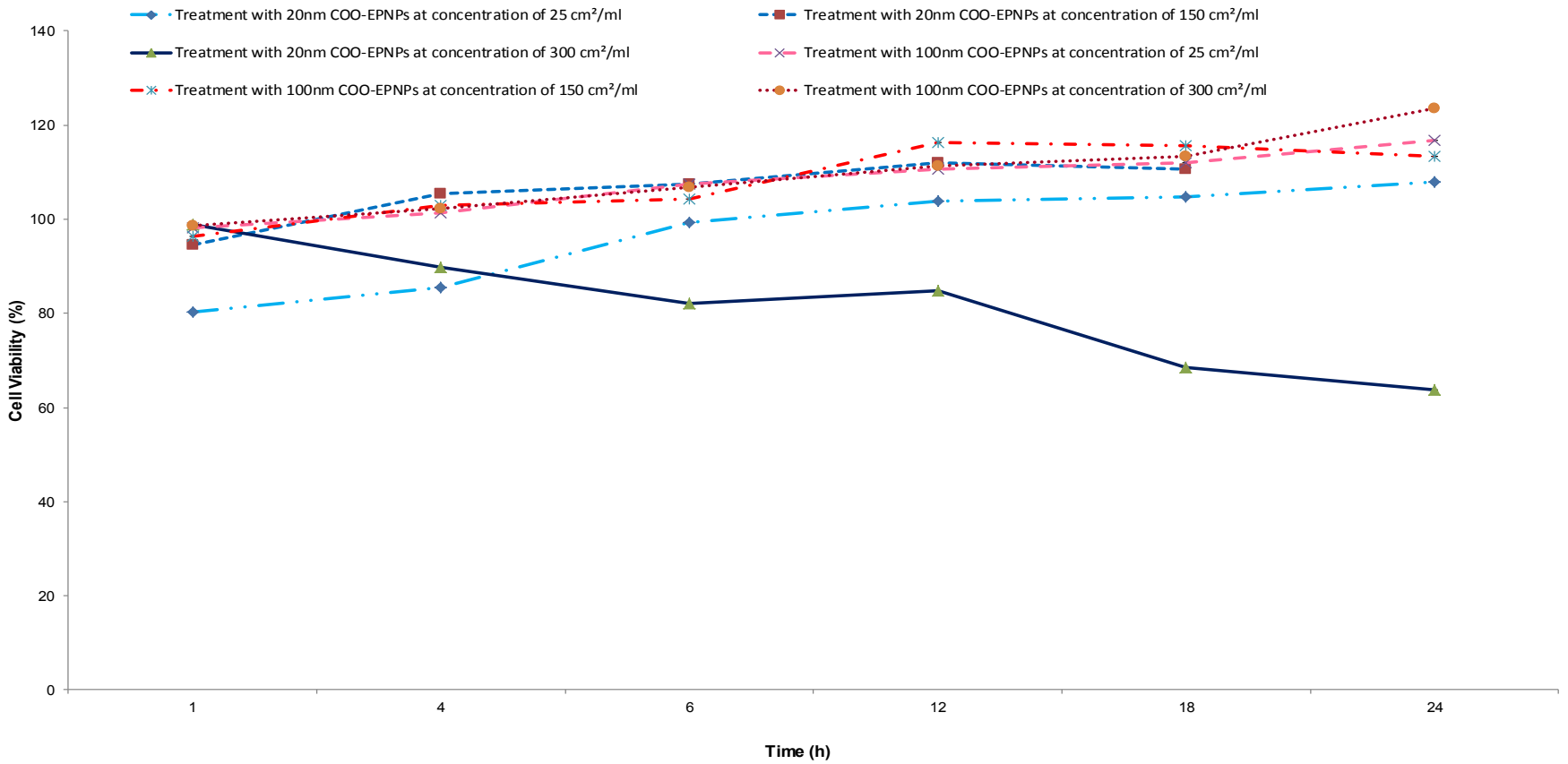


Fig. 5.1 MTT assay were performed at different time points (as specified in materials and method, see section 2.5) to evaluate the viability of BEAS-2B cells after exposure to different concentrations of COO-PS-NPs. Data show that the viability of BEAS-2B cells was decreased only after 24h treatment with 20nm COO-PS-NPs at 300cm$^2$ whereas all the other treatments with different concentrations of this 20nm sized and the 100nm sized COO-PS-NPs treatments did not significantly influence the viability of BEAS-2B cells at any time point. Investigated measurements of at least 3 samples ($n$=3) with triplicate were recorded and the error bars represent the standard error of the mean (± SEM) although they were small and could not be seen on the graph.

### 5.2.1.2 Investigation of the oxidative stress markers

#### 5.2.1.2.1 Induction of ROS by COO-PS-NPs

ROS is a key factor in both cellular toxicity and apoptosis and excess generation of ROS can trigger changes in mitochondrial membrane permeability and damages the respiratory chain, and thus induces apoptosis [Jezek et al (2005), Valko et al (2006)]. In the current study, 2',7'-dichlorodihydrofluorescein diacetate ($H_2$DCF-DA), were used to quantify ROS level in BEAS-2B cells after exposure to COO-PS-NPs to assess possible ENPs-mediated ROS-production. In the current study, ROS generation (assessed by $H_2$DCF-DA oxidation) in BEAS-2B cells was investigated at different incubation times (1, 4, 6, 12, 18 and 24h) with a range of concentrations (25, 150 and 300cm$^2$/ml) of 20nm and 100nm sized COO-PS-NPs.

The results of multiple regression conducted using SPSS demonstrated in the model that only time of incubation ($p < 0.05$) can affect the ROS generation in BEAS-2B cells whereas COO-PS-NPs concentration ($p > 0.05$) and size ($p > 0.05$) did not influence ROS level. The multiple regression model with all three predictors, i.e. independent variables, predicted the ROS production in BEAS-2B cells $F(3, 144) = 5.286$, $p < 0.05$, $R^2 = 0.099$. The multiple regression equation of ROS generation upon incubation time, concentration and size of COO-PS-NPs is:

ROS level = 23.162 + 13.08 concentration + 13.614 time – 1.918 size

However, Microsoft Excel 2010 was used to run the standard t-test (i.e. independent sample) and the results showed a significant difference in ROS production

level only after 24 hours of cell exposure to 300cm$^2$/ml of 20nm- and 100nm-sized COO-EPSNPs with a two-tailed *p* value (=0.00015478) <0.05.

The results of the experiment (Fig. 5.2) revealed that ROS generation did not change significantly when cells were exposed to different concentrations of 20nm and 100nm COO-PS-NPs at any time point except after 24h of incubation where the intracellular ROS level increased significantly with increasing concentration of the 20nm COO-PS-NPs. The highest generated ROS level in BEAS-2B cells was after incubation with 300cm$^2$/ml of the 20nm sized COO-PS-NPs for 24h while the 24h treatment of BEAS-2B cells with 150cm$^2$/ml of the 100nm sized COO-PS-NPs produced more ROS compared to other concentrations of the 100nm sized COO-PS-NPs used. Moreover, only the 18 and 24h treatment with the 20nm COO-PS-NPs at 150cm$^2$/ml and 300cm$^2$/ml significantly increased the ROS level compared to the non-treated cells whereas the other time points of incubation have no significant effect on ROS level. This would indicate that short-time exposure (<18h) may have no effect on the ROS production.

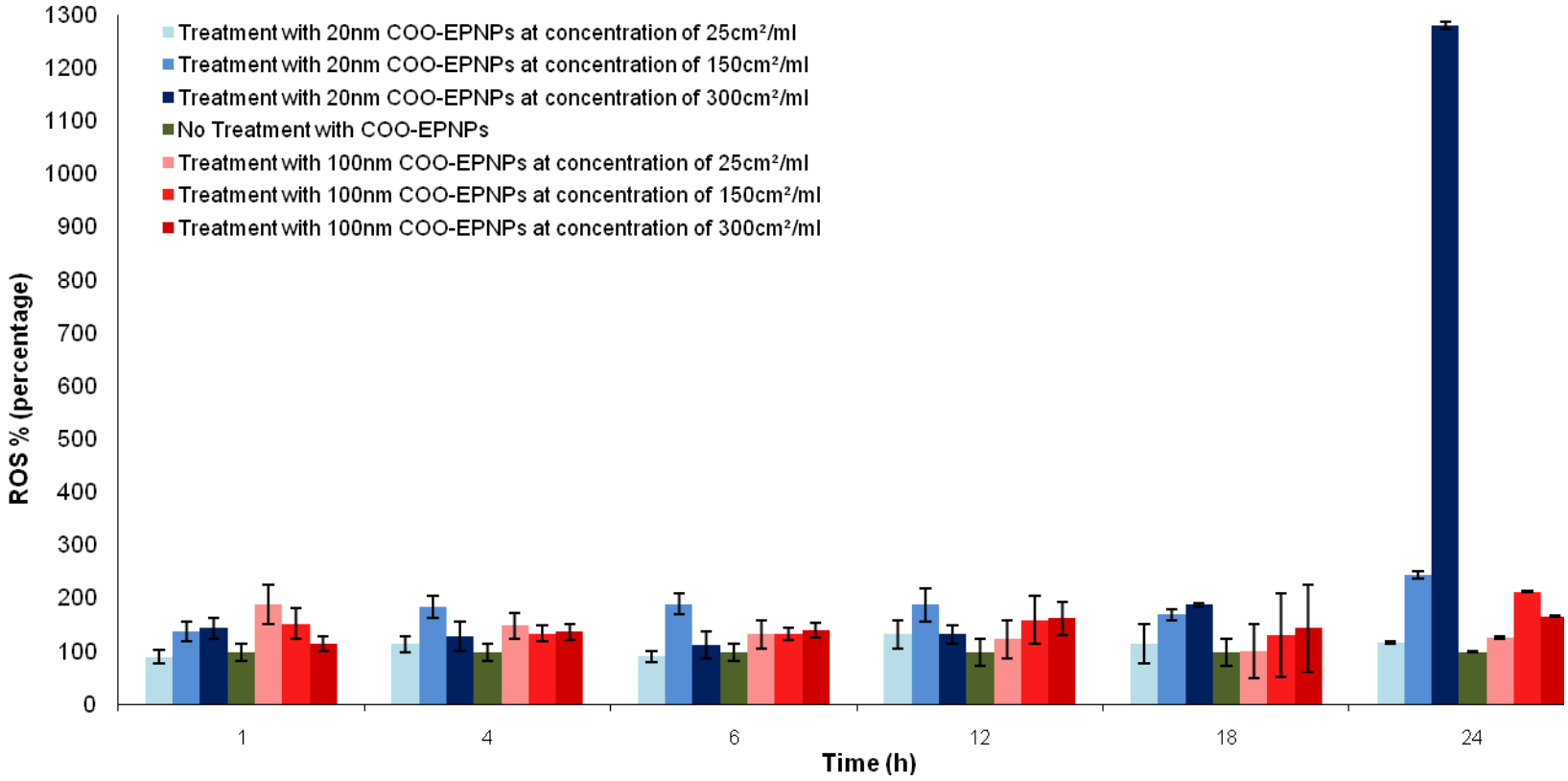


Fig. 5.2 ROS generation (assessed by $H_2$DCF-DA) did not change significantly overtime in cells exposed to different concentrations of 20nm and 100nm COO-PS-NPs except after 24h where steady increase in ROS can be seen with increasing the concentration of the 20nm COO-PS-NPs. Incubation of BEAS-2B cells with 300cm$^2$/ml of the 20nm COO-PS-NPs for 24h caused the highest ROS generation among other different treatments. Size of COO-PS-NPs and concentration used for treatment did not cause significant differences in ROS levels within one particular time of incubation. Measurements of at least 3 samples ($n$=3) were recorded and the error bars on the graph represent the standard error of the mean (± SEM).

#### 5.2.1.2.2 Depletion of intracellular GSH

GSH is an important cellular antioxidant that plays a significant role in ROS detoxification [Green et al (2006)]. Therefore, intracellular GSH levels following treatment for 24h with different concentrations of the two sized COO-PS-NPs were measured to investigate another parameter related to oxidative stress that might be altered in cells.

Multiple regression analysis was conducted to predict the average of intracellular GSH from the concentration and size of COO-PS-NPs. The results showed that the GSH depletion in COO-PS-NPs treated cells depends on both of the predictor variables, the concentration and size of COO-PS-NPs, as each of them is significant ($p < 0.05$). The multiple regression model with both predictor variables, i.e. independent variables, predicted the GSH in BEAS-2B cells $F(2, 77) = 408.267$, $p < 0.05$, $R^2 = 0.914$. The model to predict the intracellular GSH is:

Intracellular GSH = 0.722 + 0.073 size – 0.235 concentration

The results demonstrated that different concentrations of 20nm and 100nm sized COO-PS-NPs (ranging from 25 - 300 $cm^2$/ml) caused significant decreases in the total levels of GSH after 24h incubation. As can be seen (Fig. 5.3), increasing the concentrations of the 20nm and 100nm COO-PS-NPs resulted in a concentration-dependent reduction in GSH. There was a sharp decline in GSH level when BEAS-2B cells were treated with 75$cm^2$/ml of the 20nm COO-PS-NPs followed by a more gradual decline in GSH levels as the concentration of COO-PS-NPs was increased to the highest concentration of 300$cm^2$/ml. The GSH depletion caused by treatment with the 20nm

COO-PS-NPs was statistically significantly greater than that resulting from the 100nm COO-PS-NPs at equivalent concentrations.

The intracellular GSH levels were plotted against the percentage of ROS generation in BEAS-2B cells after 24h treatment with different concentrations (0, 25, 150 and 300 $cm^2$/ml) of 20nm and 100nm COO-PS-NPs (Fig. 5.4). The non-treated cells (negative control) have had the highest GSH level with the lowest ROS level and increasing the concentration of COO-PS-NPs resulted generally in a gradual increase of the ROS level associated with a steady decrease in the GSH level. Nonetheless, a significant sharp increase in ROS production was observed when cells were incubated with 300$cm^2$/ml of the 20nm COO-PS-NPs for 24h. Cells incubated for 24h with different concentrations of the100nm COO-PS-NPs behaved similarly however the highest ROS level was at 150$cm^2$/ml.

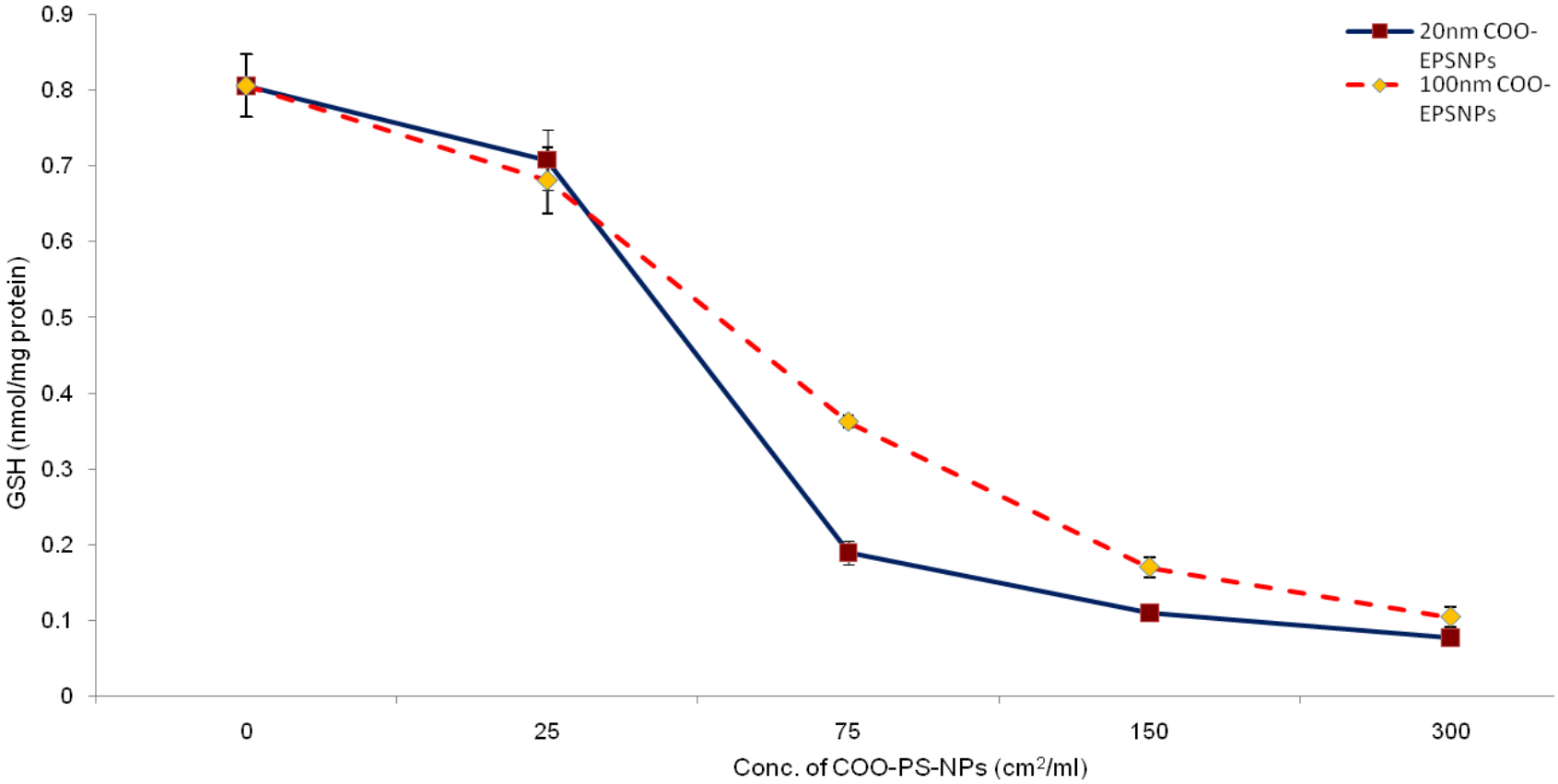


Fig. 5.3 This graph shows the depletion of intracellular level of GSH in BEAS-2B cells by COO-PS-NPs treatment for 24h. GSH level was depleted with increasing the concentrations of 20nm and 100nm of COO-PS-NPs as both caused gradual decline in GSH level with increasing the concentration of the treatment doses. Interestingly, there was a sharp drop in the cellular GSH content when cells were incubated with the 75 $cm^2$/ml of the 20nm COO-PS-NPs before retaining a more gradual decline. Measurements of four samples ($n$=4) were recorded and the error bars on the graph represent the standard error of the mean (± SEM).

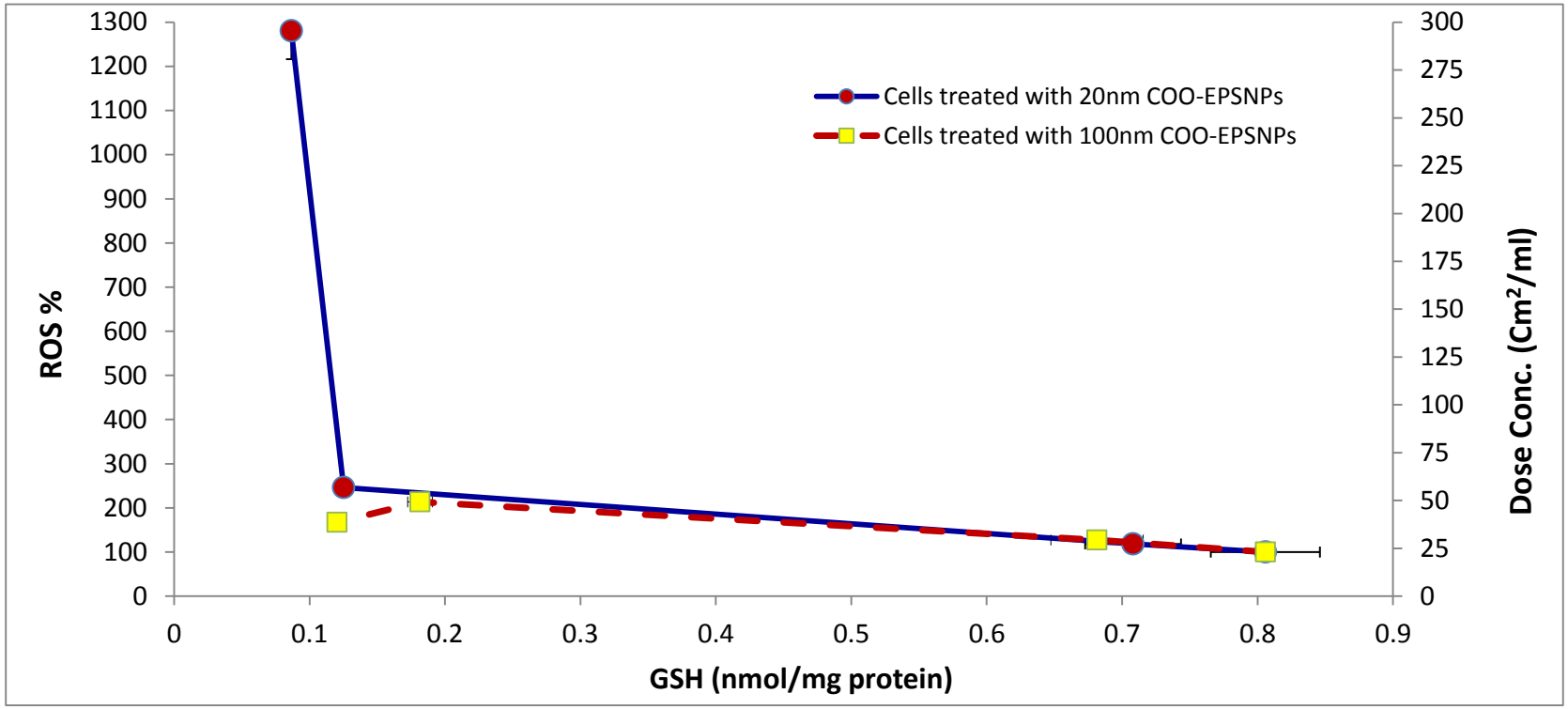


Fig. 5.4 The intracellular GSH levels plotted against the ROS generation in BEAS-2B cells exposed for 24h to different concentrations (0, 25, 150 and 300 $cm^2$/ml) of 20nm and 100nm COO-PS-NPs. The GSH level was the highest in the untreated cells while ROS level was the lowest and in general increasing the concentration of COO-PS-NPs resulted in rise of the ROS level accompanied with decline of the GSH level. In cells treated with 20nm for 24h, there were gradual increase in ROS generation and steady decrease in GSH before a sharp increase in ROS production occurred when cells were exposed to 300$cm^2$/ml. Likewise, cells treated with 100nm COO-PS-NPs for 24h followed similar pattern however the highest ROS level was at 150$cm^2$/ml.

### 5.2.1.3 Induction of DNA strand breaks

DNA single strand breaks as assessed by the comet assay were investigated by incubating BEAS-2B cells with increasing concentrations (25 and 150cm$^2$/ml) of the 20nm and 100nm COO-PS-NPs as detailed in the General Materials and Methods (see section 2.8) and the results were compared to control sample (i.e. untreated cells). Furthermore, the comet assay was used to assess the ability of the COO-PS-NPs to cause DNA strand breaks in BEAS-2B cell lysate as well as in cell suspension. The cell lysate treatments and the assays procedures carried out in this experiment were detailed in the General Materials and Methods (section 2.8.2).

SPSS was used to perform multiple regression analysis to predict the DNA damage in COO-Ps-NPs treated cell from size and concentration. The results showed that the DNA strand breaks is dependent on both ENPs concentration ($p < 0.05$) and size ($p < 0.05$) which means that both of the independent variables can affect the DNA damage in COO-PS-NPs treated cells. The multiple regression model with the two predictors produced the DNA strand breaks in BEAS-2B cells $F(2, 17) = 67.152$, $p < 0.05$, $R^2 = 0.888$. The model to predict the DNA strand breaks is:

DNA damage = 1.877 + 20.727 concentration – 5.695 size

The results of the comet assay (Fig. 5.5) show an increase in the number of DNA damaged cells after 24h treatment with 20nm and 100nm COO-PS-NPs in comparison to untreated controls. Furthermore, the amount of DNA damage was concentration-dependent and treatment with 150cm$^2$/ml resulted in more DNA damages than treatment with 25cm$^2$/ml of the same sized COO-PS-NPs. Regarding the DNA

damage measured in cell lysate and cell suspension at corresponding concentration (25 and 150cm$^2$/ml) of the 20nm COO-PS-NPs, the results revealed a lack of DNA strand breaks compared to that produced in cultured BEAS-2B cells (Fig. 5.6). Hence, this means that the DNA damage observed is real and not a result of the particles interfering with the comet assay that has been reported in some types of ENPs. The effect of the 20nm COO-PS-NPs on cell lysate and cell suspension have been investigated as these small sized ENPs caused more significant DNA injury compared with their 100nm counterparts at equivalent concentrations.

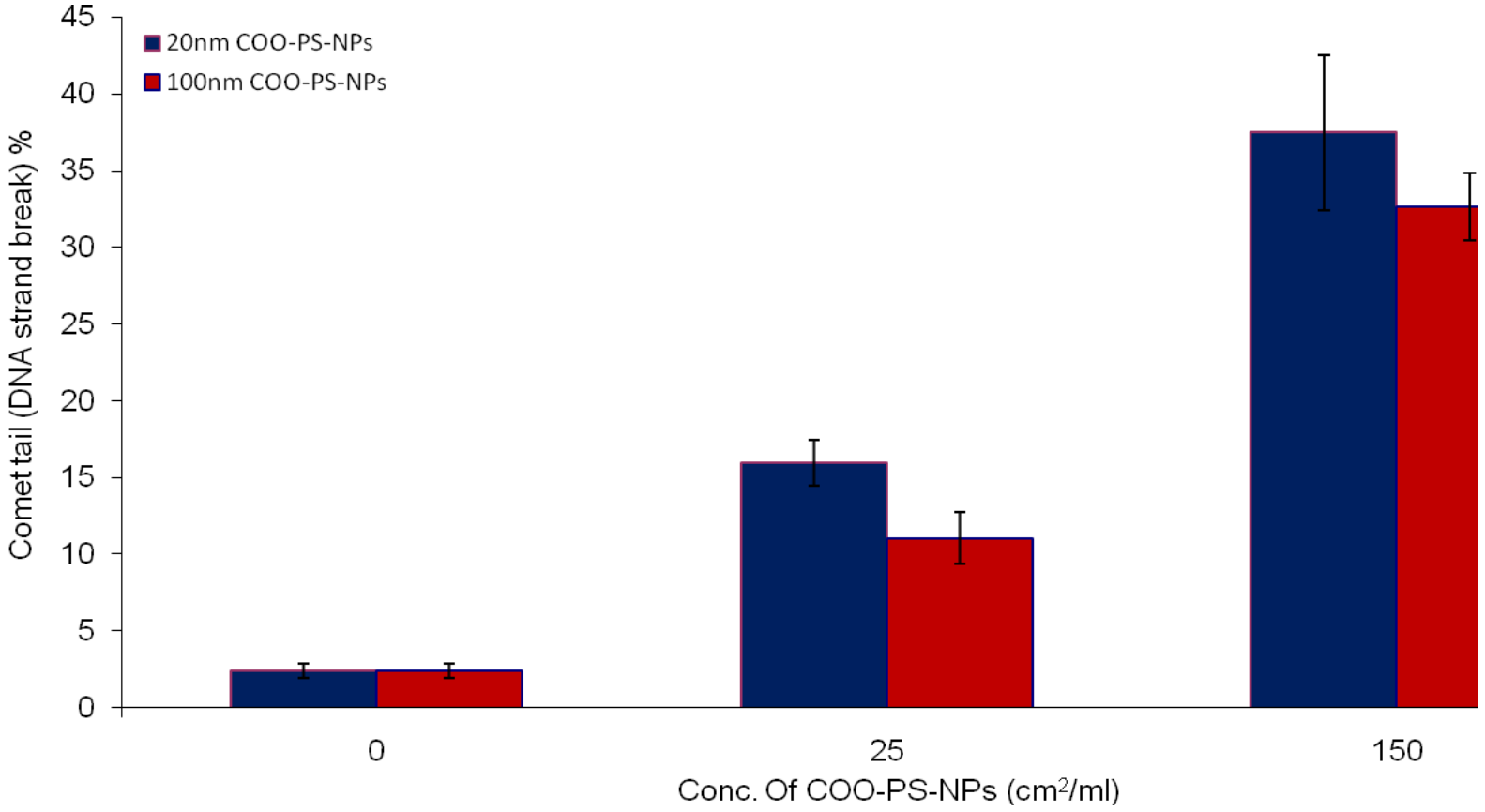


Fig. 5.5 Induction of DNA strand breaks as assessed by comet assay following 24h treatments of BEAS-2B cells with 25 and 150cm$^2$/ml of the 20nm and 100nm sized COO-PS-NPs. Results were expressed as tail intensity (percentage of DNA breaks in tail) of damaged BEAS-2B cells (at least 100 cells were counted in each sample). Significant difference can be seen in the comet tail intensity between different treatments of the same sized nanoparticles. Measurements of four samples ($n$=4) were recorded and the error bars on the graph represent the standard error of the mean (± SEM).

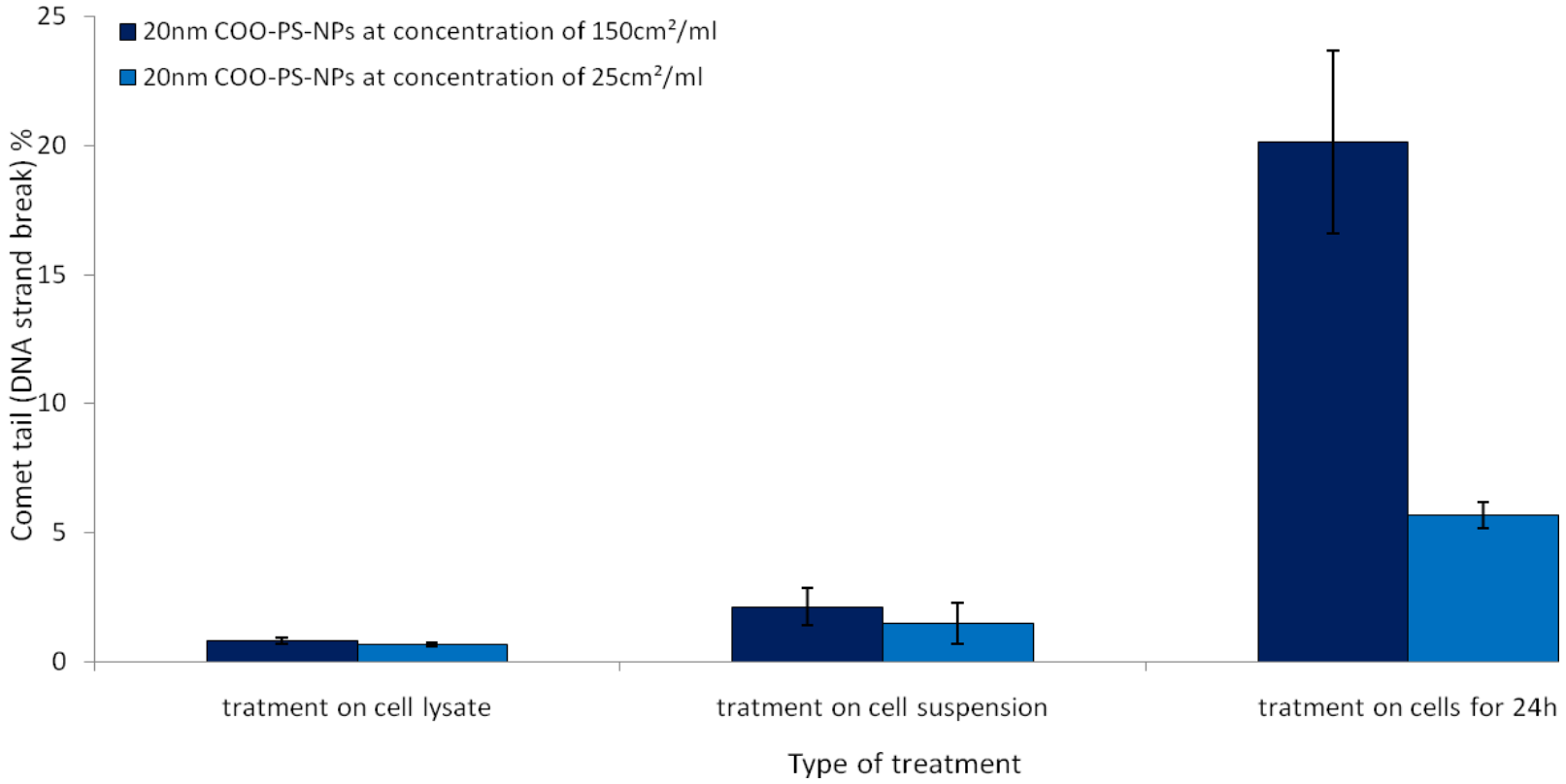


Fig. 5.6 This graph shows the DNA strand breaks detected by comet assay after various treatments with 25 and 150cm$^2$/ml of the 20nm and 100nm sized COO-PS-NPs expressed as the tail intensity (percentage of DNA breaks in tail) of damaged DNA in BEAS-2B cells, cell suspension and cell lysate (at least 100 cells were counted in each sample). There was significant difference in the comet tail intensity between the 24h treatment of whole BEAS-2B cells and the other different treatments of the same sized COO-PS-NPs. Nonetheless, no considerable variations were observed between the other treatments compared to each other or to the control. Measurements of three samples (n=3) have been recorded and the error bars represent the standard error of the mean (±SEM).

### 5.2.2 Possible role of calcium in COO-PS-NPs mediated cytotoxicity

#### 5.2.2.1 Assessment of COO-PS-NPs influenced cell viability after treatment with BAPTA

$Ca^{2+}$ is an important second messenger that is involved in regulation of several cellular processes including cell death since elevation of cytoplasmic calcium level can activate and accelerate this mechanism [Nicotera et al (1992)]. In this study, BEAS-2B cells were pretreated for 1h with 5μM BAPTA-AM (calcium chelator) before treatment with a single concentration of COO-PS-NPs for 24h and cell viability was then assessed by the MTT assay.

Statistical analysis (multiple regression) was carried out using SPSS to predict viability of cell pretreated with BAPTA-AM from NPs' size, concentration and BAPTA treatment. Statistical analysis (multiple regression) was carried out using SPSS to predict viability of cell pretreated with BAPTA-AM from NPs' size, concentration and BAPTA treatment. The results revealed that the viability of cells is dependent on size ($p < 0.05$) and BAPTA treatment ($p < 0.05$) but independent from concentration ($p > 0.05$). This means that size of COO-PS-NPs and pretreatment with BAPTA (but not concentration of COO-PS-NPs) can affect the cell viability indicating a relationship between BAPTA pretreatment and size of COO-PS-NPs used for post-treatment of cells in changing the viability of BEAS-2B cells. The multiple regression model with all three predictors, i.e. independent variables, predicted the viability of BEAS-2B cells $F(3, 216) = 29.29$, $p < 0.05$, $R^2 = 0.289$. The model to predict the viability is:

Viability = 0.951 + 0.021 size – 0.006 concentration – 0.124 BAPTA pretreatment

Likewise, independent sample t-tests performed using Microsoft Excel 2010 have showed significant differences in the viability of BEAS-2B cells treated with the 20nm-sized COO-EPSNPs only compared to cells pre-exposed to 5μM BAPTA-AM for 1h except at the 300cm$^2$/ml with two-tailed *p value*s <0.05. In contrast, excluding at the 300cm$^2$/ml, no significant differences were indicated in the viability between cells exposed first to BAPTA-AM for 1h at ahead of a treatment with 100nm-sized COO-EPSNPs and cells presented purely to the 100nm-sized COO-EPSNPs for 24h with two-tailed *p* values >0.05.

This would mean that the 1h 5μM BAPTA-AM pretreatment could significantly affect the viability of BEAS-2B cells when treated with the 20nm-sized COO-PS-NPs (Fig. 5.7) since this caused a considerable decrease in the MTT reduction of BEAS-2B cell in comparison to cells exposed only to 20nm COO-PS-NPs. On the other hand, this 1h pre-exposure to 5μM BAPTA-AM could not significantly affect the cell viability treated with the 100nm-sized COO-EPSNPs (Fig. 5.8).

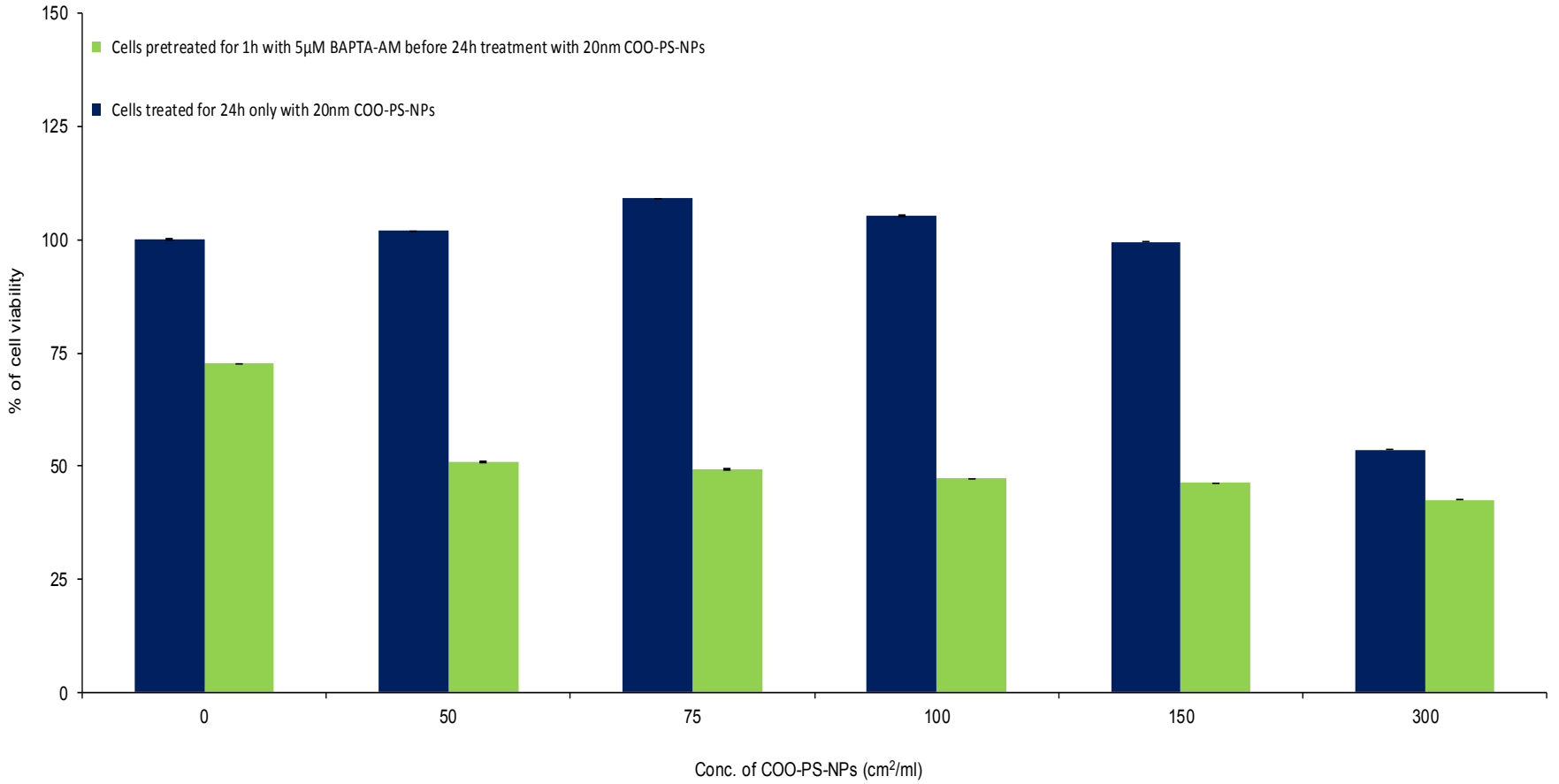


Fig. 5.7 The MTT assay showed that the 1h pretreatment with BAPTA-AM (5µM) followed by 24h exposure to 20nm sized COO-PS-NPs (ranged 50 -300 $cm^2$/ml) caused a reduction in the viability of BEAS-2B cells in comparison with the 24h exposure to COO-PS-NPs at their own. Measurements of five samples (n=5) were recorded and the error bars on the graph represent the standard error of the mean (± SEM).

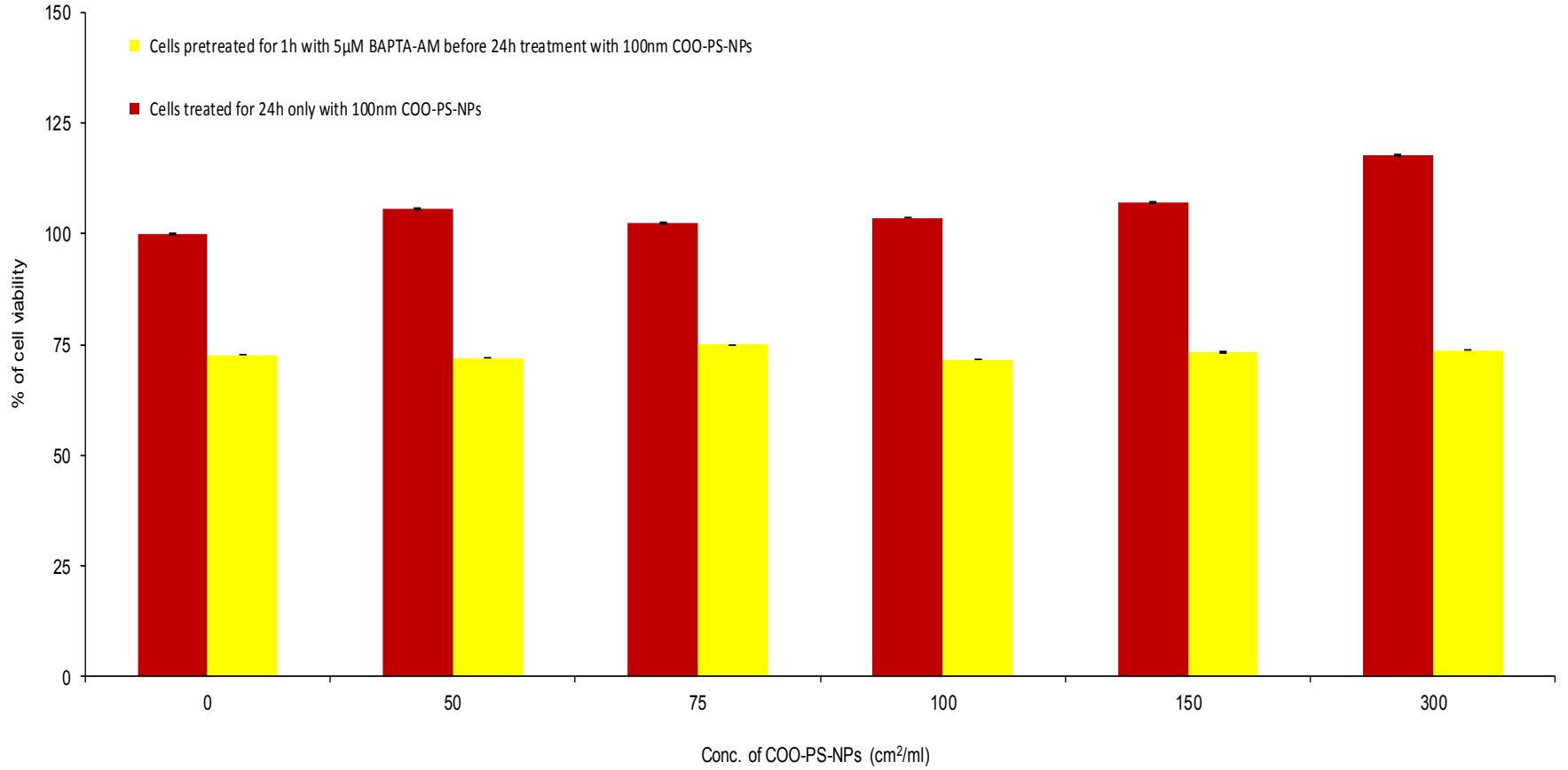


Fig. 5.8 The MTT assay results revealed that the viability of BEAS-2B cells pre-exposed to BAPTA-AM (5µM) for 1h followed by 24h treatment with 100nm sized COO-PS-NPs (ranged 50 -300 $cm^2$/ml) was significantly decreased compared the 24h treatment solely with equivalent concentrations of COO-PS-NPs. Measurements of five samples (n=5) were recorded and the error bars on the graph represent the standard error of the mean (± SEM).

#### 5.2.2.2 Measurement of COO-PS-NPs induced ROS level after treatment with BAPTA

The same treatments used for investigating the role of $Ca^{2+}$ on the cell viability (as assessed by the MTT assay) were also used to evaluate the possible effect of $Ca^{2+}$ on ROS production in BEAS-2B cells following individual exposure to two different concentrations (75 and 150$cm^2$/ml) of 20nm and 100nm COO-PS-NPs for 24h preceded by 1h treatment with BAPTA-AM (5μM). The results (Fig. 5.9) demonstrated significant differences in the ROS generation caused in cells treated only with COO-PS-NPs for 24h and that caused in cells pretreated with BAPTA-AM (5μM) for 1h before 24h treatment with COO-PS-NPs (of 20nm and 100nm) at equivalent concentration (of 75 and 150$cm^2$/ml). It showed that 1h pretreatment with BAPTA-AM statistically and significantly increased the ROS generation before treatment with COO-PS-NPs 24h compared to the 24h treatment with COO-PS-NPs only.

Three independent variables (that are BAPTA, size and concentration of COO-PS-NPs) were involved in multiple regression analysis using SPSS to predict ROS generation in BEAS-2B cells. The results revealed that the viability of cells is dependent on size of COO-PS-NPs ($p < 0.05$) and BAPTA ($p < 0.05$) but independent from concentration ($p > 0.05$). The multiple regression model with all three independent variables predicted the level of ROS in BEAS-2B cells $F(3, 36) = 10.028$, $p < 0.05$, $R^2 = 0.455$. The model to predict the ROS is:

$$ROS = 43.598 + 3.695\ BAPTA + 0.003\ concentration - 0.111\ size$$

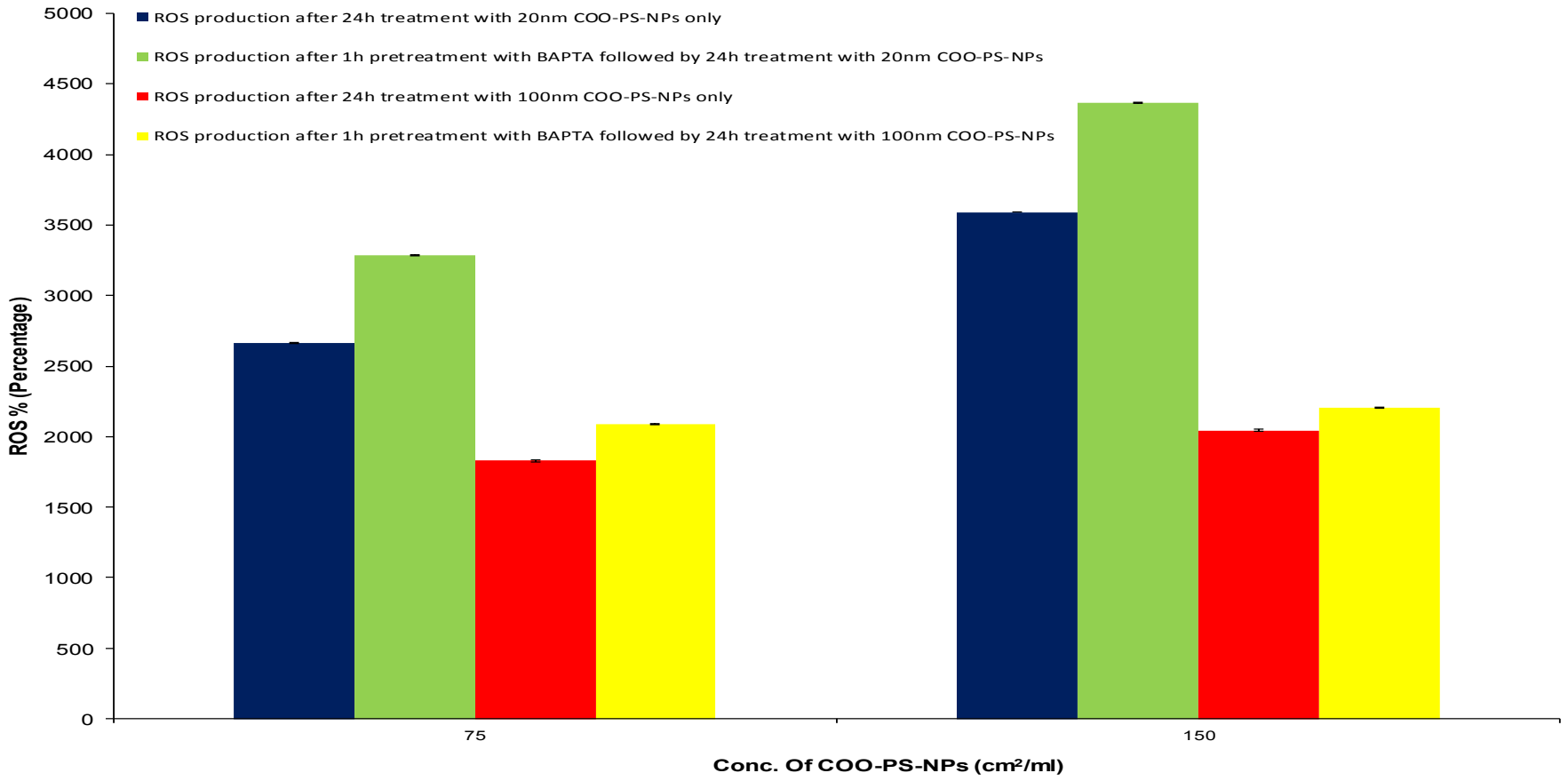


Fig. 5.9 The results showed that ROS generated in cells pretreated with BAPTA-AM for 1h before being exposed to COO-PS-NPs for 24h is significantly increased in comparison to ROS generated in cells exposed for 24h only to same sized COO-PS-NPs (at corresponding concentration). ROS generation seems to be stimulated by the BAPTA-AM pretreatment. Measurements of four samples (n=4) were recorded and the error bars on the graph represent the standard error of the mean (± SEM).

### 5.2.3 Induction of caspase-3/7 activity by COO-PS-NPs

Activation of caspases-3 and -7 is an important event in apoptosis that results in irreversible commitment to cell death [Cullen and Martin (2009)]. Thus, measurement of the activity of the caspases-3/7 was conducted to investigate whether COO-PS-NPs induced cell death involves activation of caspases or not. The results (Fig. 5.10) revealed that only the 24h treatment with the 20nm sized COO-PS-NPs resulted in significant caspases-3/7 activation.

Multiple regression was performed as a statistical analysis by SPSS to predict the caspases-3/7 activity using size and concentration of COO-PS-NPs. The results showed that the caspases-3/7 activation in BEAS-2B cells is significantly dependent on the size of COO-PS-NPs ($p < 0.05$) but not on their concentration ($p > 0.05$). This means that only the size of COO-PS-NPs influences the activation of caspases-3/7 in BEAS-2B cells treated with COO-PS-NPs. The multiple regression model with the two independent variables predicted the caspases-3/7 activity in BEAS-2B cells $F(2, 162) = 5.922$, $p < 0.05$, $R^2 = 0.068$. The model to predict the activation of caspases-3/7 is:

Caspases-3/7 activity = 3287.278 + 33.268 concentration - 337.447 size.

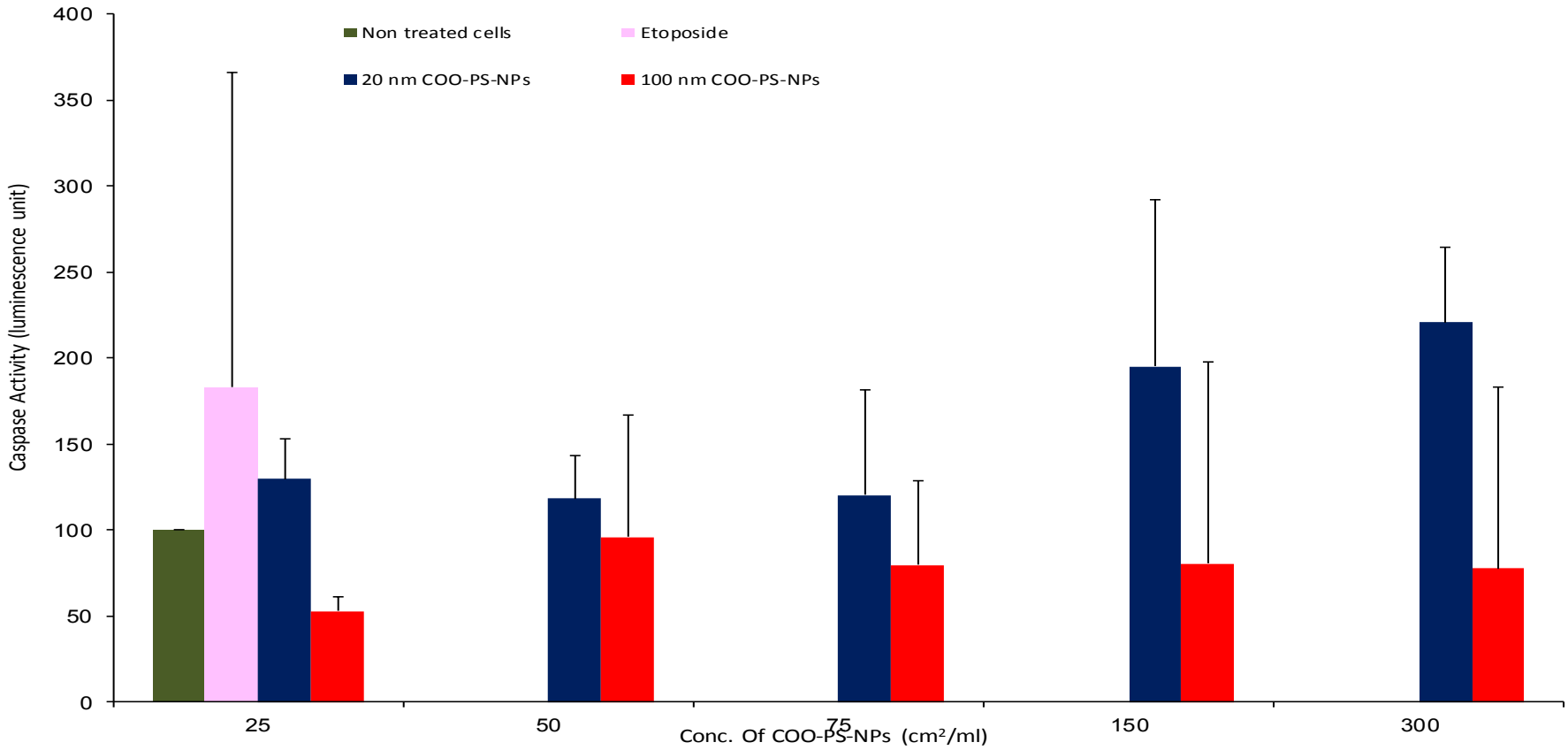


Fig. 5.10 BEAS-2B cells were incubated for 1hr with the caspase reagent following treatment with different concentrations (25-300cm$^2$/ml) of 20nm and 100nm COO-PS-NPs for 24h or with Etoposide (as +Ve control) for 2h before measuring the luminescence. Compared to the negative control sample, the results showed that only the 20nm sized COO-PS-NPs significantly activated caspases-3/7 in BEAS-2B cells in a concentration-dependent manner (to some extent) while the 24h treatment with the 100nm COO-PS-NPs did not cause caspases-3/7 activation. Measurements of at least five samples were recorded and the error bars represent the standard error of the mean (± SEM).

### 5.2.4 Depletion of the GSH by COO-PS-NPs in cell-free systems

ENPs are known to adsorb and bind proteins and other bio-molecules in biological fluids forming a corona [Lundqvist et al (2008), Cedervall et al[b] (2007)]. Results of a previous experiment in this chapter of current study have shown a depletion of the intracellular GSH content after 24h incubation of BEAS-2B cells. Consequently, it was of interest to investigate whether the mechanism of GSH depletion was due to detoxification of the COO-PS-NPs generated ROS or due to a direct physical interaction between COO-PS-NPs and GSH molecules. This was performed in cell-free systems where GSH compound (final concentration of 3.25μM) were left alone in one tube or mixed well with single concentration (25 or 150 $cm^2$/ml) of the 20nm or 100nm sized COO-PS-NPs in another tube before all being incubated on ice for 1hr. The GSH level was then measured in these solutions as detailed in the General Materials and Methods (section 2.12.1).

Statistical multiple regression analysis was conducted using SPSS to predict cell GSH level from size and concentration of COO-PS-NPs. The results demonstrated that the GSH level in cell-free solutions is significantly dependent on the concentration of COO-PS-NPs ($p < 0.05$) but not on their size ($p > 0.05$). This means that only the concentration of COO-PS-NPs has an impact on the GSH level measured in cell-free system. The multiple regression model with the two independent variables predicted the GSH level $F(2, 57) = 6.718$, $p < 0.05$, $R^2 = 0.191$. The model to predict the GSH level is:

GSH level = 1.042 + 0.009 size – 0.154 concentration.

The results (Fig. 5.11) demonstrated that incubation of COO-PS-NPs with GSH in cell free solutions resulted in significant COO-PS-NPs concentration-dependent decreases in the concentrations of detectable GSH. The GSH content was at high concentration (of approximately 1.5μg/ml) in GSH solution but dropped in solutions containing GSH mixed with the 20nm sized COO-PS-NPs (at concentrations of 25 and 150$cm^2$/ml to 1.21 and 0.74μg/ml respectively) and in solutions containing GSH mixed with the 100nm sized COO-PS-NPs (at concentrations of 25 and 150$cm^2$/ml to 1.28 and 0.83μg/ml respectively). The decline was found to be slightly more in the 20nm COO-PS-NPs containing solutions than those with 100nm COO-PS-NPs. However, the GSH level was higher in these cell-free systems in comparison to the GSH level measured in the BEAS-2B cells following 24h treatments with various concentrations (25 and 150$cm^2$/ml) of the 20nm and 100nm COO-PS-NPs.

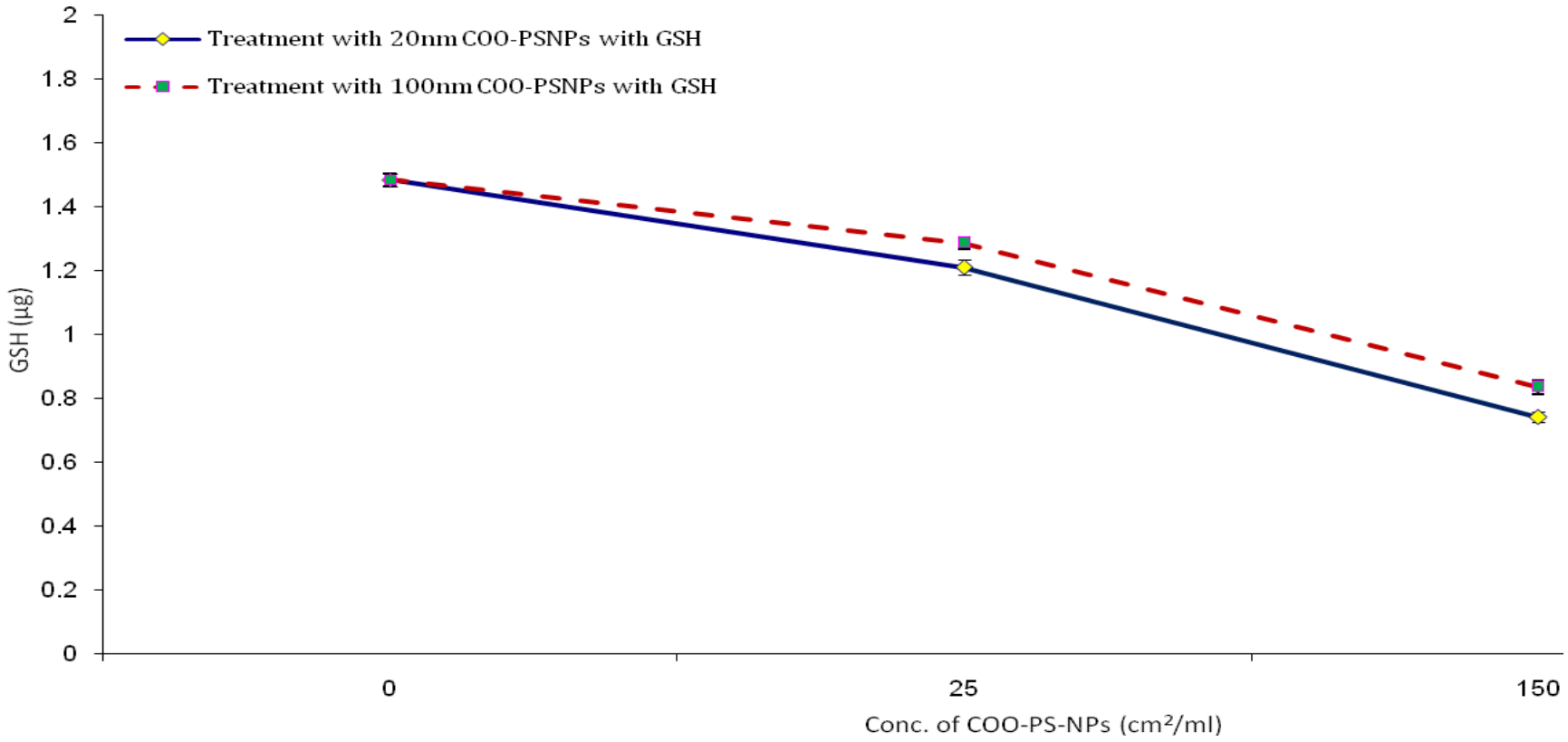


Fig. 5.11 The GSH level was measured (µg) in different cell-free solutions that were composed of GSH compound mixed with individual concentration of COO-PS-NPs (20nm or 100nm) at different concentrations (25 and 150$cm^2$/ml while the zero concentration represents GSH compound only without COO-PS-NPs molecules). The results showed that the GSH level declined in a dose-dependent manner in COO-PS-NPs containing cell-free solutions and that the 20nm sized COO-PS-NPs caused more decrease compared to the 100nm at the same concentrations. Measurements of four samples (n=4) have been recorded and error bars represent the standard error of the mean (±SEM).

### 5.2.5 Evaluation of the GSH level in COO-PS-NPs treated cell lysate

Because incubation of GSH solutions with COO-PS-NPs in cell-free system could decrease the concentration of measurable GSH, it was important to investigate whether a similar effect could be observed when COO-PS-NPs were incubated with GSH containing cell extracts prepared from BEAS-2B cells. Therefore, BEAS-2B cells were cultured for 24h before extracting the lysate that was then exposed to COO-PS-NPs for 1h and the GSH level was measured in this cell lysate.

The results illustrated that incubation of cells extracts with both of 20nm and 100nm sized COO-PS-NPs caused significant decreases in detectable GSH levels in cell lysates compare to the non-treated lysate (Fig. 5.12). However, no significant differences in GSH level were observed neither between the 20nm and the 100nm COO-PS-NPs used for treatment at equivalent concentrations nor between different concentrations of the same sized COO-PS-NPs.

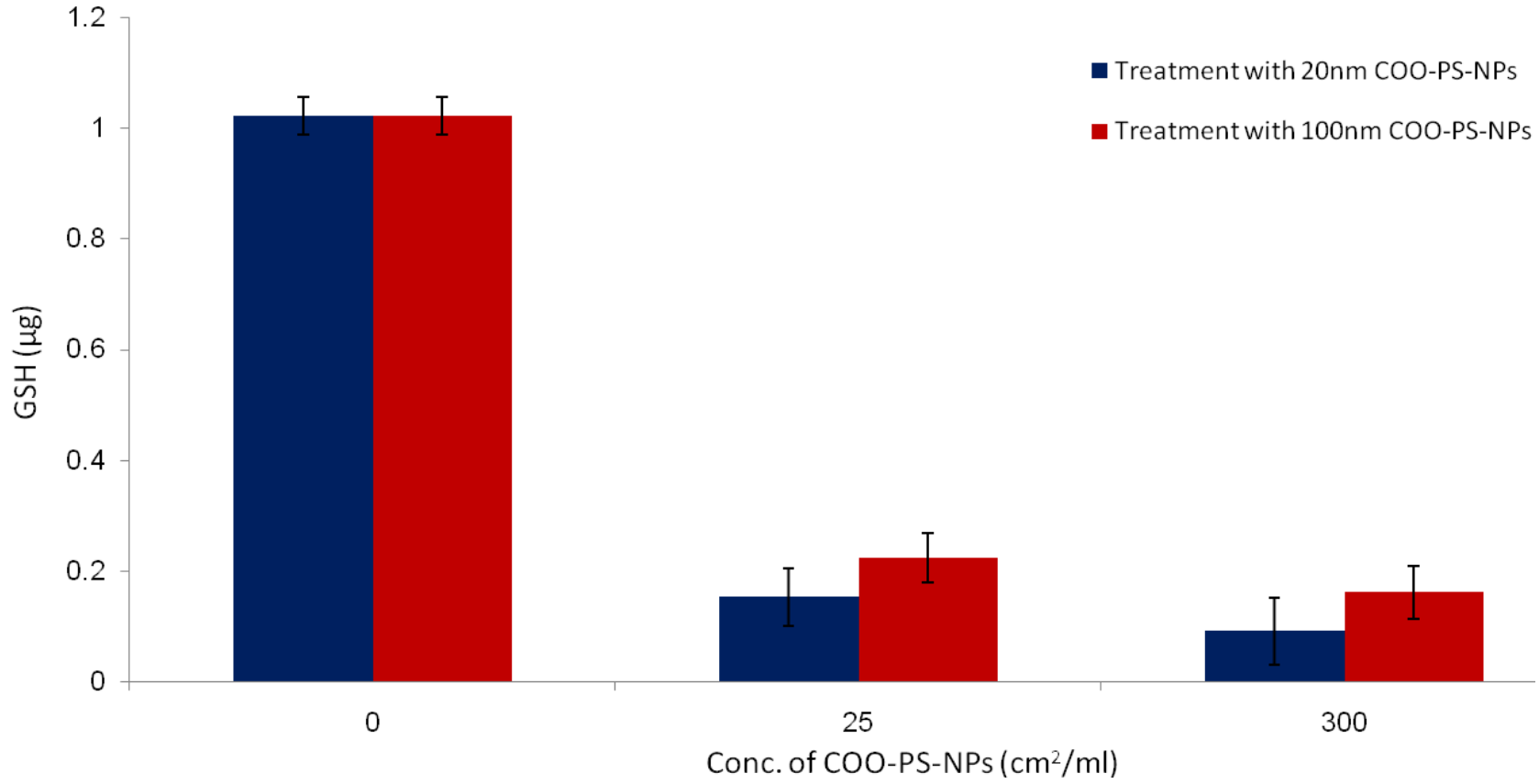


Fig. 5.12 The GSH level measured in cell lysates treated with 20nm and 100nm COO-PS-NPs at various concentrations (of 25 and 300$cm^2$/ml) for 1h showed significant decreases compared with non-treated lysate. The GSH level decline was not significantly in concentration- or size-dependent manner. Measurements of six samples (n=6) have been recorded and the error bars represent the standard error of the mean (±SEM).

## 5.3 Discussion

This study used a range of concentrations (25-300$cm^2$/ml) of two different sized COO-PS-NPs (20nm and 100nm) to treat BEAS-2B cells for different time points (1-24h) before investigating different biological markers related to toxicity. The results of MTT assay showed that the 100nm sized COO-PS-NPs were not toxic as assessed by this assay at any of the concentrations investigated over the time course. Likewise, the cell viability as assessed by MTT assay in BEAS-2B cells treated with low concentrations (≤ 150$cm^2$/ml) of the 20nm sized COO-PS-NPs was not significantly altered following up to 24h treatment. In contrast, treatment with the 20nm sized COO-PS-NPs at high concentration (300$cm^2$/ml) caused significant cell death in a time-dependent manner but mainly after 24h incubation (Fig. 5.1). Previous literatures that studied the toxicity of a variety of nanoparticles on several cell lines have proposed that the toxicological effect of nanoparticles depends on the NPs' composition [Sohaebuddin et al (2010)], NPs' size [(Fröhlich et al[b] (2012)], NPs' concentration [Çiftçi et al (2013)] and time of incubation [Bottini et al (2006)]. In agreement, the cell viability results of this study indicate that the COO-PS-NPs toxicity is particle's size-, concentration- and time-dependant. This concentration-dependent decrease in BEAS-2B cell viability was associated with a concentration-dependent elevation of the intracellular ROS level (Fig. 5.2) induced by the 20nm COO-PS-NPs. In contrast, there was little evidence of ROS formation in cells treated with 100nm COO-PS-NPs at any of the concentration investigated. Consequently, the cell viability decrease might be attributed to the oxidative stress stimulated by 20nm COO-PS-NPs and several previous studies have reported that increased ROS levels is a

possible mechanism of toxicity for COO-PS-NPs including induction of programmed cell death [(Fröhlich et al[a] (2012)]. Moreover, the three factors (i.e. incubation time, COO-PS-NPs' size and concentration) seem to work altogether to affect the ROS production since the ROS level did not change significantly over incubation time in COO-PS-NPs treated cells in comparison with the non-treated ones except when incubated with the 20nm COO-PS-NPs at high concentrations ($\geq$150cm$^2$/ml) for long period of time ($\geq$18h). A number of concerns have challenged using this dye for evaluating the intracellular redox status change. It has been reported, for instance, that DCF (the oxidized fluorescent product) might leach out of cells which lead to underestimation of the oxidative stress [Jakubowski and Bartosz (1997)]. Additionally, cytochrome *c* release from the mitochondria during apoptosis has been reported to be a strong oxidative catalyst for $H_2$DCF-DA and can result in overestimation of the oxidative stress [Lawrence et al (2003)]. Therefore, $H_2$DCF-DA should be carefully used for oxidative stress measurements when apoptosis occurs as a result of ENPs exposure. Moreover, this possible mitochondrial release of cytochrome *c* might explain the big ROS resulted at high concentration of the 20nm COO-PS-NPs.

It is well known that GSH has an essential role as a cellular anti-oxidant [Jefferies et al (2003)] and that elevated levels of ROS can deplete the intracellular GSH. In the current study, cell treatment with both of the 20nm and 100nm sized COO-PS-NPs caused GSH status of cells to be reduced in a concentration-dependent manner (as can be seen in Fig. 5.3). GSH level was severely dropped at 75cm$^2$/ml of the 20nm COO-PS-NPs after which the GSH level retains the gradual decrease trend down to the high dose

concentration of 300 $cm^2$/ml. Taken together, our experimental results would suggest that the cell toxicity observed is caused by ROS elevated levels in BEAS-2B cells treated with high concentrations (300$cm^2$/ml) of 20nm COO-PS-NPs accompanied with a decline in the intracellular GSH content level as it becomes oxidised in response to NP-induced oxidative stress. Continuous ROS generation at high concentration of the 20nm sized COO-PS-NPs results in excessive ROS accumulation that would exhaust GSH (and other protective factors) and exceed the cellular defensive mechanism leading to the reduced cell viability observed. In contrast, cells exposure to the 100nm COO-PS-NPs or to low concentrations (≤150$cm^2$/ml) of the 20nm COO-PS-NPs did not significantly reduce cell viability because although cells were stressed other sufficient cellular non-enzymatic antioxidants (such as vitamin C) might remain in the cell and can hence still counteract the damaging effects of ROS and maintain cell viability. Furthermore, DNA damage is known to be caused by several stimuli including cellular ROS [Hoeijmakers (2001)] and the current study showed that COO-PS-NPs induced ROS generation in BEAS-2B cells (as assessed by $H_2$DCF-DA) in a ENPs' size-dependent manner at a particular time point. Taken together, this mean that the 20nm COO-PS-NPs produced higher ROS level than the 100nm COO-PS-NPs and this would be the reason that make the 20nm sized COO-PS-NPs to be more toxic leading to more DNA damages in BEAS-2B cells after 24h compared to the 100nm sized COO-PS NPs at the same concentration (of 25 and 150$cm^2$/ml) investigated. Moreover, no significant DNA strand breaks have been observed when COO-PS-NPs were individually introduced directly to cell lysate and cell suspension (Fig. 5.6) indicating that the DNA damage was not due to direct interaction

between COO-PS-NPs and the DNA since both (the DNA and COO-PS-NPs) are negatively charged molecules.

$Ca^{2+}$ has many key roles in cellular functions and it is involved, for example, in regulating apoptosis by inducing caspases-3 activation in response to various stimuli [Hajnoczky et al (2003), Orrenius et al (2003), Tantral et al (2004)]. Disrupting the intracellular $Ca^{2+}$ has been suggested to be a possible mechanism of toxicity of ENPs [Xia et al (2008)]. BAPTA ($Ca^{2+}$ chelator) was used therefore to control the cytosolic $Ca^{2+}$ activity in BEAS-2B cells and subsequently enable investigating the possible role of $Ca^{2+}$ in COO-PS-NPs toxicity. The results of cell viability (as assessed by MTT assay) showed that the cell pretreatment with BAPTA-AM did not prevent cell death by the 20nm COO-PS-NPs after 24h exposure. This would suggest that although $Ca^{2+}$ is important in multi cellular functions, but this divalent cation might not fundamentally contribute in the COO-PS-NPs-induced cell death mechanism in BEAS-2B cells and that other $Ca^{2+}$-independent pathway might be involved in mediating the cytotoxicity, for instance via rupture of the mitochondrial transmembrane due to COO-PS-NPs co-localisation and release of the mitochondrial components such as cytochrome *c* into the cytosol which would hence lead to cell death. It has been stated that increasing the intracellular $Ca^{2+}$ is not crucial for apoptotic mechanism [Kluck et al (1994)] and the cellular $Ca^{2+}$ homeostasis disruption has been suggested to be a downstream event that takes place at late phase while GSH depletion occurs at earlier stage in oxidant-induced cell death [Macho et al (1997)]. In contrast, the exposure of BEAS-2B cells to COO-PS-NPs (at 20nm) following pretreatment with BAPTA-AM has surprisingly reduced the cell

viability even at low (non-toxic) concentrations that did not considerably show any effect by their own (Fig. 5.7 and 5.8). BAPTA-AM has been stated to induce apoptosis causing death of cultured cells [Kluck et al (1994)]. Moreover, the ROS generation (as assessed by the $H_2$DCF-DA assay) was significantly increased by COO-PS-NPs in BAPTA pretreated BEAS-2B cells in the current study (Fig. 5.9) and these data would suggest that the ROS generation induced by COO-PS-NPs is not triggered by $Ca^{2+}$ but it may have some role.

Caspase-3 and -7 are executioner (effector) caspases and considered major mediators for the execution of apoptosis since their activation by initiator caspases (in an upstream cascade) is a crucial event to cleave other substrates in a downstream proteolytic process that can lead to apoptosis (programmed cell self-destruction) [Cullen and Martin (2009)]. Therefore, activation of caspases-3and -7 was assessed in BEAS-2B cells following treatment with COO-PS-NPs to investigate their role in decreasing cell viability. The results (Fig. 5.10) showed that COO-PS-NPs caused caspases-3/7 activation in BEAS-2B cells only when treated with 20nm COO-PS-NPs mainly at high concentration of 300$cm^2$/ml where cell viability was significantly decreased as assessed by the MTT assay. This would suggest that the toxicity of the 20nm sized COO-PS-NPs in BEAS-2B cells is mediated through the activation of caspases-3/7. This caspases-3/7 activation caused by the 20nm sized COO-PS-NPs can be attributed to their capability to colocalise into the mitochondria as observed by confocal microscopy (see previous chapter) and this ability seems to be the reason that makes the 20nm sized COO-PS-NPs more toxic than the 100nm counterparts. Such mechanism of caspases-3/7 activation

dependent toxicity (that cause cell death) has been observed in different cells when treated with small sized ENPs such as amine-modified polystyrene nanoparticles (NH-PS-NPs) introduced to human brain astrocytoma cells [Bexiga et al (2011)] and to macrophages (RAW 264.7) at size of 60nm [Xia et al (2008)] as well as in bronchial epithelial (16HBE14o) cells exposed individually to carbon nanoparticles (CB-NPs) at size of 13nm and to titanium dioxide ($TiO_2$ NPs) at size of 15nm [Hussain et al (2010)].

The levels of GSH in cell-free solutions incubated with COO-PS-NPs (20nm or 100nm) were measured to investigate whether GSH depletion observed in the COO-PS-NPs treated BEAS-2B cells was related to detoxification of the COO-PS-NPs induced ROS or due to direct interaction between GSH and COO-PS-NPs. The results (Fig. 5.11) have shown significant decreases of the GSH levels compared to the solution of GSH only (that was in a NPs-free system) and this would reveal possible binding between GSH and COO-PS-NPs under certain conditions. It is well-known that GSH is a stable tri-peptide molecule with net negative electrical charge on the C-end of the Gly residue under physiological pH conditions, however it has a zwitterion (i.e. hybrid ions) on the N-end of the Glu residue of its structure [Yan et al (2007)]. This means that the GSH would be able to react with acids and bases and thus these GSH molecules might have interacted with (and bound to) the negatively charged COO-PS-NPs through the zwitterionic surface on the N-terminus forming nanoparticle induced GSH aggregation and causing a drop in the GSH level observed in free-cell systems. The GSH level in the cell-free systems was inversely correlated with the concentration of the COO-PS-NPs used in these solutions (Fig. 5.11). Moreover, the GSH levels in these cell-free systems

were generally higher than that in the COO-PS-NPs treated BEAS-2B cells at equivalent concentrations since the ROS molecules in the biological system (beside the COO-PS-NPs) would take part in depleting the GSH level. In addition, there would be some free GSH molecules (i.e. COO-PS-NPs boundless GSH molecules) in the cell-free system that came from the added GSH compound. Furthermore, there was a drop in the GSH level in cell lysate and cell suspension exposed to the 20nm and 100nm COO-PS-NPs (Fig. 5.12) which support the findings about the capability of the COO-PS-NPs to bind GSH.

In conclusion, these experiments show that 24h treatment of BEAS-2B cells with the 20nm COO-PS-NPs at high concentrations ($300cm^2/ml$) can cause $Ca^{2+}$-independent generation of ROS, GSH depletion, ROS-mediated oxidative stress and DNA damage leading consequently to cell death (mainly apoptosis) that involves caspase-3/7 activation. Results would suggest that raising the cytosolic $Ca^{2+}$ do not have a direct role in the COO-PS-NPs-induced cell death mechanism in BEAS-2B cells and that other cytosolic $Ca^{2+}$-independent pathway seems to be involved in the cytotoxicity of the COO-PS-NPs, via mitochondrial damage for example since mitochondria are vital organelles for cellular energy production. This can happen as consequence of the COO-PS-NPs co-localisation into the mitochondria which would have a toxic effect in the cell.

# CHAPTER SIX:

# GENERAL DISCUSSIION

## 6.1 General discussion

NPs are materials with at least one external nano-scaled dimension (≤100nm) and they have increasingly been synthesized and used widely for various applications because of their unique physicochemical characteristics. However, they might also cause a risk of harmful effects on health and environment as several researches have reported that their use can cause cell death through ROS generation and oxidative stress which have been suggested to result in NPs-induced apoptosis [Nel et al (2006), De Stefano et al (2012)]. Moreover, many global researches are ongoing for further investigations of the physicochemical characteristics of ENPs that might help in making it possible to use them for other applications. This widespread use of ENPs makes exposure to them inevitable and inhalation is the primary potential exposure route of the body making the lung a major target for NP-mediated toxicities [Mühlfeld et al (2007)]. The toxicological effects of ENPs need consequently to be individually investigated to identify possible risk on environment and human health before employing them in medical and other industrial applications.

COO-PS-NPs have potential applications as vehicles for drug delivery, for example anti-tuberculosis drug in addition to take part in other wide range of applications. It has therefore been recommended that special attention should be paid to ENPs designed for drug delivery or for food components and systematic investigations [Hoet et al (2004)]. Accordingly, it is of great importance to assess the potential risks of COO-PS-NPs to lungs at the cellular level and understand how they would cause their biological and toxicological effect. Furthermore, monitoring the uptake and co-

localisation of these COO-PS-NPs into different organelles would be helpful in elucidating the possible role of the physicochemical properties of COO-PS-NPs. This study was conducted *in vitro* (BEAS-2B lung epithelial cells) with a range of concentrations (25-300$cm^2$/ml) of two different sized fluorescently labelled COO-PS-NPs (20nm and 100nm in diameter) to investigate the role of size and concentration on uptake and to observe their co-localisation within different cellular compartments with the ultimate aim of studying their biological effects.

MTT assay is widely used technique and considered as an easy, fast and powerful colorimetric method to assess the cell viability by evaluating the mitochondrial activity of cells [Horie et al (2012)] using the yellow 3-(4,5-dimethyl-2-thiazolyl)-2,5-diphenyl-tetrazolium bromide and simple optical density reader machine to yield reproducible results. The MTT results in this study showed significant decrease in viability of BEAS-2B cells when treated with the 20nm sized COO-PS-NPs only at 300$cm^2$/ml but not after treatment with 100nm sized COO-PS-NPs at any concentration. Furthermore, cells appeared morphologically normal by microscopy suggesting that the MTT assay was an appropriate measure and indication in this system. However, it has been argued that media additives including serum (which might alter the media pH) may result in deceptive outcomes about cell viability while the cell number is steady [Laaksonen et al (2007)] and that ENPs may interfere with cell viability assays such as the MTT assay [Kroll et al (2012)] making it complicated to connect the metabolically reduced tetrazolium salts measurement to cellular viability [Marquis et al (2009)]. It would have been useful to have another endpoint of cell viability if time would allow doing so.

PS-NPs have been reported to have high affinity for proteins and have been observed to form large aggregates in protein-containing systems [Fröhlich et al[a] (2012)]. The characterisation results of this study have revealed that the 20nm COO-PS-NPs (especially at high concentration) tend to aggregate heavily in the cell culture LHC-9 SFM while their 100nm counterparts were more stable with less agglomeration. Although no serum is added to the LHC-9 media, it seems that other protein molecules are present in the LHC-9 SFM in addition to proteins produced by the cells in biological systems and these proteins caused the COO-PS-NPs (especially the 20nm) to undergo aggregation. This yielded COO-PS-NPs with larger size that represents the aggregates more than the individual NP and would change their physicochemical characteristics. The lowest cellular uptake of COO-PS-NPs was seen after exposure to 25cm$^2$/ml and the uptake then increased in a concentration-dependent manner (in both of the 20 and the 100nm sized COO-PS-NPs) towards the concentration of 150cm$^2$/ml as assessed by flow cytometry and CLSM (Fig. 4.1 and Fig. 4.2 respectively). This increase attained a plateau at the 300cm$^2$/ml possibly due to saturation status since thermodynamic equilibrium has been suggested to control the cellular internalisation of ENPs over time and concentrations [Chithrani et al (2006), Zhang et al (2009)]. Images of live BEAS-2B cells by CLSM demonstrated rapid COO-PS-NPs uptake into BEAS-2B cells as fluorescent COO-PS-NPs were easily identified in cells after only 45min incubation. This is consistent with findings of a recent study that observed fast cellular uptake of fluorescent COO-PS-NPs into the cytoplasm of HEp-2 cells [Hemmerich and Mikecz (2013)]. Nevertheless, BEAS-2B cells internalised more 100nm COO-PS-NPs than the 20nm ones possibly due to aggregation observed in LHC-9 SFM that increased their size. The cellular endocytosis of

ENPs has been reported to be an active process that involves surrounding them by the cell membrane before internalisation [Gao et al (2005)]. Consequently, the aggregated 20nm COO-PS-NPs in LHC-9 would require more time and energy to be enclosed by the membrane and engulfed into the cells resulting therefore in lower uptake into BEAS-2B cells compared to the 100nm COO-PS-NPs. This would explain the low uptake of the 20nm COO-PS-NPs in comparison to the 100nm COO-PS-NPs at equivalent concentration and exposure time. These data are consistent with findings by Win and colleagues who have argued that 100-200nm ENPs are an optimum size for internalisation as greater concentration-dependent uptake of the 100 and 200nm sized PS-NPs by Caco-2 cells was observed compared to small sized (50nm) and large sized (500-1000nm) ones investigated [Win et al (2005)].

Although there was less uptake of the 20nm COO-PS-NPs compared to the 100nm ones in this study, only these 20nm sized ENPs caused significant death of BEAS-2B cells after 24h treatment at high concentration (300$cm^2$/ml). The images of CLSM experiments indicated the presence of small fractions of the 20nm COO-PS-NPs within the mitochondria after 24h incubation (Fig. 4.8 A and C) but no evidence of mitochondrial co-localisation of the 100nm COO-PS-NPs was clearly observed (Fig. 4.8 B and D). It is known that mitochondrial changes (at the structure and function levels) play an important role in a wide variety of cellular processes including apoptosis [Green and Reed (1998)]. These results would therefore suggest that the toxicity of the 20nm sized COO-PS-NPs (at 300$cm^2$/ml) may be mediated by their partial co-localisation in the mitochondria. This co-localisation into the mitochondria might cause the opening of the permeability transition pore (PTP) which may consequently result in influx of water and

solutes from the cytosol which lead in turn to alteration of mitochondrial $Ca^{2+}$ homeostasis, swelling of the mitochondrial matrix and then to the rupture of the mitochondrial trans-membrane [Bernardi and Rasola (2007)]. This would be accompanied with release of cytochrome *c* and apoptosis-inducing factor (AIF) from the mitochondrial inter-membrane space into the cytosol [Giacomello et al (2007), Pizzo and Pozzan (2007)]. Cytochrome *c* has been suggested to be involved in activating the caspase cascade (including caspases-3/7) whereas AIF that translocates in the nucleus can contribute in chromatin condensation and DNA fragmentation leading at the end to cell death [Zhivotovsky and Orrenius (2011)]. In agreement with this, our results showed that the 300$cm^2$/ml of the 20nm COO-PS-NPs caused activation of caspases-3/7 in BEAS-2B cells (Fig. 5.10) and this would indicate that ROS-mediated caspases activation induced in response to the treatment with the 300$cm^2$/ml of the 20nm COO-PS-NPs is involved in cell death mechanism.

In addition to the cellular response discussed above, there was a decline in the GSH content in cell-free systems following incubation with both 20nm and 100nm COO-PS-NPs and this would suggest that these negatively charged COO-PS-NPs might be able to bind to GSH through the zwitterionic surface on the N-terminus of the Glu residue hence reducing their levels in solutions. Similarly, intracellular GSH levels were decreased in BEAS-2B cells after incubation with the 20nm and 100nm COO-PS-NPs (Fig. 5.3). However, only treatment with the 20nm sized COO-PS-NPs (at high concentrations ≥150$cm^2$/ml for long incubation time ≥18h) caused significant increase in the intracellular ROS generation (Fig. 5.2). This would propose that the produced ROS were not efficiently detoxified by the anti-oxidant system (including GSH and vitamins)

and hence excessively accumulated in the cell leading to toxic oxidative stress. The 20nm sized COO-PS-NPs seem to be capable of causing DNA damage in BEAS-2B cells indirectly by generating ROS but not by direct interaction between DNA and COO-PS-NPs due to two reasons. Firstly, they could not get direct access to DNA as they were too large (due to aggregation in media) to enter the nucleus via nuclear pores and so no nuclear co-localisation of COO-PS-NPs were observed although Hemmerich and colleagues have reported co-localisation of fluorescent COO-PS-NPs (of 50nm in diameter) in the nucleus of Hep-2 cells [Hemmerich and Mikecz (2013)]. Secondly, there was lack of DNA strand breaks when COO-PS-NPs were introduced to cell lysate and cell suspension (Fig. 5.6) potentially because both the DNA and COO-PS-NPs are negatively charged molecules. This toxicity is unlikely be related to metal element content since the analysis of major metals such as Cu, Fe and Zn in the COO-PS-NPs stock solution sample significantly demonstrated very low concentrations of these elements (Fig. 3.12). Moreover, the COO-PS-NPs would undergo dilution by the cell culture media and this would make the elements concentrations even smaller compared with the stock solution.

In summary, genotoxic and cytotoxic methodologies were employed to investigate the activity of COO-PS-NPs in this study which revealed that the toxicity of COO-PS-NPs is size-dependent as the 20nm sized COO-PS-NPs (at 300$cm^2$/ml) showed more toxic effect than their 100nm sized counterparts in BEAS-2B cells and this was consistent with results of other studies used similar COO-PS-NPs [Fröhlich et al[a] (2012)]. The results indicated that the toxicity of the 20nm sized COO-PS-NPs (at 300$cm^2$/ml) in BEAS-2B cells after 24h treatment is mediated through mitochondrial co-localisation

which caused generation of ROS and GSH depletion leading to oxidative stress, DNA damage and consequently to $Ca^{2+}$-independent cell death (mainly apoptosis) that involves caspase-3/7 activation. $Ca^{2+}$ is important for multi cellular functions however this study indicated that it does not fundamentally participate in the COO-PS-NPs-induced cell death mechanism in BEAS-2B cells. In contrast, in vitro exposure to the 100nm COO-PS-NPs (at all the concentrations investigated) or to low concentrations ($\leq$150cm$^2$/ml) of the 20nm COO-PS-NPs did not significantly reduce cell viability. This is because although they were taken up by cells and caused oxidative stress however other sufficient cellular non-enzymatic antioxidants (such as vitamin C) might remain in the cell and could counteract the damaging effects of ROS and hence maintain cell viability. In conclusion, 100-200nm has been suggested earlier to be the optimum size for ENPs internalisation [Win et al (2005)] and Polymer-based NPs (including PS-NPs) have been reported as good drug carrier systems to lungs [Sung et al (2007)]. The results of the current study have revealed that the 100nm sized COO-PS-NPs are not toxic to BEAS-2B cells at any concentration investigated since they did not cause reduction of viability of BEAS-2B cells with higher cellular uptake compared to the 20nm sized ones. This would provide a versatile platform that the 100nm COO-PS-NPs can therefore be suitable for use as carrier system for drug delivery (e.g. anti-tuberculosis). However, further studies should be carried out to attain deeper understanding of the toxicity of COO-PS-NPs after the drugs are mounted (conjugated) to them as this conjugation might alter their physicochemical properties.

Since the results and observations of literatures showed differences (and sometimes contradictions) in the possible cellular uptake of NPs and the proposed

mechanism of toxicity, it seems that several parameters such as cell line, NPs' size, NPs' concentration, NPs' type (chemical nature) and incubation time are important factors that affect both of the cellular uptake [Davda and Labhasetwar (2002)], the toxicity [Fröhlich et al[b] (2012)] and the cell death mechanism of ENPs [De Stefano et al (2012)]. Some studies, for example, have proposed that generation of cellular ROS, GSH depletion and toxic oxidative stress are the mechanism of toxicity of various NPs that would involve mitochondrial co-localisation and damage [Xia et al (2006), Bhattacharjee et al (2010)]. Another study has suggested that the NPs co-localisation in endosomes and lysosomes (but not in the mitochondria) is the reason for ROS generation-independent cellular damage and death [Fröhlich et al (2009)]. This diversity in the NPs intracellular localisation between different cells can be attributed to different endocytotic capabilities of these cell lines [Mailänder and Landfester (2009)]. Other factors including ENPs administration procedures, dispersion method and processing technique can also contribute in affecting the results of ENPs uptake, cytotoxicity and cell death mechanism [Lai et al (2013)].

Omics are fast growing disciplines that are used to give comprehensive information about the biochemical and functional status of a biological system, expression of the whole gene as well as the changes caused by chemical compounds [Ramirez et al (2013)]. Thus, the use of different omics techniques (including transcriptomic and metabolomic endpoints and modern proteomic approaches such as two-dimensional electrophoresis, mass spectrometry and protein microarrays) can be useful tools in suggested future work to investigate the genotoxicity (by evaluating the changes in exposure biomarkers), understand the possible mechanism(s) of action and

detect the potential targets of these COO-PS-NPs in BEAS-2B cells. In addition, experiments can be designed and conducted to investigate the required time for a cell to recover following removal of the COO-PS-NPs by cell washing and incubating in fresh media. Different techniques, methods and assays are recommended to be used in parallel for COO-PS-NPs characterisation and for investigating the biomarkers following treatment with COO-PS-NPs. This is to overcome the restrictions of a technique (such as the amount of sample required) and the bias that might result from the accuracy of one instrument and/or the operator although this would boost up the cost and time and may produce dissimilar (or even conflict) results. The outcomes from different machines can be compared to each other to get additional information and the results of investigating various biomarkers using different techniques (that tell different information) can be combined to provide more information from one sample. Moreover, further characterisation of the COO-PS-NPs to study the changes of their physicochemical properties (such as morphology and size) and behaviour in physiological systems that might affect the cell exposure to them, their uptake, cellular fate and interpretation of results. Techniques of scanning electron microscopy (SEM) and atomic force microscopy (AFM) can be used for such characterisation while nanoparticle tracking analysis (NTA) can be used to visualise the size, distribution and real time events (such as aggregation/dissolution) of NPs with high resolution video in addition to calculate the ζ-potential and concentration in liquid solutions. Different batches of the same fluorescently labelled COO-PS-NPs might display slightly different physicochemical properties but result in varied outcomes of one experimental analysis in cells and a significant challenge was therefore getting reproducible outcomes which required

consequently several repetition albeit limitations of time and cost. Thus, finding a way to avoid the polydispersity of nanoparticles batches might be needed.

# CHAPTER SEVEN:

# REFERENCES

1. Agarwal, M., M. Murugan, et al. (2013). "Nanoparticles and its Toxic Effects: A Review." Int. J. Curr. Microbiol. App. Sci **2**(10): 76-82.

2. Allaker, R. P. and G. Ren (2008). "Potential impact of nanotechnology on the control of infectious diseases." Trans R Soc Trop Med Hyg **102**(1): 1-2.

3. Alvarez-Roman, R., A. Naik, et al. (2004). "Skin penetration and distribution of polymeric nanoparticles." J Control Release **99**(1): 53-62.

4. Ames, B. N., M. K. Shigenaga, et al. (1993). "Oxidants, antioxidants, and the degenerative diseases of aging." Proc Natl Acad Sci U S A **90**(17): 7915-7922.

5. AshaRani, P. V., G. Low Kah Mun, et al. (2009). "Cytotoxicity and genotoxicity of silver nanoparticles in human cells." ACS Nano **3**(2): 279-290.

6. ATCC. available online (last accessed on 14 January 2014): http://www.lgcstandards-atcc.org/products/all/CRL-9609.aspx?geo_country=gb#357C3571006A4259B64650D34DF19048

7. Baalousha, M., Y. Ju-Nam, et al. (2012). "Characterisation of cerium oxide nanoparticles-part 1: size measurements." Environ Toxicol Chem **31**(5): 983-993.

8. Baalousha, M., Y. Ju-Nam, et al. (2012). "Characterisation of cerium oxide nanoparticles-part 2: nonsize measurements." Environ Toxicol Chem **31**(5): 994-1003.

9. Bains, J. S. and C. A. Shaw (1997). "Neurodegenerative disorders in humans: the role of glutathione in oxidative stress-mediated neuronal death." Brain Res Brain Res Rev **25**(3): 335-358.

10. Barth, S., D. Glick, et al. (2010). "Autophagy: assays and artifacts." J Pathol **221**(2): 117-124.

11. Bass, D. A., J. W. Parce, et al. (1983). "Flow cytometric studies of oxidative product formation by neutrophils: a graded response to membrane stimulation." J Immunol **130**(4): 1910-1917.

12. Bass, R., L. W. Ruddock, et al. (2004). "A major fraction of endoplasmic reticulum-located glutathione is present as mixed disulfides with protein." J Biol Chem **279**(7): 5257-5262.

13. Baudouin-Cornu, P., G. Lagniel, et al. (2012). "Glutathione degradation is a key determinant of glutathione homeostasis." J Biol Chem **287**(7): 4552-4561.

14. Bauer, I. W., S. P. Li, et al. (2008). "Internalisation of hydroxyapatite nanoparticles in liver cancer cells." J Mater Sci Mater Med **19**(3): 1091-1095.

15. Bernardi, P. and A. Rasola (2007). "Calcium and cell death: the mitochondrial connection." Subcell Biochem **45**: 481-506.

16. Beurel, E. and Richard S. Jope (2006). "The paradoxical pro-and anti-apoptotic actions of GSK3 in the intrinsic and extrinsic apoptosis signaling pathways." Progress in neurobiology **79**(4): 173-189.

17. Bexiga, M. G., J. A. Varela, et al. (2011). "Cationic nanoparticles induce caspase 3-, 7- and 9-mediated cytotoxicity in a human astrocytoma cell line." Nanotoxicology **5**(4): 557-567.

18. Bhattacharjee, S., J. Y. Chen, et al. (2000). "DLVO interaction energy between spheroidal particles and a flat surface." Colloids and Surfaces - A - Physiochemical and Engineering Aspects **165**(1-3): 143–156.

19. Bhattacharjee, S., L. H. de Haan, et al. (2010). "Role of surface charge and oxidative stress in cytotoxicity of organic monolayer-coated silicon nanoparticles towards macrophage NR8383 cells." Part Fibre Toxicol **7**: 25.

20. Bhattacharya, K., M. Davoren, et al. (2009). "Titanium dioxide nanoparticles induce oxidative stress and DNA-adduct formation but not DNA-breakage in human lung cells." Part Fibre Toxicol **6**: 17.

21. Bihari, P., M. Vippola, et al. (2008). "Optimized dispersion of nanoparticles for biological in vitro and in vivo studies." Part Fibre Toxicol **5**: 14.

22. Boatright, K. M. and G. S. Salvesen (2003). "Mechanisms of caspase activation." Curr Opin Cell Biol **15**(6): 725-731.

23. Bottini, M., S. Bruckner, et al. (2006). "Multi-walled carbon nanotubes induce T lymphocyte apoptosis." Toxicol Lett **160**(2): 121-126.

24. Boveris, A. and B. Chance (1973). "The mitochondrial generation of hydrogen peroxide. General properties and effect of hyperbaric oxygen." Biochem J **134**(3): 707-716.

25. Bozzola, J. J. (2007). "Conventional specimen preparation techniques for transmission electron microscopy of cultured cells." Methods Mol Biol **369**: 1-18.

26. Bradford, M. M. (1976). "A rapid and sensitive method for the quantitation of microgram quantities of protein utilizing the principle of protein-dye binding." Anal Biochem **72**: 248-254.

27. Brar, S. K. and M. Verma (2011). "Measurement of nanoparticles by light-scattering techniques." TrAC Trends in Analytical Chemistry **30**(1): 14.

28. Braun, A., O. Couteau, et al. (2011). "Validation of dynamic light scattering and centrifugal liquid sedimentation methods for nanoparticle characterisation." Advanced Powder Technology **22**(6): 766-770.

29. Brown, D. M., K. Donaldson, et al. (2004). "Calcium and ROS-mediated activation of transcription factors and TNF-alpha cytokine gene expression in macrophages exposed to ultrafine particles." Am J Physiol Lung Cell Mol Physiol **286**(2): L344-353.

30. Brown, D. M., M. R. Wilson, et al. (2001). "Size-dependent proinflammatory effects of ultrafine polystyrene particles: a role for surface area and oxidative stress in the enhanced activity of ultrafines." Toxicol Appl Pharmacol **175**(3): 191-199.

31. Brunner, D., J. Frank, et al. (2010). "Serum-free cell culture: the serum-free media interactive online database." ALTEX **27**(1): 53-62.

32. , Carrasco, R. A., N. B. Stamm, et al. (2003). "One-step cellular caspase-3/7 assay." Biotechniques **34**(5): 1064-1067.

33. Cedervall, T., I. Lynch, et al. (2007a). "Detailed Identification of Plasma Proteins Adsorbed on Copolymer Nanoparticles." Angewandte Chemie International Edition **46**(30): 5754-5756.

34. Cedervall, T., I. Lynch, et al. (2007b). "Understanding the nanoparticle-protein corona using methods to quantify exchange rates and affinities of proteins for nanoparticles." Proc Natl Acad Sci U S A **104**(7): 2050-2055.

35. Chang, L. and M. Karin (2001). "Mammalian MAP kinase signalling cascades." Nature **410**(6824): 37-40.

36. Chen, Y., Y. Huang, et al. (2012). "Temperature effect on the aggregation kinetics of CeO2 nanoparticles in monovalent and divalent electrolytes." Journal of Environmental & Analytical Toxicology **2**(7).

37. Chithrani, B. D., A. A. Ghazani, et al. (2006). "Determining the size and shape dependence of gold nanoparticle uptake into mammalian cells." Nano Lett **6**(4): 662-668.

38. ÇİFTÇİ, H. T., Mustafa; TAMER, Uğur; KARAHAN, Siyami; MENEMEN, Yusuf (2013). "Silver NPs: cytotoxic, apoptotic and necrotic effects on MCF-7 cells." Turkish Journal of Biology **37**(5.): 9.

39. Collatz, M. B., R. Rudel, et al. (1997). "Intracellular calcium chelator BAPTA protects cells against toxic calcium overload but also alters physiological calcium responses." Cell Calcium **21**(6): 453-459.

40. Collins, A. R. (2004). "The comet assay for DNA damage and repair: principles, applications, and limitations." Mol Biotechnol **26**(3): 249-261.

41. Commission Recommendation on the definition of nanomaterial. Brussels, 2011]. available online (last accessed on 14 January 2014): http://ec.europa.eu/environment/chemicals/nanotech/pdf/commission_recommendation.pdf

42. Compton, S. J. and C. G. Jones (1985). "Mechanism of dye response and interference in the Bradford protein assay." Anal Biochem **151**(2): 369-374.

43. Conner, S. D. and S. L. Schmid (2003). "Regulated portals of entry into the cell." Nature **422**(6927): 37-44.

44. Cortez, C., E. Tomaskovic-Crook, et al. (2007). "Influence of size, surface, cell line, and kinetic properties on the specific binding of A33 antigen-targeted multilayered particles and capsules to colorectal cancer cells." ACS Nano **1**(2): 93-102.

45. Cullen, S. P. and S. J. Martin (2009). "Caspase activation pathways: some recent progress." Cell Death Differ **16**(7): 935-938.

46. Dausend, J., A. Musyanovych, et al. (2008). "Uptake mechanism of oppositely charged fluorescent nanoparticles in HeLa cells." Macromol Biosci **8**(12): 1135-1143.

47. Davda, J. and V. Labhasetwar (2002). "Characterisation of nanoparticle uptake by endothelial cells." Int J Pharm **233**(1-2): 51-59.

48. De Jong, W. H. and P. J. Borm (2008). "Drug delivery and nanoparticles: applications and hazards." Int J Nanomedicine **3**(2): 133-149.

49. De Stefano, D., R. Carnuccio, et al. (2012). "Nanomaterials toxicity and cell death modalities." J Drug Deliv **2012**: 167896.

50. Dechsakulthorn, F., A. Hayes, et al. (2007). "In vitro cytotoxicity of selected nanoparticles using human skin fibroblasts." Alternatives to Animal Testing and Experimentation **14**(Special issue): 397-400.

51. Decuzzi, P. and M. Ferrari (2008). "The receptor-mediated endocytosis of nonspherical particles." Biophys J **94**(10): 3790-3797.

52. Deponte, M. (2012). "Glutathione catalysis and the reaction mechanisms of glutathione-dependent enzymes." Biochim Biophys Acta **1830**(5): 3217-3266.

53. Desai, M. P., V. Labhasetwar, et al. (1997). "The mechanism of uptake of biodegradable microparticles in Caco-2 cells is size dependent." Pharm Res **14**(11): 1568-1573.

54. Dojindo Molecular Technologies Incorporation website (for BAPTA-AM reaction). available online (last accessed on 14 January 2014): http://www.dojindo.com/store/p/560-BAPTA-AM.html

55. Dolmetsch, R. E., R. S. Lewis, et al. (1997). "Differential activation of transcription factors induced by Ca2+ response amplitude and duration." Nature **386**(6627): 855-858.

56. Donaldson, K., V. Stone, et al. (2003). "Oxidative stress and calcium signaling in the adverse effects of environmental particles (PM10)." Free Radic Biol Med **34**(11): 1369-1382.

57. Donaldson, K., V. Stone, et al. (2001). "Ultrafine particles." Occup Environ Med **58**(3): 211-216, 199.

58. Donaldson, K., L. Tran, et al. (2005). "Combustion-derived nanoparticles: a review of their toxicology following inhalation exposure." Part Fibre Toxicol **2**: 10.

59. Dos Santos, T., J. Varela, et al. (2011). "Effects of transport inhibitors on the cellular uptake of carboxylated polystyrene nanoparticles in different cell lines." PLoS One **6**(9): e24438.

60. Ehrenberg, M. and J. L. McGrath (2005). "Binding between particles and proteins in extracts: implications for microrheology and toxicity." Acta Biomater **1**(3): 305-315.

61. Eidi, H., O. Joubert, et al. (2012). "Drug delivery by polymeric nanoparticles induces autophagy in macrophages." Int J Pharm **422**(1-2): 495-503.

62. Elmore, S. (2007). "Apoptosis: a review of programmed cell death." Toxicol Pathol **35**(4): 495-516.

63. Ercal, N., H. Gurer-Orhan, et al. (2001). "Toxic metals and oxidative stress part I: mechanisms involved in metal-induced oxidative damage." Curr Top Med Chem **1**(6): 529-539.

64. Ermak, G. and K. J. Davies (2002). "Calcium and oxidative stress: from cell signaling to cell death." Mol Immunol **38**(10): 713-721.

65. Farkas, J., P. Christian, et al. (2011). "Uptake and effects of manufactured silver nanoparticles in rainbow trout (Oncorhynchus mykiss) gill cells." Aquat Toxicol **101**(1): 117-125.

66. Fatisson, J., I. R. Quevedo, et al. (2012). "Physicochemical characterisation of engineered nanoparticles under physiological conditions: effect of culture media components and particle surface coating." Colloids Surf B Biointerfaces **91**: 198-204.

67. Flora, S. J., M. Mittal, et al. (2008). "Heavy metal induced oxidative stress & its possible reversal by chelation therapy." Indian J Med Res **128**(4): 501-523.

68. Freitas, C. and R. H. Müller (1998). "Effect of light and temperature on zeta potential and physical stability in solid lipid nanoparticle (SLN™) dispersions." International Journal of Pharmaceutics **168**(2): 221-229.

69. Frigault, M. M., J. Lacoste, et al. (2009). "Live-cell microscopy - tips and tools." J Cell Sci **122**(Pt 6): 753-767.

70. Froberg, J. C., O. J. Rojas, et al. (1999). "Surfaces force and measuring techniques." International journal of mineral process **56**(1): 1-30.

71. Frohlich, E., C. Meindl, et al. (2012a). "Action of polystyrene nanoparticles of different sizes on lysosomal function and integrity." Part Fibre Toxicol **9**: 26.

72. Frohlich, E., C. Meindl, et al. (2012b). "Cytotoxity of nanoparticles is influenced by size, proliferation and embryonic origin of the cells used for testing." Nanotoxicology **6**(4): 424-439.

73. Frohlich, E., C. Samberger, et al. (2009). "Cytotoxicity of nanoparticles independent from oxidative stress." J Toxicol Sci **34**(4): 363-375.

74. Fubini, B., M. Ghiazza, et al. (2010). "Physicochemical features of engineered nanoparticles relevant to their toxicity." Nanotoxicology **4**: 347-363.

75. Fusi, F., S. Saponara, et al. (2001). "2,5-Di-t-butyl-1,4-benzohydroquinone (BHQ) inhibits vascular L-type $Ca^{2+}$ channel via superoxide anion generation." Br J Pharmacol **133**(7): 988-996.

76. Gao, H., W. Shi, et al. (2005). "Mechanics of receptor-mediated endocytosis." Proc Natl Acad Sci U S A **102**(27): 9469-9474.

77. Geiser, M. (2010). "Update on macrophage clearance of inhaled micro- and nanoparticles." J Aerosol Med Pulm Drug Deliv **23**(4): 207-217.

78. Geiser, M., B. Rothen-Rutishauser, et al. (2005). "Ultrafine particles cross cellular membranes by nonphagocytic mechanisms in lungs and in cultured cells." Environ Health Perspect **113**(11): 1555-1560.

79. Genestra, M. (2007). "Oxyl radicals, redox-sensitive signalling cascades and antioxidants." Cell Signal **19**(9): 1807-1819.

80. Geng, Y., P. Dalhaimer, et al. (2007). "Shape effects of filaments versus spherical particles in flow and drug delivery." Nat Nanotechnol **2**(4): 249-255.

81. Gharagozloo, P. E. and K. E. Goodson (2011). "Temperature-dependent aggregation and diffusion in nanofluids." International Journal of Heat and Mass Transfer **54**(4): 797-806.

82. Giacomello, M., I. Drago, et al. (2007). "Mitochondrial Ca2+ as a key regulator of cell life and death." Cell Death Differ **14**(7): 1267-1274.

83. Glick, D., S. Barth, et al. (2010). "Autophagy: cellular and molecular mechanisms." J Pathol **221**(1): 3-12.

84. Gottstein, C., G. Wu, et al. (2013). "Precise quantification of nanoparticle internalisation." ACS Nano **7**(6): 4933-4945.

85. Gowda R, Sun H, et al. (2009). "Effects of Particle Surface Charge, Species, Concentration, and Dispersion Method on the Thermal Conductivity of Nanofluids." Advances in Mechanical Engineering **2010**.

86. Grant, B. D. and M. Sato (2006). "Intracellular trafficking." WormBook: 1-9.

87. Grant, C. M., F. H. MacIver, et al. (1996). "Glutathione is an essential metabolite required for resistance to oxidative stress in the yeast Saccharomyces cerevisiae." Current Genetics **29**(6): 511-515.

88. Green, D. R. and J. C. Reed (1998). "Mitochondria and apoptosis." Science **281**(5381): 1309-1312.

89. Green, R. M., M. Graham, et al. (2006). "Subcellular compartmentalization of glutathione: correlations with parameters of oxidative stress related to genotoxicity." Mutagenesis **21**(6): 383-390.

90. GSH Oxidation. available online (last accessed on 14 January 2014): http://david-bender.co.uk/metonline/CHO/favism/images/GSH.png

91. GSH synthesis. available online (last accessed on 14 January 2014): http://www.gsh.com.tw/images/glutathione_synthesis.gif

92. Hai, N. H., N. H. Luong, et al. (2009). "Preparation of magnetic nanoparticles embedded in polystyrene microspheres." Journal of Physics: Conference Series **187**(1).

93. Hajnoczky, G., E. Davies, et al. (2003). "Calcium signaling and apoptosis." Biochem Biophys Res Commun **304**(3): 445-454.

94. Halliwell, B. (1999). "Antioxidant defence mechanisms: from the beginning to the end (of the beginning)." Free radical research **31**(4): 261-272.

95. Hanley, C., J. Layne, et al. (2008). "Preferential killing of cancer cells and activated human T cells using ZnO nanoparticles." Nanotechnology **19**(29): 295103.

96. Harush-Frenkel, O., N. Debotton, et al. (2007). "Targeting of nanoparticles to the clathrin-mediated endocytic pathway." Biochem Biophys Res Commun **353**(1): 26-32.

97. Harush-Frenkel, O., E. Rozentur, et al. (2008). "Surface charge of nanoparticles determines their endocytic and transcytotic pathway in polarized MDCK cells." Biomacromolecules **9**(2): 435-443.

98. Hassellov, M., J. W. Readman, et al. (2008). "Nanoparticle analysis and characterisation methodologies in environmental risk assessment of engineered nanoparticles." Ecotoxicology **17**(5): 344-361.

99. He, C., Y. Hu, et al. (2010). "Effects of particle size and surface charge on cellular uptake and biodistribution of polymeric nanoparticles." Biomaterials **31**(13): 3657-3666.

100. He, C. and D. J. Klionsky (2009). "Regulation mechanisms and signaling pathways of autophagy." Annu Rev Genet **43**: 67-93.

101. Hellstrand, E., I. Lynch, et al. (2009). "Complete high-density lipoproteins in nanoparticle corona." Febs J **276**(12): 3372-3381.

102. Hemmerich, P. H. and A. H. von Mikecz (2013). "Defining the subcellular interface of nanoparticles by live-cell imaging." PLoS One **8**(4): e62018.

103. Hengartner, M. O. (2000). "The biochemistry of apoptosis." PLoS One **407**: 770-776.

104. Hocherl, A., M. Dass, et al. (2012). "Competitive cellular uptake of nanoparticles made from polystyrene, poly(methyl methacrylate), and polylactide." Macromol Biosci **12**(4): 454-464.

105. Hoeijmakers, J. H. (2001). "Genome maintenance mechanisms for preventing cancer." Nature **411**(6835): 366-374.

106. Hoet, P. H., I. Bruske-Hohlfeld, et al. (2004). "Nanoparticles - known and unknown health risks." J Nanobiotechnology **2**(1): 12.

107. Holzapfel, V., A. Musyanovych, et al. (2005). "Preparation of Fluorescent Carboxyl and Amino Functionalized Polystyrene Particles by Miniemulsion Polymerization as Markers for Cells." Macromolecular Chemistry and Physics **206**(24): 10.

108. Horie, M., H. Kato, et al. (2012). "In vitro evaluation of cellular response induced by manufactured nanoparticles." Chem Res Toxicol **25**(3): 605-619.

109. Hu, X., S. Cook, et al. (2010). "In vitro evaluation of cytotoxicity of engineered carbon nanotubes in selected human cell lines." Sci Total Environ **408**(8): 1812-1817.

110. Hume, D. A. (2006). "The mononuclear phagocyte system." Curr Opin Immunol **18**(1): 49-53.

111. Hussain, S., L. Thomassen, et al. (2010). "Carbon black and titanium dioxide nanoparticles elicit distinct apoptotic pathways in bronchial epithelial cells." Particle and fibre toxicology **7**: 10.

112. Jakubowski, W. and G. Bartosz (1997). "Estimation of oxidative stress in Saccharomyces cerevisae with fluorescent probes." Int J Biochem Cell Biol **29**(11): 1297-1301.

113. Jefferies, H., J. Coster, et al. (2003). "Glutathione." ANZ J Surg **73**(7): 517-522.

114. Jezek, P. and L. Hlavata (2005). "Mitochondria in homeostasis of reactive oxygen species in cell, tissues, and organism." Int J Biochem Cell Biol **37**(12): 2478-2503.

115. Jiang, X., J. Dausend, et al. (2010a). "Specific effects of surface amines on polystyrene nanoparticles in their interactions with mesenchymal stem cells." Biomacromolecules **11**(3): 748-753.

116. Jiang, X., A. Musyanovych, et al. (2011). "Specific effects of surface carboxyl groups on anionic polystyrene particles in their interactions with mesenchymal stem cells." Nanoscale **3**(5): 2028-2035.

117. Jiang, X., S. Weise, et al. (2010b). "Quantitative analysis of the protein corona on FePt nanoparticles formed by transferrin binding." Journal of The Royal Society Interface **7**(Suppl 1): S5-513.

118. Johnston, H. J., M. Semmler-Behnke, et al. (2010). "Evaluating the uptake and intracellular fate of polystyrene nanoparticles by primary and hepatocyte cell lines in vitro." Toxicol Appl Pharmacol **242**(1): 66-78.

119. Jones, C. F. and D. W. Grainger (2009). "In vitro assessments of nanomaterial toxicity." Adv Drug Deliv Rev **61**(6): 438-456.

120. Joris, F., B. B. Manshian, et al. (2013). "Assessing nanoparticle toxicity in cell-based assays: influence of cell culture parameters and optimized models for bridging the in vitro-in vivo gap." Chem Soc Rev **42**(21): 8339-8359.

121. Kajita, M., K. Hikosaka, et al. (2007). "Platinum nanoparticle is a useful scavenger of superoxide anion and hydrogen peroxide." Free Radical Research **41**(6): 615-626.

122. Karlsson, H. L. (2010). "The comet assay in nanotoxicology research." Analytical and Bioanalytical Chemistry **398**(2): 651 -666.

123. Kendall, M., L. Brown, et al. (2004). "Molecular adsorption at particle surfaces: a PM toxicity mediation mechanism." Inhal Toxicol **16 Suppl 1**: 99-105.

124. Kluck, R. M., C. A. McDougall, et al. (1994). "Calcium chelators induce apoptosis--evidence that raised intracellular ionised calcium is not essential for apoptosis." Biochim Biophys Acta **1223**(2): 247-254.

125. Kroll, A., M. H. Pillukat, et al. (2012). "Interference of engineered nanoparticles with in vitro toxicity assays." Arch Toxicol **86**(7): 1123-1136.

126. Kulinskii, V. I. and L. S. Kolesnichenko (2009). "Glutathione system. I. Synthesis, transport, glutathione transferases, glutathione peroxidases." Biomed Khim **55**(3): 255-277.

127. Kyriakis, J. M. and J. Avruch (2001). "Mammalian mitogen-activated protein kinase signal transduction pathways activated by stress and inflammation." Physiol Rev **81**(2): 807-869.

128. Laaksonen, T., H. Santos, et al. (2007). "Failure of MTT as a toxicity testing agent for mesoporous silicon microparticles." Chem Res Toxicol **20**(12): 1913-1918.

129. Laborda, F., J. Jimenez-Lamana, et al. (2011). "Selective identification, characterisation and determination of dissolved silver(i) and silver nanoparticles based on single particle detection by inductively coupled plasma mass spectrometry." Journal of Analytical Atomic Spectrometry **26**(7): 1362-1371.

130. Lai, W., Z. Hu, et al. (2013). "The Concerns on Biosafety of Nanomaterials." JSM Nanotechnology & Nanomedicine.

131. Lam, C. W., J. T. James, et al. (2004). "Pulmonary toxicity of single-wall carbon nanotubes in mice 7 and 90 days after intratracheal instillation." Toxicol Sci **77**(1): 126-134.

132. Lanone, S., F. Rogerieux, et al. (2009). "Comparative toxicity of 24 manufactured nanoparticles in human alveolar epithelial and macrophage cell lines." Particle and fibre toxicology **6**: 14-25.

133. Lawrence, A., C. M. Jones, et al. (2003). "Evidence for the role of a peroxidase compound I-type intermediate in the oxidation of glutathione, NADH, ascorbate, and dichlorofluorescin by cytochrome *c*/H2O2. Implications for oxidative stress during apoptosis." J Biol Chem **278**(32): 29410-29419.

134. LeBel, C. P., H. Ischiropoulos, et al. (1992). "Evaluation of the probe 2',7'-dichlorofluorescin as an indicator of reactive oxygen species formation and oxidative stress." Chem Res Toxicol **5**(2): 227-231.

135. Lee, K. H., H. S. Jung, et al. (2010). "Rapid detection of intracellular nanoparticles by electron microscopy." Journal of analytical science and technology **1**(1): 71-73.

136. Levine, B. and J. Yuan (2005). "Autophagy in cell death: an innocent convict?" J Clin Invest **115**(10): 2679-2688.

137. Lewinski, N., V. Colvin, et al. (2008). "Cytotoxicity of Nanoparticles." Small **4**(1): 26-49.

138. Li, N., C. Sioutas, et al. (2003). "Ultrafine particulate pollutants induce oxidative stress and mitochondrial damage." Environ Health Perspect **111**(4): 455-460.

139. Li, Y. and N. Gu (2010). "Thermodynamics of charged nanoparticle adsorption on charge-neutral membranes: a simulation study." J Phys Chem B **114**(8): 2749-2754.

140. Liu, G. and P. Liu (2009). "Preparation of carboxyl-coated polystyrene nanoparticles using oleic acid." IET Nanobiotechnol **3**(2): 23-27.

141. Lorenz, M. R., V. Holzapfel, et al. (2006). "Uptake of functionalized, fluorescent-labelled polymeric particles in different cell lines and stem cells." Biomaterials **27**(14): 2820-2828.

142. Lovric, J., H. S. Bazzi, et al. (2005). "Differences in subcellular distribution and toxicity of green and red emitting CdTe quantum dots." J Mol Med (Berl) **83**(5): 377-385.

143. Lu, S. C. (2013). "Glutathione synthesis." Biochim Biophys Acta **1830**(5): 3143-3153.

144. Lucking, A. J., M. Lundback, et al. (2008). "Diesel exhaust inhalation increases thrombus formation in man." Eur Heart J **29**(24): 3043-3051.

145. Lundqvist, M., J. Stigler, et al. (2008). "Nanoparticle size and surface properties determine the protein corona with possible implications for biological impacts." Proc Natl Acad Sci U S A **105**(38): 14265-14270.

146. Lunov, O., T. Syrovets, et al. (2011a). "Differential uptake of functionalized polystyrene nanoparticles by human macrophages and a monocytic cell line." ACS Nano **5**(3): 1657-1669.

147. Lunov, O., T. Syrovets, et al. (2011b). "Amino-functionalized polystyrene nanoparticles activate the NLRP3 inflammasome in human macrophages." ACS Nano **5**(12): 9648-9657.

148. Lynch, I., A. Ahluwalia, et al. (2013). "The bio-nano-interface in predicting nanoparticle fate and behaviour in living organisms: towards grouping and categorising nanomaterials and ensuring nanosafety by design." BioNanoMaterials **14**(3-4): 22.

149. Lynch, I., T. Cedervall, et al. (2007). "The nanoparticle-protein complex as a biological entity; a complex fluids and surface science challenge for the 21st century." Adv Colloid Interface Sci **134-135**: 167-174.

150. Lynch, I. and K. A. Dawson (2008). "Protein-nanoparticle interactions." Nano Today **3**(1–2): 40-47.

151. Macho, A., T. Hirsch, et al. (1997). "Glutathione depletion is an early and calcium elevation is a late event of thymocyte apoptosis." J Immunol **158**(10): 4612-4619.

152. Magder, S. (2006). "Reactive oxygen species: toxic molecules or spark of life?" Crit Care **10**(1): 208.

153. Magdolenova, Z., D. Bilanicova, et al. (2012). "Impact of agglomeration and different dispersions of titanium dioxide nanoparticles on the human related in vitro cytotoxicity and genotoxicity." J Environ Monit **14**(2): 455-464.

154. Mailander, V. and K. Landfester (2009). "Interaction of nanoparticles with cells." Biomacromolecules **10**(9): 2379-2400.

155. Makino, K., N. Yamamoto, et al. (2003). "Phagocytic uptake of polystyrene microspheres by alveolar macrophages: effects of the size and surface properties of the microspheres." Colloids and Surfaces B: Biointerfaces **27**(1): 33-39.

156. Marquis, B. J., S. A. Love, et al. (2009). "Analytical methods to assess nanoparticle toxicity." Analyst **134**(3): 425-439.

157. McFadyen, P. and D. Fairhurst (1993). "Zeta potentials of nanoceramic materials - measurement and interpretation." in British Ceramic Proceedings. A paper presented at the Canadian Mineral Analyst Meeting, Winipeg, Manitoba, Canada.

158. Meister, A. (1988). "Glutathione metabolism and its selective modification." J Biol Chem **263**(33): 17205-17208.

159. Mohanraj, V. J. and Y. Chen (2006). "Nanoparticles - A review." Tropical Journal of Pharmaceutical Research **5**(1): 561-573.

160. Mohora, M., M. Greabu, et al. (2009). "Redox sensitive signaling factors and antioxidants." Farmacia **57**(4): 399-411.

161. Mosmann, T. (1983). "Rapid colorimetric assay for cellular growth and survival: application to proliferation and cytotoxicity assays." J Immunol Methods **65**(1-2): 55-63.

162. Muhlfeld, C., B. Rothen-Rutishauser, et al. (2007). "Visualization and quantitative analysis of nanoparticles in the respiratory tract by transmission electron microscopy." Part Fibre Toxicol **4**: 11.

163. Muller, G., S. Wied, et al. (2008). "Hydrogen peroxide-induced translocation of glycolipid-anchored (c)AMP-hydrolases to lipid droplets mediates inhibition of lipolysis in rat adipocytes." Br J Pharmacol **154**(4): 901-913.

164. Murthy, S. K. (2007). "Nanoparticles in modern medicine: state of the art and future challenges." Int J Nanomedicine **2**(2): 129-141.

165. Nagashima, K., J. Zheng, et al. (2011). "Biological tissue and cell culture specimen preparation for TEM nanoparticle characterisation." Methods Mol Biol **697**: 83-91.

166. Nel, A., T. Xia, et al. (2006). "Toxic potential of materials at the nanolevel." Science **311**(5761): 622-627.

167. Nel, A. E., L. Madler, et al. (2009). "Understanding biophysicochemical interactions at the nano-bio interface." Nat Mater **8**(7): 543-557.

168. Nemmar, A., M. F. Hoylaerts, et al. (2002). "Ultrafine particles affect experimental thrombosis in an in vivo hamster model." Am J Respir Crit Care Med **166**(7): 998-1004.

169. Newman C (2003). "Serum-free cell culture - the ethical, scientific and economic choice." The Biomedical Scientist **47**: 941-942.

170. Ng, C. T., J. J. Li, et al. (2010). "Localising cellular uptake of nanomaterials in vitro by transmission electron microscopy." Microscopy: Science, Technology, Applications and Education **1**: 316-320.

171. Nicotera, P., G. Bellomo, et al. (1992). "Calcium-mediated mechanisms in chemically induced cell death." Annu Rev Pharmacol Toxicol **32**: 449-470.

172. Oberdörster, G., A. Maynard, et al. (2005a). "Principles for characterising the potential human health effects from exposure to nanomaterials: elements of a screening strategy." Particle and fibre toxicology **2**(1): 35.

173. Oberdörster, G., E. Oberdörster, et al. (2005b). "Nanotoxicology: an emerging discipline evolving from studies of ultrafine particles." Environmental health perspectives **113**(7): 17.

174. Oh, W. K., S. Kim, et al. (2010). "Cellular uptake, cytotoxicity, and innate immune response of silica-titania hollow nanoparticles based on size and surface functionality." ACS Nano **4**(9): 5301-5313.

175. Olivier, V., C. Riviere, et al. (2004). "Uptake of polystyrene beads bearing functional groups by macrophages and fibroblasts." Colloids and Surfaces B: Biointerfaces **33**(1): 9.

176. Orrenius, S., B. Zhivotovsky, et al. (2003). "Regulation of cell death: the calcium-apoptosis link." Nat Rev Mol Cell Biol **4**(7): 552-565.

177. Palakurthi, S., V. K. Yellepeddi, et al. (2011). "Nanocarriers for Cytosolic Drug and Gene Delivery in Cancer Therapy." Biomedical Engineering, Trends, Research and Technologies. Dr. Sylwia Olsztynska (Ed.), INTECH Open Access Publisher, available online (last accessed on 14 January 2014): http://www.intechopen.com/books/biomedical-engineering-trends-research-and-technologies/nanocarriers-for-cytosolic-drug-and-gene-delivery-in-cancer-therapy

178. Panyam, J. and V. Labhasetwar (2010). "Biodegradable nanoparticles for drug and gene delivery to cells and tissue." Advanced drug delivery reviews **64**: 11.

179. Park, E. J., J. Yi, et al. (2008). "Oxidative stress and apoptosis induced by titanium dioxide nanoparticles in cultured BEAS-2B cells." Toxicol Lett **180**(3): 222-229.

180. Parrish, A. B., C. D. Freel, et al. (2013). "Cellular mechanisms controlling caspase activation and function." Cold Spring Harb Perspect Biol **5**(6).

181. Parton, R. G. and K. Simons (2007). "The multiple faces of caveolae." Nat Rev Mol Cell Biol **8**(3): 185-194.

182. Pastore, A., G. Federici, et al. (2003). "Analysis of glutathione: implication in redox and detoxification." Clin Chim Acta **333**(1): 19-39.

183. Patil, S., A. Sandberg, et al. (2007). "Protein adsorption and cellular uptake of cerium oxide nanoparticles as a function of zeta potential." Biomaterials **28**(31): 4600-4607.

184. Pavlin, M. and V. B. Bregar (2012). "Stability of nanoparticle suspensions in different biologically relevant media." Dig J Nanomater Biostr **7**(4): 1389–1400.

185. Petosa, A. R., D. P. Jaisi, et al. (2010). "Aggregation and deposition of engineered nanomaterials in aquatic environments: role of physicochemical interactions." Environ Sci Technol **44**(17): 6532-6549.

186. Pizzo, P. and T. Pozzan (2007). "Mitochondria-endoplasmic reticulum choreography: structure and signaling dynamics." Trends Cell Biol **17**(10): 511-517.

187. Pochard, I., J.-P. Boisvert, et al. (2003). "Surface charge, effective charge and dispersion/aggregation properties of nanoparticles." Polymer International **52**(4): 619-624.

188. Poda, A. R., A. J. Bednar, et al. (2011). "Characterisation of silver nanoparticles using flow-field flow fractionation interfaced to inductively coupled plasma mass spectrometry." J Chromatogr A **1218**(27): 4219-4225.

189. Porter, A. E., K. Muller, et al. (2006). "Uptake of C60 by human monocyte macrophages, its localisation and implications for toxicity: studied by high resolution electron microscopy and electron tomography." Acta Biomater **2**(4): 409-419.

190. Porter, A. G. (1999). "Protein translocation in apoptosis." Trends in Cell Biology **9**(10): 394-401.

191. Prokop, A. and J. M. Davidson (2008). "Nanovehicular intracellular delivery systems." J Pharm Sci **97**(9): 3518-3590.

192. Qiao, R., A. P. Roberts, et al. (2007). "Translocation of C60 and its derivatives across a lipid bilayer." Nano Lett **7**(3): 614-619.

193. Ramirez, T., M. Daneshian, et al. (2013). "Metabolomics in toxicology and preclinical research." ALTEX **30**(2): 209-225.

194. Reisner, A. H., P. Nemes, et al. (1975). "The use of Coomassie Brilliant Blue G250 perchloric acid solution for staining in electrophoresis and isoelectric focusing on polyacrylamide gels." Anal Biochem **64**(2): 509-516.

195. Rejman, J., V. Oberle, et al. (2004). "Size-dependent internalisation of particles via the pathways of clathrin- and caveolae-mediated endocytosis." Biochem J **377**(Pt 1): 159-169.

196. Revell, P. A. (2006). "The biological effects of nanoparticles." Nanotechnology Perceptions: a Review of Ultraprecision Engineering **2**(3): 283 - 298.

197. Riedl, S. J. and Y. Shi (2004). "Molecular mechanisms of caspase regulation during apoptosis." Nat Rev Mol Cell Biol **5**(11): 897-907.

198. Rigas, B. and Y. Sun (2008). "Induction of oxidative stress as a mechanism of action of chemopreventive agents against cancer." Br J Cancer **98**(7): 1157-1160.

199. Risom, L., P. Moller, et al. (2005). "Oxidative stress-induced DNA damage by particulate air pollution." Mutat Res **592**(1-2): 119-137.

200. Robinson, K. M., M. S. Janes, et al. (2006). "Selective fluorescent imaging of superoxide in vivo using ethidium-based probes." Proc Natl Acad Sci U S A **103**(41): 15038-15043.

201. Rocker, C., M. Potzl, et al. (2009). "A quantitative fluorescence study of protein monolayer formation on colloidal nanoparticles." Nat Nanotechnol **4**(9): 577-580.

202. Roduner, E. (2006). "Size matters: why nanomaterials are different." Chem Soc Rev **35**(7): 583-592.

203. Rothen-Rutishauser, B., C. Muhlfeld, et al. (2007). "Translocation of particles and inflammatory responses after exposure to fine particles and nanoparticles in an epithelial airway model." Part Fibre Toxicol **4**: 9.

204. Rothen-Rutishauser, B. M., S. Schurch, et al. (2006). "Interaction of fine particles and nanoparticles with red blood cells visualized with advanced microscopic techniques." Environ Sci Technol **40**(14): 4353-4359.

205. Roveri, A., M. Coassin, et al. (1992). "Effect of hydrogen peroxide on calcium homeostasis in smooth muscle cells." Arch Biochem Biophys **297**(2): 265-270.

206. Roy, S. S. and G. Hajnoczky (2008). "Calcium, mitochondria and apoptosis studied by fluorescence measurements." Methods **46**(3): 213-223.

207. Sabuncu, A. C., J. Grubbs, et al. (2012). "Probing nanoparticle interactions in cell culture media." Colloids Surf B Biointerfaces **95**: 96-102.

208. Sager, T. M. and V. Castranova (2009). "Surface area of particle administered versus mass in determining the pulmonary toxicity of ultrafine and fine carbon black: comparison to ultrafine titanium dioxide." Part Fibre Toxicol **6**: 15.

209. Sahay, G., D. Y. Alakhova, et al. (2010). "Endocytosis of nanomedicines." J Control Release **145**(3): 182-195.

210. Salvati, A., A. S. Pitek, et al. (2013). "Transferrin-functionalized nanoparticles lose their targeting capabilities when a biomolecule corona adsorbs on the surface." Nat Nanotechnol **8**(2): 137-143.

211. Samaj, J., F. Baluska, et al. (2004). "Endocytosis, actin cytoskeleton, and signaling." Plant Physiol **135**(3): 1150-1161.

212. Sametband, M., I. Shweky, et al. (2007). "Application of nanoparticles for the enhancement of latent fingerprints." Chem Commun (Camb) (11): 1142-1144.

213. SCENIHR (2007a). "Opinion on: The scientific aspects of the existing and proposed definitions relating to products of nanoscience and nanotechnologies." European Commission, Brussels.

214. SCENIHR (2007b). "Opinion on: The appropriateness of the risk assessment methodology in accordance with the technical guidance documents for new and existing substances for assessing the risks of nanomaterials." European Commission, Brussels.

215. Scheffer, A., C. Engelhard, et al. (2008). "ICP-MS as a new tool for the determination of gold nanoparticles in bioanalytical applications." Anal Bioanal Chem **390**(1): 249-252.

216. Schrand, A. M., J. J. Schlager, et al. (2010). "Preparation of cells for assessing ultrastructural localisation of nanoparticles with transmission electron microscopy." Nat Protoc **5**(4): 744-757.

217. Seaton, A., L. Tran, et al. (2010). "Nanoparticles, human health hazard and regulation." J R Soc Interface **7 Suppl 1**: S119-129.

218. Shang, L., K. Nienhaus, et al. (2014). "Engineered nanoparticles interacting with cells: size matters." J Nanobiotechnology **12**: 5.

219. Shi, Y. (2002). "Mechanisms of caspase activation and inhibition during apoptosis." Mol Cell **9**(3): 459-470.

220. Shi, Y., F. Wang, et al. (2010). "Titanium dioxide nanoparticles cause apoptosis in BEAS-2B cells through the caspase 8/t-Bid-independent mitochondrial pathway." Toxicol Lett **196**(1): 21-27.

221. Shintani, T. and D. J. Klionsky (2004). "Autophagy in health and disease: a double-edged sword." Science **306**(5698): 990-995.

222. Silva, V. M., N. Corson, et al. (2005). "The rat ear vein model for investigating in vivo thrombogenicity of ultrafine particles (UFP)." Toxicol Sci **85**(2): 983-989.

223. Singh, N. P., M. T. McCoy, et al. (1988). "A simple technique for quantitation of low levels of DNA damage in individual cells." Exp Cell Res **175**(1): 184-191.

224. Slater, T. F., B. Sawyer, et al. (1963). "Studies on Succinate-Tetrazolium Reductase Systems. Iii. Points of Coupling of Four Different Tetrazolium Salts." Biochim Biophys Acta **77**: 383-393.

225. Soenen, S. J., P. Rivera-Gil, et al. (2011). "Cellular toxicity of inorganic nanoparticles: Common aspects and guidelines for improved nanotoxicity evaluation." Nano Today **6**(5): 446-465.

226. Sohaebuddin, S., P. Thevenot, et al. (2010). "Nanomaterial cytotoxicity is composition, size, and cell type dependent." Particle and fibre toxicology **7**: 22.

227. Stearns, R. C., J. D. Paulauskis, et al. (2001). "Endocytosis of ultrafine particles by A549 cells." Am J Respir Cell Mol Biol **24**(2): 108-115.

228. Stephen, D. W. and D. J. Jamieson (1996). "Glutathione is an important antioxidant molecule in the yeast Saccharomyces cerevisiae." FEMS Microbiol Lett **141**(2-3): 207-212.

229. Stern, S., P. Adiseshaiah, et al. (2012). "Autophagy and lysosomal dysfunction as emerging mechanisms of nanomaterial toxicity." Particle and fibre toxicology **9**(1): 20.

230. Stone, V. and K. Donaldson (2006). "Nanotoxicology: signs of stress." Nat Nanotechnol **1**(1): 23-24.

231. Stone, V., B. Nowack, et al. (2010). "Nanomaterials for environmental studies: classification, reference material issues, and strategies for physicochemical characterisation." Sci Total Environ **408**(7): 1745-1754.

232. Sung, J. C., B. L. Pulliam, et al. (2007). "Nanoparticles for drug delivery to the lungs." Trends Biotechnol **25**(12): 563-570.

233. Szeto, Y. T., I. F. Benzie, et al. (2005). "A buccal cell model comet assay: development and evaluation for human biomonitoring and nutritional studies." Mutat Res **578**(1-2): 371-381.

234. Tallury, P., A. Malhotra, et al. (2010). "Nanobioimaging and sensing of infectious diseases." Adv Drug Deliv Rev **62**(4-5): 424-437.

235. Tantral, L., K. Malathi, et al. (2004). "Intracellular calcium release is required for caspase-3 and -9 activation." Cell Biochem Funct **22**(1): 35-40.

236. Teeguarden, J. G., P. M. Hinderliter, et al. (2007). "Particokinetics in vitro: dosimetry considerations for in vitro nanoparticle toxicity assessments." Toxicol Sci **95**(2): 300-312.

237. Thubagere, A. and B. M. Reinhard (2010). "Nanoparticle-induced apoptosis propagates through hydrogen-peroxide-mediated bystander killing: insights from a human intestinal epithelium in vitro model." ACS Nano **4**(7): 3611-3622.

238. The Nanotechnology Consumer Products Inventory. available online (last accessed on 14 January 2014): http://www.nanotechproject.org/inventories/consumer/

239. Tsai, Y. Y., J. Oca-Cossio, et al. (2007). "Novel synthesis of cerium oxide nanoparticles for free radical scavenging." Nanomedicine (Lond) **2**(3): 325-332.

240. Tsoli, M., H. Kuhn, et al. (2005). "Cellular uptake and toxicity of Au55 clusters." Small **1**(8-9): 841-844.

241. Tsuji, J. S., A. D. Maynard, et al. (2006). "Research strategies for safety evaluation of nanomaterials, part IV: risk assessment of nanoparticles." Toxicol Sci **89**(1): 42-50.

242. Unfried, K., U. Sydlik, et al. (2008). "Carbon nanoparticle-induced lung epithelial cell proliferation is mediated by receptor-dependent Akt activation." Am J Physiol Lung Cell Mol Physiol **294**(2): L358-367.

243. Valko, M., C. J. Rhodes, et al. (2006). "Free radicals, metals and antioxidants in oxidative stress-induced cancer." Chem Biol Interact **160**(1): 1-40.

244. Van der Valk, J., D. Mellor, et al. (2004). "The humane collection of fetal bovine serum and possibilities for serum-free cell and tissue culture." Toxicol In Vitro **18**(1): 1-12.

245. Van Meerloo, J., G. J. Kaspers, et al. (2011). "Cell sensitivity assays: the MTT assay." Methods Mol Biol **731**: 237-245.

246. Varela, J. A., M. G. Bexiga, et al. (2012). "Quantifying size-dependent interactions between fluorescently labelled polystyrene nanoparticles and mammalian cells." J Nanobiotechnology **10**: 39.

247. Vippola, M., G. C. Falck, et al. (2009). "Preparation of nanoparticle dispersions for in-vitro toxicity testing." Hum Exp Toxicol **28**(6-7): 377-385.

248. Vranic, S., N. Boggetto, et al. (2013). "Deciphering the mechanisms of cellular uptake of engineered nanoparticles by accurate evaluation of internalisation using imaging flow cytometry." Part Fibre Toxicol **10**: 2.

249. Wang, H. and J. A. Joseph (1999). "Quantifying cellular oxidative stress by dichlorofluorescein assay using microplate reader." Free Radic Biol Med **27**(5-6): 612-616.

250. Wang, X. Z., L. Liu, et al. (2009). "Online characterisation of nanoparticle suspensions using dynamic light scattering, ultrasound spectroscopy and process tomography." Chemical Engineering Research and Design **87**(6): 874-884.

251. Waris, G. and H. Ahsan (2006). "Reactive oxygen species: role in the development of cancer and various chronic conditions." J Carcinog **5**: 14.

252. Wei, J. and E. Khun (2014). "Determination of critical coagulation concentration of silicon nanoparticles." Adv Mat Lett **5**(1): 2-5.

253. Wesierska-Gadek, J., M. Gueorguieva, et al. (2005). "A new multiplex assay allowing simultaneous detection of the inhibition of cell proliferation and induction of cell death." J Cell Biochem **96**(1): 1-7.

254. Wilson, M. R., J. H. Lightbody, et al. (2002). "Interactions between ultrafine particles and transition metals in vivo and in vitro." Toxicol Appl Pharmacol **184**(3): 172-179.

255. Win, K. Y. and S. S. Feng (2005). "Effects of particle size and surface coating on cellular uptake of polymeric nanoparticles for oral delivery of anticancer drugs." Biomaterials **26**(15): 2713-2722.

256. Wong, Y. W. H., C. W. M. Yuen, et al. (2006). "Selected applications of nanotechnology in textiles." AUTEX Research Journal **6**(1): 8.

257. Wu, L., Y. Zhang, et al. (2014). "Tuning Cell Autophagy by Diversifying Carbon Nanotube's Surface Chemistry." ACS Nano.

258. Xia, T., M. Kovochich, et al. (2006). "Comparison of the abilities of ambient and manufactured nanoparticles to induce cellular toxicity according to an oxidative stress paradigm." Nano Lett **6**(8): 1794-1807.

259. Xia, T., M. Kovochich, et al. (2008). "Cationic polystyrene nanosphere toxicity depends on cell-specific endocytic and mitochondrial injury pathways." ACS Nano **2**(1): 85-96.

260. Xie, Z. and D. J. Klionsky. (2007). "Autophagosome formation: core machinery and adaptations." Nat. Cell Biol **9**(10): 1102-1109.

261. Xu, P., J. Xu, et al. (2012). "In vitro toxicity of nanosized copper particles in PC12 cells induced by oxidative stress." Journal of Nanoparticle Research **14**(6): 1-9.

262. Yacobi, N. R., L. Demaio, et al. (2008). "Polystyrene nanoparticle trafficking across alveolar epithelium." Nanomedicine **4**(2): 139-145.

263. Yacobi, N. R., N. Malmstadt, et al. (2010). "Mechanisms of alveolar epithelial translocation of a defined population of nanoparticles." Am J Respir Cell Mol Biol **42**(5): 604-614.

264. Yacobi, N. R., H. C. Phuleria, et al. (2007). "Nanoparticle effects on rat alveolar epithelial cell monolayer barrier properties." Toxicol In Vitro **21**(8): 1373-1381.

265. Yamamoto, N., F. Fukai, et al. (2002). "Dependence of the phagocytic uptake of polystyrene microspheres by differentiated HL60 upon the size and surface properties of the microspheres." Colloids and Surfaces - B - Biointerfaces **25**(2): 6.

266. Yan, H., H. Zhu, et al. (2007). "Molecular dynamics simulation study on zwitterionic structure to maintain the normal conformations of Glutathione." Science in China Series B: Chemistry **50**(5): 660-664.

267. Yang, Z., Z. W. Liu, et al. (2010). "A review of nanoparticle functionality and toxicity on the central nervous system." J R Soc Interface **7 Suppl 4**: S411-422.

268. Zabirnyk, O., M. Yezhelyev, et al. (2007). "Nanoparticles as a novel class of autophagy activators." Autophagy **3**(3): 278-281.

269. Zauner, W., N. A. Farrow, et al. (2001). "In vitro uptake of polystyrene microspheres: effect of particle size, cell line and cell density." J Control Release **71**(1): 39-51.

270. Zhang, D. X. and D. D. Gutterman (2007). "Mitochondrial reactive oxygen species-mediated signaling in endothelial cells." Am J Physiol Heart Circ Physiol **292**(5): H2023-2031.

271. Zhang, S., J. Li, et al. (2009). "Size-Dependent Endocytosis of Nanoparticles." Adv Mater **21**: 419-424.

272. Zhao, F., Y. Zhao, et al. (2011). "Cellular uptake, intracellular trafficking, and cytotoxicity of nanomaterials." Small **7**(10): 1322-1337.

273. Zhivotovsky, B. and S. Orrenius (2011). "Calcium and cell death mechanisms: a perspective from the cell death community." Cell Calcium **50**(3): 211-221.

274. Zhong, W., M. Lü, et al. (2013). "Autophagy as new emerging cellular effect of nanomaterials." Chinese Science Bulletin **58**(33): 4031-4038.

275. Zhu, Z. J., R. Carboni, et al. (2010). "Surface properties dictate uptake, distribution, excretion, and toxicity of nanoparticles in fish." Small **6**(20): 2261-2265.

276. Zucker, R. M., E. J. Massaro, et al. (2010). "Detection of TiO2 nanoparticles in cells by flow cytometry." Cytometry A **77**(7): 677-685.